

**Analysis and Design of Sheet Pile Ribs for Slope Stabilization**

by

James Ryan Bartz

A thesis submitted in partial fulfillment of the requirements for the degree of

Master of Science

in

Geotechnical Engineering

Department of Civil and Environmental Engineering  
University of Alberta

© James Ryan Bartz, 2017

## **ABSTRACT**

An unconventional slope stabilization technique locally known in Alberta as “Hardy Ribs” or “Hardy Walls” was implemented by Canadian National Railway Company (CN) to stabilize a very slow moving landslide. This site is located along the Assiniboine River valley in western Manitoba at CN Mile 191.4 of the Rivers Subdivision. The Hardy Ribs consist of a series of parallel sheet pile walls that are installed oriented parallel to the direction of slope movement and driven through the landslide mass into the underlying soil or bedrock. Hardy Ribs have proven to be a suitable option for the railway industry at locations where transporting materials and equipment can be too costly for more conventional slope stabilization techniques. Since this slope stabilization technique is relatively unknown, there are no currently accepted design procedures. This thesis summarizes an analysis of the performance of the slope at CN Mile 191.4 Rivers Subdivision after remediation with Hardy Ribs and a design methodology for Hardy Ribs is developed.

The Hardy Ribs installed at CN Mile 191.4 Rivers Subdivision have been effective to reduce the rate of landslide displacement which ultimately reduces the ongoing railway maintenance requirements and associated costs. Some displacement after construction is expected and is required to develop resistance as the Hardy Ribs are a passive system. The ultimate lateral resistance for laterally loaded sheet pile walls and the effect of the spacing between sheet pile walls was estimated using limit equilibrium theory and further investigated by finite element modelling. Based on these findings, a seven step procedure was developed to design Hardy Ribs which consists of a de-coupled approach. The landslide loads and required increase in resistance are calculated from a two-dimensional limit equilibrium stability analysis. The resistance from

the Hardy Ribs is calculated from a laterally loaded pile analysis utilizing soil resistance versus pile deflection ( $p-y$ ) curves.

## **ACKNOWLEDGEMENTS**

I would like express my sincerest gratitude to my wife, Jenna Bartz, for all of her support through this master's degree. Your encouragement and willingness to move away from your family and friends to support me are greatly appreciated. Our time in Edmonton has been an amazing opportunity for our relationship to grow and I'm excited to see what lies ahead.

I would also like to thank Dr. C. Derek Martin and Dr. Michael Hendry for supervising my research. Their guidance and feedback was invaluable in completing this project. They provided me the opportunity to work on this very interesting research project and numerous opportunities to network in the engineering and research communities. The positive experience I have had at the University of Alberta has inspired me to further consider a career path in academics and pursue a Ph.D. in geotechnical engineering.

Lastly, I would like to thank the partners of the Railway Ground Hazard Research Program which includes Canadian National Railway, Canadian Pacific Railway, and Transport Canada. I would like to thank Tom Edwards and Melissa Ruel of CN for their help and insight related to my research project.

Scholarships to fund this research were provided by Natural Sciences and Engineering Research Council of Canada (NSERC), Alberta Innovates Technology Futures (AITF), the University of Alberta, and the Government of Alberta.

# TABLE OF CONTENTS

ABSTRACT .....	ii
ACKNOWLEDGEMENTS.....	iv
TABLE OF CONTENTS .....	v
LIST OF TABLES.....	x
LIST OF FIGURES.....	xi
1.0 INTRODUCTION .....	1
1.1 Background .....	1
1.2 Description of Problem .....	1
1.3 Research Scope and Limitations .....	2
1.4 Research Objectives and Methodology.....	2
1.5 Overview of Thesis .....	3
2.0 SLOPE STABILIZATION USING LATERALLY LOADED PILES .....	5
2.1 Slope Stabilization using Pile Walls .....	5
2.2 Ultimate Lateral Soil Resistance.....	6
2.2.1 Wedge Failure Mode .....	6
2.2.1.1 Cohesive Soil.....	6
2.2.1.2 Cohesionless Soil.....	10
2.2.2 Flow-Around Failure Mode.....	14
2.2.2.1 Cohesive Soil.....	14
2.2.2.2 Cohesionless Soil.....	20
2.2.3 Spacing Effects and Reduction Factor .....	23
2.2.3.1 Laboratory Testing on Cohesive Soil.....	24
2.2.3.2 Laboratory Testing on Cohesionless Soil.....	26

2.3	Design Methods for Slope Stabilization with Piles .....	28
2.3.1	Evaluating Required Shear Force to Stabilize Slope .....	29
2.3.2	Evaluating Maximum Shear Force from Stabilizing Piles.....	30
2.3.2.1	Viggiani's (1981) Method .....	30
2.3.2.2	Load Transfer Method with <i>p-y</i> Curves.....	34
2.3.3	Selecting Pile Location, Type and Number .....	36
2.4	Selection of <i>p-y</i> Curves .....	36
2.4.1	<i>p-y</i> Curves for Soft Clay .....	36
2.4.2	<i>p-y</i> Curves for Stiff Clay without Free Water.....	37
2.4.3	<i>p-y</i> Curves for Stiff Clay with Free Water.....	38
2.4.4	<i>p-y</i> Curves for Sand.....	40
2.4.5	<i>p-y</i> Curves for Weak Rock.....	41
2.4.6	Method of Georgiadis for Layered Soil.....	42
2.5	Summary of Laterally Loaded Piles for Slope Stabilization .....	43
3.0	HARDY RIBS CASE STUDY SITE .....	44
3.1	Site Location and Slope Geometry.....	44
3.2	Site Geology and Stratigraphy .....	50
3.3	Site Instrumentation and Monitoring .....	52
3.4	Hardy Ribs Design and Construction .....	55
3.5	Performance of Hardy Ribs .....	60
3.6	Summary of Hardy Ribs at CN Mile 191.4 Rivers Subdivision.....	63
4.0	LATERALLY LOADED SHEET PILE WALLS .....	65
4.1	Block-Soil Model .....	66
4.2	Broms' (1983) Pile Group in Clay Model.....	68

4.3	Two-Dimensional Finite Element Model.....	69
4.3.1	2D F.E. Model Setup .....	70
4.3.1.1	Boundary Conditions .....	70
4.3.1.2	Material Properties.....	71
4.3.2	Model Calibration .....	72
4.3.2.1	Sensitivity of Number of Piles.....	72
4.3.2.2	Sensitivity of Elastic Properties of Clay .....	73
4.3.2.3	Sensitivity of Pile-Soil Adhesion.....	75
4.3.2.4	Sensitivity of Pile Geometry .....	77
4.3.2.5	Sensitivity of Pile Spacing.....	79
4.3.2.6	Sensitivity of Clay Shear Strength .....	81
4.3.2.7	Sensitivity of Pile Width.....	82
4.3.3	Sheet Pile Geometry Effects.....	83
4.4	Summary of Laterally Loaded Sheet Pile Walls .....	88
5.0	SHEET PILE WALL SPACING EFFECTS .....	90
5.1	Critical Sheet Pile Spacing .....	90
5.1.1	Cohesive Soil.....	90
5.1.2	Cohesionless Soil.....	93
5.2	Three-Dimensional Finite Element Modeling.....	96
5.2.1	3D F.E. Model Geometry and Mesh .....	96
5.2.1.1	Boundary Conditions .....	98
5.2.1.2	Material Properties.....	99
5.2.2	Sheet Pile Spacing Results.....	100
5.3	<i>p-y</i> Curves for Closely Spaced Sheet Pile Walls.....	109

5.4	Summary of Spacing Effects .....	109
6.0	PROPOSED DESIGN METHODOLOGY FOR HARDY RIBS .....	111
6.1	Details of Proposed Design Steps .....	112
6.1.1	Determine Landslide Loads.....	112
6.1.2	Strength Parameters for Laterally Loaded Pile Analysis .....	112
6.1.3	Determine Critical Spacing of Sheet Pile Walls .....	113
6.1.4	Develop <i>p-y</i> Curves.....	114
6.1.4.1	Option 1: Assumed Continuous Wall .....	114
6.1.4.2	Option 2: Assumed Equivalent Pile Diameter .....	115
6.1.5	Numerically Model Soil-Pile Interaction .....	116
6.1.6	Check Structural Capacity of Sheet Piles.....	118
6.1.7	Select Location to Install Hardy Ribs .....	118
6.2	Example Calculations for Hardy Ribs at CN Mile 191.4 Rivers Subdivision .....	119
6.2.1	Landslide Loads at CN Study Site .....	119
6.2.2	Strength Parameters at CN Study Site for Laterally Loaded Pile Analysis .....	121
6.2.3	Critical Spacing of Sheet Pile Walls at CN Study Site.....	123
6.2.4	<i>p-y</i> Curves for CN Study Site .....	123
6.2.5	Soil-Pile Interaction at CN Study Site .....	126
6.2.6	Structural Capacity of Sheet Pile Walls at CN Study Site .....	131
6.2.7	Location of Sheet Pile Walls at CN Study Site .....	131
6.3	Comparison to Viggiani’s (1981) Method.....	134
6.4	Summary of Design Methodology .....	136
7.0	CONCLUSIONS.....	138
7.1	Key Contributions.....	138



7.2 Summary of CN Mile 191.4 Rivers Subdivision ..... 139

7.3 Recommendations for Future Research..... 141

REFERENCES..... 143

APPENDIX A: BOREHOLE LOGS..... 148

## LIST OF TABLES

Table 2.1: Suggested pile wall type and approximate construction cost (from Abdelaziz et al., 2011).....	5
Table 2.2: Representative values of $\epsilon_{50}$ for normally consolidated clays (from Peck et al., 1974). 37	
Table 2.3: Representative values for overconsolidated clays (from Reese et al, 1975). ....	39
Table 3.1: Groundwater data monitored on Dec. 11, 2014. ....	53
Table 4.1: Calibrated material properties for 2D finite element model of laterally loaded piles..	78
Table 6.1: Estimated FS before remediation at CN Mile 191.4 Rivers Subdivision. ....	121
Table 6.2: Maximum bending moment and shear force in sheet pile walls.....	130

## LIST OF FIGURES

Figure 2.1: Pile and soil deformation under lateral load (Adapted from Wang & Reese, 1986 with permission of Center for Transportation Research).....	6
Figure 2.2: Assumed passive wedge failure for clay. (a) Shape of wedge (b) Forces acting on wedge (from Wang & Reese, 1986 with permission of Center for Transportation Research). .....	7
Figure 2.3: Passive wedge failure of piles in a row (from Wang & Reese, 1986 with permission of Center for Transportation Research).....	8
Figure 2.4: Soil deformation and gaps observed in experimental study (from Wang & Reese, 1986 with permission of Center for Transportation Research).....	9
Figure 2.5: Distribution of ultimate lateral soil resistance with depth (Adapted from Broms, 1964 with permission from ASCE). ....	10
Figure 2.6: Assumed passive wedge-type failure in sand. (a) General wedge shape (b) Forces on wedge (c) Forces on pile (from Reese et al., 1974. Copyright 1974, Society of Petroleum Engineers Inc. Reproduced with permission of SPE. Further reproduction prohibited without permission). ....	12
Figure 2.7: Assumed passive wedge for piles in a row. (a) General view (b) Plane view (c) Side view (Adapted from Wang & Reese, 1986 with permission of Center for Transportation Research). ....	13
Figure 2.8: Example study of ultimate soil resistance in sand with pile diameter of 30 in. (Adapted from Wang & Reese, 1986 with permission of Center for Transportation Research). ....	14
Figure 2.9: Assumed lateral flow-around type of failure for clay using block-soil model. (a) Section through pile (b) Mohr-Coulomb diagram (c) Forces acting on pile (Adapted from Wang & Reese, 1986 with permission of Center for Transportation Research). ....	15
Figure 2.10: Ultimate lateral soil resistance from slip-line theory (Adapted from Broms, 1964 with permission from ASCE). ....	16
Figure 2.11: Slip-line field for a single square pile (Adapted from Wang & Reese, 1986 with permission of Center for Transportation Research).....	16
Figure 2.12: Lateral resistance of a pile group in clay (After Broms, 1983).....	17
Figure 2.13: Comparison of test results and calculated ultimate lateral soil resistance (After Broms, 1983).....	18

Figure 2.14: Variation of  $N_c$  with friction ratio (Adapted. Republished with permission of ICE Publishing, from Randolph & Houlsby, 1984; permission conveyed through Copyright Clearance Centre, Inc.). ..... 19

Figure 2.15: The ultimate soil resistance on a circular pile for flow around failure based on the slip-line theory (Republished with permission of ICE Publishing, from Randolph & Houlsby, 1984; permission conveyed through Copyright Clearance Centre, Inc.). ..... 19

Figure 2.16: Assumed lateral flow-around type of failure for sand using block-soil model. (a) Section through pile (b) Mohr-Coulomb diagram (From Wang & Reese, 1986 with permission of Center for Transportation Research). ..... 21

Figure 2.17: Lateral resistance of a pile group in sand (After from Broms, 1983). ..... 22

Figure 2.18: Comparison of test results and calculated ultimate lateral soil resistance of sand (After Broms, 1983). ..... 23

Figure 2.19: Reduction factors for closely space piles (Adapted. Republished with permission of ASCE, from Reese et al., 1992; permission conveyed through Copyright Clearance Centre Inc.). ..... 24

Figure 2.20: Efficiency of pile groups in clay (Adapted. Republished with permission from Cox et al., 1984, copyright ASTM International, 100 Barr Harbor Drive, West Conshohocken, PA 19428). ..... 25

Figure 2.21: Ultimate load ratio (reduction factor) for soft clay (From Wang & Reese, 1986 with permission of Center for Transportation Research). ..... 26

Figure 2.22: Ultimate load ratio (reduction factor) for loose sand (From Wang & Reese, 1986 with permission of Center for Transportation Research). ..... 27

Figure 2.23: Ultimate load ratio (reduction factor) for dense sand (From Wang & Reese, 1986 with permission of Center for Transportation Research). ..... 27

Figure 2.24: Modified reduction factor vs spacing ratio (Adapted. Republished with permission of ASCE, from Reese et al., 1992; permission conveyed through Copyright Clearance Centre Inc.). ..... 28

Figure 2.25: Simplified scheme of problem (Adapted from Viggiani, 1981 with permission of Taylor and Francis). ..... 30

Figure 2.26: Failure modes for short piles (Adapted from Viggiani, 1981 with permission of Taylor and Francis). ..... 31

Figure 2.27: Failure modes for long piles (Adapted from Viggiani, 1981 with permission of Taylor and Francis). ..... 33

Figure 2.28: Model for pile under lateral loading with p-y curves. (a) Elevation view (b) As elastic line (c) p-y curves (From Reese., 1997 with permission from ASCE).....	35
Figure 2.29: p-y curve for stiff clay with free water (Adapted from Reese et al., 1975. Copyright 1975, Society of Petroleum Engineers, Inc. Reproduced with permission of SPE. Further reproduction prohibited without permission). .....	38
Figure 2.30: Values of $A_s$ and $A_c$ (Adapted from Reese et al., 1975. Copyright 1975, Society of Petroleum Engineers, Inc. Reproduced with permission of SPE. Further reproduction prohibited without permission).....	39
Figure 2.31: p-y Curve for Sand (Adapted from Reese et al., 1974. Copyright 1974, Society of Petroleum Engineers Inc. Reproduced with permission of SPE. Further reproduction prohibited without permission).....	40
Figure 2.32: Non-dimensional coefficients A and B for ultimate soil resistance vs depth (Adapted from Reese et al., 1974. Copyright 1974, Society of Petroleum Engineers Inc. Reproduced with permission of SPE. Further reproduction prohibited without permission). .....	41
Figure 2.33: p-y curve for weak rock (Adapted from Reese, 1997 with permission from ASCE).42	
Figure 3.1: Location of study site. ....	45
Figure 3.2: Topographic contour plan of CN study site. ....	47
Figure 3.3: Cross sections showing valley geometry. ....	48
Figure 3.4: LIDAR data in CloudCompare. a) Point cloud showing regional topography b) Mesh showing landslide region. ....	50
Figure 3.5: Stratigraphic sections at CN Mile 191.4 Rivers Subdivision .....	52
Figure 3.6: S.I. monitoring data from BH14-1. ....	53
Figure 3.7: S.I. monitoring data from BH14-2. ....	54
Figure 3.8: S.I. monitoring data from BH14-3. ....	54
Figure 3.9: Dimensions of PZC 26 sheet pile.....	55
Figure 3.10: Layout of sheet piles for Hardy Ribs at CN Mile 191.4 Rivers Sub.....	56
Figure 3.11: Plan view showing as-built layout of sheet pile walls. ....	57
Figure 3.12: Cross section showing as-built layout of sheet pile walls. ....	58
Figure 3.13: Hoisting sheet pile with crane (Source: CN).....	58

Figure 3.14: Advancing sheet piles with vibratory hammer (Source: CN).....	59
Figure 3.15: Driving sheet piles with diesel hammer (Source: CN).....	59
Figure 3.16: Rows of installed sheet pile walls (Source: CN).....	60
Figure 3.17: S.I. monitoring data from BH15-3. ....	61
Figure 3.18: Total landslide displacement with time. ....	62
Figure 3.19: Photos from October 5, 2016. (a) Looking downslope from rail line (b) Looking north from over top of Hardy Ribs (c) Looking upslope from access road downslope of Hardy Ribs (d) Shore line of Assiniboine River showing signs of erosion. (Photos by J.R. Bartz). 63	63
Figure 4.1: Soil and sheet pile deformation under lateral load.....	65
Figure 4.2: Assumed block failure model for clay. (a) Section through sheet pile (b) Mohr-Coulomb diagram (c) Forces acting on sheet pile. ....	67
Figure 4.3: Lateral resistance of a sheet pile group in clay.....	68
Figure 4.4: Ultimate resistance in clay for sheet pile groups in clay. (a) Adhesion factor of 1.0 (b) Adhesion factor of 0.5. ....	69
Figure 4.5: General 2D finite element model setup.....	70
Figure 4.6: RS <sup>2</sup> model geometry for sensitivity analysis of number of piles. (a) Two square piles (b) Four square piles.....	72
Figure 4.7: Displacement versus soil resistance showing sensitivity to number of piles. ....	73
Figure 4.8: Displacement versus lateral soil resistance showing sensitivity to clay Young's Modulus. ....	74
Figure 4.9: Displacement versus lateral soil resistance showing sensitivity to clay Poisson's ratio. ....	75
Figure 4.10: Modeled p-y curve showing sensitivity to soil-pile adhesion. ....	76
Figure 4.11: Modeled p-y curve showing sensitivity to joint stiffness. ....	77
Figure 4.12: Modeled p-y curve comparing circular and square pile geometry.....	78
Figure 4.13: RS <sup>2</sup> output for calibrated model of laterally loaded circular piles showing total displacement contours. (a)Entire model geometry (b) Left half of model geometry.....	79
Figure 4.14: Modeled p-y curve showing sensitivity to pile spacing. ....	80

Figure 4.15: Comparison of 2D F.E. model results and laboratory testing results by Broms (1983). .....	81
Figure 4.16: Sensitivity to clay undrained shear strength. (a) p-y curves (b) $c_u$ versus $p_{ult}$ . .....	82
Figure 4.17: Sensitivity to square pile width. (a) Modeled p-y curves (b) Pile width versus $p_{ult}$ . 83	
Figure 4.18: RS <sup>2</sup> model showing sheet pile geometry. ....	84
Figure 4.19: RS <sup>2</sup> output for model of rectangular piles. (a)Entire model geometry (b) Left half of model geometry. ....	85
Figure 4.20: Sensitivity to sheet pile dimensions with adhesion factor of 1.0. (a) Modeled p-y curves (b) $B_2/B_1$ versus $p_{ult}$ . ....	86
Figure 4.21: Sensitivity to sheet pile geometry with adhesion factor of 0.5. (a) Modeled p-y curve (b) $B_2/B_1$ versus $p_{ult}$ . ....	87
Figure 4.22: Distribution of ultimate soil resistance with depth. ....	89
Figure 5.1: Closely spaced sheet pile walls in cohesive soil.....	91
Figure 5.2: Closely spaced sheet pile walls in cohesionless soil. ....	94
Figure 5.3: RS <sup>3</sup> model geometry.....	97
Figure 5.4: Mesh of RS <sup>3</sup> model.....	98
Figure 5.5: Boundary conditions of RS <sup>3</sup> model. ....	99
Figure 5.6: Total displacement contours for S=0.9 m. ....	101
Figure 5.7: Total displacement contours for S=1.9 m. ....	101
Figure 5.8: Total displacement contours for S=2.9 m. ....	102
Figure 5.9: Total displacement contours for S=3.9 m. ....	102
Figure 5.10: Total displacement contours for S=4.9 m. ....	103
Figure 5.11: Total displacement contours for S=5.9 m. ....	103
Figure 5.12: Yielded elements contours for S=0.9 m.....	104
Figure 5.13: Yielded elements contours for S=1.9 m.....	104
Figure 5.14: Yielded elements contours for S=2.9 m.....	105

Figure 5.15: Yielded elements contours for $S=3.9$ m.....	105
Figure 5.16: Yielded elements contours for $S=4.9$ m.....	106
Figure 5.17: Yielded elements contours for $S=5.9$ m.....	106
Figure 5.18: Total displacement contours and vectors for 160 mm for sheet pile displacement with spacing of 1.9 m.....	107
Figure 5.19: RS <sup>3</sup> results of sheet pile spacing vs clay deflection. (a) Leading edge of sheet piles (b) At mid-length of sheet piles. ....	108
Figure 6.1: Equivalent pile diameter for Option 2a and Option 2b. ....	116
Figure 6.2: Potential slide planes. ....	119
Figure 6.3: Slide 7.0 model of cross section at CN Mile 191.4 River Subdivision .....	120
Figure 6.4: Simplified soil properties for laterally loaded pile analysis at CN Mile 191.4 Rivers Subdivison. ....	122
Figure 6.5: $p_{ult}$ with depth at CN Mile 191.4 Rivers Subdivision.....	125
Figure 6.6: Custom p-y curves for Option 1. ....	126
Figure 6.7: RSPile output showing pile displacement, moment, and shear force from soil displacement.....	127
Figure 6.8: Estimated lateral displacement of sheet pile. ....	128
Figure 6.9: Estimated bending moment profile of sheet pile. ....	129
Figure 6.10: Estimated shear force profile of sheet pile. ....	129
Figure 6.11: Slide 7.0 model of potential upper slope slide plane.....	132
Figure 6.12: Slide 7.0 model of potential lower slope slide plane. ....	133
Figure 6.13: Slide 7.0 model of potential deep slide plane. ....	134



# 1.0 INTRODUCTION

## 1.1 Background

Landslides in Prairie river valleys are common, and the slope movements can have detrimental impact on the human use of the land. This includes damage to existing structures and buildings, and damage to linear infrastructure such as pipelines, roads and railways. The owners of linear infrastructure are constantly looking for cost effective solutions for maintaining their infrastructure. For example, railways generally attempt to manage landslides by avoiding the hazard, stabilizing the hazard, or using monitoring and signals to ensure that safe track conditions can be maintained (Bunce and Chadwick, 2012). Where access to sites is limited, current mitigation techniques can be difficult or costly to construct. Some of the current mitigation techniques to stabilize landslides include regrading and reconstructing the site to a new geometry, constructing granular shear keys or columns, and/or installing pile groups. Many of the rail lines in western Canada have limited access, and thus new slope stabilization techniques are required.

An unconventional slope stabilization method has been developed utilizing a series of parallel sheet pile walls where the sheet pile walls are installed oriented parallel to the movement of the landslide. This counter-intuitive slope stabilization method is known locally in Edmonton, but has seen limited application since it was first introduced by Dr. R.M Hardy. Recently, Canadian National Railway Company (CN) utilized the method, referred to as “Hardy Ribs” or “Hardy Walls”, to stabilize a slope along the Assiniboine River near the Birdtail Sioux First Nation in western Manitoba. Hardy Ribs were also implemented by CN in the past to stabilize a slope near Peace River, Alberta to protect its rail line.

## 1.2 Description of Problem

Due to the limited use and limited case histories of the Hardy Ribs slope stabilization method, there is no generally accepted design methodology. Passive stabilization methods are particularly challenging from a design perspective, as the loads on the walls are unknown. It is anticipated that the Hardy Ribs will resist landslide displacement in a manner similar to the passive

resistance provided by installing a row of circular piles. The difference in geometry between a sheet pile wall and a circular pile is expected to have an impact on the lateral resistance that can be passively developed. The spacing between adjacent rows of sheet piles is also expected to effect the resistance developed from each sheet pile wall.

### **1.3 Research Scope and Limitations**

The scope of this research includes developing a methodology for the design of Hardy Ribs as a slope stabilization technique. Since the Hardy Ribs slope stabilization technique is not a common or well-known method, there are currently no existing published design procedures. Developing a design procedure involves studying the potential failure mechanisms of the moving soil above the landslide shear plane and the stable soil below the shear plane. The design procedure developed as part of this research utilizes similar procedures and methodologies developed for the design of a row of circular piles for slope stabilization. This method consists of a two-dimensional limit equilibrium slope stability analysis and lateral loaded pile analysis which geotechnical engineers are familiar with.

There are limitations in the currently available knowledge base regarding Hardy Ribs which includes a lack of documented and monitored case studies. There is a relatively small amount of instrumentation installed at the CN case study site to measure landslide displacement and monitor the performance of the Hardy Ribs. Also, there is no lab scale or field scale testing of laterally loaded sheet piles that are loaded in the appropriate orientation to be representative of the Hardy Ribs system. These limitations should be kept in mind and it should be understood that the design procedure developed is based on the assumptions stated herein.

### **1.4 Research Objectives and Methodology**

There are several key objectives for this research on the Hardy Ribs slope stabilization method. This includes estimating the ultimate lateral load capacity of the sheet piles, estimating the ultimate lateral load capacity when considering group and spacing effects from adjacent sheet pile walls, and developing a design procedure for Hardy Ribs.

The ultimate lateral load capacity of the sheet piles to resist the flow around failure of the soil was estimated. The methodology included performing theoretical calculations and performing two-dimensional finite element method modeling which provides further insight into the development of resistance with relative displacement between the soil and sheet piles. These calculations consider plane-strain conditions and therefore are only suitable for the performance of a single sheet pile wall or sheet pile walls that are spaced sufficiently far apart.

Hardy Ribs consists of a row of parallel sheet pile walls that are spaced relatively close to each other. Therefore, spacing effects are expected and the ultimate lateral load capacity of each sheet pile wall in a series would differ from that of a single sheet pile wall. The maximum resistance against landslide loading can be achieved by spacing the parallel sheet pile walls close enough together. This prevents the potential failure of soil from squeezing between the rows of sheet piles. The methodology to estimate the ultimate lateral load capacity included performing limit equilibrium calculations to estimate the critical spacing between sheet pile walls to prevent soil squeezing between sheet piles. Also, the ultimate lateral load capacity for the Hardy Ribs with sufficiently small sheet pile wall spacing was estimated. The limit equilibrium theory results were then supported with three-dimensional finite element method modelling.

After developing an appropriate calculation for the ultimate lateral soil resistance, the design procedure was then developed by borrowing concepts and methodologies from slope stabilization with circular piles. The design guidelines are used to analyze the Hardy Ribs installed at CN Mile 191.4 Rivers Subdivision and the monitoring results are compared to those provided by the design guidelines.

## **1.5 Overview of Thesis**

Chapter 1 provides background information regarding Hardy Ribs, a description of the problem, the research scope and limitations, and the research objectives and methodology. Chapter 2 summarizes a review of literature related to slope stabilization with piles and laterally loaded pile analysis. The case study for the CN site where Hardy Ribs were implemented is discussed in detail in Chapter 3. Chapter 4 presents the findings regarding the ultimate lateral load resistance

for sheet pile walls installed parallel to the direction of loading. Chapter 5 presents the findings regarding effects from the spacing between adjacent rows of sheet piles which compose the Hardy Ribs. Chapter 6 summarizes the recommended design procedure for the Hardy Ribs method for slope stabilization and provides an example of performing the design procedure on the Hardy Ribs case study at CN Mile 191.4 River Subdivision. Chapter 7 summarizes the conclusions of this research and provides recommendations for further research.

## 2.0 SLOPE STABILIZATION USING LATERALLY LOADED PILES

This chapter summarizes a review of literature related to slope stabilization and laterally loaded pile analysis. This includes a review of slope stabilization using pile walls, the ultimate lateral soil resistance for laterally loaded piles, design methods for slope stabilization using piles and the selection of adequate soil resistance versus pile deflection ( $p$ - $y$ ) curves.

### 2.1 Slope Stabilization using Pile Walls

Various authors have studied pile walls for slope stabilization; e.g. Viggiani (1981); Poulos (1995); Reese, Wang & Fouse (1992); and Vessely, Yamasaki & Strom (2007) amongst many others. Pile walls for stabilizing landslides are classified as passive piles, where the forces acting on the piles are mobilized due to lateral soil movement (Abdelaziz, Proudfoot & Skirrow, 2011). By mobilizing the available soil reaction in the stable ground mass below the slide plane, resistance is transmitted to the overlying sliding soil mass (Vessely et al., 2007). Most pile wall designs consist of large diameter piles of 0.61 m to 1.83 m with centre-to-centre spacing ranging from 1.5 to 3.0 times the pile diameter to create a line of piles or a pile wall (Cornforth, 2012).

Abdelaziz et al. (2011) studied 28 sites in Alberta where pile walls were installed to stabilize a slope between 1988 and 2011. Pile walls were considered as an attractive alternative at these sites because of site specific constraints including conflicts with existing utilities, minimizing disruption to highway traffic, land acquisition issues, and water bodies located within or at the toe of the slide mass. The pile types at these study sites varied from cast-in-place (CIP) concrete piles to driven steel, and some of the sites included tie backs. Based on the 28 sites in Alberta, Abdelaziz et al. (2011) made the following recommendations shown in Table 2.1 for selecting the pile wall type based on the depth of the slide plane. The included approximate cost is based on information for pile walls installed from 2005 to 2011.

Table 2.1: Suggested pile wall type and approximate construction cost (from Abdelaziz et al., 2011).

Depth to Slip Surface	Pile Wall Type	Cost/m of Wall
0 to 3 m	Cantilever pile wall (H piles)	\$6,500 to \$7,500
4 to 6 m	Cantilever pile wall (CIP piles)	\$12,000 to \$16,000
>6 m	Tied-back pile wall	\$20,000 to \$30,000

## 2.2 Ultimate Lateral Soil Resistance

The ultimate lateral resistance per unit length of pile ( $p_{ult}$ ) for soil failure around a laterally loaded pile can be distinguished between two failure mechanisms shown in Figure 2.1. At shallow depths, a passive wedge of soil develops and moves upward and away from the pile (Wang & Reese, 1986). At greater depths, the soil is limited to plane-strain conditions and fails by flowing around the pile (Wang & Reese, 1986). This section describes the wedge failure mode and the flow-around failure mode in detail for both cohesive and cohesionless soil types. The effect of closely spaced adjacent piles on the ultimate lateral soil resistance is also discussed.

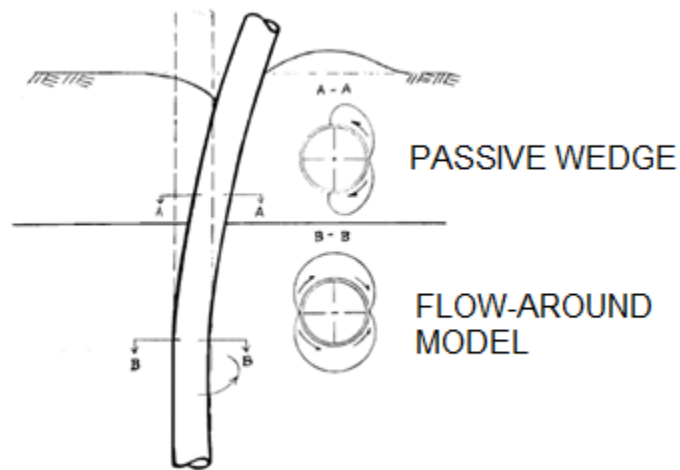


Figure 2.1: Pile and soil deformation under lateral load (Adapted from Wang & Reese, 1986 with permission of Center for Transportation Research).

### 2.2.1 Wedge Failure Mode

Various theoretical solutions for calculating the ultimate lateral soil resistance per unit length of pile ( $p_{ult}$ ) for a potential wedge failure near ground surface of laterally loaded piles are described for cohesive and cohesionless soils below.

#### 2.2.1.1 Cohesive Soil

Reese (1958) developed a soil model for calculating the ultimate soil resistance for a wedge-type failure near ground surface for lateral loading of a single pile in cohesive soil. A free-body diagram and the assumed failure geometry is shown in Figure 2.2. It was assumed that the full shear strength of the soil develops along planes ACE, BDF, and ABEF. It was assumed that the

shear strength developed along plane CDEF is equal to  $ac_u$  where  $a$  is an adhesion factor between 0 and 1 and  $c_u$  is the undrained shear strength of the soil. If  $\theta$  is assumed to be  $45^\circ$ , then the ultimate lateral soil resistance per unit length of pile ( $p_{ult}$ ) can be calculated using Reese (1958):

$$p_{ult} = 2c_u b + \gamma b H + 2.83c_u H \quad (\text{for } a = 0) \quad 2-1$$

$$p_{ult} = 3c_u b + \gamma b H + 2.83c_u H \quad (\text{for } a = 1) \quad 2-2$$

where  $b$  is the pile diameter,  $\gamma$  is the soil unit weight, and  $H$  is the height of the wedge (see Figure 2.2). Since the mode of failure is assumed and may not match actual failure modes, Equations 2-1 and 2-2 should be considered as approximate and should be modified with experimental results (Welch & Reese, 1972). Field tests completed by Matlock (1970) indicate that the factor 2.83 in Equation 2-1 and 2.2 should be in the order of 0.25 to 0.5 for soft clays.

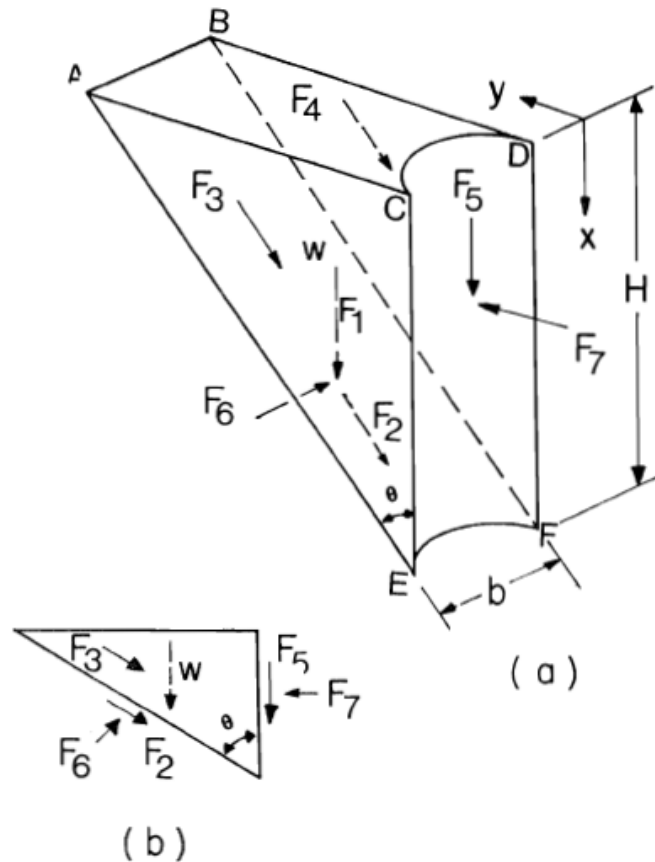


Figure 2.2: Assumed passive wedge failure for clay. (a) Shape of wedge (b) Forces acting on wedge (from Wang & Reese, 1986 with permission of Center for Transportation Research).

When piles are in a row, the resistance for each pile is equal to that of a single pile if the spacing between piles is large (Wang & Reese, 1986). The difference in resistance for a single pile and pile groups becomes negligible when the centre-to-centre spacing to pile diameter ratio reaches 3 to 4 (Cornforth, 2005; Reese et al., 1992). If the spacing is too narrow however, the soil block between piles will move with the passive wedge and a continuous failure plane will develop (Wang & Reese, 1986). The soil model developed by Wang & Reese (1986) for pile group behaviour is shown in Figure 2.3. This behaviour was observed in laboratory testing performed by Wang & Reese (1986) where a continuous gap of soil developed behind closely spaced piles as shown in Figure 2.4.

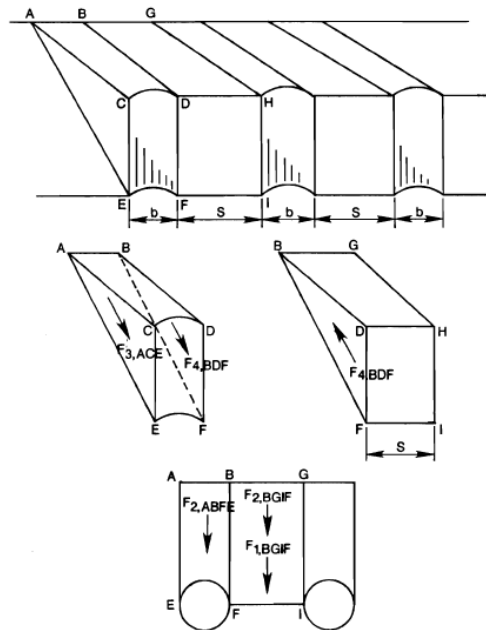


Figure 2.3: Passive wedge failure of piles in a row (from Wang & Reese, 1986 with permission of Center for Transportation Research).



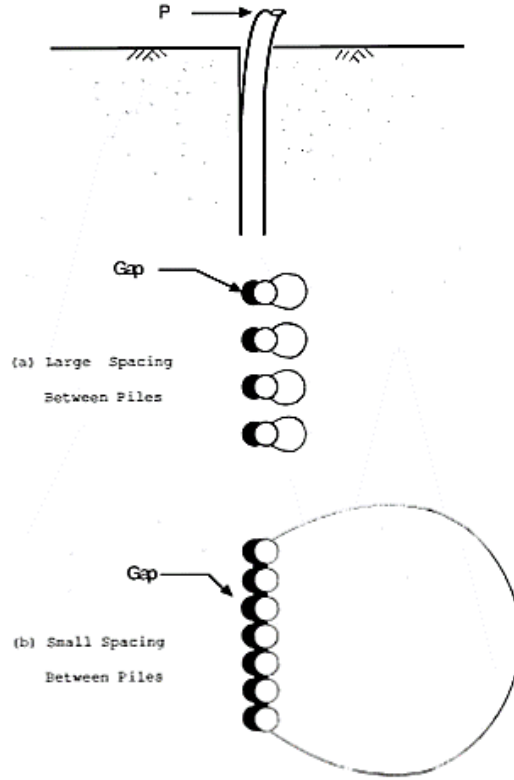


Figure 2.4: Soil deformation and gaps observed in experimental study (from Wang & Reese, 1986 with permission of Center for Transportation Research).

According to Wang & Reese (1986), if the adhesion between the pile and soil ( $a$ ) is assumed to be equal to 0,  $\theta$  is assumed to be  $45^\circ$ , and if the forces  $F_{3,ACE} + F_{4,BDF} > F_{1,BGIF} + F_{2,BGIF}$  (see Figure 2.3), then:

$$p_{ult} = 2c_u(b + S) + \gamma(b + S)H + c_uS \quad 2-3$$

where  $S$  is the clear spacing between piles. When  $S$  is equal to 0, then  $p_{ult}$  is equivalent to the Rankine passive earth pressure for a continuous wedge failure. According to Wang & Reese (1986), the critical spacing ( $S_{cr}$ ) between piles where the failure mechanism changes from the individual passive wedge failure to a group wedge failure can be calculated using:

$$S_{cr} = \frac{2.828c_uH}{\gamma H + 6c_u} \quad 2-4$$

Alternatively, Reese (1958) suggested that the ultimate soil lateral resistance is approximately equal to  $2c_u b$  at surface and increases with depth to a depth of approximately  $3b$  where the overburden pressure is great enough to force the flow-around method to become more critical. The pressure distribution with depth is illustrated in Figure 2.5. The distribution with depth is often simplified in practice and assumed to increase linearly between  $2c_u b$  at ground surface to  $9c_u b$  at a depth of  $3b$  to  $3.5b$  (Cornforth, 2012; Poulos, 1995).

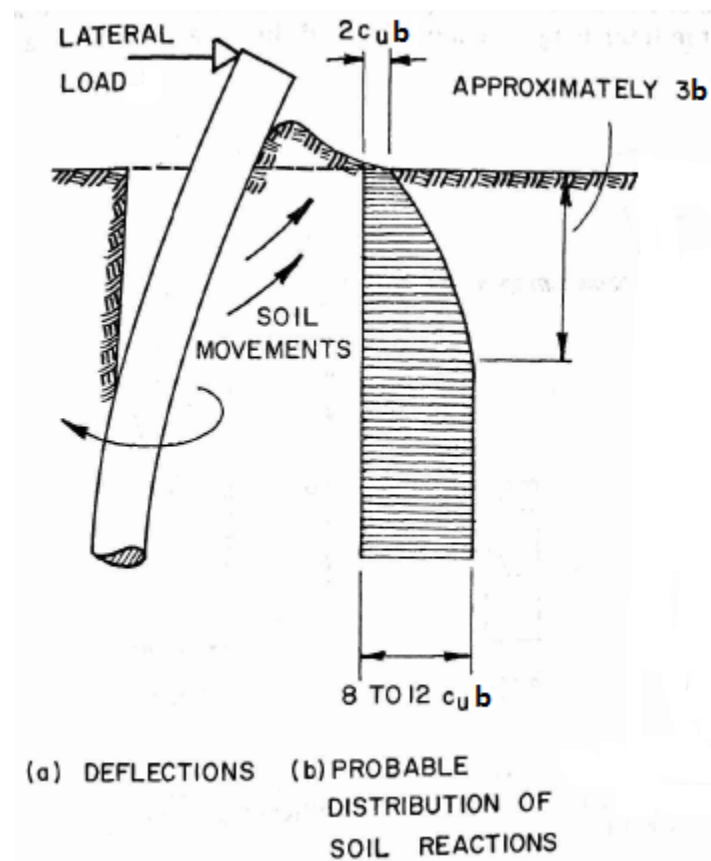


Figure 2.5: Distribution of ultimate lateral soil resistance with depth (Adapted from Broms, 1964 with permission from ASCE).

### 2.2.1.2 Cohesionless Soil

At soil failure for a laterally loaded pile in cohesionless soil, the soil in front of the soil moves upward in front of the piles and soil at the back of the pile will move downward to fill the void (Broms, 1964). Lateral displacement of a laterally loaded pile causes passive lateral resistance to develop on the front of the pile and active lateral resistance on the back of the pile. Due to the lateral stress distribution in the soil, the passive lateral resistance is greater than that of a

continuous wall and the active lateral resistance is less than that of a continuous wall. Broms (1964) assumed that the active earth pressure on the pile is small compared to the passive earth pressure and can be neglected. Broms (1964) assumed that the passive resistance developed by a single frictionless laterally loaded pile can be estimated to be three times the lateral passive earth pressure calculated by Rankine earth pressure theory. Broms (1964) calculated the ultimate lateral resistance of laterally loaded piles based on these assumptions and compared the results to test data. The results indicated that the proposed method consistently under predicts the ultimate lateral resistance by approximately 50% and is therefore conservative. The ultimate lateral soil resistance for cohesionless soil increases linearly with depth and can be conservatively calculated as:

$$p_{ult} = 3b\gamma'zK_p \quad 2-5$$

where  $\gamma'$  is the effective soil unit weight,  $z$  is the depth below ground surface, and  $K_p$  is the passive earth pressure calculated by Rankine earth pressure theory. Poulos (1995) has suggested that the factor of 3 in Equation 2-5 could range from 3 to 5.

Reese, Cox & Koop (1974) developed a soil model for calculating the ultimate resistance of a single pile near ground surface in sand as shown in Figure 2.6. The horizontal force acting on the pile can be calculated by summing the horizontal components of all forces, and the resulting force can be differentiated with respect to the depth. According to Reese et al. (1974),  $p_{ult}$  of a single pile can be calculated as:

$$p_{ult} = K_p\gamma bH + K_p\gamma(\tan\alpha)(\tan\beta)H^2 + K_o\gamma(\tan\beta)(\tan\phi - \tan\alpha)H^2 - K_a\gamma bH \quad 2-6$$

where  $\alpha$  and  $\beta$  are angles defining the geometry of the passive wedge as shown in Figure 2.6,  $H$  is the height of the soil wedge,  $\phi$  is the friction angle of the soil,  $K_o$  is the at-rest earth pressure coefficient, and  $K_a$  is the Rankine theory active earth pressure coefficient.

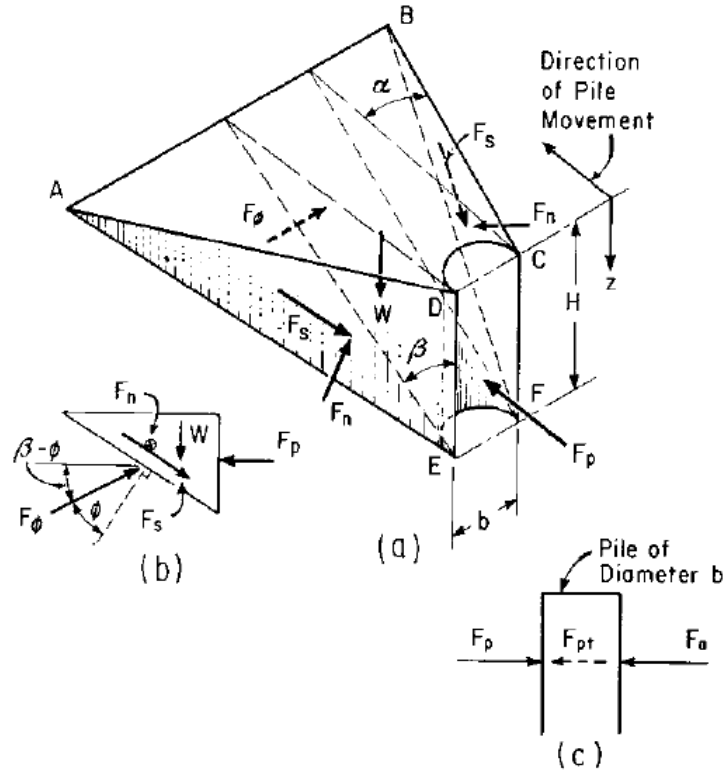


Figure 2.6: Assumed passive wedge-type failure in sand. (a) General wedge shape (b) Forces on wedge (c) Forces on pile (from Reese et al., 1974. Copyright 1974, Society of Petroleum Engineers Inc. Reproduced with permission of SPE. Further reproduction prohibited without permission).

Where a row of piles are spaced close to each other, the passive wedge developed in front of each pile will overlap and the lateral resistance per pile will decrease (Wang & Reese, 1986). This is illustrated in Figure 2.7. Wang & Reese (1986) suggested that  $p_{ult}$  for a pile in a group can be calculated by summing the horizontal components of all forces on the assumed passive wedge, and differentiating with respect to the depth:

$$\begin{aligned}
 p_{ult} = & K_p \gamma b (H - H_1) + K_p (\tan \alpha) (\tan \beta) \gamma (H^2 - H_1^2) & 2-7 \\
 & - K_p (\tan \alpha) (\tan \beta) \gamma S H_1 (\cot \alpha) (\cot \beta) + K_p \gamma H_1 (b + S) \\
 & + K_o \gamma \tan \beta (\tan \phi - \tan \alpha) (H - H_1)^2 + K_o \gamma S H_1 (\tan \phi \cot \alpha - 1) \\
 & - K_a \gamma b H
 \end{aligned}$$

where the height  $H_1$  is indicated in Figure 2.7 and is equal to  $H-(S/2)\cot\alpha\cot\beta$ . Wang and Reese (1986) calculated  $p_{ult}$  for an example study and varied the pile spacing from  $S/b = 0$  to  $S/b = 5$  as shown in Figure 2.8. The units in the example study are in imperial units. The ultimate lateral resistance when there is zero spacing between piles is approximately half that of a single pile and is equal to Rankine passive earth pressure minus Rankine active earth pressure.

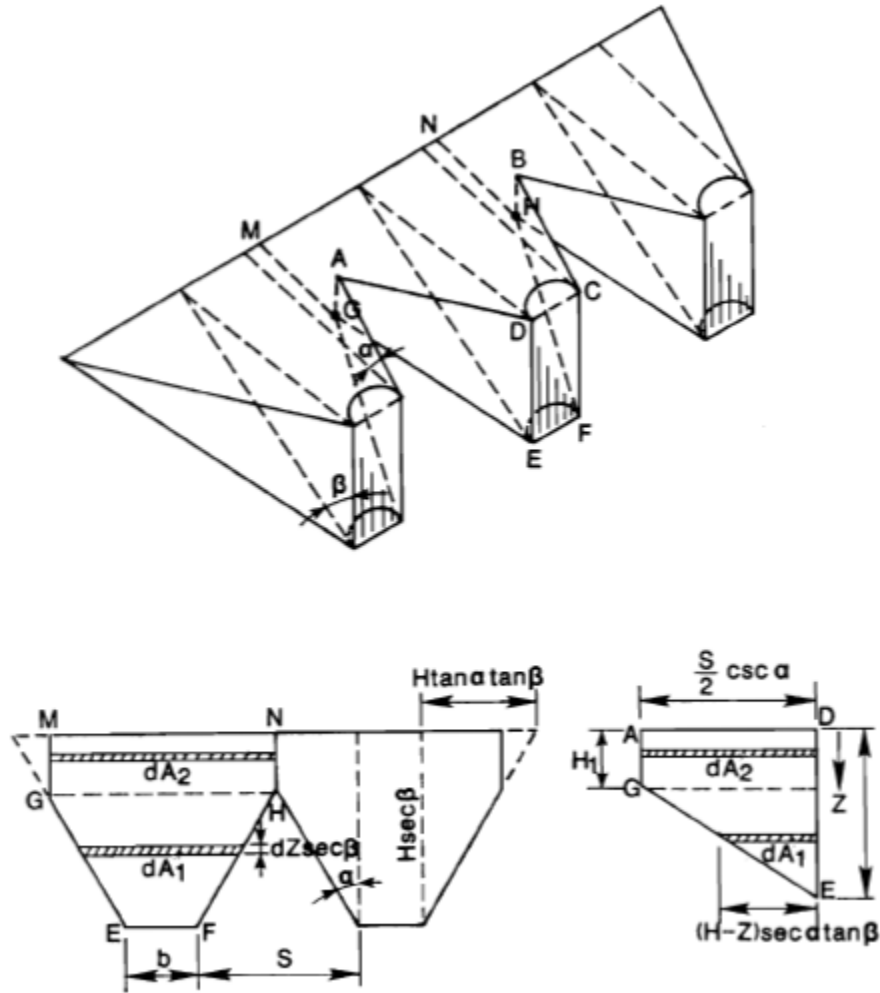


Figure 2.7: Assumed passive wedge for piles in a row. (a) General view (b) Plane view (c) Side view (Adapted from Wang & Reese, 1986 with permission of Center for Transportation Research).

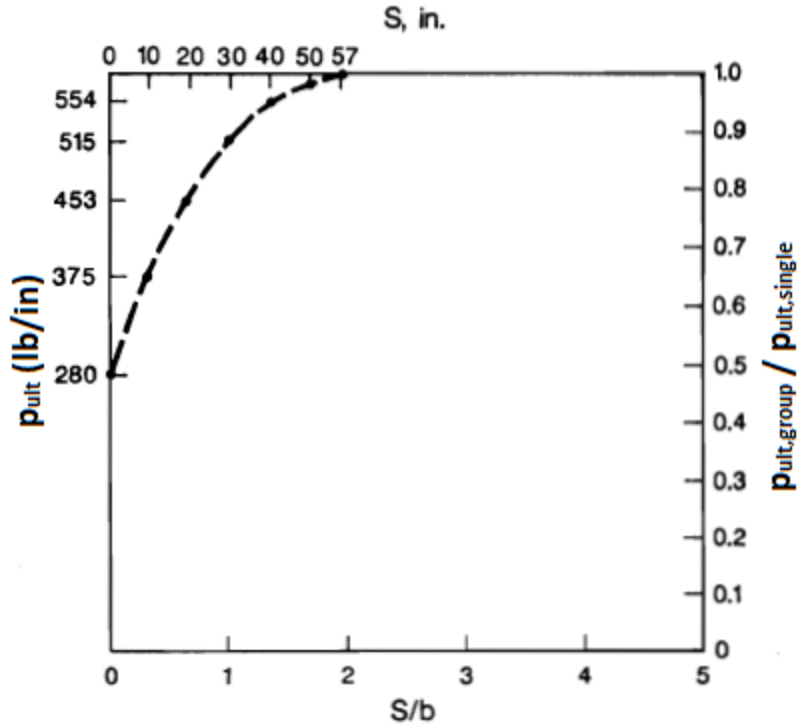


Figure 2.8: Example study of ultimate soil resistance in sand with pile diameter of 30 in. (Adapted from Wang & Reese, 1986 with permission of Center for Transportation Research).

## 2.2.2 Flow-Around Failure Mode

Various theoretical and experimental solutions for calculating  $p_{ult}$  for a potential flow-around failure at depth for laterally loaded piles are described for cohesive soils in Section 2.2.2.1 and for cohesionless soils in Section 2.2.2.2.

### 2.2.2.1 Cohesive Soil

Various authors (Reese, 1958; Broms, 1964; Broms, 1983; Randolph and Houlsby, 1984) have estimated the ultimate lateral resistance for failure of soil at depth where the soil flows from the front to the back of the pile. For purely cohesive soils, an empirical correlation is commonly used to estimate the ultimate lateral resistance using:

$$p_{ult} = N_c c_u b \quad 2-8$$

where  $p_{ult}$  is the ultimate lateral resistance of the soil per unit length on the pile,  $N_c$  is a lateral bearing capacity factor,  $c_u$  is the undrained shear strength, and  $b$  is the pile diameter. A wide

range of values for  $N_c$  have been proposed by Reese (1958), Broms (1964), Broms (1983), and Randolph and Houlsby (1984) as described below in this section. A value of  $N_c$  equal to 9 is widely used in practice however (Broms, 1964; Vessely, Yamasaki & Strom, 2007; Cornforth, 2005).

A block-soil model was proposed by Reese (1958) which is illustrated in Figure 2.9. Square blocks with side lengths of  $b$  surround a circular pile of diameter  $b$ . Lateral displacement of the pile is assumed to cause blocks 1, 2, 4, and 5 to fail in shear and block 3 develops resistance by sliding. The stress conditions are shown in Figure 2.9b and the free body diagram shown in Figure 2.9c can be examined to calculate a lateral bearing capacity factor  $N_c$  equal to 11. The side friction on the pile is assumed to be half of the undrained shear strength in this case. If side friction is not considered however,  $N_c$  is equal to 10.

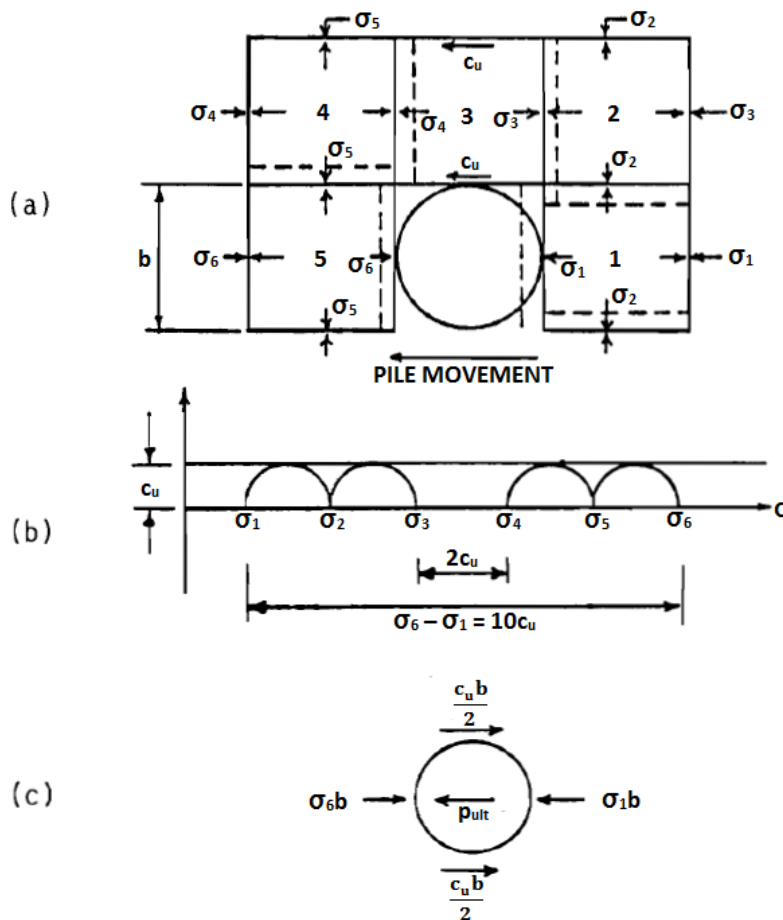


Figure 2.9: Assumed lateral flow-around type of failure for clay using block-soil model. (a) Section through pile (b) Mohr-Coulomb diagram (c) Forces acting on pile (Adapted from Wang & Reese, 1986 with permission of Center for Transportation Research).

Broms (1964) calculated the ultimate lateral resistance for the plane-strain conditions using the slip line theory. Depending on the pile geometry and whether a smooth or rough surface was assumed,  $N_c$  ranged from 8.28 to 12.56 as shown in Figure 2.10.

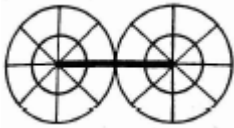
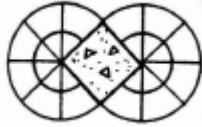
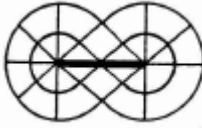
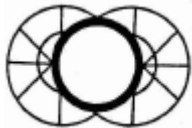
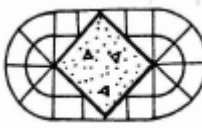
Slip Field Pattern	Surface	$N_c$
	Rough	12.56
	Rough	11.42
	Smooth	11.42
	Smooth	9.14
	Smooth	8.28

Figure 2.10: Ultimate lateral soil resistance from slip-line theory (Adapted from Broms, 1964 with permission from ASCE).

Wang and Reese (1986) stated that to avoid plastic interference between adjacent piles, the clear spacing between piles should be greater than  $1.414b$ . This is based on the assumption that the piles are square for simplicity and with a consistent slip-line field as assumed by Broms (1964). This is illustrated in Figure 2.11.

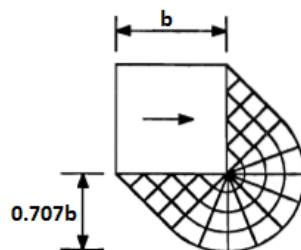


Figure 2.11: Slip-line field for a single square pile (Adapted from Wang & Reese, 1986 with permission of Center for Transportation Research).



Broms (1983) suggested that the ultimate lateral resistance increases as pile spacing decreases for the plane-strain condition. To simplify calculations, square piles were assumed as shown in Figure 2.12.  $N_c$  was assumed to consist of an end bearing component equal to 5.14 and friction along the sides of the piles was assumed to increase the lateral pressure acting on the pile. The ultimate lateral resistance can then be calculated as:

$$p_{ult} = bc_u \left( 5.14 + \frac{2aS_{c-c}}{S} \right) \tag{2-9}$$

where  $a$  is an adhesion factor,  $S_{c-c}$  is the centre-to-centre spacing of the piles, and  $S$  is the clear spacing between piles. The adhesion factor  $a$  normally varies between 0.5 for hard stiff clay to 1.0 for soft clay (Broms, 1983). Based on this equation, the estimated ultimate lateral resistance will approach infinity as the clear spacing between piles approaches zero.

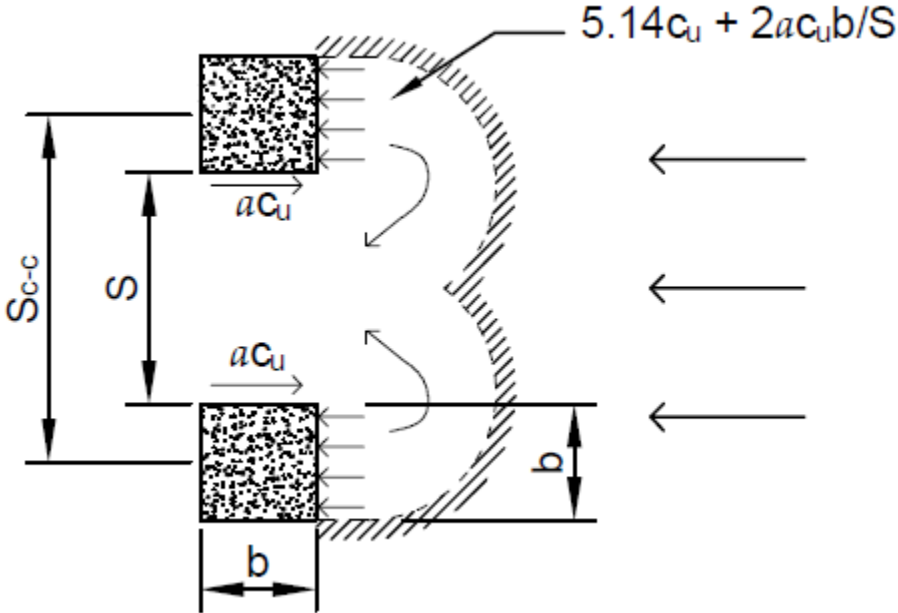


Figure 2.12: Lateral resistance of a pile group in clay (After Broms, 1983).

Broms (1983) performed laboratory testing for the plane-strain conditions and for a range of pile spacing with an interval ratio ( $S/S_{c-c}$ ) from approximately 0.2 to 0.9, the results of which are shown in Figure 2.13. The experimental results were very close to the calculated  $p_{ult}$  from Equation 2-9 assuming the adhesion factor was equal to 1.0 for the soft clay.

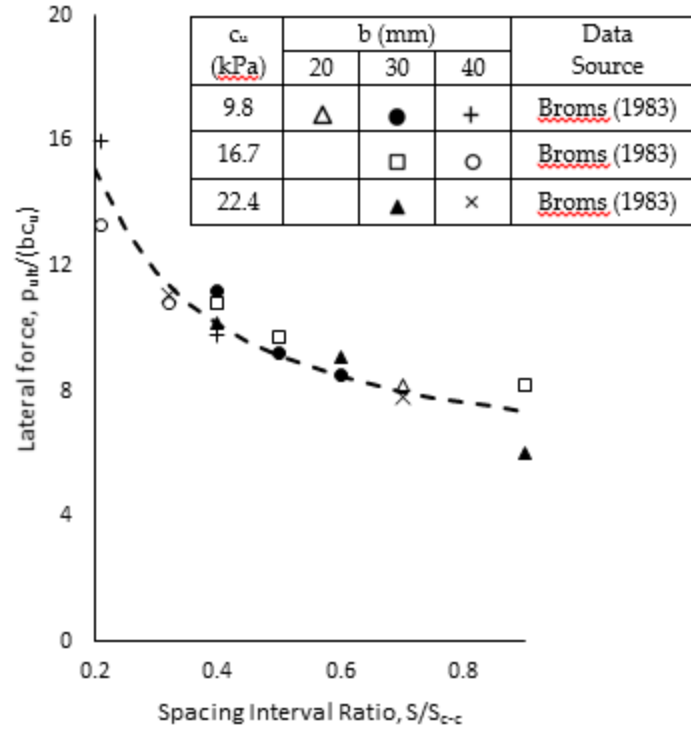


Figure 2.13: Comparison of test results and calculated ultimate lateral soil resistance (After Broms, 1983).

An exact analytical solution using the upper bound and lower bound theorems of limit analysis for the flow around a circular pile was presented by Randolph and Houlsby (1984). Friction along the pile-soil interface ( $f_s$ ) that is less than or equal to the shear strength of the soil is considered in this analysis. Randolph and Houlsby (1984) suggested that the ultimate lateral resistance per unit length of the pile is equal to:

$$p_{ult} = c_u b \left[ \pi + 2\omega + 4\cos\left(\frac{\pi}{4} - \frac{\omega}{4}\right) \left( 1.414 + \sin\left(\frac{\pi}{4} - \frac{\omega}{4}\right) \right) \right] \quad 2-10$$

where  $\omega$  is equal to  $\sin^{-1}(f_s/c_u)$ . The variation of  $N_c$  versus  $f_s/c_u$  is shown in Figure 2.14 and  $N_c$  ranges from 9.14 for a smooth pile to 11.94 for a rough pile. The slip line fields for soil flowing around a circular pile with and without friction between the soil-pile interface is shown in Figure 2.15.

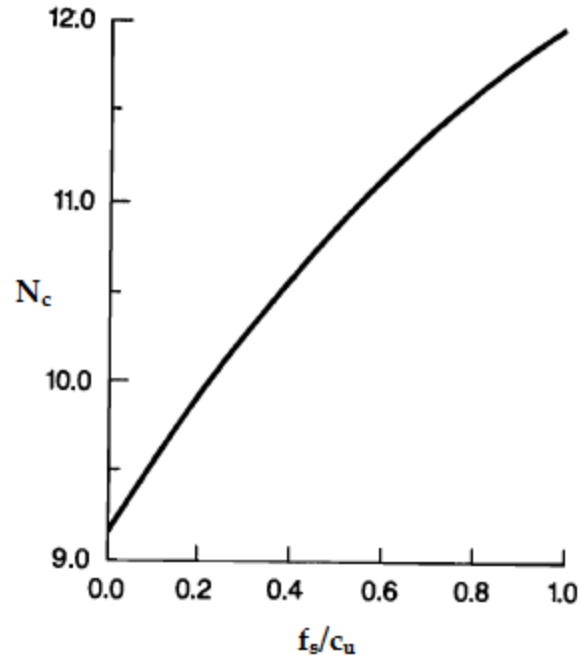


Figure 2.14: Variation of  $N_c$  with friction ratio (Adapted. Republished with permission of ICE Publishing, from Randolph & Houlsby, 1984; permission conveyed through Copyright Clearance Centre, Inc.).

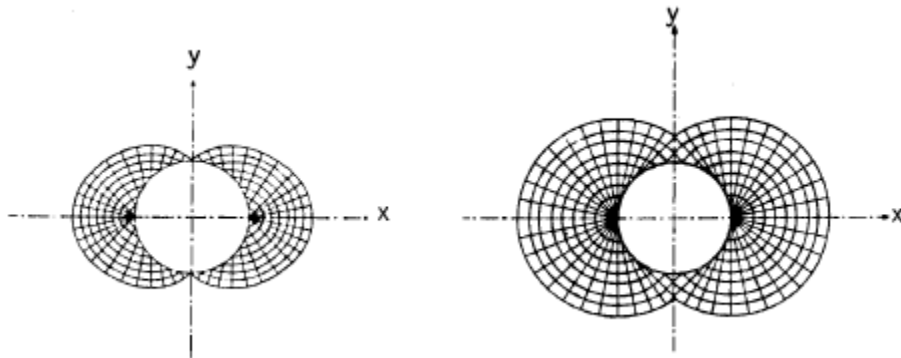


Figure 2.15: The ultimate soil resistance on a circular pile for flow around failure based on the slip-line theory (Republished with permission of ICE Publishing, from Randolph & Houlsby, 1984; permission conveyed through Copyright Clearance Centre, Inc.).

The ultimate lateral resistance for soil flowing around a square or circular pile has been studied by various authors beyond the ones mentioned. Despite the variation in assumptions made,  $N_c$  typically ranges between 8 and 12 for the various calculations made by various authors.

Since most case studies have been performed with circular piles, Reese & Van Impe (2011) suggested the following expression to calculate an equivalent pile diameter ( $b_{eq}$ ) to calculate  $p_{ult}$  for a rectangular pile. Reese & Van Impe (2011) suggested that  $b_{eq}$  can be calculated as:

$$b_{eq} = B_1 \left[ \frac{p_{ult,c} + 2 \left( B_2 - \frac{B_1}{2} \right) ac_u}{p_{ult,c}} \right] \quad 2-11$$

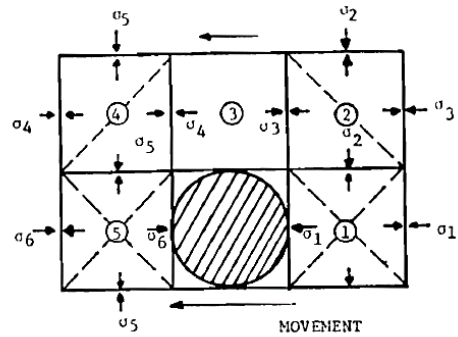
where  $B_1$  is the pile width perpendicular to the applied load,  $B_2$  is the length parallel to the load, and  $p_{ult,c}$  is equal to the ultimate resistance of a circular section with a diameter  $b$  equal to  $B_1$ .

### 2.2.2.2 Cohesionless Soil

A flow-around failure mode will occur where soil moves from the front to the back of the pile at depth, however this depth is relatively large for cohesionless soil (Broms, 1964). Approximate calculations performed by Broms (1964) indicate that a critical depth of approximately  $50b$  is required for the flow-around failure mode to occur based on a friction angle of  $30^\circ$ .

A block-soil model was proposed by Wang & Reese (1986) to approximate the ultimate lateral soil capacity for sand at depth which is illustrated in Figure 2.16. Square blocks with side lengths of  $b$  surround a circular pile of diameter  $b$ . Lateral pile displacement is assumed to cause blocks 1,2,4, and 5 to fail in shear and block 3 develops resistance by sliding. The stress conditions are shown in Figure 2.16b. The stress at the back of the pile ( $\sigma_1$ ) is assumed to be greater than the active earth pressure so that the soil does not fail by slumping. The ultimate soil resistance for horizontal flow around the pile given by Wang & Reese (1986) as:

$$p_{ult} = K_a \gamma b z (\tan^8 \beta - 1) + K_o \gamma b z (\tan \phi) (\tan^4 \beta) \quad 2-12$$



(a)

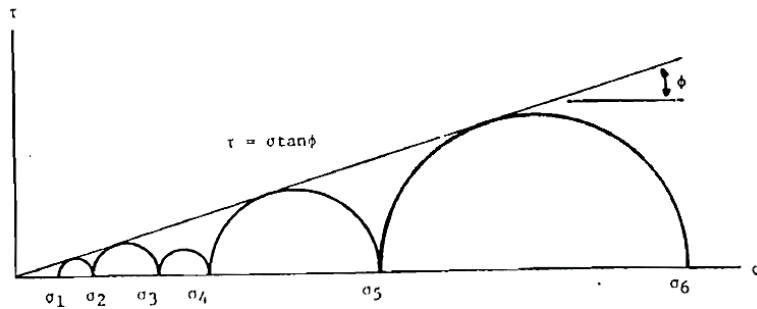


Figure 2.16: Assumed lateral flow-around type of failure for sand using block-soil model. (a) Section through pile (b) Mohr-Coulomb diagram (From Wang & Reese, 1986 with permission of Center for Transportation Research).

Similar to the model for a row of piles in cohesive soils, Broms (1983) suggested that the ultimate lateral resistance increases as pile spacing decreases for the plane-strain condition. To simplify calculations, square piles were assumed as shown in Figure 2.17. The ultimate lateral resistance ( $p_{ult}$ ) can then be calculated as:

$$p_{ult} = P_{h2}' N_q \quad 2-13$$

where  $P_{h2}'$  is the effective confining pressure and  $N_q$  is the bearing capacity factor which is a function of the friction angle ( $\phi$ ). The confining pressure  $P_{h2}'$  is affected by the friction on the sides of the piles which depends on the effective normal pressure  $K_p P_h'$  and the friction resistance along the soil-pile interface ( $\phi_a$ ). Integrating the friction force along the side of the pile provides:

$$P_{h2}' = K_0 \gamma z \exp(2bK_p \tan \phi_a / S) \text{ and;} \quad 2-14$$

$$p_{ult} = K_0 \gamma z \exp(2bK_p \tan \phi_a / S) N_q \quad 2-15$$

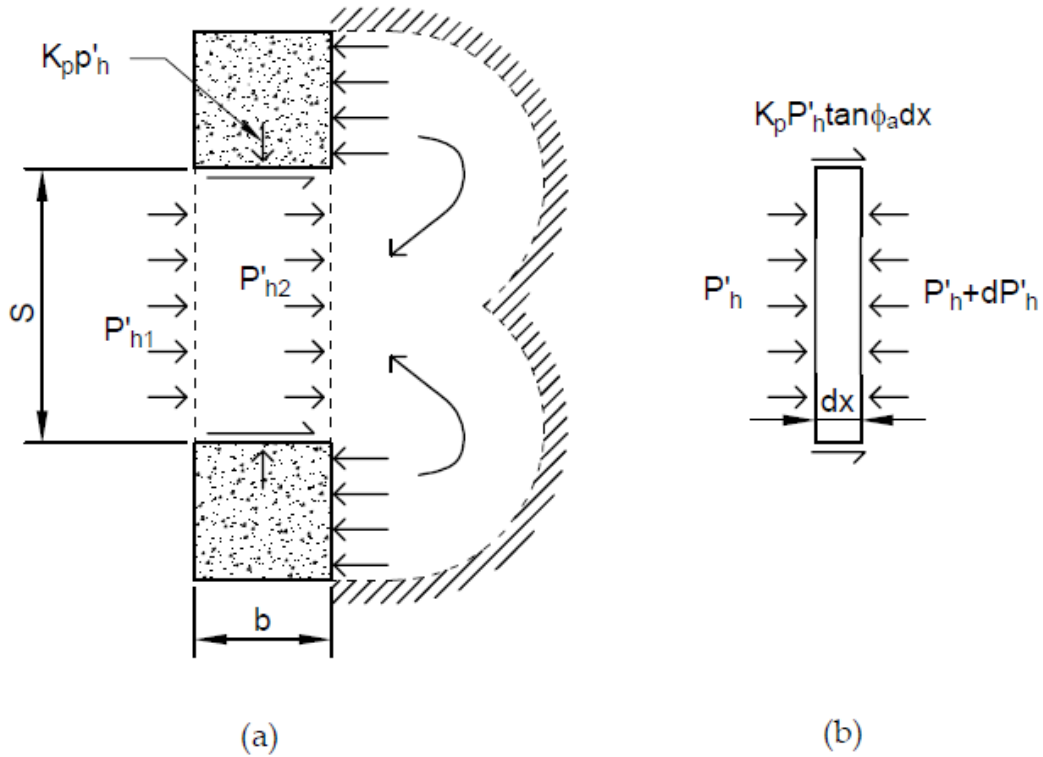


Figure 2.17: Lateral resistance of a pile group in sand (After from Broms, 1983).

Based on this equation, the estimated ultimate lateral resistance will approach infinity as the clear spacing between piles approaches zero. Broms (1983) performed laboratory testing for the plane-strain conditions and for a range of pile spacing with an interval ratio ( $S/S_{c-c}$ ) from approximately 0.73 to 0.93, the results of which are shown in Figure 2.18. The experimental results were very close to the calculated value of  $p_{ult}$ . The coefficient of at rest lateral earth pressure  $K_0$  was assumed to be 0.5 and  $\phi_a$  was assumed to be  $25^\circ$ .

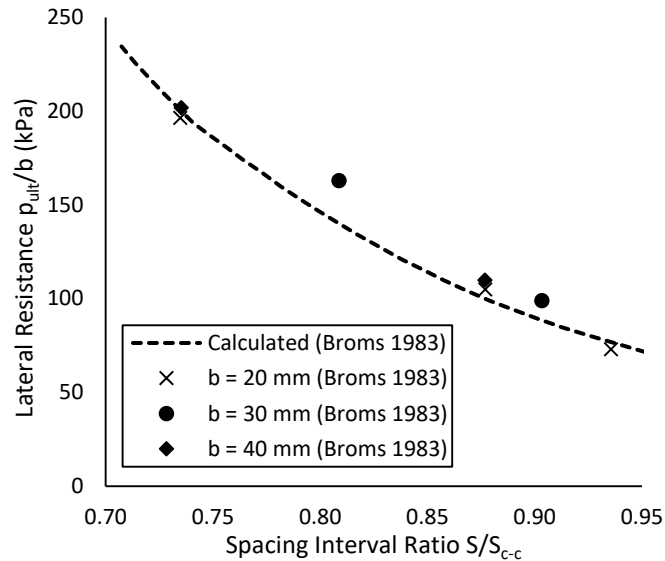


Figure 2.18: Comparison of test results and calculated ultimate lateral soil resistance of sand (After Broms, 1983).

### 2.2.3 Spacing Effects and Reduction Factor

Various authors have conducted laboratory testing to study the spacing effects for a row of piles and how the magnitude of  $p_{ult}$  is effected by changing the distance of the spacing between adjacent piles. Experimental laboratory testing was completed by Prakash (1962), Cox, Dixon & Murphy (1984), Wang & Reese (1986), and Lieng (1988) to study the spacing effects of a row of piles. The data from these tests was compiled by Reese et al. (1992) and the reduction factor ( $P$ ) is plotted vs the pile spacing in terms of centre-to-centre spacing over pile diameter ( $S_{c-c}/b$ ) as shown in Figure 2.19. The reduction factor ( $P$ ) is defined by Reese et al. (1992) as the ratio of the averaged capacity of individual piles in a group to that of a single isolated pile. The reduction in pile capacity is negligible when the centre-to-centre spacing between piles is approximately  $3b$  to  $4b$ . Wang, Vasquez & Xu (2013) suggest that if there is no spacing between piles, then the reduction factor should be between 0.5 (lower bound) to 0.7 (upper bound). Reese and Van Impe (2011) reviewed additional experimental data for side-by-side piles and recommended calculating the reduction factor as:

$$P = 0.64 \left( \frac{S_{c-c}}{b} \right)^{0.34} \text{ for } 1 \leq \left( \frac{S_{c-c}}{b} \right) < 3.75$$

for  $S_{c-c}/b$  less than 3.75. Based on this calculation,  $P$  is equal to 0.64 for a contiguous row of piles and  $P$  should be assumed equal to 1 for  $S_{c-c}$  greater than 3.75.

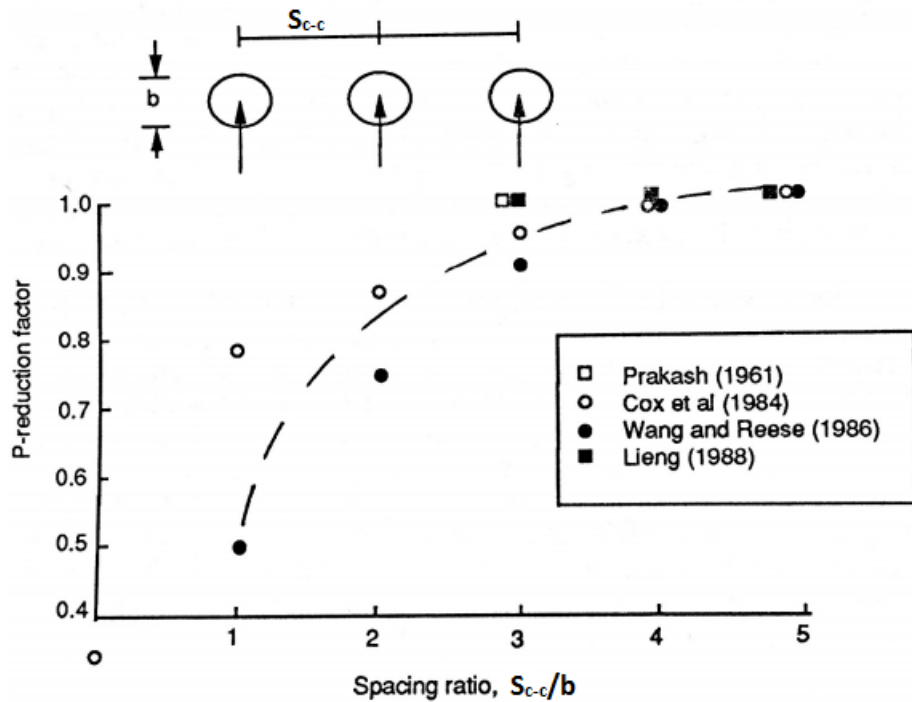


Figure 2.19: Reduction factors for closely space piles (Adapted. Republished with permission of ASCE, from Reese et al., 1992; permission conveyed through Copyright Clearance Centre Inc.).

The experimental laboratory tests that comprise the results shown Figure 2.19 are discussed in further detail in Section 2.2.3.1 for testing on cohesive soil and in Section 2.2.3.2 for testing on cohesionless soil.

### 2.2.3.1 Laboratory Testing on Cohesive Soil

Experimental laboratory testing was completed by Cox et al. (1984) on very soft clay where a lateral load was applied to a pile or group of piles at slow displacement rates approaching static conditions. The piles were 25.4 mm in diameter and were tested as an individual pile and as groups of 3 or 5 piles with clear spacing of 0.5, 1, 2, and 3 pile diameters for side-by-side testing. The clay in the testing was very soft with an undrained shear strength of approximately 2 kPa.



The results of the experimental data for pile groups arranged side-by-side are shown in Figure 2.20. Cox et al. (1984) expressed the results with an average group efficiency as a percentage, where 100% corresponds to the reduction factor ( $P$ ) of 1.

It appears as though the data point from Cox et al. (1984) in Figure 2.19 by Reese et al. (1992) for centre-to-centre spacing of 1.0 should actually be plotted at a spacing of 1.5 to be consistent with the results in Figure 2.20.

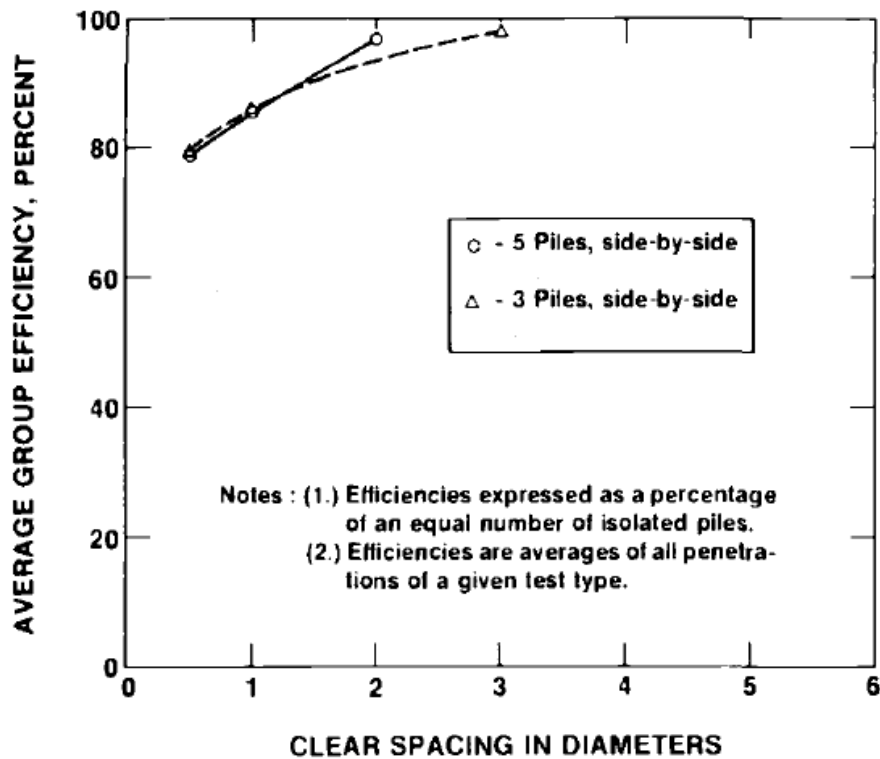


Figure 2.20: Efficiency of pile groups in clay (Adapted. Republished with permission from Cox et al., 1984, copyright ASTM International, 100 Barr Harbor Drive, West Conshohocken, PA 19428).

Wang and Reese (1986) completed laboratory testing on soft clay with piles that were similarly 25.4 mm in diameter. The clay had an average undrained shear strength of 5.5 kPa at the top of the container and 7.6 kPa at the bottom of the container. Results from the laboratory testing are shown in Figure 2.21.

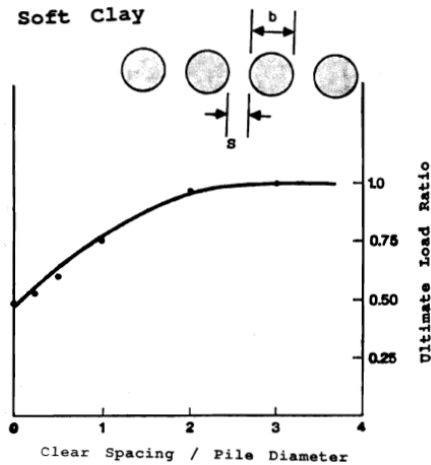


Figure 2.21: Ultimate load ratio (reduction factor) for soft clay (From Wang & Reese, 1986 with permission of Center for Transportation Research).

### 2.2.3.2 Laboratory Testing on Cohesionless Soil

Prakash (1962) performed laboratory testing on laterally loaded piles of 12.7 mm in diameter piles and embedded in sand. Pile groups of 4 piles and 9 piles were tested and a single pile was tested for comparison. Prakash (1962) concluded that the pile group has less resistance than that of the sum of the individual piles when the centre-to-centre spacing is less than  $3b$ .

Wang and Reese (1986) completed laboratory testing on loose sand and dense sand with piles that were 25.4 mm in diameter. Results from the laboratory testing are shown in Figure 2.22 and Figure 2.23 for loose sand and dense sand, respectively. Similar trends are observed regardless of soil type. The reduction factor is approximately 0.5 where there is zero spacing between piles and there is no reduction factor when centre-to-centre spacing is greater than  $3b$  or  $4b$ .

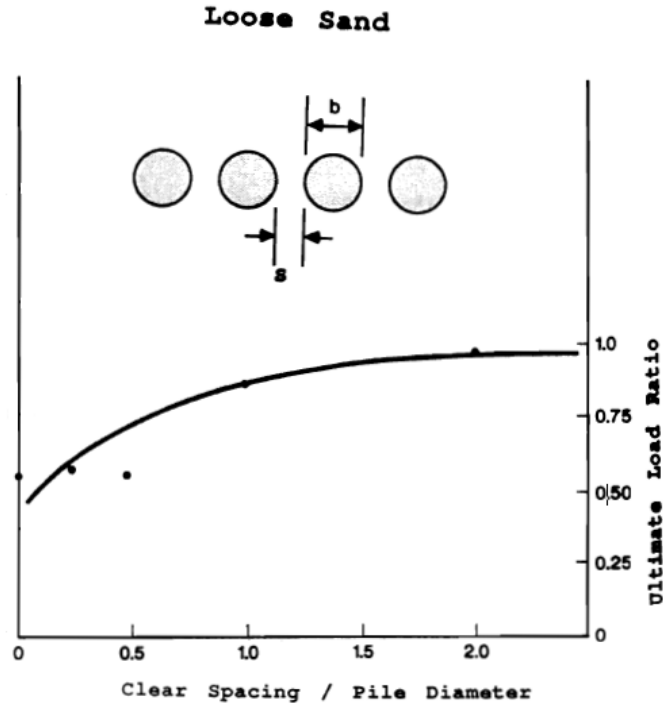


Figure 2.22: Ultimate load ratio (reduction factor) for loose sand (From Wang & Reese, 1986 with permission of Center for Transportation Research).

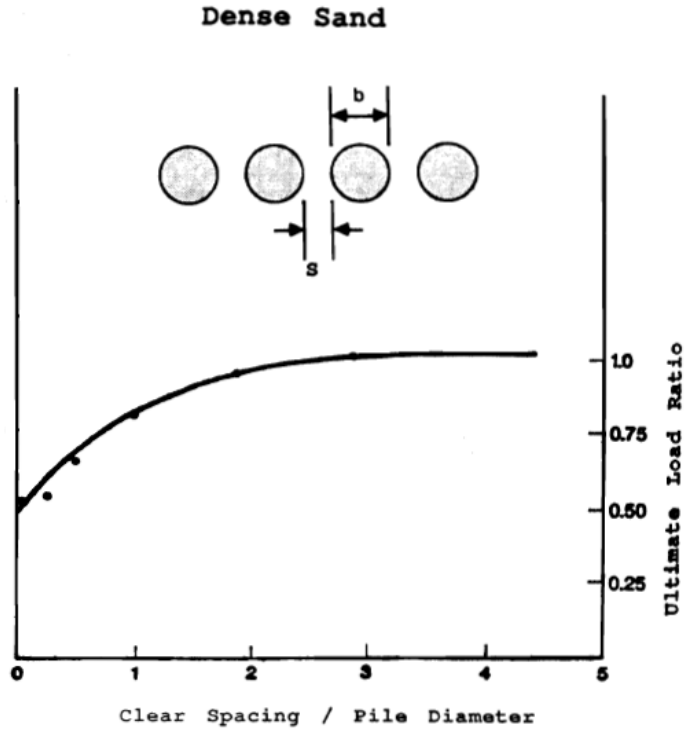


Figure 2.23: Ultimate load ratio (reduction factor) for dense sand (From Wang & Reese, 1986 with permission of Center for Transportation Research).

Lieng (1988) performed laboratory testing on laterally loaded piles of 150 mm diameter and 2.6 m length embedded in sand. Pile groups of two piles were tested and compared to results of testing a single pile. Lieng (1988) found no sign of the ultimate load being disturbed by the neighbouring pile for centre to centre spacing down to  $3b$ .

After reviewing the source data for Figure 2.19, a modification is proposed where the data point from Cox et al. (1984) for a centre-to-centre spacing of  $1b$  should be moved to a spacing of  $1.5b$  to be consistent with the results shown in Figure 2.20. The modified plot of reduction factor vs pile spacing is shown in Figure 2.24. By correcting the data, there is less scatter in the results when comparing the various data sources.

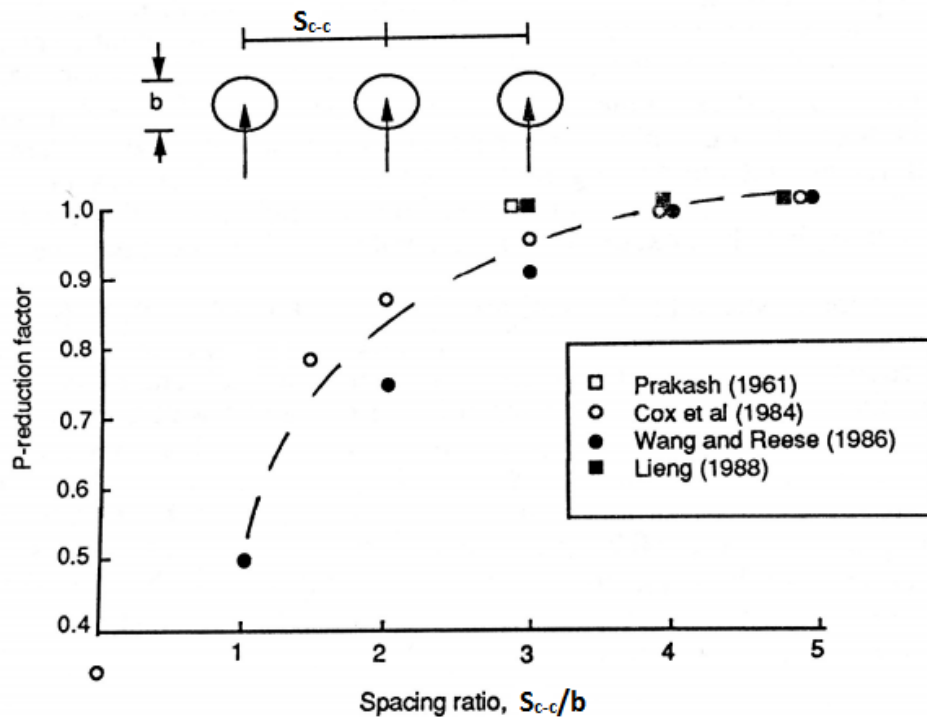


Figure 2.24: Modified reduction factor vs spacing ratio (Adapted. Republished with permission of ASCE, from Reese et al., 1992; permission conveyed through Copyright Clearance Centre Inc.).

### 2.3 Design Methods for Slope Stabilization with Piles

Lateral loads on landslide stabilizing piles induce bending moments and shear forces in the pile which can lead to failure of the pile. Various authors have developed methodologies for analysis and design of stabilizing piles using a de-coupled approach where a separate slope stability

analysis and laterally loaded pile analysis are performed. Three basic steps were described by Viggiani (1981) as general design steps which include: (1) evaluating the total shear force needed to increase the factor of safety of the slope to a desired value; (2) evaluating the maximum shear force that each pile can provide as resistance against sliding of the unstable soil; and (3) selecting the most suitable location on the slope as well as the number and type of piles to be installed.

### 2.3.1 Evaluating Required Shear Force to Stabilize Slope

The shear force required to stabilize a landslide can be estimated based on a two-dimensional limit equilibrium slope stability analysis. An initial analysis can be performed to determine the current estimated factor of safety. For an active landslide, the calculated factor of safety should be near unity. The factor of safety ( $FS$ ) can be defined as:

$$FS = \frac{\Sigma R}{\Sigma F_D} \quad 2-17$$

where  $\Sigma R$  is the sum of resisting forces along the critical surface and  $\Sigma F_D$  is the sum of disturbing forces along the critical surface. Poulos (1995) described an expression to determine the additional resistance ( $\Delta R$ ) that must be provided by the piles to achieve a desired target factor of safety ( $FS_T$ ). The target factor of safety can be defined as:

$$FS_T = \frac{\Sigma R + \Delta R}{\Sigma F_D} \quad 2-18$$

Based on equations 2-17 and 2-18, the additional resistance required to achieve the target factor of safety can be calculated from the following equation where  $\Delta R$  represents the stabilizing force per unit width of the soil that must be provided by the soil:

$$\Delta R = \Sigma F_D (FS_T - FS) \quad 2-19$$

### 2.3.2 Evaluating Maximum Shear Force from Stabilizing Piles

Two methodologies for estimating the maximum shear force that can be achieved from installing piles to resist landslide loading include Viggiani's (1981) method and the load-transfer method using  $p$ - $y$  curves.

#### 2.3.2.1 Viggiani's (1981) Method

Viggiani (1981) developed a method to evaluate the maximum shear force that an individual pile can provide in resisting the landslide. The problem is idealized as shown in Figure 2.25 where a constant displacement occurs above a slide plane which separates two soil layers. Both soil layers are assumed to be saturated clays where the sliding soil mass has an undrained shear strength of  $c_{u1}$  and a depth of  $l_1$ . The stable soil mass has an undrained shear strength of  $c_{u2}$  and the length between the shear plane and bottom of the pile is  $l_2$ . Viggiani (1981) considers that the lateral bearing capacity factor may differ above and below the slide plane and has introduced  $N_{c1}$  for the sliding soil mass and  $N_{c2}$  for the stable soil.

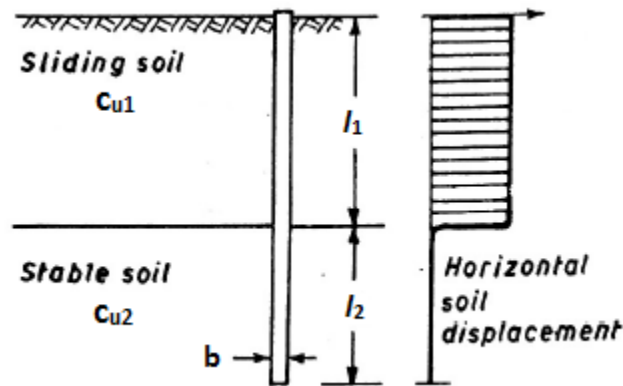


Figure 2.25: Simplified scheme of problem (Adapted from Viggiani, 1981 with permission of Taylor and Francis).

Viggiani (1981) described three possible failures models for short piles, where the pile is rigid and the yield moment of the pile is greater than the bending moments acting on it. The three failure modes are shown in Figure 2.26 and are labelled mode A through C. In failure mode A, the piles translate laterally with the moving soil and the soil-pile contact pressure reaches the yield value only in the soil in the stable zone below the slide plane. In failure mode B, the piles rotates and the soil fails along the entire length of the pile. In failure mode C, the piles remains in place and

the soil flows around the pile above the slide plane. The soil reaction is shown in Figure 2.26 where the soil is assumed to fail when the soil-pile contact pressure exceeds  $N_c c_u b$  for the failure mechanism of soil flowing around the pile. The possible wedge failure mechanism near ground surface was not considered and  $N_c c_u b$  was considered to be constant with depth for each respective layer. Viggiani (1981) suggested that the lateral bearing capacity factor for the sliding soil ( $N_{c1}$ ) was likely to be equal to 4 and the lateral bearing capacity factor for the stable soil ( $N_{c2}$ ) was likely to be equal to 8. The lower value  $N_c$  for the sliding soil mass should be due to the proximity to the ground surface where a wedge-type failure is expected to occur as opposed to the flow-around failure mechanism (Conte & Troncone, 2004).

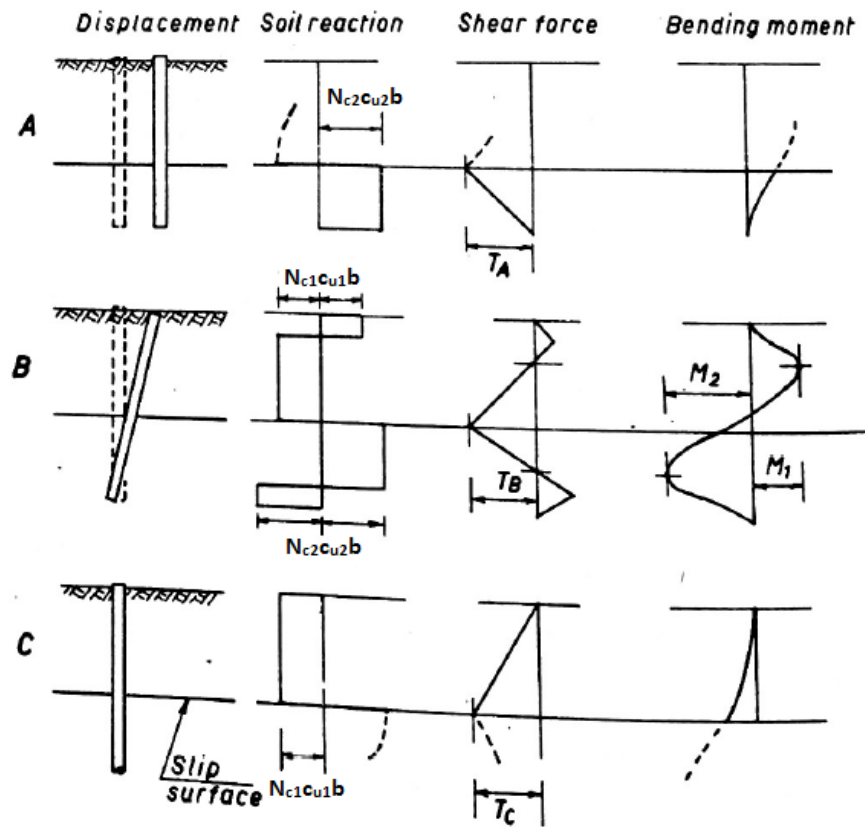


Figure 2.26: Failure modes for short piles (Adapted from Viggiani, 1981 with permission of Taylor and Francis).

Viggiani (1981) derived formulas to calculate the shear force at the slip surface ( $T$ ) for each of the three short pile failure modes and the developed bending moments for failure mode B as shown below:

Mode A:

$$T_A = N_{c1}c_{u1}bl_1 \left[ \frac{\lambda}{\chi} \right] \quad 2-20$$

Mode B:

$$T_B = N_{c1}c_{u1}bl_1 \left[ \sqrt{\left( \frac{1+\lambda}{1+\chi} \right)^2 + \frac{\lambda^2 + \chi}{\chi(1+\chi)}} - \frac{1+\lambda}{1+\chi} \right] \quad 2-21$$

$$M_1 = N_{c1}c_{u1}bl_1^2 \left[ \frac{1}{4} \left( 1 - \frac{T_B}{N_{c1}c_{u1}bl_1} \right)^2 \right] \quad 2-22$$

$$M_2 = N_{c1}c_{u1}bl_1^2 \left[ \frac{1}{4\chi} \left( \lambda - \frac{T_B}{N_{c1}c_{u1}bl_1} \right)^2 \right] \quad 2-23$$

Mode C:

$$T_c = N_{c1}c_{u1}bl_1 \quad 2-24$$

where  $T_A$ ,  $T_B$ , and  $T_c$  are the shear force at the slip plane for failure modes A, B, and C, respectively.  $M_1$  and  $M_2$  are the maximum bending moments developed in failure mode B below and above the slide plane, respectively.  $\lambda$  is the ratio of  $l_2/l_1$  and  $\chi$  is the ratio of  $N_{c1}c_{u1}/N_{c2}c_{u2}$ .

Viggiani (1981) also described three possible failures models for long piles, where the bending moments acting on the pile are greater than the yield moment of the pile and one or two hinges develop. The three failure modes are shown in Figure 2.27 and are labelled mode B1, BY and B2. In failure mode B1, a plastic hinge forms in the pile in the sliding soil mass. In failure mode BY, plastic hinges form in the pile in both the sliding soil and stable soil. In failure mode B2, a plastic hinge forms in the pile in the stable soil mass. The soil reaction is shown in Figure 2.27 where the soil is assumed to fail when the soil-pile contact pressure exceeds  $N_c c_u b$  for the failure mechanism



of soil flowing around the pile. The possible wedge failure mechanism near ground surface was similarly not considered.

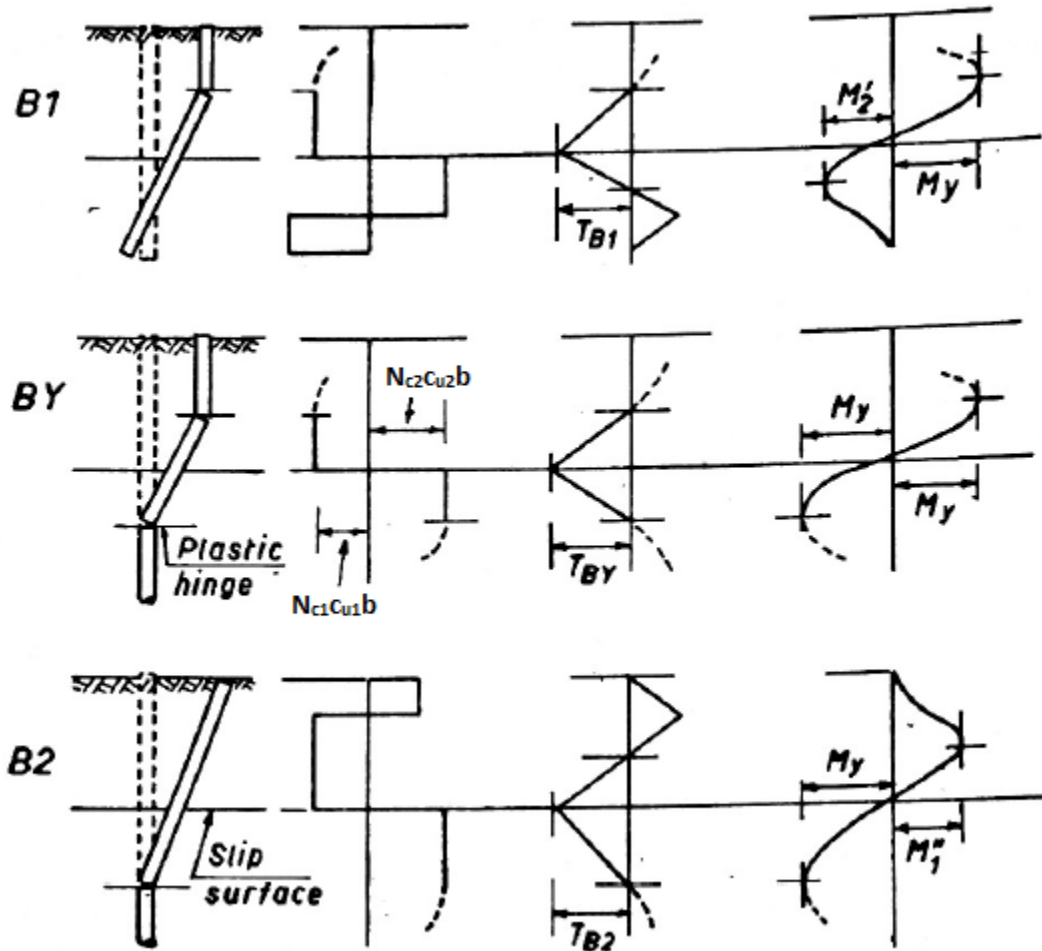


Figure 2.27: Failure modes for long piles (Adapted from Viggiani, 1981 with permission of Taylor and Francis).

Viggiani (1981) derived formulas to calculate the shear force at the slip surface ( $T$ ) for each of the three long pile failure modes and the bending moments for failure modes B1 and B2 as shown below:

Mode B1:

$$T_{B1} = N_{c1}c_{u1}bl_1 \left[ \frac{\lambda}{\chi + 2} \left( \sqrt{\frac{2\chi + 2}{\lambda} + \frac{\chi + 2}{\lambda^2} \frac{4M_y}{N_{c1}c_{u1}bl_1^2}} - 1 \right) \right] \quad 2-25$$

$$M'_2 = N_{c1}c_{u1}bl_1^2 \left[ \frac{1}{4\chi} \left( \lambda - \chi \frac{T_{B1}}{N_{c1}c_{u1}bl_1} \right)^2 \right] \quad 2-26$$

Mode BY:

$$T_{BY} = N_{c1}c_{u1}bl_1 \left[ 2 \sqrt{\frac{1}{1 + \chi} \frac{M_y}{N_{c1}c_{u1}bl_1^2}} \right] \quad 2-27$$

Mode B2:

$$T_{B2} = N_{c1}c_{u1}bl_1 \left[ \frac{1}{1 + 2\chi} \left( \sqrt{1 + (1 + 2\chi) \left( 1 + \frac{4M_y}{N_{c1}c_{u1}bl_1^2} \right)} - 1 \right) \right] \quad 2-28$$

$$M''_1 = N_{c1}c_{u1}bl_1^2 \left[ \frac{1}{4} \left( 1 - \frac{T_{B2}}{N_{c1}c_{u1}bl_1} \right)^2 \right] \quad 2-29$$

where  $T_{B1}$ ,  $T_{BY}$ , and  $T_{B2}$  are the shear force at the slip plane for failure modes B1, BY, and B2, respectively.  $M''_1$  and  $M'_2$  are the bending moments developed and illustrated in Figure 2.27.  $M_y$  is the yield moment of the pile.

Poulos (1995) described some limitations regarding the solutions provided by Viggiani (1981) including: (i) they only provide solutions for purely cohesive soils and the shear strength is constant with depth for each layer; (ii) they only apply to the ultimate state and do not indicate the development of pile resistance with soil displacement; and (iii) they are constrained to a simplified assumption that the soil displacement is constant above the slide plane.

### 2.3.2.2 Load Transfer Method with $p$ - $y$ Curves

Numerical analyses can be utilized to determine the deflection, shear force, and bending moments in the pile and the soil reaction for a laterally loaded pile (Vessely et al., 2007; Cornforth,

2012). Software such as LPILE by Ensoft, Inc. or RSPile by Rocscience Inc. are capable of solving the differential equation of a beam-column using nonlinear lateral load-transfer ( $p$ - $y$ ) curves. A physical model for a laterally loaded pile is shown in Figure 2.28 where the soil is replaced with a spring-mass model. The soil reaction ( $p$ ) as a force per unit length of the pile is a function of the distance along the pile length measured from the pile head ( $x$ ) and the lateral deflection ( $y$ ) as defined by  $p$ - $y$  curves.

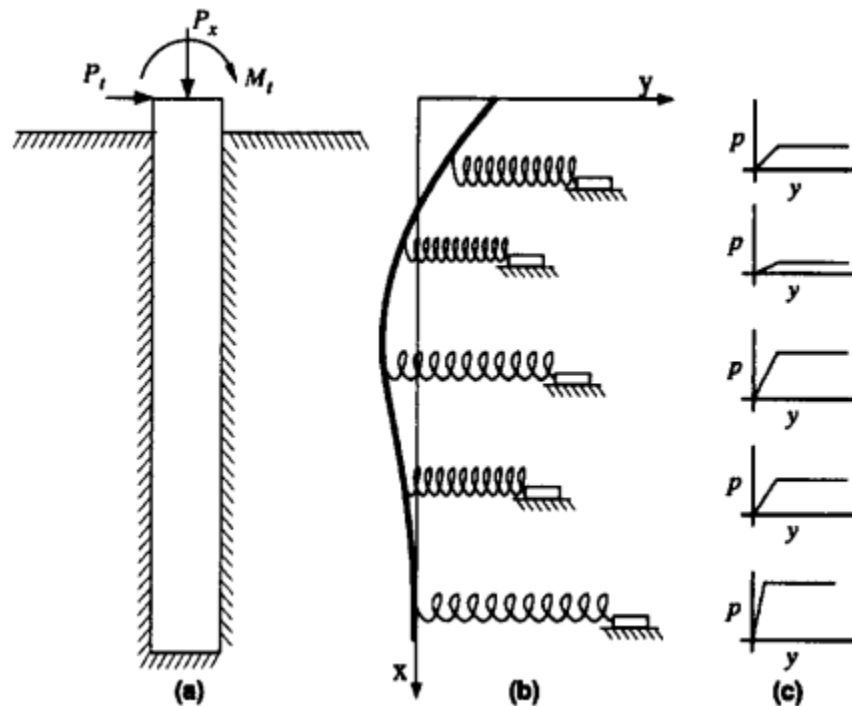


Figure 2.28: Model for pile under lateral loading with  $p$ - $y$  curves. (a) Elevation view (b) As elastic line (c)  $p$ - $y$  curves (From Reese., 1997 with permission from ASCE).

Behaviour of the laterally loaded pile can be obtained by solving the following differential equation (Hetenyi, 1946):

$$E_p I_p \frac{d^4 y}{dx^4} + P_x \frac{d^2 y}{dx^2} - p + W = 0 \quad 2-30$$

where  $P_x$  is the axial load on the pile,  $x$  is the pile length coordinate,  $y$  is the lateral deflection of the pile at point  $x$ ,  $p$  is the soil reaction per unit length,  $E_p I_p$  is the flexural rigidity of the pile, and

$W$  is the distributed load along the pile. Equation 2-30 is readily solved by difference-equation techniques and converging to the required points on the non-linear  $p$ - $y$  curves by iteration. Various authors have developed expressions for  $p$ - $y$  curves which are typically a function of soil properties, pile geometry, and the method of loading (Reese et al., 1992). The development of  $p$ - $y$  curves and the selection of appropriate  $p$ - $y$  curves is discussed in further detail in Section 2.4 of the literature review.

### **2.3.3 Selecting Pile Location, Type and Number**

Although there are no well-established guidelines for selecting the optimal location of piles to stabilize a slope, Poulos (1995) has suggested the following characteristics to make stabilizing piles effective: (i) the piles must be relatively stiff and large to generate a reasonably large stabilizing force without failing the pile; (ii) the piles must extend sufficiently deep beyond the critical failure surface so that it is not shifted downward below the piles with a factor of safety less than the target value; (iii) the piles should be located near the centre of the moving landslide mass in order to prevent shifting the critical failure surface behind or in front of the piles.

## **2.4 Selection of $p$ - $y$ Curves**

The critical step in the laterally loaded pile analysis using the load-transfer method is selecting correct  $p$ - $y$  curves (Vessely et al., 2007). Various authors have developed  $p$ - $y$  curves for sand or clay and under different loading conditions. For piles used in stabilizing a slope, the response of the soil to sustained loading must be considered (Reese et al., 1992). Established  $p$ - $y$  curves for piles in different soil types including soft clay (Matlock, 1970), stiff clay without free water (Welch & Reese, 1972), stiff clay with free water (Reese, Cox & Koop, 1975), sand (Reese et al., 1974), and weak rock (Reese, 1997) are discussed in this section. These established  $p$ - $y$  curves are some of the built-in functions included in lateral pile analysis software such as LPILE and RSPILE.

### **2.4.1 $p$ - $y$ Curves for Soft Clay**

Matlock (1970) developed the following expression for  $p$ - $y$  curves for piles in soft clay:

$$\frac{p}{p_{\text{ult}}} = 0.5 \left( \frac{y}{y_{50}} \right)^{\frac{1}{3}} \quad 2-31$$

where  $p$  is the soil reaction,  $y$  is the pile deflection and  $y_{50}$  is the deflection at one-half the ultimate resistance.  $y_{50}$  can be estimated as  $2.5\varepsilon_{50}b$  where  $\varepsilon_{50}$  is strain corresponding to one-half the maximum principal stress difference. The magnitude of  $p_{\text{ult}}$  varies with depth ( $z$ ) and can be calculated according to Matlock (1970) as the lesser of:

$$p_{\text{ult}} = 9c_u b \quad 2-32$$

$$p_{\text{ult}} = \left[ 3 + \frac{\gamma'}{c_u} z + \frac{0.5}{b} z \right] c_u b \quad 2-33$$

$\gamma'$  should be taken as the average effective unit weight from ground surface to the  $p$ - $y$  curve depth. Peck, Hanson & Thorburn (1974) suggested the values shown in Table 2.2 for  $\varepsilon_{50}$  based on the average undrained shear strength for normally consolidated clays.

Table 2.2: Representative values of  $\varepsilon_{50}$  for normally consolidated clays (from Peck et al., 1974).

Consistency of Clay	Undrained Shear Strength, $c_u$ (kPa)	Strain, $\varepsilon_{50}$
Soft	<48	0.020
Medium	45-96	0.010
Stiff	96-192	0.005

#### 2.4.2 $p$ - $y$ Curves for Stiff Clay without Free Water

Welch and Reese (1972) developed the following expression for  $p$ - $y$  curves for stiff clay without access to free water:

$$\frac{p}{p_{\text{ult}}} = 0.5 \left( \frac{y}{y_{50}} \right)^{\frac{1}{4}} \quad 2-34$$

where  $p_{\text{ult}}$  is the lesser of:

$$p_{ult} = 9c_{u,a}b \quad 2-35$$

$$p_{ult} = \left[ 3 + \frac{\gamma'}{c_{u,a}}z + \frac{0.5}{b}z \right] c_{u,a}b \quad 2-36$$

where  $c_{u,a}$  is the averaged undrained shear strength at depth  $z$ . The expression for the  $p$ - $y$  curve is similar to that for the soft clay but with an exponent of  $\frac{1}{4}$  instead of  $\frac{1}{3}$ . If no value of  $\epsilon_{50}$  is available, then a value of 0.005 or 0.01 can be selected, with the larger value being more conservative (Welch & Reese, 1972).

### 2.4.3 $p$ - $y$ Curves for Stiff Clay with Free Water

Reese et al. (1975) developed an expression for  $p$ - $y$  curves for stiff clay with access to free water with the same input as for the case without free water, with an additional input of  $k_s$  to define the initial slope. The  $p$ - $y$  curve is shown in Figure 2.29 below.

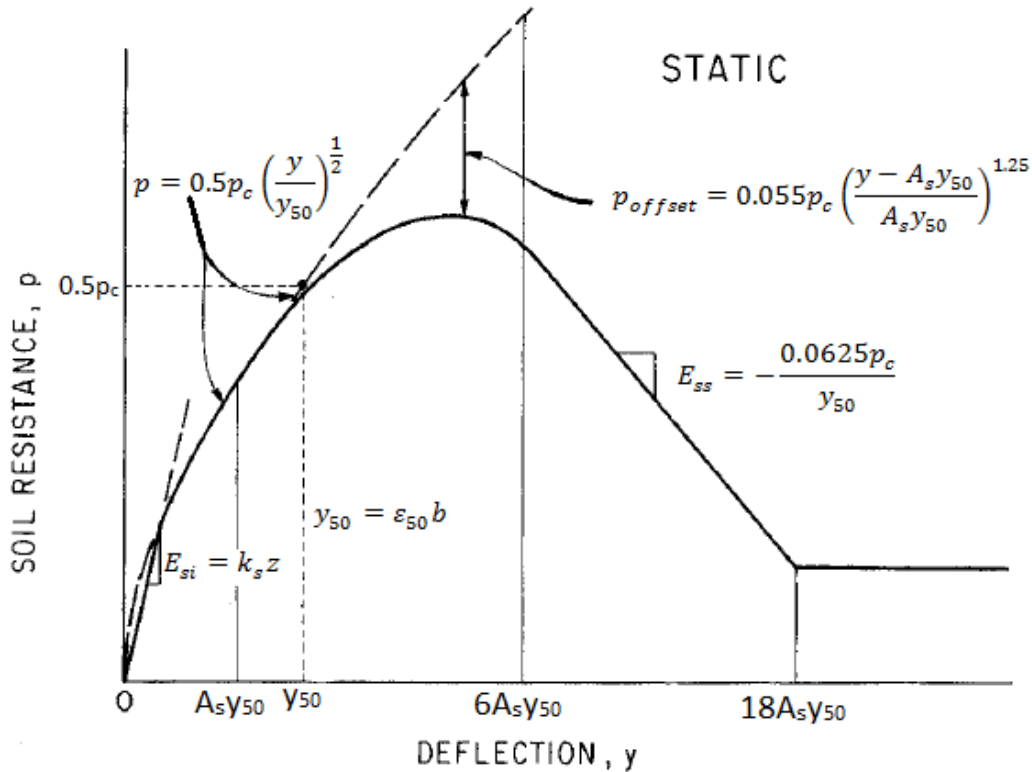


Figure 2.29:  $p$ - $y$  curve for stiff clay with free water (Adapted from Reese et al., 1975. Copyright 1975, Society of Petroleum Engineers, Inc. Reproduced with permission of SPE. Further reproduction prohibited without permission).

Reese et al. (1975) suggested values for  $\epsilon_{50}$  and  $k_s$  based on the undrained shear strength of the clay as shown in Table 2.3. The coefficient  $A_s$  can be selected from Figure 2.30.  $p_c$  can be selected as the lesser value from the equations below.

$$p_c = 2c_{u,a}b + \gamma'bz + 2.83c_{u,a}z \quad 2-37$$

$$p_c = 11c_u b \quad 2-38$$

Table 2.3: Representative values for overconsolidated clays (from Reese et al, 1975).

Undrained Shear Strength ( $c_{u,a}$ )	50-100	100-200	200-400
Strain, $\epsilon_{50}$	0.007	0.005	0.004
$k_s$ - static (MN/m <sup>3</sup> )	135	270	540
$k_s$ - cyclic (MN/m <sup>3</sup> )	55	110	540

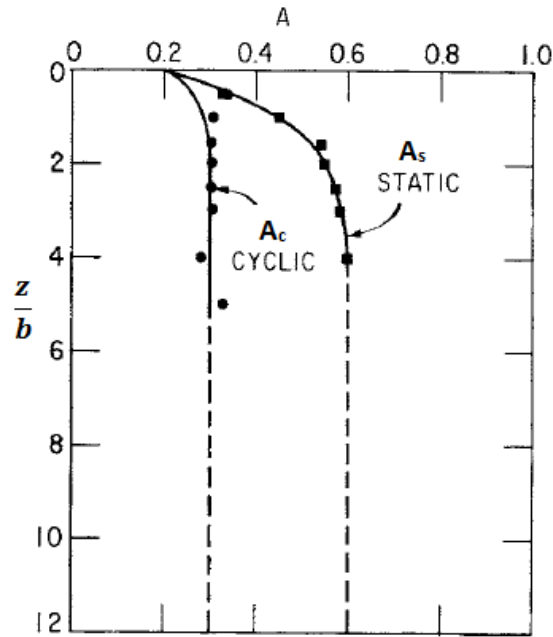


Figure 2.30: Values of  $A_s$  and  $A_c$  (Adapted from Reese et al., 1975. Copyright 1975, Society of Petroleum Engineers, Inc. Reproduced with permission of SPE. Further reproduction prohibited without permission).

#### 2.4.4 p-y Curves for Sand

Reese et al. (1974) developed an expression for  $p$ - $y$  curves for sand based on the friction angle ( $\phi$ ) and effective soil unit weight and is shown in Figure 2.31. The variable  $k_{py}$  defines the initial straight portion of the  $p$ - $y$  curve. The inflection point with soil resistance ( $p_k$ ) and pile deflection ( $y_k$ ) are calculated from  $p_m$ ,  $p_{ult}$ ,  $y_m$  and  $y_u$ . If  $y_k$  is greater than  $y_u$ , then the  $p$ - $y$  curve is linear from the origin to the point of  $p_{ult}$  and  $y_u$ .

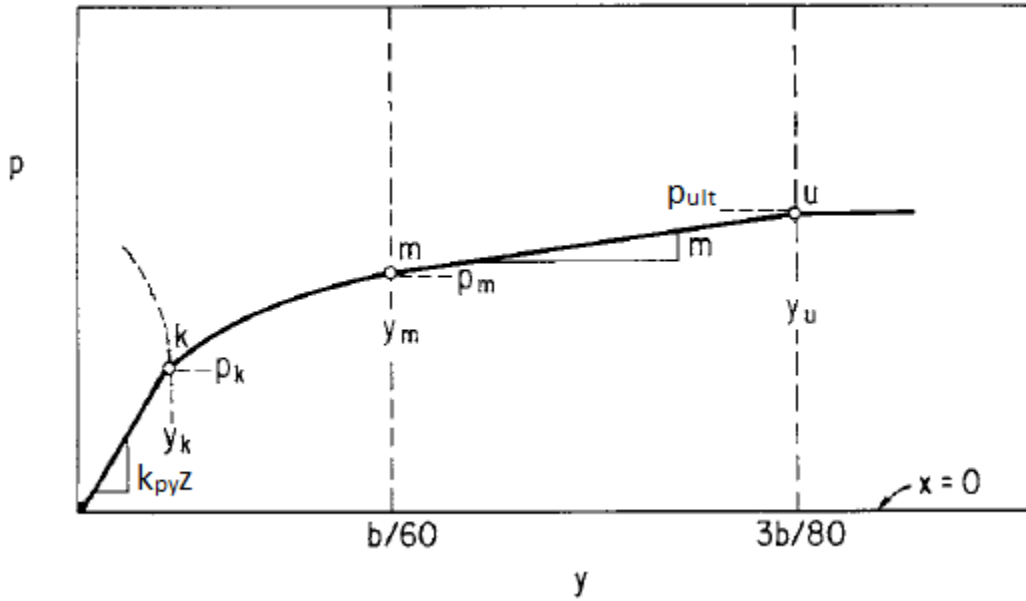


Figure 2.31:  $p$ - $y$  Curve for Sand (Adapted from Reese et al., 1974. Copyright 1974, Society of Petroleum Engineers Inc. Reproduced with permission of SPE. Further reproduction prohibited without permission).

$p_{ult}$  and  $p_m$  are calculated by first calculating  $p_s$  as the smaller of:

$$p_s = \gamma'z \left[ \frac{K_o z \tan \phi \sin \beta}{\tan(\beta - \phi) \cos \alpha} + \frac{\tan \beta}{\tan(\beta - \phi)} (b + z \tan \beta \tan \alpha) \right. \\ \left. + K_o z \tan \beta (\tan \phi \sin \beta - \tan \alpha) - K_a b \right] \quad 2-39$$

$$p_s = K_a b \gamma'z (\tan^8 \beta - 1) + K_o b \gamma'z \tan \phi \tan^4 \beta \quad 2-40$$

where  $\alpha$  is equal to  $\phi/2$ ,  $\beta$  is equal to  $45 + \phi/2$ ,  $K_o$  is assumed to equal 0.4 and  $K_a$  is the Rankine theory active earth pressure coefficient.  $p_{ult}$  and  $p_m$  are then calculated as:



$$p_{ult} = A_s p_s \quad 2-41$$

$$p_m = B_s p_s \quad 2-42$$

where the coefficients  $A_s$  and  $B_s$  can be selected from Figure 2.32 for static conditions.

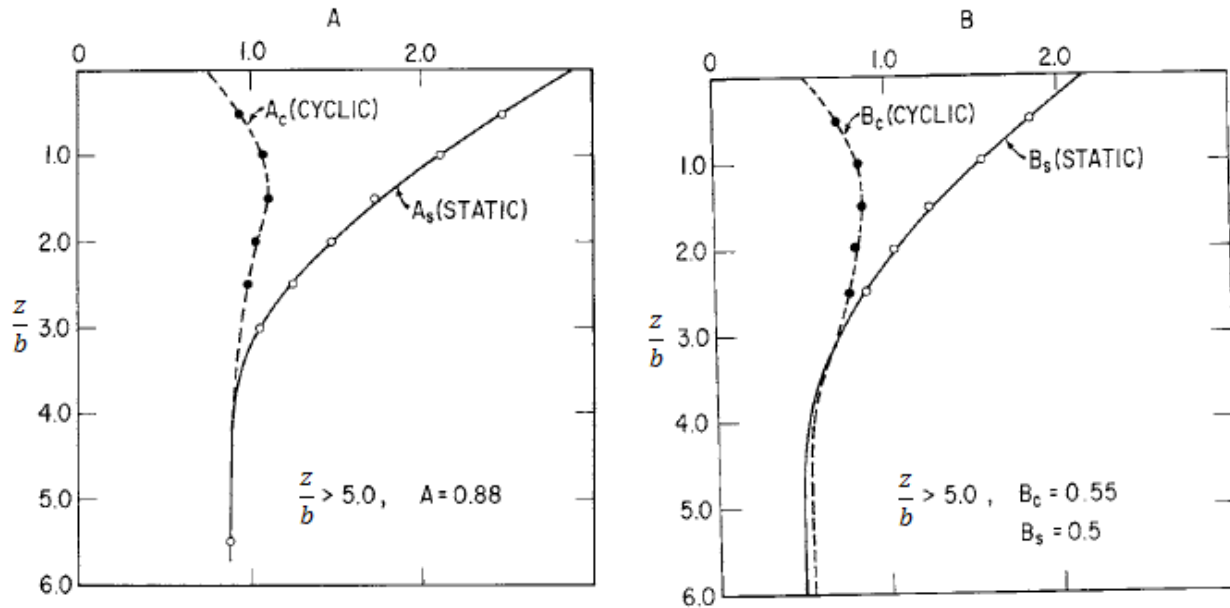


Figure 2.32: Non-dimensional coefficients  $A$  and  $B$  for ultimate soil resistance vs depth (Adapted from Reese et al., 1974. Copyright 1974, Society of Petroleum Engineers Inc. Reproduced with permission of SPE. Further reproduction prohibited without permission).

#### 2.4.5 $p$ - $y$ Curves for Weak Rock

Reese (1997) developed an expression for  $p$ - $y$  curves for weak rock based on the uniaxial compressive strength, reaction modulus of the rock, the rock quality designation ( $RQD$ ), and a strain factor ( $k_{rm}$ ).  $k_{rm}$  ranges from 0.0005 to 0.00005 and can be taken as the compression strain at one half of the uniaxial compressive strength. The  $p$ - $y$  curve for weak rock is shown in Figure 2.33.  $K_{ir}$  defines the initial modulus until it intersects with the curved portion of the curve.  $k_{rm}$  serves to establish the overall stiffness of the curve and  $y_{rm}$  can be calculated as  $k_{rm}b$  (Reese, 1997).

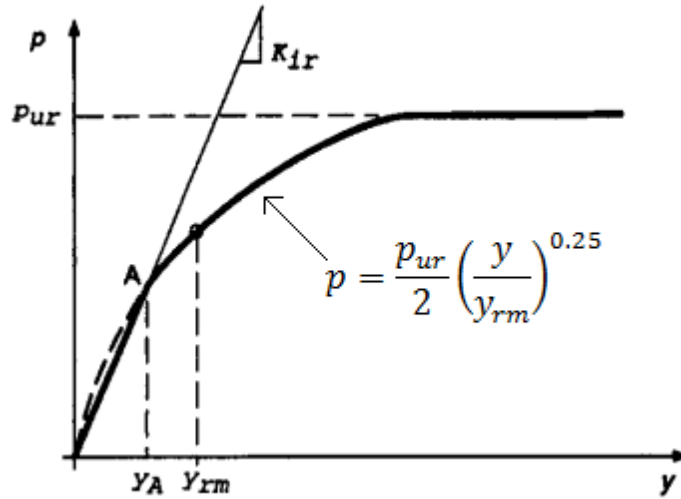


Figure 2.33:  $p$ - $y$  curve for weak rock (Adapted from Reese, 1997 with permission from ASCE).

The ultimate resistance of the rock ( $p_{ur}$ ) can be taken as the lesser of:

$$p_{ur} = \alpha_r q_{ur} b \left( 1 + 1.4 \frac{z_r}{b} \right) \quad 2-43$$

$$p_{ur} = 5.2 \alpha_r q_{ur} b \quad 2-44$$

where  $q_{ur}$  is the compressive strength of the rock,  $z_r$  is depth below the rock surface, and  $\alpha_r$  is a strength reduction factor calculated as follows:

$$\alpha_r = 1 - \left( \frac{2 RQD\%}{3 \cdot 100\%} \right) \quad 2-45$$

#### 2.4.6 Method of Georgiadis for Layered Soil

A method was developed by Georgiadis (1983) to analyze layered soils. This method is based on calculating an equivalent depth of all soil layers existing below the top layer. The equivalent depth ( $z_2$ ) of the layer below the top layer is found from equating the integrals of the ultimate soil resistance over depth for the two layers with  $z_1$  as the depth of the top layer (Reese & Van Impe, 2011).

$$F_1 = \int_0^{z_1} p_{ult1} dz \quad 2-46$$

$$F_1 = \int_0^{z_2} p_{ult2} dz \quad 2-47$$

The values of  $p_{ult}$  are calculated as described throughout Section 2.4 for the various soil and rock types. Equations 2-46 and 2-47 are solved simultaneously for  $z_2$ . The  $p$ - $y$  curves for the second layer are computed using the equivalent thickness ( $z_2$ ) of the upper layer along with the soil properties of the second layer (Reese and Van Impe, 2011). The  $p$ - $y$  curves of the second layer are computed starting at  $z_2$  (actual depth,  $z_1$ ) with depth until reaching another layer in terms of actual depth. This method can be used for the length of the pile as it crosses additional soil layers.

## 2.5 Summary of Laterally Loaded Piles for Slope Stabilization

A row of shear piles can improve the resistance to landslide loading at the weak shear zone of a landslide (Cornforth, 2005). This remediation option is applicable for the common landslide condition in stiff clays where a discrete shear zone exists where the clay is at residual strength that is much weaker than the landslide mass (Cornforth, 2012). Cornforth (2005) described several advantages and disadvantages to using a row of shear piles for landslide stabilization. These advantages include: (1) the piles do not have to be anchored near the top if lateral deflection is not a concern; (2) the top of piles can be buried; (3) individual shear piles provide greater passive resistance per pile than a group or contiguous row; and (4) the installation location is flexible. Disadvantages described by Cornforth (2005) include they are relatively expensive to construct and cast-in-place concrete piles can't be installed in moving landslides.

### **3.0 HARDY RIBS CASE STUDY SITE**

The application of Hardy Ribs for slope stabilization was introduced in Alberta by Dr. R. M. Hardy. The only documented application of Hardy Ribs available to the author is a site near the Birdtail Sioux First Nation in western Manitoba. The Hardy Ribs were implemented in 2015 to stabilize a slope along the Assiniboine River to protect a CN rail line. Information regarding the site conditions and the construction of the Hardy Ribs were provided by CN. The author was not involved in the design or construction of the case study Hardy Ribs. This chapter describes the site location, geology, stratigraphy, instrumentation and monitoring, design, construction, and performance of the Hardy Ribs stabilization works.

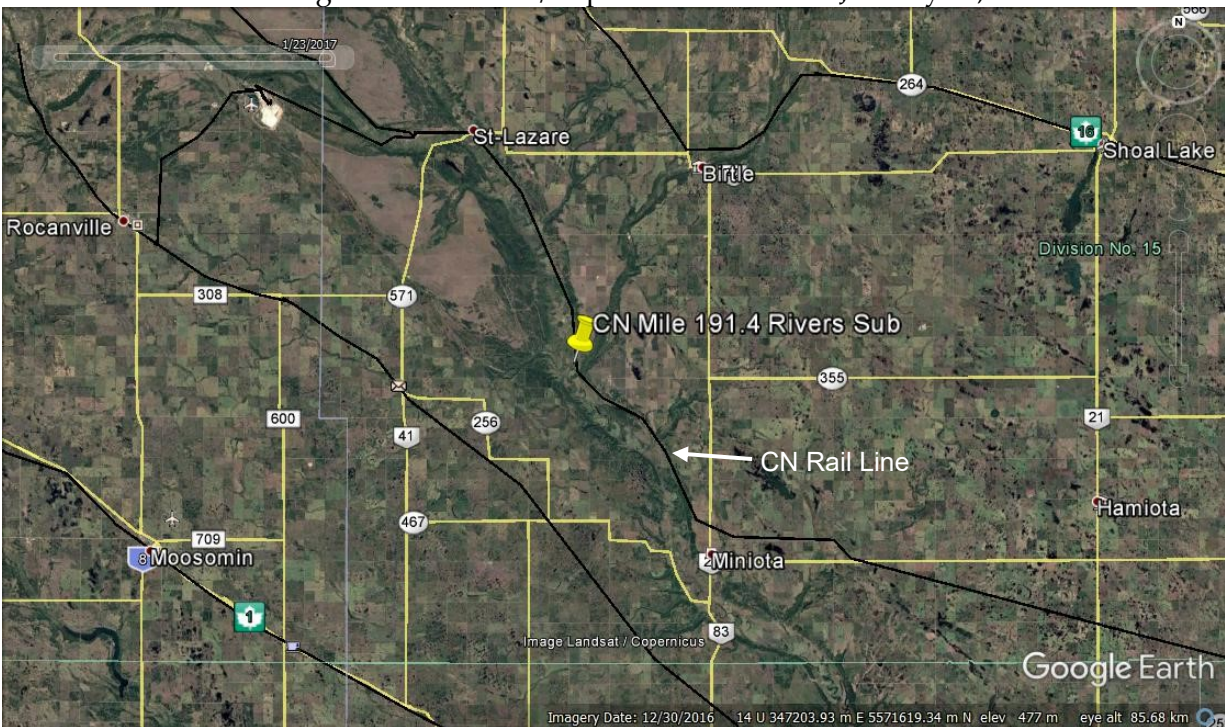
#### **3.1 Site Location and Slope Geometry**

The landslide study site is located along an outside bend of the Assiniboine River valley at NW18-15-27-W1 in south-western Manitoba, adjacent to a CN rail line at Mile 191.4 of the Rivers Subdivision. The general location of the study site is shown in Figure 3.1 with satellite imagery from Google Earth. Figure 3.1a shows the location in relation to the Canadian provinces and Figure 3.1b shows the location of the site along the Assiniboine River Valley between Miniota, Manitoba and St. Lazare, Manitoba. Approximately 110 m of the track was affected by the very slow (Cruden and Varnes, 1996) moving landslide as estimated by the required ongoing track maintenance prior to the construction of slope stabilization works.

The site was inspected in October, 2014 by staff of CN. At the time of inspection, a head scarp of the landslide was observed to intersect the rail line at the south extent of the landslide. The outside bank of the Assiniboine River comes within 90 m of the track and signs of active erosion were observed along the outside meander.



(a) Google Earth V 7.1.7.2606. (December 13, 2015). Canada. 15U 493616.52 m E, 6037239.40 m N, eye alt 4189.03 km. IBCAO. SIO, NOAA, U.S. Navy, NGA, GEBCO. Google 2016. Landsat/Copernicus. Accessed January 23, 2017.



(b) Google Earth V 7.1.7.2606. (December 30, 2016). Canada. 14U 347203.93 m E, 5571619.34 m N, eye alt 85.68 km. Landsat/Copernicus. Accessed January 23, 2017.

Figure 3.1: Location of study site.

LIDAR data was collected along the Assiniboine River valley between CN Mile 191 to Mile 192 of the Rivers subdivision in November of 2015. A topographic contour map was developed based on the LIDAR data and is shown in Figure 3.2. Three cross sections of the slope that intersect the rail line and that are within the extent of the landslide are shown in Figure 3.3 and the location of the cross sections is shown in plan on Figure 3.2. The LIDAR data does not capture the elevation of the river bottom and therefore the Assiniboine River appears to be level in Figures 3.2 and 3.3. Cross Sections A and C are separated by 110 m and are near the southern and northern extents of the landslide mass. Cross Section B is approximately near the centre of the landslide and is in line with the majority of the boreholes and instrumentation on the site. The LIDAR data was collected after completion of the stabilization works in summer of 2015.

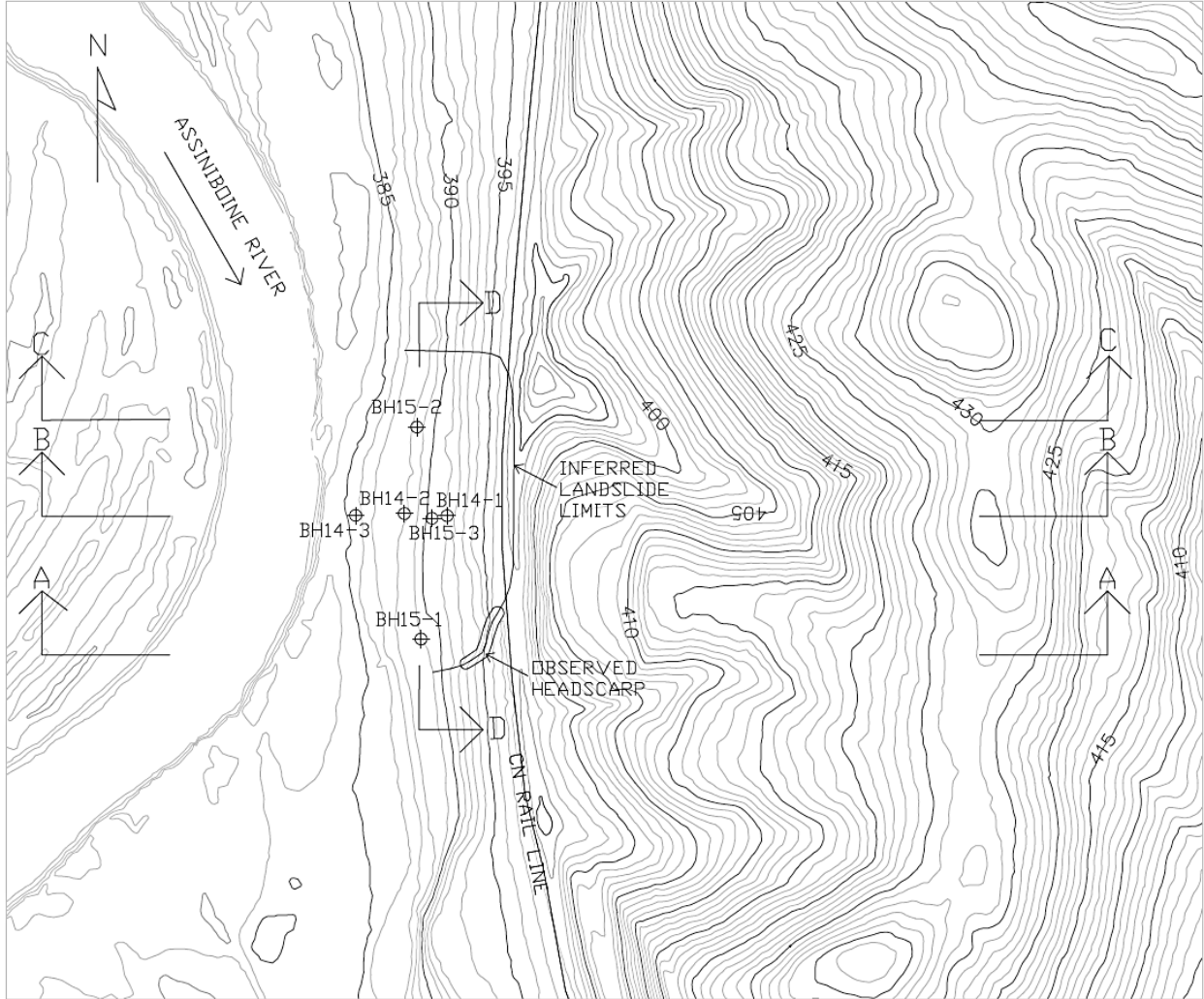
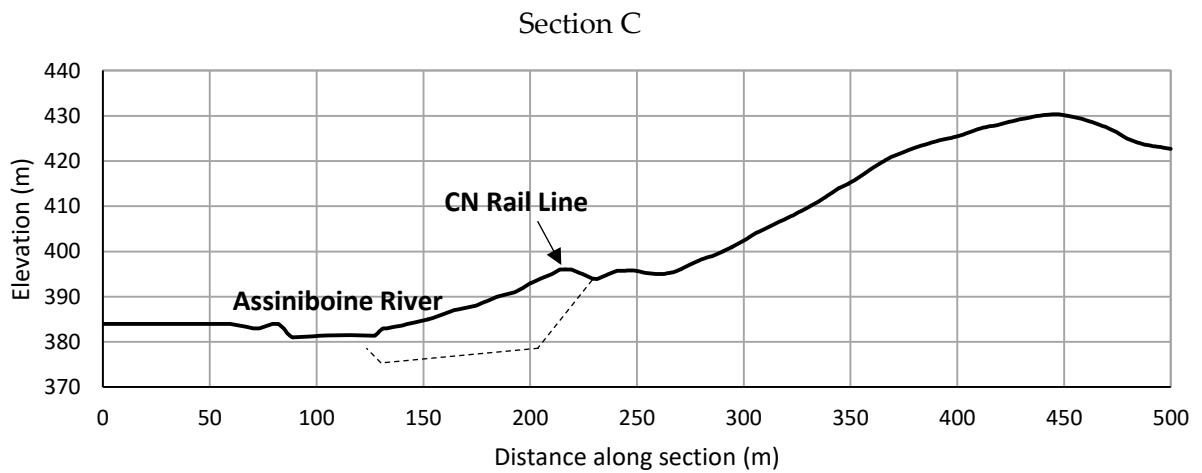
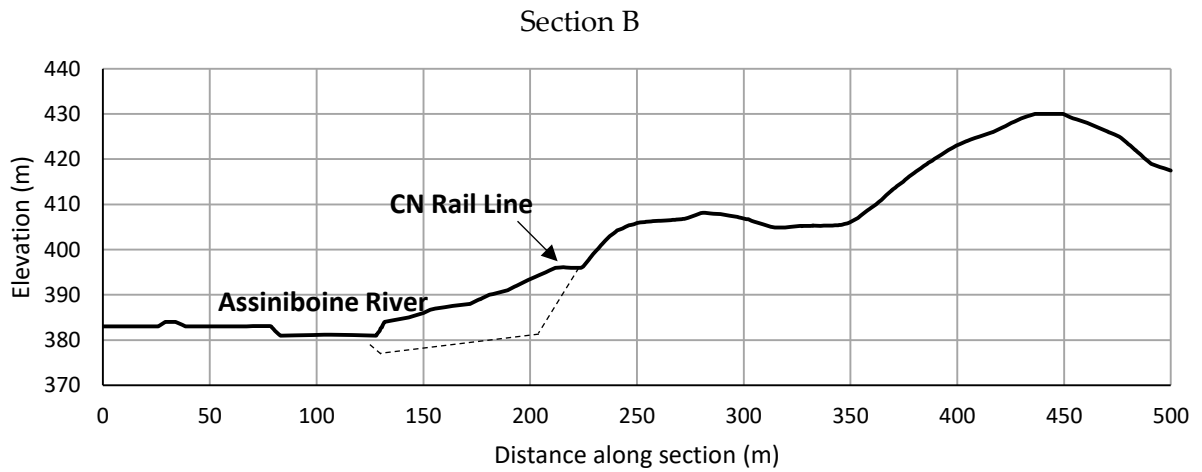
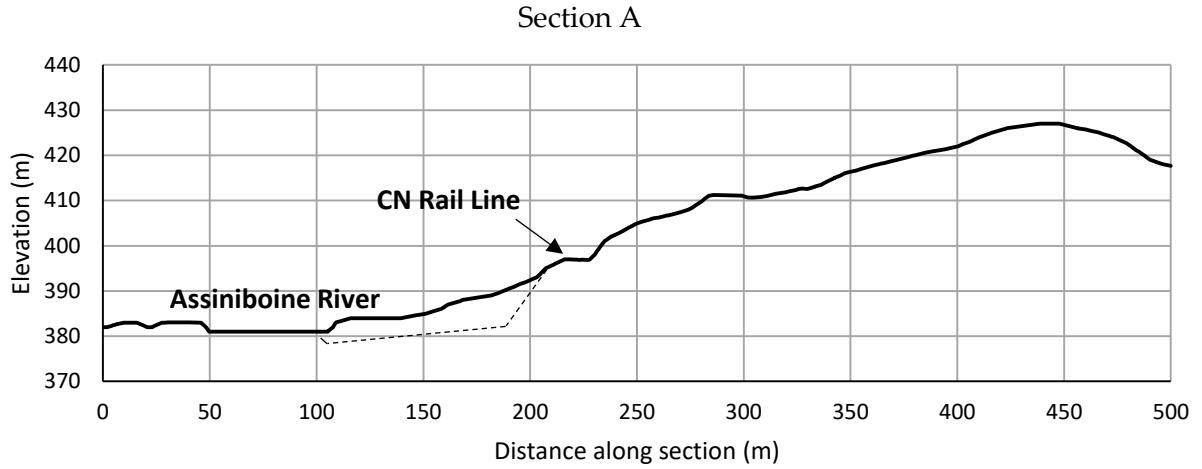


Figure 3.2: Topographic contour plan of CN study site.

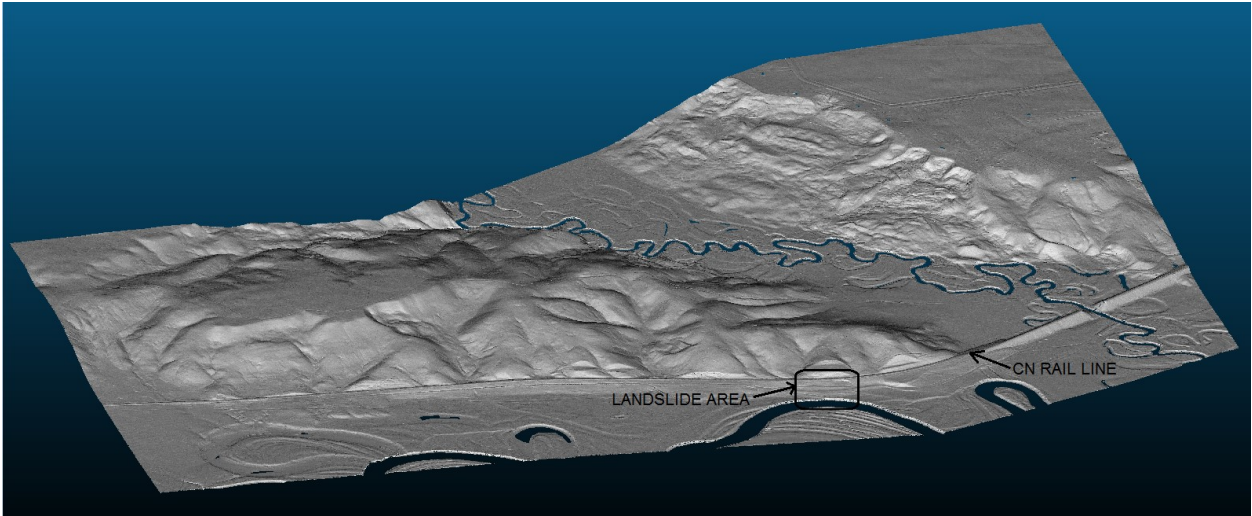


*Figure 3.3: Cross sections showing valley geometry.*

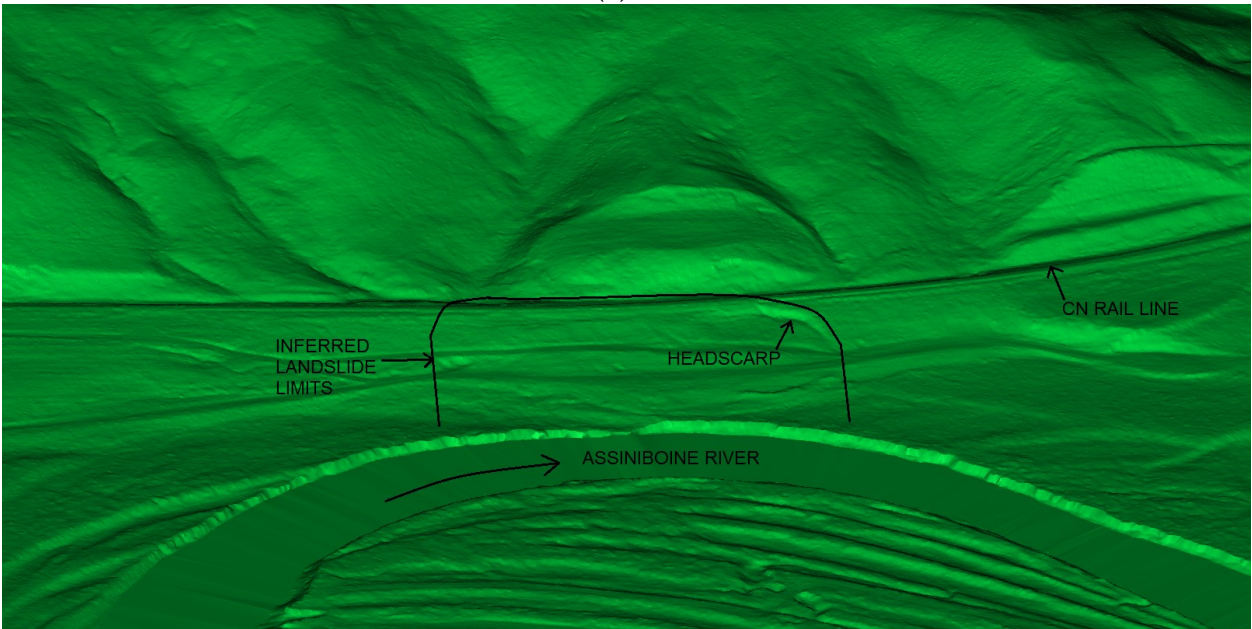
To show the topography of the region and the scale of the landslide, the LIDAR data was analyzed using CloudCompare (2017) which is an open source software for 3D point cloud and mesh



processing. Visuals from CloudCompare with the LIDAR data are shown in Figure 3.4. The regional topography is evident in the LIDAR point cloud shown in Figure 3.4a. The railway embankment can be observed running along the edge of the Assiniboine River valley and crossing the smaller Birdtail River. The landslide of concern is located along the outside bend of the Assiniboine River. Figure 3.4b shows a mesh developed from the point cloud and shows the region in the vicinity of the landslide. The headscarp of the landslide which approaches the railway that was observed during site inspections can similarly be observed in Figure 3.4b. The steep banks on the outside bend of the Assiniboine River and the point bar observed on the inside bend are signs that the active and ongoing erosion is occurring at the toe of the landslide slope.



(a)



(b)

Figure 3.4: LIDAR data in CloudCompare. a) Point cloud showing regional topography b) Mesh showing landslide region.

### 3.2 Site Geology and Stratigraphy

The Assiniboine River is an underfit stream within a trench-shaped valley formed as a meltwater channel during deglaciation of the region approximately 12,000 to 15,000 years ago (Klassen, 1975). The bedrock in this region consists of marine clay shale of the Cretaceous Riding Mountain Formation and the valley bottom fill consists of alluvial sediments (Klassen, 1975).

A geotechnical drilling program was conducted at this site in November 2014 and is summarized by Clifton Associates (2015). The sonic drilling method was utilized with an 80 mm diameter core

barrel and 130 mm diameter casing. Additional geotechnical drilling programs were conducted in June 2015 during construction of the Hardy Ribs and November 2015 following completion of the Hardy Ribs to install instrumentation. All boreholes were extended into the shale bedrock. The location of the boreholes is shown in plan on Figure 3.2. Boreholes from the November 2014 drilling program are labelled BH14-1, BH14-2, and BH14-3. Boreholes from the June and November 2015 drilling programs are labelled BH15-1, BH15-2, and BH15-3. BH15-1 and BH15-2 were drilled approximately near the southern and northern extents of the land slide, respectively. Borehole logs with data from the geotechnical drilling programs are attached in Appendix A.

As part of the geotechnical investigation program conducted in November 2014, laboratory testing was conducted on disturbed and undisturbed soil samples as described by Clifton Associates (2015). Water content analyses were performed on each sample collected. Dry density tests, Atterberg limits tests and the Unified Soil Classification System (USCS) classification was performed on select samples. The undrained shear strength was estimated for disturbed samples by performing pocket penetrometer tests and laboratory vane tests. The laboratory testing results are shown on the borehole logs attached in Appendix A.

Based on the geotechnical drilling program, the stratigraphy at the site is interpreted to consist of a thin layer of fill at ground surface underlain by clay and shale bedrock. The shale above the slide plane was observed to be heavily disturbed. The general stratigraphy is shown in Figure 3.5 for the alignment of Cross Section B and Cross Section D. The cross sections are shown in plan view in Figure 3.2. The elevation of the shale layer is observed to be inclined and sloping downward towards the Assiniboine River. The depth to the intact shale is greater towards the north side of the Hardy Ribs alignment.

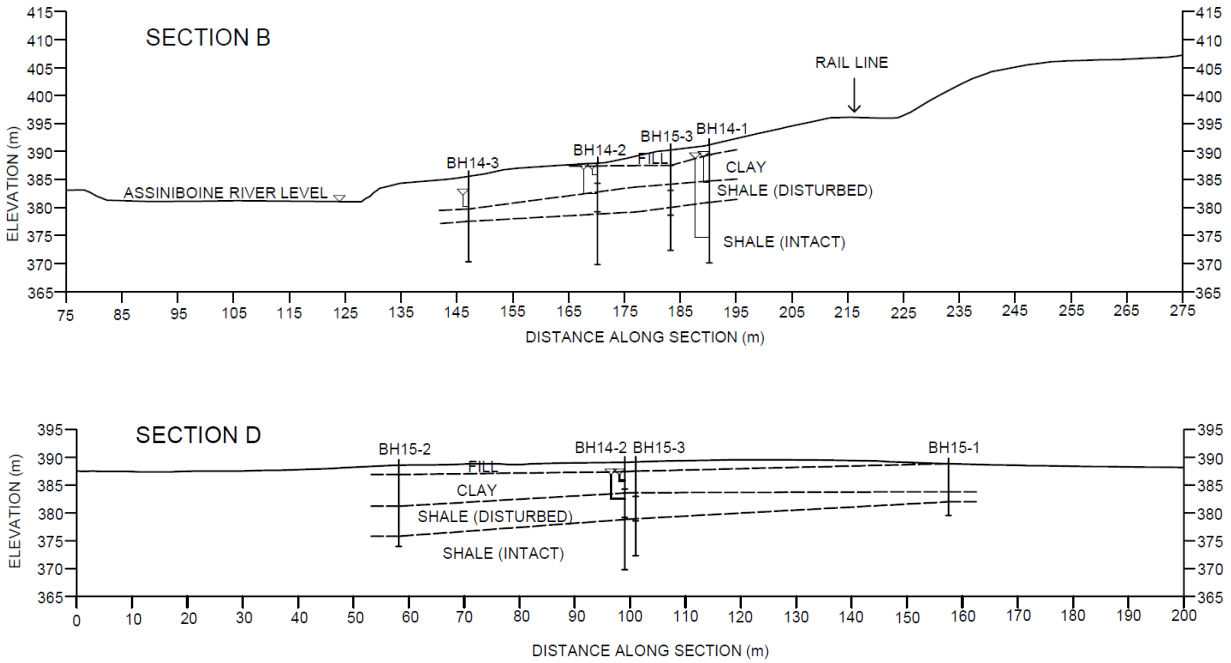


Figure 3.5: Stratigraphic sections at CN Mile 191.4 Rivers Subdivision

### 3.3 Site Instrumentation and Monitoring

Instrumentation installed during the November 2014 geotechnical drilling program by Clifton Associates (2015) included five vibrating wire piezometers and three slope inclinometers (S.I.). Two vibrating wire piezometers were installed in each of BH14-1 and BH14-2, and one vibrating wire piezometer was installed in BH14-3. A slope inclinometer was installed in each of BH14-1, BH14-2, and BH14-3.

The groundwater elevations as measured from the vibrating wire piezometers on December 11, 2014 is shown in Table 3.1 and in Figure 3.5. Based on the piezometer monitoring data presented in Table 3.1 as measured on December 11, 2014, the piezometric surface ranged between 1.3 m to 3.3 m below ground surface. The vertical groundwater gradient was negligible at BH14-1 and BH14-2. The groundwater elevation was measured to decrease towards the Assiniboine River.

Table 3.1: Groundwater data monitored on Dec. 11, 2014.

Borehole	Ground Elevation (m)	Tip Elevation (m)	Groundwater Elevation (m)	Monitoring Zone
BH14-1	391.521	374.7	388.7	Clay/Shale Interface
	391.521	384.5	388.9	Shale
BH14-2	388.099	382.5	386.8	Clay
	388.099	385.8	386.8	Shale
BH14-3	385.513	380.2	382.2	Clay

The slope inclinometers were monitored two times and plots showing the displacement to December 11, 2014 are shown in Figures 3.6., 3.7 and 3.8 for BH14-1, BH14-2 and BH14-3, respectively.

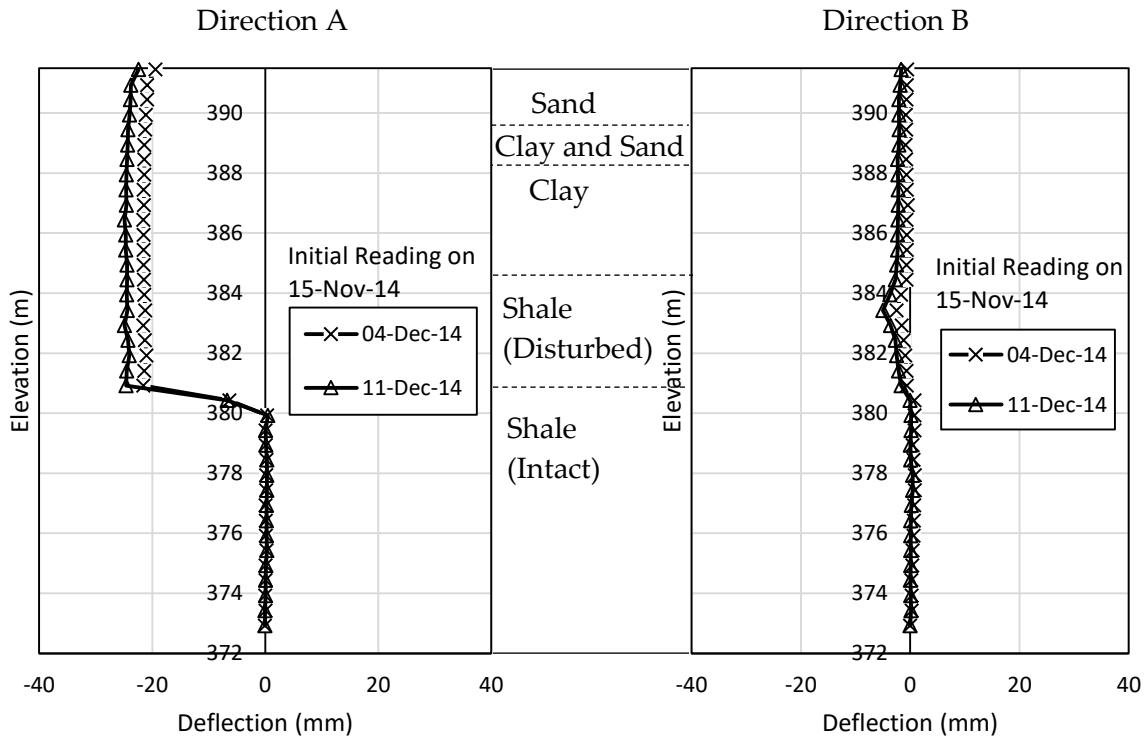


Figure 3.6: S.I. monitoring data from BH14-1.

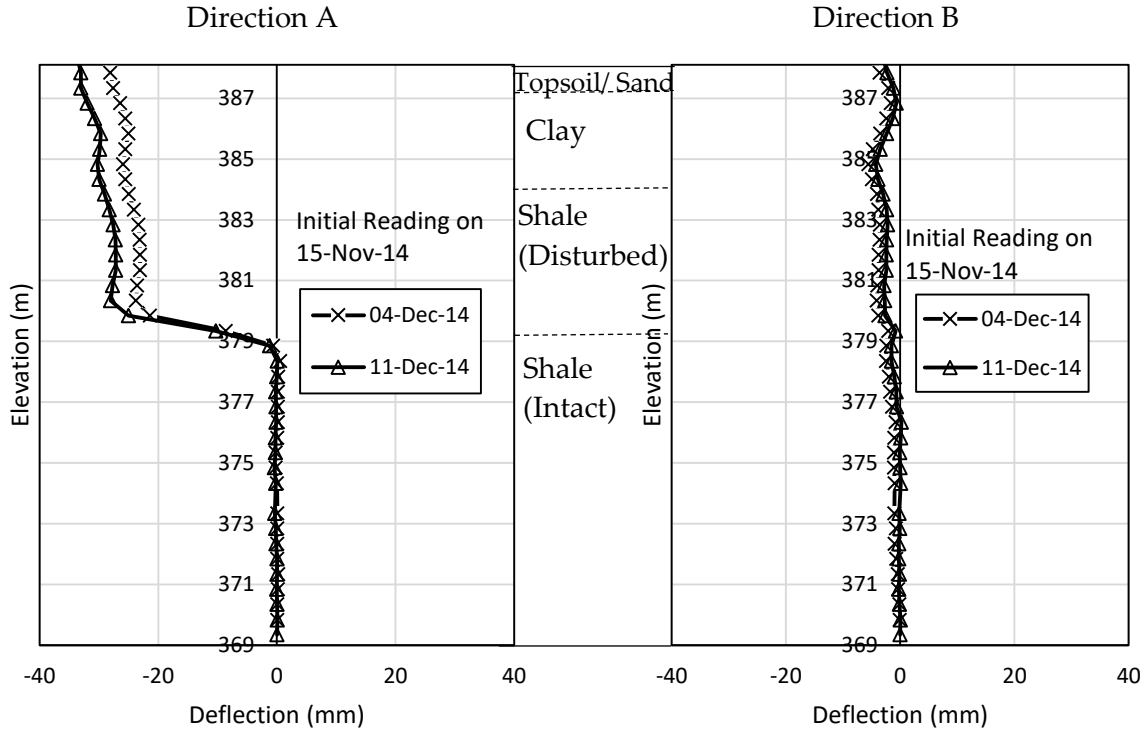


Figure 3.7: S.I. monitoring data from BH14-2.

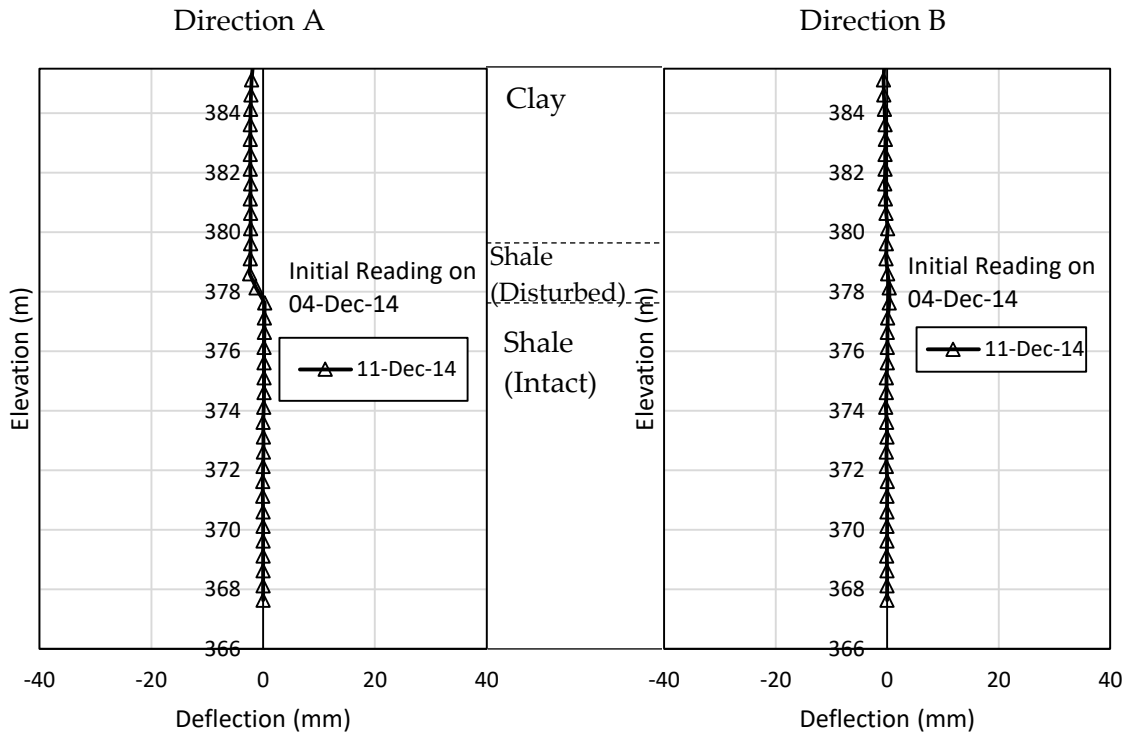


Figure 3.8: S.I. monitoring data from BH14-3.

The S.I. plots identify significant slope movement at an approximate elevation of 381 m, 380 m and 378 m at BH14-1, BH14-2 and BH14-3, respectively. The slide plane is inclined and decreases in elevation towards the river with an approximate slope of 14H:1V. Over the 26 day monitoring period shown in the S.I. data in Figure 3.6 and 3.7, the rate of displacement in the A-direction was approximately equal to 1 mm per day. BH14-3 was only monitored over a 6 day period, however the displacement along the slide plane is comparable to the displacement between the December 4, 2014 and December 11, 2014 readings from BH14-1 and BH14-2. The S.I. casings had deformed beyond their functional limits by the summer of 2015 and there was no S.I. monitoring during construction of the Hardy Ribs.

### 3.4 Hardy Ribs Design and Construction

The Hardy Ribs slope stabilization works at CN Mile 191.4 Rivers Subdivision were constructed in June and July of 2015 over a span of approximately 40 days. The Hardy Ribs consisted of 37 sheet pile walls installed parallel to each other and spaced 3.0 m apart centre-to-centre. Each sheet pile wall consisted of ten PZC-26 steel sheet pile sections with an overall length of approximately 7.08 m. The sheet piles were approximately 12.19 m to 13.72 m in length and were installed to a minimum of approximately 1.83 m beyond the shear plane. The shear plane was deeper below ground surface on the north end of the site and therefore the longer sheet piles were used towards the northern extent of the site. The dimensions of a PZC-26 sheet pile are shown in Figure 3.9 and the arrangement of the sheet pile walls are shown in Figure 3.10.

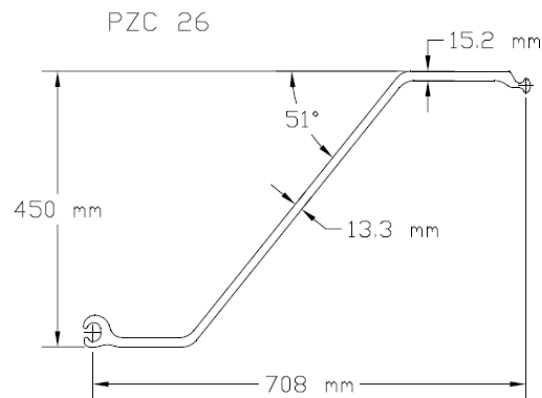


Figure 3.9: Dimensions of PZC 26 sheet pile.

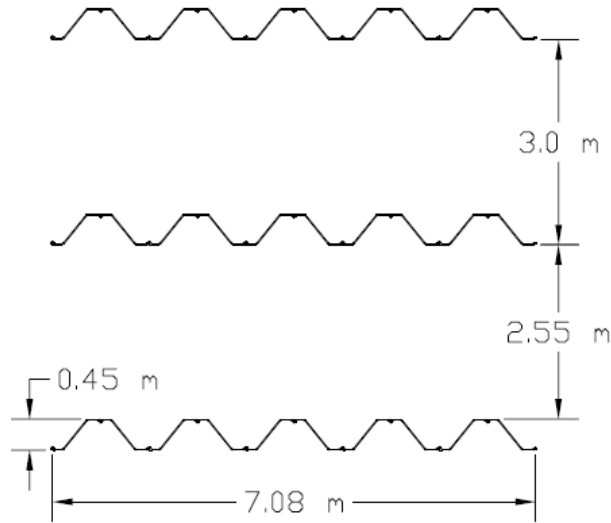


Figure 3.10: Layout of sheet piles for Hardy Ribs at CN Mile 191.4 Rivers Sub.

The as-constructed layout and location of the sheet pile walls are shown in plan in Figure 3.11 and in cross section in Figure 3.12. An inferred limits of the landslide are shown in Figure 3.11 as estimated from an observed landslide scarp on the southern limits of the landslide and based on deflections in the rail. The sheet pile walls that comprise the Hardy Ribs do not extend along the entire width of the landslide. The ten sheet piles that comprise each sheet pile wall were installed as five pairs of two. The alignment shown in Figure 3.11 that is labelled as “pair 5 alignment” represents the most upslope pair of sheet piles for each wall. The depth of the sheet piles shown in the Figure 3.12 is representative of the most downslope pair of sheet pile for each wall and the depth of subsequent pairs for each wall varies.



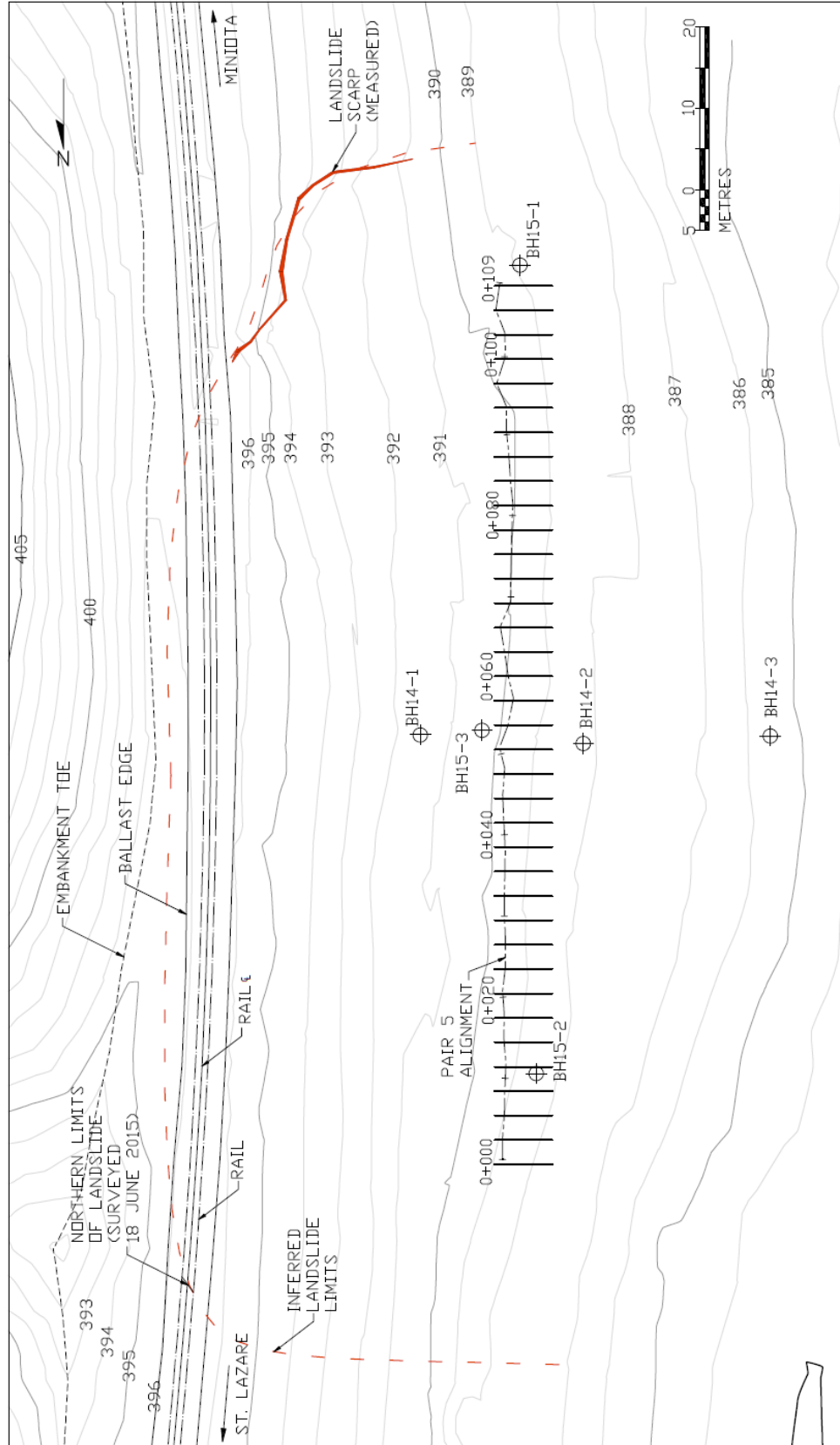


Figure 3.11: Plan view showing as-built layout of sheet pile walls.

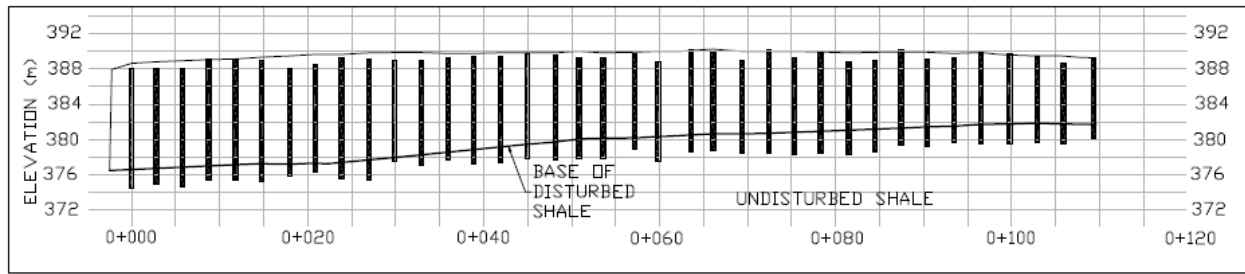


Figure 3.12: Cross section showing as-built layout of sheet pile walls.

The sheet piles were installed by initially vibrating each sheet pile to a depth of approximately 5.5 m using a crane hoisted vibratory hammer. The sheet piles were then driven to the design elevation with a crane hoisted diesel hammer. The sheet piles were intended to be installed to a minimum of 1.83 m beyond the slide plane although the installation depth did vary. Finally, the extra length of the sheet pile above ground was cut off prior to regrading the site to the final slope geometry. Photos showing the installation method are shown in Figures 3.13 to 3.16.



Figure 3.13: Hoisting sheet pile with crane (Source: CN).



Figure 3.14: Advancing sheet piles with vibratory hammer (Source: CN).



Figure 3.15: Driving sheet piles with diesel hammer (Source: CN).



*Figure 3.16: Rows of installed sheet pile walls (Source: CN).*

### **3.5 Performance of Hardy Ribs**

The S.I. casings installed in BH14-1, BH14-2 and BH14-3 were no longer functional by the summer of 2015 during construction of the Hardy Ribs. An S.I. casing was installed in BH15-3 which was drilled in November, 2015 and therefore there was no S.I. monitoring data between December, 2014 and November, 2015. BH15-3 was drilled upslope of the Hardy Ribs and between the locations of BH14-1 and BH14-2. The S.I. monitoring data from BH15-3 is shown below in Figure 3.17.

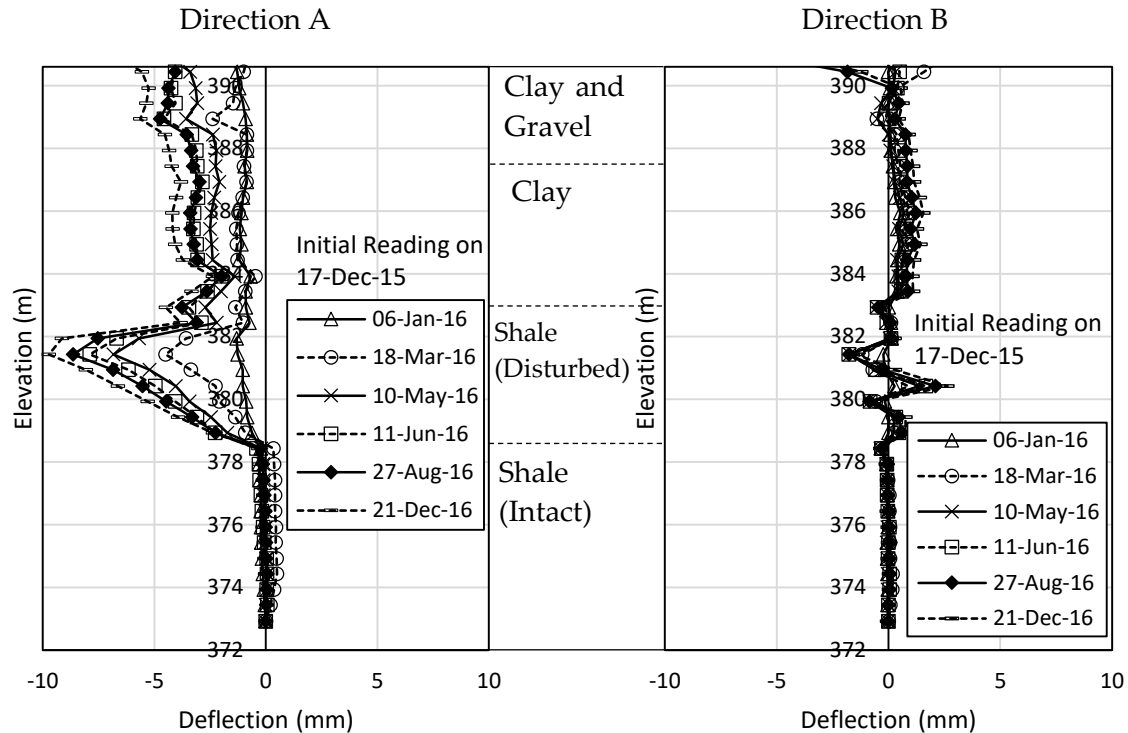


Figure 3.17: S.I. monitoring data from BH15-3.

Based on the S.I. monitoring results shown in Figure 3.17, there has been ongoing slope displacement since construction of the Hardy Ribs. The magnitude of the slope displacement is most significant between approximate elevations of 379 m to 382 m. The maximum displacement is occurring at approximate elevation of 381.4 m where the cumulative displacement was 9.7 mm from December, 2015 to December, 2016. The displacement rate during this time period was less than 1 mm per month. The soil has continued to move downslope along the length of the Hardy Ribs which suggests that the sheet pile walls may be moving laterally or rotating about the bottom. The increased lateral soil displacement from elevations 379 to 382 m may indicate that the soil is shearing or squeezing between the sheet pile walls within the disturbed shale, but the magnitudes of displacement are minor to date. The total A-direction S.I. displacement from BH14-1 and BH15-3 has been plotted with time in Figure 3.18. There is a considerable time gap in the slope inclinometer data, however it is evident that the rate of displacement has significantly decreased since installation of the Hardy Ribs. Although the landslide displacement rate has significantly decreased, there may be continued long term displacement due to creep behaviour of the clay and shale.

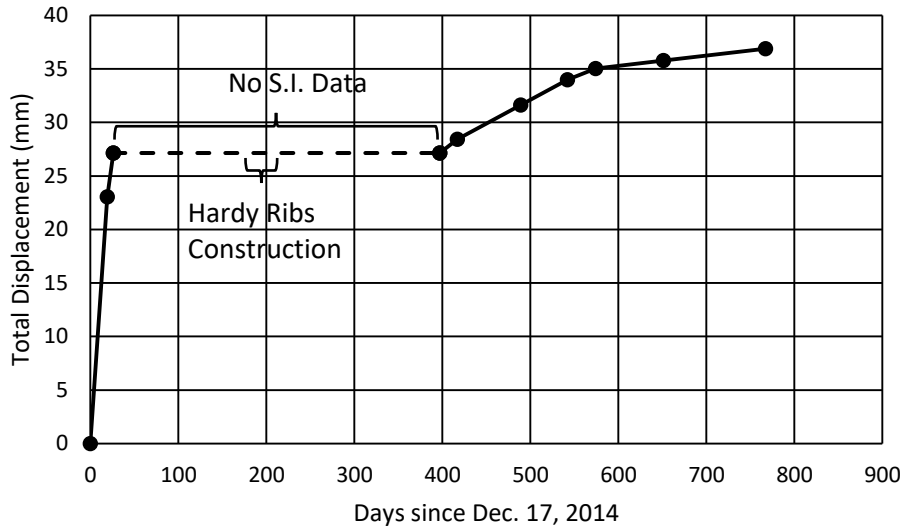


Figure 3.18: Total landslide displacement with time.

General site photos from an October, 2016 site visit are shown in Figure 3.19 to show the site conditions post-construction and after vegetation has been re-established. Vegetation has been re-established over the Hardy Ribs and there is little evidence of the works as observed in Figures 3.19a, 3.19b, and 3.19c. Signs of ongoing erosion at the toe of the slope along the outside bend of the Assiniboine River are observed in Figure 3.19d.



(a)



(b)



(c)



(d)

Figure 3.19: Photos from October 5, 2016. (a) Looking downslope from rail line (b) Looking north from over top of Hardy Ribs (c) Looking upslope from access road downslope of Hardy Ribs (d) Shore line of Assiniboine River showing signs of erosion. (Photos by J.R. Bartz).

### 3.6 Summary of Hardy Ribs at CN Mile 191.4 Rivers Subdivision

The Hardy Ribs installed at CN Mile 191.4 Rivers Subdivision consisted of 37 parallel sheet pile walls spaced 3.0 m apart centre-to-centre. Each sheet pile wall consisted of 10 PZC-26 steel sheet piles. The sheet piles were driven through the landslide mass and into the underlying stable shale bedrock.

S.I. monitoring before and after construction of the Hardy Ribs has shown a significant decrease in the rate of landslide movement. Prior to remediation, the landslide was moving along a discrete shear plane at an approximate rate of 1 mm per day. Some displacement has continued since construction of the Hardy Ribs which is expected since it is a passive system and requires movement to develop resistance. The ongoing downslope displacement is greatest in the

disturbed shale layer and suggests that the disturbed shale may be shearing or squeezing between the sheet piles. The magnitudes of displacement are very small however in the disturbed shale with a rate less than 1 mm per month. Based on the latest S.I. monitoring data, the Hardy Ribs have effectively reduced the rate of landslide displacement which will reduce the requirements for track maintenance and realignment.



## 4.0 LATERALLY LOADED SHEET PILE WALLS

There are no existing solutions that the author is aware of for calculating the ultimate lateral soil resistance ( $p_{ult}$ ) for a sheet pile wall loaded in the orientation consistent with the Hardy Ribs slope stabilization method, i.e. the load is parallel to the long dimension of the wall. Also, there are no acceptable  $p$ - $y$  curves that have been developed for this loading case. This chapter consists of the derivation of several proposed theoretical solutions for calculating the ultimate lateral load capacity for a single sheet pile wall in cohesive soil, based on the concepts developed for circular piles discussed in Chapter 2.

A laterally loaded sheet pile wall for a Hardy Rib is illustrated in Figure 4.1 below. It is anticipated that similar to laterally loaded circular piles, the soil near the ground surface will form a passive wedge and the soil at depth will flow around the pile. The ultimate lateral soil capacity of a single sheet pile wall is expected to be greater than that of a circular pile with equal width due the frictional resistance that would develop along the sides of the sheet piles. The shear resistance along the sides of the sheet pile wall must be exceeded prior to the soil failing as a passive wedge or in the flow-around mechanism. Therefore, the initial stiffness of the load-deflection or  $p$ - $y$  curve is anticipated to increase with increasing sheet pile length.

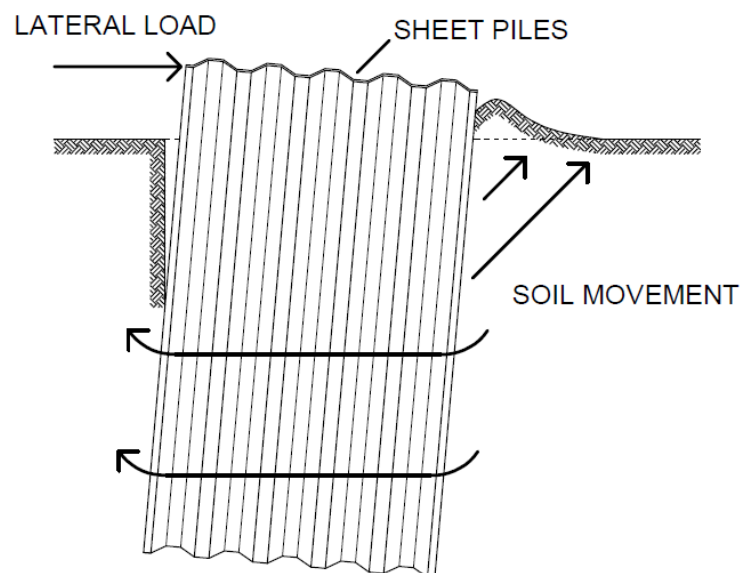


Figure 4.1: Soil and sheet pile deformation under lateral load.

Several theoretical solutions are proposed for calculating the ultimate lateral soil capacity for sheet pile walls. These solutions are based on the block-soil model by Reese (1958) for circular piles, the lab testing results by Broms (1983) for square piles, and by performing two-dimensional finite element modeling.

#### **4.1 Block-Soil Model**

The block-soil model developed by Reese (1958) for estimating the ultimate lateral soil resistance for a laterally loaded circular pile was modified to estimate  $p_{ult}$  for a laterally loaded sheet pile wall. A sheet pile wall with width  $B_1$  and length  $B_2$  are surrounded by square blocks with side length  $B_2$  and a rectangular block with dimensions of  $B_1$  by  $B_2$  as shown in Figure 4.2a. Lateral displacement of the pile is assumed to cause blocks 1,2,4, and 5 to fail in shear and block 3 develops resistance by sliding. The stress conditions are shown in Figure 4.2b and the free body diagram shown in Figure 4.2c can be examined to calculate the lateral bearing capacity factor.

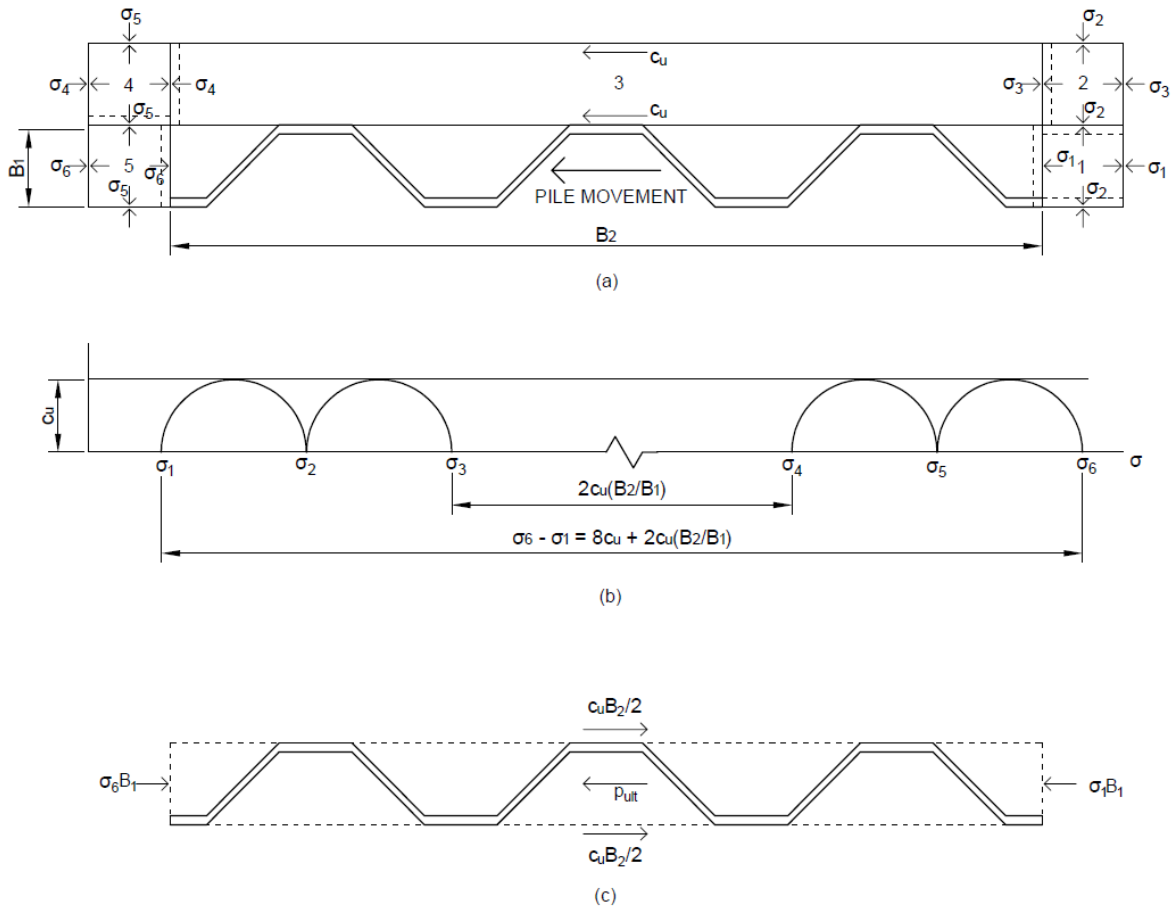


Figure 4.2: Assumed block failure model for clay. (a) Section through sheet pile (b) Mohr-Coulomb diagram (c) Forces acting on sheet pile.

If the side friction on the pile is assumed to be half of the undrained shear strength consistent with the assumption by Reese (1958), then the lateral bearing capacity ( $N_c$ ) can be calculated as:

$$N_c = 8 + 3 \frac{B_2}{B_1} \quad 4-1$$

where  $B_1$  is the sheet pile wall width and  $B_2$  is the sheet pile wall length.  $p_{ult}$  for the flow-around failure mode is then calculated by multiplying  $N_c$  by  $c_u B_1$ . If the sides are assumed to be frictionless, then  $N_c$  can be calculated as:

$$N_c = 8 + 2 \frac{B_2}{B_1} \quad 4-2$$

## 4.2 Broms' (1983) Pile Group in Clay Model

The model proposed by Broms (1983) for pile groups of square piles in clay is extended to rectangular piles as an approximate representation of a sheet pile wall. The frictional resistance along the length of the piles is assumed to be proportional to the pile length as shown in Figure 4.3.

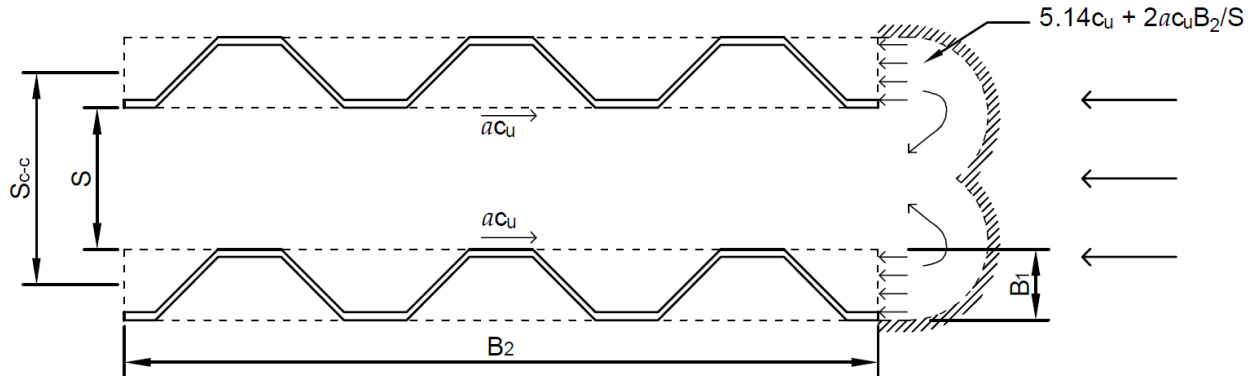


Figure 4.3: Lateral resistance of a sheet pile group in clay.

$p_{ult}$  can then be calculated based on the pile geometry as:

$$p_{ult} = 5.14c_u B_1 + 2ac_u B_2 \left( \frac{S_{c-c}}{S} \right) \quad 4-3$$

where  $B_1$  is the sheet pile wall width,  $B_2$  is the sheet pile wall length,  $S$  is the clear spacing between sheet pile walls and  $S_{c-c}$  is the centre-to-centre spacing between sheet pile walls.

Figure 4.4 shows the estimated relationship between  $p_{ult}$  and the pile spacing interval ratio ( $S/S_{c-c}$ ) as calculated from Equation 4-3 and for varying ratios of sheet pile length ( $B_2$ ) to sheet pile width ( $B_1$ ). Figure 4.4a has an adhesion value ( $a$ ) of 1.0 and Figure 4.4b has  $a$  of 0.5. Soft clay is expected to have  $a$  of 0.8 to 1.0 and stiff clay is expected to have  $a$  of 0.4 to 0.5 (Broms, 1983).

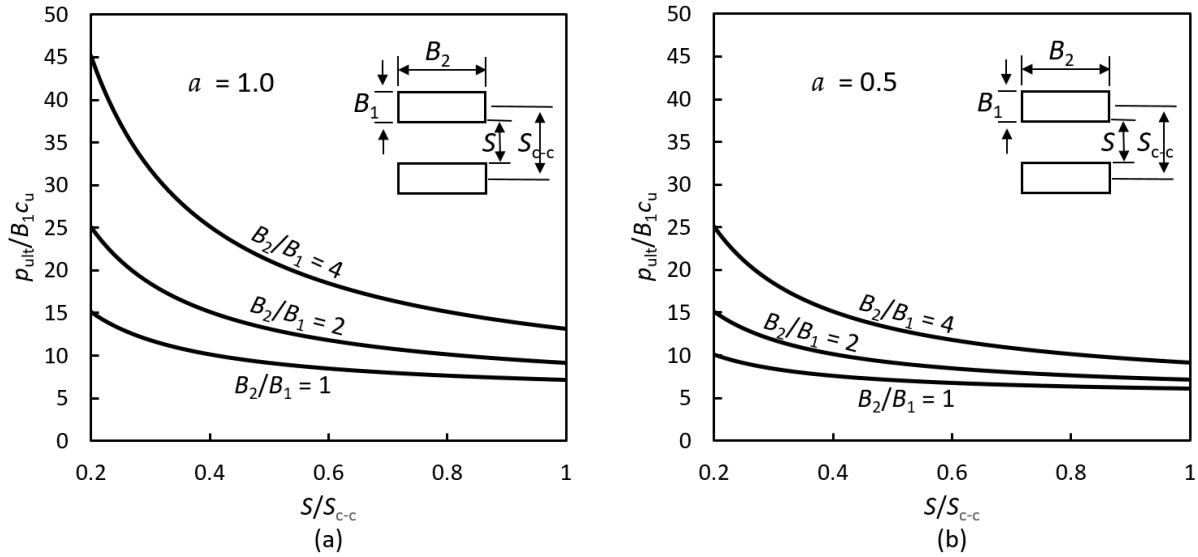


Figure 4.4: Ultimate resistance in clay for sheet pile groups in clay. (a) Adhesion factor of 1.0 (b) Adhesion factor of 0.5.

The ultimate soil resistance for a single sheet pile in clay for the flow-around failure method can be calculated from Equation 4-3 and can be observed from Figure 4.4 where the spacing between sheet piles is infinitely far where  $S_{c-c}/S = 1$ . The magnitude of  $p_{ult}$  for a single sheet pile can then be calculated as:

$$p_{ult} = 5.14c_u B_1 + 2ac_u B_2 \quad 4-4$$

### 4.3 Two-Dimensional Finite Element Model

Two-dimensional (2D) finite element (F.E.) modeling was performed using RS<sup>2</sup> (Rocscience, 2016) to investigate the performance of laterally loaded sheet pile walls. The load-deformation ( $p$ - $y$ ) curve and the ultimate lateral soil resistance ( $p_{ult}$ ) were estimated for the flow-around failure mechanism for a laterally loaded sheet pile in saturated clay. The 2D finite element model was calibrated to replicate the  $p$ - $y$  curve developed by Matlock (1970) from field testing for a circular pile in soft saturated clay. The model was also calibrated to reasonably match the spacing effects measured by Broms (1983) from lab testing of square piles in plane-strain conditions. After calibrating the model, the general setup of the model and assumptions made were then used to model sheet piles to estimate the load-deformation behaviour. The 2D F.E. model is described in

this section including the model setup in Section 4.3.1, model calibration in Section 4.3.2, and sheet pile geometry effects in Section 4.3.3.

#### 4.3.1 2D F.E. Model Setup

The 2D model was set up as a plan view of square or circular piles to analyze the load resistance which is passively developed from displacement of soil towards the piles. Since the model represents plane-strain conditions, the lateral load capacity is only representative of soil at depths where the overburden pressure is great enough to prevent upward heaving of the soil. A schematic of the general model set up is shown in Figure 4.5.

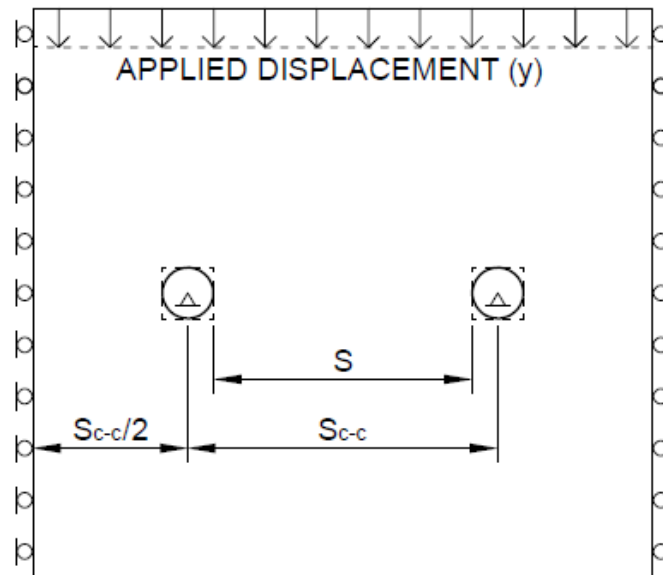


Figure 4.5: General 2D finite element model setup.

A graded mesh with 6 noded triangle elements was used to develop the mesh. The element density was increased near the pile regions. The quality of the mesh was checked to ensure there were no bad elements prior to running the models. In this case, bad elements were defined as elements with a maximum to minimum side length ratio greater than 30, elements with an angle less than  $2^\circ$ , elements with an angle greater than  $175^\circ$ , or inverted elements.

##### 4.3.1.1 Boundary Conditions

The piles are modeled as a square or circular material boundary within the boundaries of the model. The piles have a centre-to-centre spacing of  $S_{c-c}$  and the side outer boundaries are spaced

at  $S_{c-c}/2$  away from the centre of the piles. These side boundaries are fixed in the x-direction and are free to move in the y-direction. This is intended to represent the centre line between another pile outside of the model geometry to model an infinite series of piles. The only fixed nodes in the model are the centre of each pile.

Loading of the piles is simulated by applying a displacement to the top boundary of the soil mass towards the piles. The displacement in these preliminary models for calibration of the model was applied in numerous stages with an increment of 1 mm per stage. After computing, a query was applied along the top boundary where the displacement was applied to determine the y-direction reaction force. The y-direction force for each node along the top boundary was summed to calculate the lateral resistance for a given displacement. The lateral resistance was then divided by the number of piles to determine the lateral resistance per pile.

There is no stress or displacement boundary condition applied to the bottom boundary in the model. Therefore, this model setup with the applied boundary conditions are not suitable for frictional materials where the shear strength is dependent on the stress state. The boundary conditions will only provide reasonable results for purely cohesive soil.

#### **4.3.1.2 Material Properties**

An elastic-plastic constitutive model was applied to the clay with the shear strength governed by purely cohesive soil. The tensile strength of the clay was input as two times the cohesion. There was no reduction of shear strength or tensile strength for the input residual strength. Sensitivity analyses were performed by varying the elastic properties and strength properties of the clay as explained in detail in Section 4.3.2 to calibrate the 2D F.E. model.

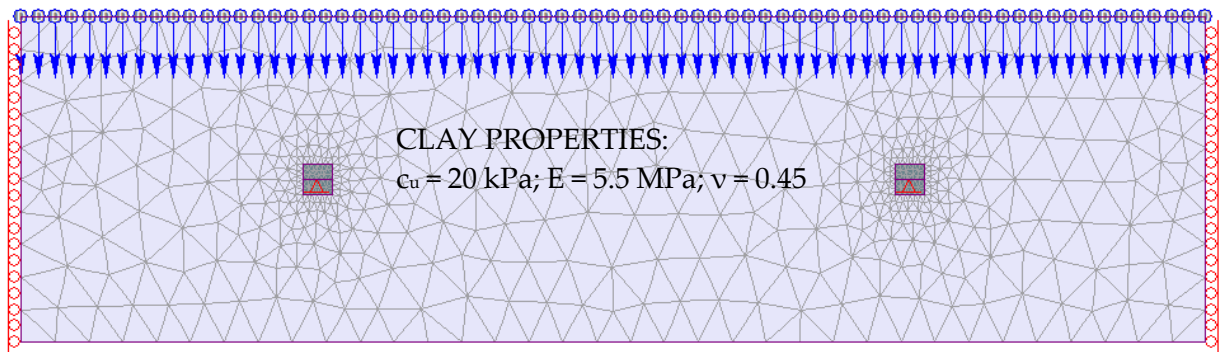
An elastic constitutive model was applied to the pile material properties. An elastic modulus of 200 GPa was applied to this material type with Poisson's ratio ( $\nu$ ) of 0.3 to be representative of the elastic properties of steel. The pile material is considerably stiff compared to the clay and will not yield. Therefore the resistance will develop passively from the deformation of the clay around the piles.

### 4.3.2 Model Calibration

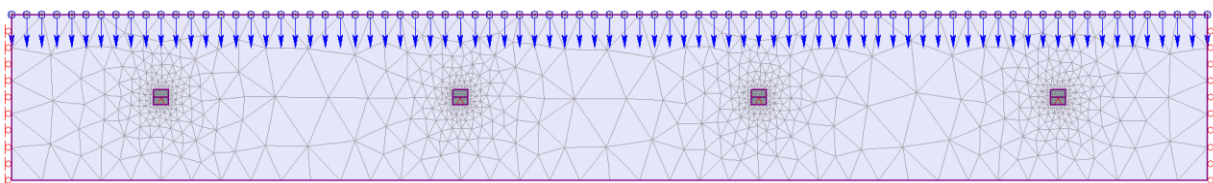
The 2D finite element model was calibrated to replicate the spacing effects for laterally loading square piles in plane-strain conditions as recorded by Broms (1983) as well as to replicate the  $p$ - $y$  curve by Matlock (1970) for circular piles. Square piles with a width of 40 mm in clay with undrained shear strength of 20 kPa were initially modeled which is in the range of pile dimensions and clay shear strength in the lab testing by Broms (1983).

#### 4.3.2.1 Sensitivity of Number of Piles

A sensitivity analysis for varying number of piles was initially performed to determine if the model geometry and boundary conditions represent an infinite series of piles. Figure 4.6 shows the arrangement of two square piles in Figure 4.6a and the arrangement of four square piles in Figure 4.6b. The pile dimensions and all material properties were modeled consistently for the two cases.



(a)



(b)

Figure 4.6:  $RS^2$  model geometry for sensitivity analysis of number of piles. (a) Two square piles (b) Four square piles.



The sum of the vertical reaction force for all nodes along the top boundary where the displacement was applied was divided by the number of piles to determine the resisting force per pile. The initial input elastic and strength parameters for the clay are shown in Figure 4.6. The piles were initially modeled with a spacing ratio of  $S/S_{c-c}$  equal to 0.95 so that there is negligible interference between adjacent piles. Figure 4.7 shows the displacement versus resisting force for the model with two piles and four piles. The results indicate that regardless of the number of piles, if the spacing between the outer piles and the side boundary is equal to half of the centre to centre pile spacing, then the load-deformation response is consistent. Therefore, the model setup represents an infinite series of piles and further models are all set up to include only two piles to decrease the number of nodes and simplify the model.

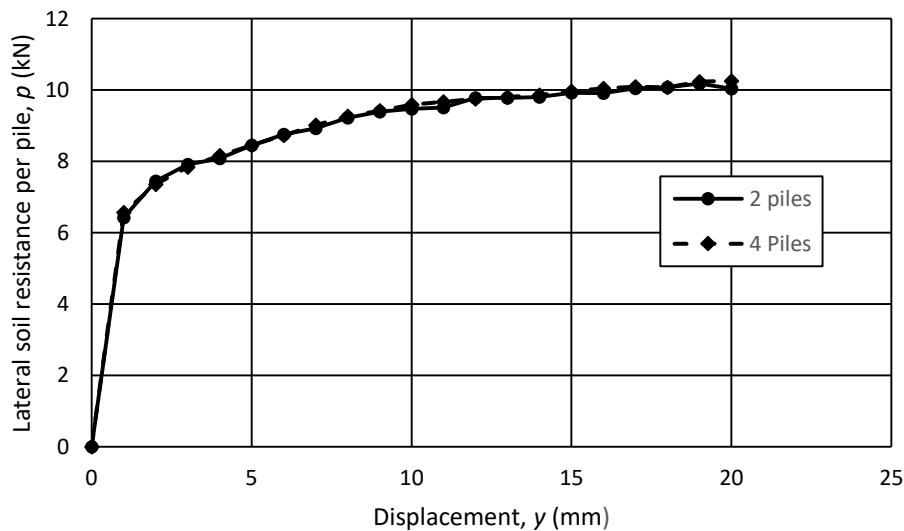


Figure 4.7: Displacement versus soil resistance showing sensitivity to number of piles.

#### 4.3.2.2 Sensitivity of Elastic Properties of Clay

Sensitivity analyses were then performed on the elastic clay properties including the Young's modulus and Poisson's ratio to observe the effect on  $p_{ult}$  and the load-deformation relationship.

For clays, the Young's modulus ( $E$ ) is usually related to the undrained shear strength and at relatively low load levels,  $E$  can be expected to range from  $150c_u$  to  $400c_u$  (Poulos and Davis, 1980). A sensitivity analysis was performed with  $E$  of 3.0 MPa, 5.5 MPa, and 8.0 MPa which is

equal to  $150c_u$ ,  $275c_u$ , and  $400c_u$  for the modelled undrained shear strength of 20 kPa. Figure 4.8 shows the  $p$ - $y$  relationship for the varying magnitudes of  $E$  for the clay.

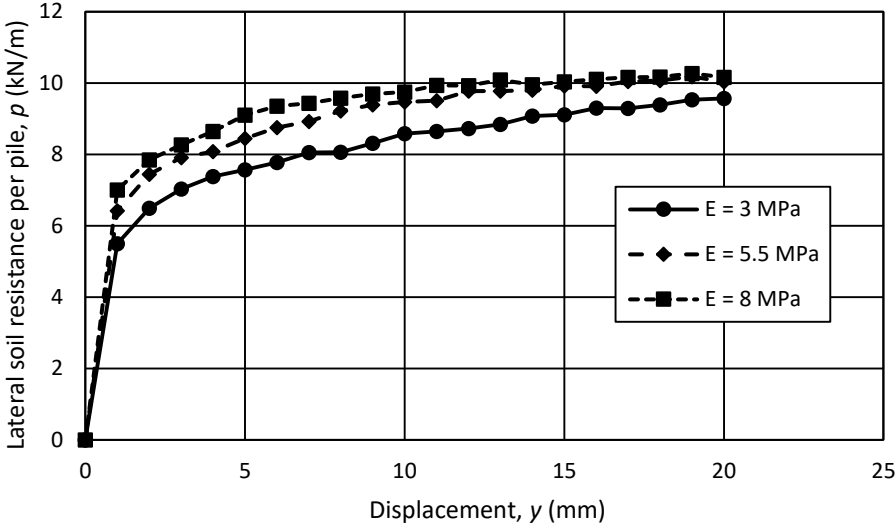


Figure 4.8: Displacement versus lateral soil resistance showing sensitivity to clay Young's Modulus.

The Poisson's ratio for saturated clay typically ranges from 0.4 to 0.5 (Bowles, 1996). A sensitivity analysis was performed with  $\nu$  of 0.4, 0.45, and 0.49. Figure 4.9 shows the  $p$ - $y$  relationship for the varying magnitudes of  $\nu$  with a constant  $E$  of 5.5 MPa.

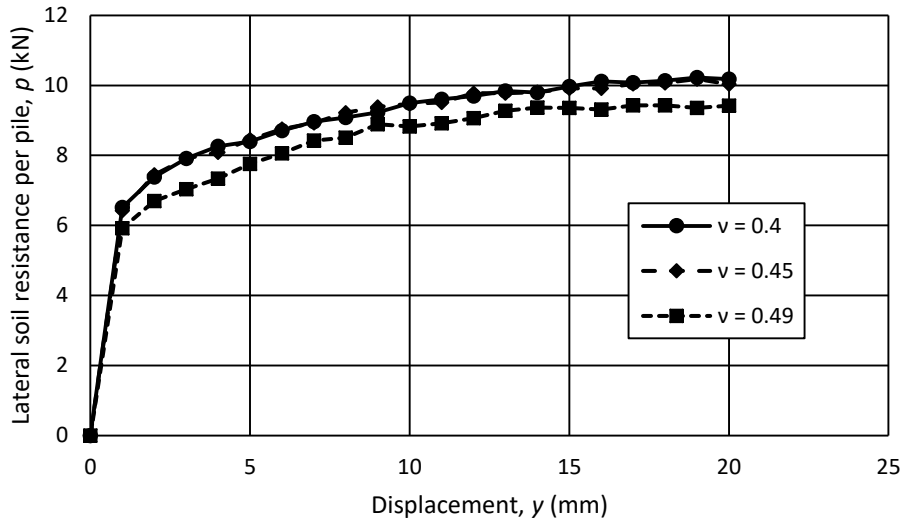


Figure 4.9: Displacement versus lateral soil resistance showing sensitivity to clay Poisson's ratio.

Based on the results shown in Figures 4.8 and 4.9, a laterally loaded pile in a stiffer clay with a greater  $E$  and lower  $\nu$  will result in a greater  $p_{ult}$  than a pile installed in a softer clay with a lower  $E$  and greater  $\nu$ . Moving further in the calibration of the 2D F.E. model,  $E$  of  $275c_u$  and  $\nu$  of 0.45 were input. This is in the middle of the expected range of Young's modulus (Poulos and Davis, 1980) and expected range of Poisson's ratio (Bowles, 1996) for saturated clay.

#### 4.3.2.3 Sensitivity of Pile-Soil Adhesion

In order to model varying magnitudes of adhesion between the pile and soil interface, a joint between the clay and steel pile boundary was introduced. Sensitivity analyses were performed on the shear strength of the joint and the stiffness of the joint.

The joint shear strength was modeled as a function of the undrained shear strength according to  $ac_u$  where  $a$  is an adhesion factor. The joint shear strength was modeled as 0, 10, and 20 kPa for an  $a$  of 0, 0.5, and 1.0 respectively. There is no tensile strength along the joint and was input as 0 kPa. The  $p$ - $y$  curves for the varying joint shear strengths is shown in Figure 4.10. It can be observed that  $p_{ult}$  decreases as the joint shear strength of soil-pile adhesion decreases. For soft clay with an undrained shear strength of 20 kPa as was modeled,  $a$  is expected to be near 1.0. The joint normal and shear stiffness was initially modelled equal to 55 MPa/m.

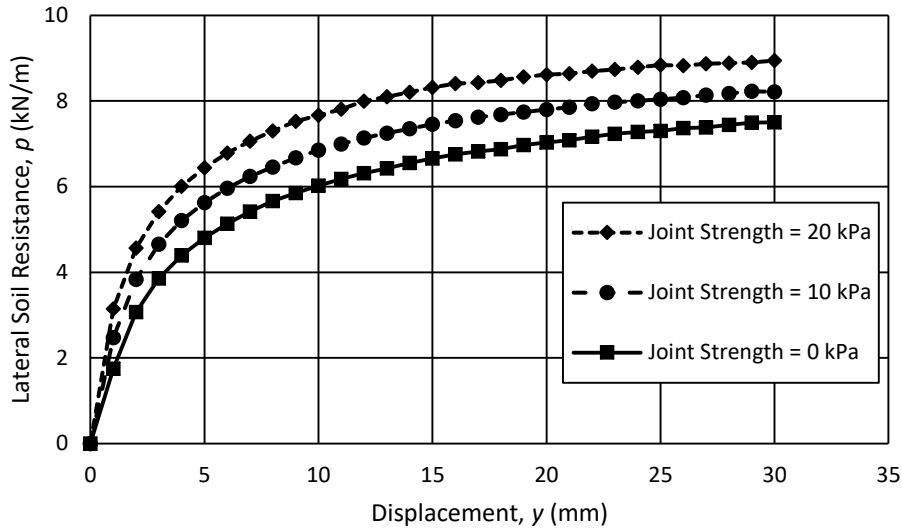


Figure 4.10: Modeled  $p$ - $y$  curve showing sensitivity to soil-pile adhesion.

A sensitivity analysis was also performed on the stiffness of the joint between the clay and steel pile boundary. The normal and shear stiffness were modelled to be equal in magnitude. The joint stiffness ( $k_n$ ) can be calculated from Pariseau (2007) as:

$$k_n = \frac{E_j}{h} \quad 4-5$$

where  $E_j$  is the Young's modulus of the joint and  $h$  is the thickness of the joint.  $E_j$  was taken as  $E$  of the clay.  $h$  was estimated as 0.01 m, 0.05 m and 0.1 m which resulted in a calculated  $k_n$  of 550 MPa/m, 110 MPa/m, and 55 MPa/m, respectively. The joint stiffness was modelled with these varying magnitudes to determine the effect of joint stiffness on the  $p$ - $y$  curve. Figure 4.11 shows the  $p$ - $y$  curves for the varying magnitudes of joint stiffness where the joint shear strength was input as 20 kPa. It can be observed that  $p_{ult}$  is relatively consistent regardless of the joint stiffness, however the initial stiffness and overall shape of the  $p$ - $y$  curve changes. A joint stiffness of 55 MPa/m provides the best fit to calibrate the  $p$ - $y$  curve to match Matlock's (1970) curve shown in Figure 4.12.

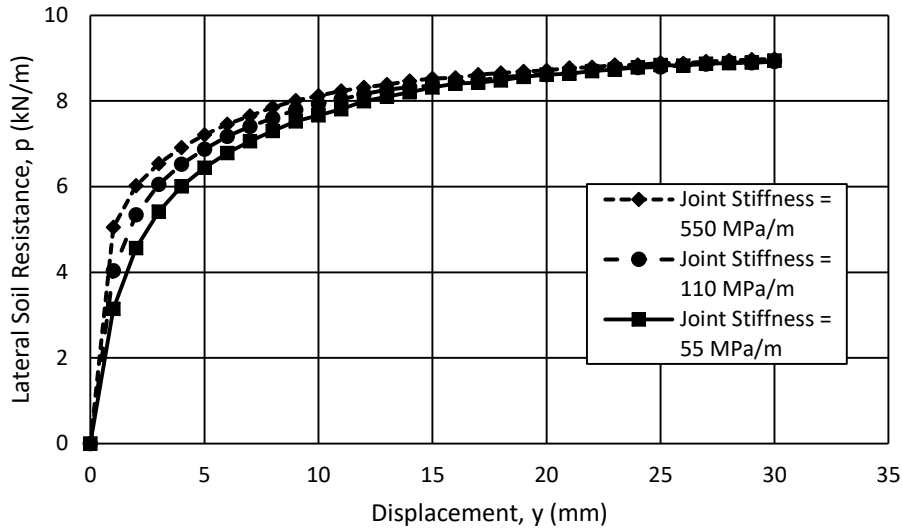


Figure 4.11: Modeled  $p$ - $y$  curve showing sensitivity to joint stiffness.

#### 4.3.2.4 Sensitivity of Pile Geometry

The pile geometry was modeled as both a square and circular pile. The modeled  $p$ - $y$  curve for both the square pile and circular pile is shown in Figure 4.12. The ultimate lateral resistance is greater for a square pile which is consistent with the theoretical calculations by Broms (1964). The expected  $p$ - $y$  curve for saturated soft clays as developed by Matlock (1970) is also shown in Figure 4.12. The Matlock (1970) curve shown in Figure 4.12 was plotted by calculating  $y_{50}$  assuming  $\epsilon_{50}$  of 0.02 as recommended by Peck et al. (1974) for soft clay and calculating  $p_{ult}$  as  $9c_u b$ . The 2D F.E. model reasonably predicts the resisting force for a given displacement based on Matlock's (1970) equation. Therefore, the model is reasonably calibrated with the following properties outlined in Table 4.1.

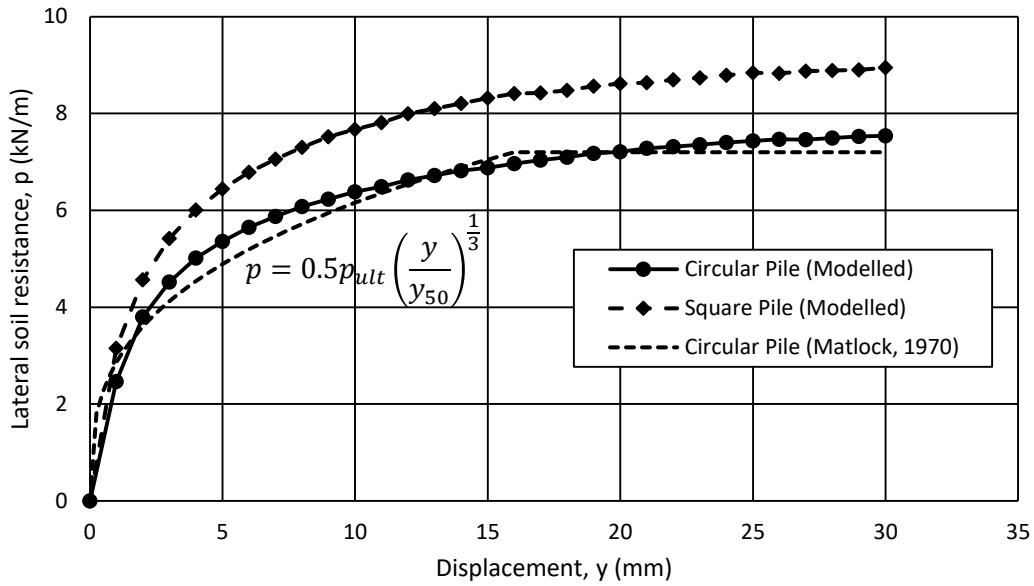
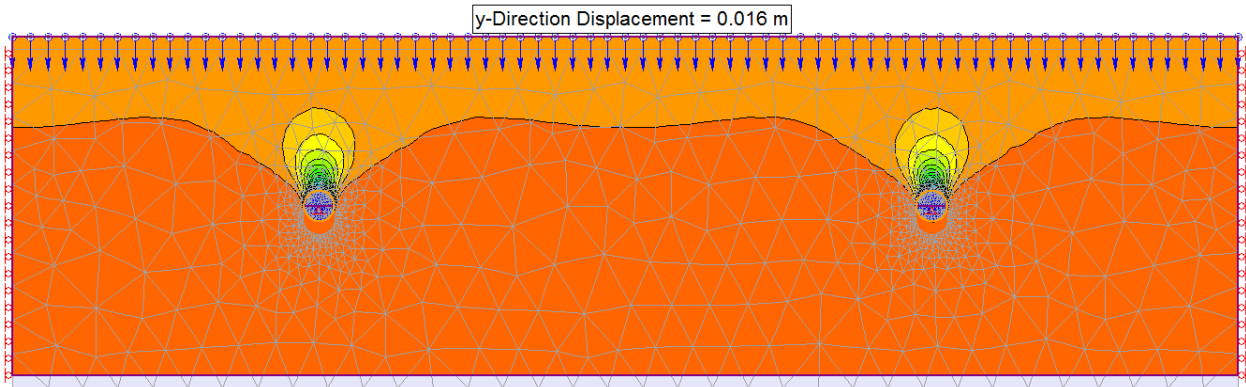


Figure 4.12: Modeled  $p$ - $y$  curve comparing circular and square pile geometry.

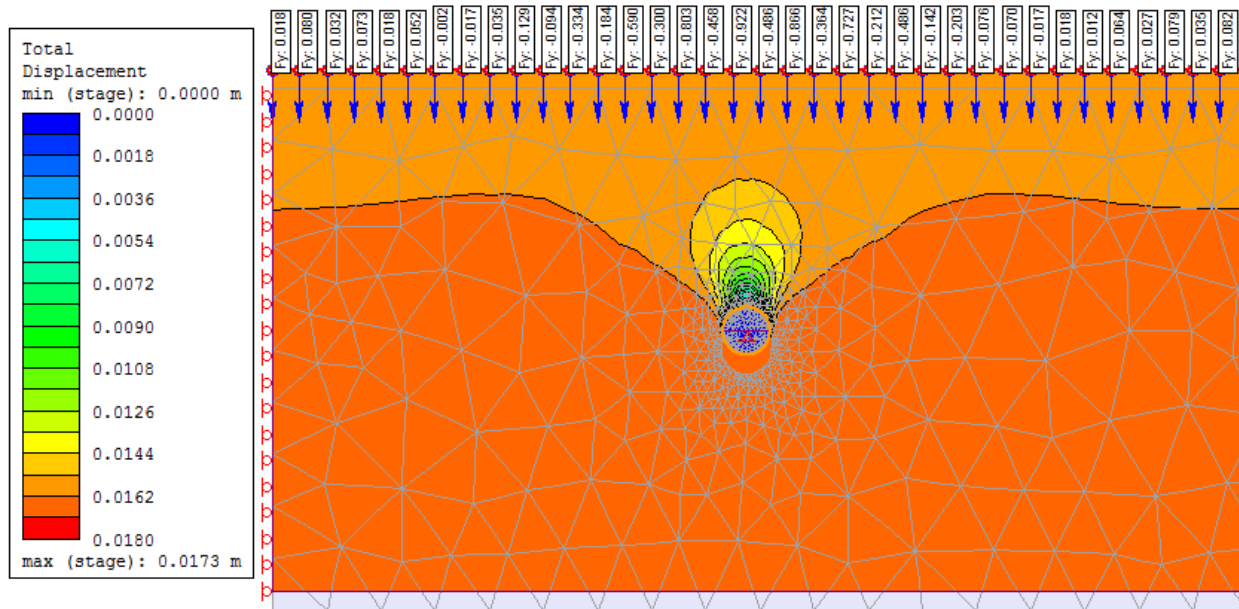
Table 4.1: Calibrated material properties for 2D finite element model of laterally loaded piles.

Property	Magnitude
Young's Modulus of Clay (kPa)	$275c_u$
Poisson's Ratio of Clay (kPa)	0.45
Tensile Strength of Clay (kPa)	$2c_u$
Shear Strength of Clay-Pile Interface (kPa)	$c_u$
Tensile Strength of Clay-Pile Interface (kPa)	0
Normal Stiffness of Clay-Pile Interface (kN/m)	$E/0.1 = 2750c_u$
Shear Stiffness of Clay-Pile Interface (kN/m)	$E/0.1 = 2750c_u$

Output from RS<sup>2</sup> for the calibrated model for a circular pile is shown below in Figure 4.13 below for a displacement of 16 mm along the top boundary. Figure 4.13a shows the entire model geometry and Figure 4.13b shows the left half of the model geometry to show a larger scale and more clearly display the results. Contours of total displacement are shown as well as the deformed mesh. The  $y$ -direction force is also shown in Figure 4.13b for each node along the top boundary.



(a)



(b)

Figure 4.13: RS<sup>2</sup> output for calibrated model of laterally loaded circular piles showing total displacement contours. (a) Entire model geometry (b) Left half of model geometry.

#### 4.3.2.5 Sensitivity of Pile Spacing

A sensitivity analysis was performed for varying spacing between square piles. Broms (1983) performed laboratory testing for this scenario with laterally loaded square piles in a plane-strain condition. Figure 4.14 shows the modelled  $p$ - $y$  curves for varying ratios of pile spacing  $S/S_{c-c}$ . The material properties in Table 4.1 were applied to the clay and clay-pile interface.

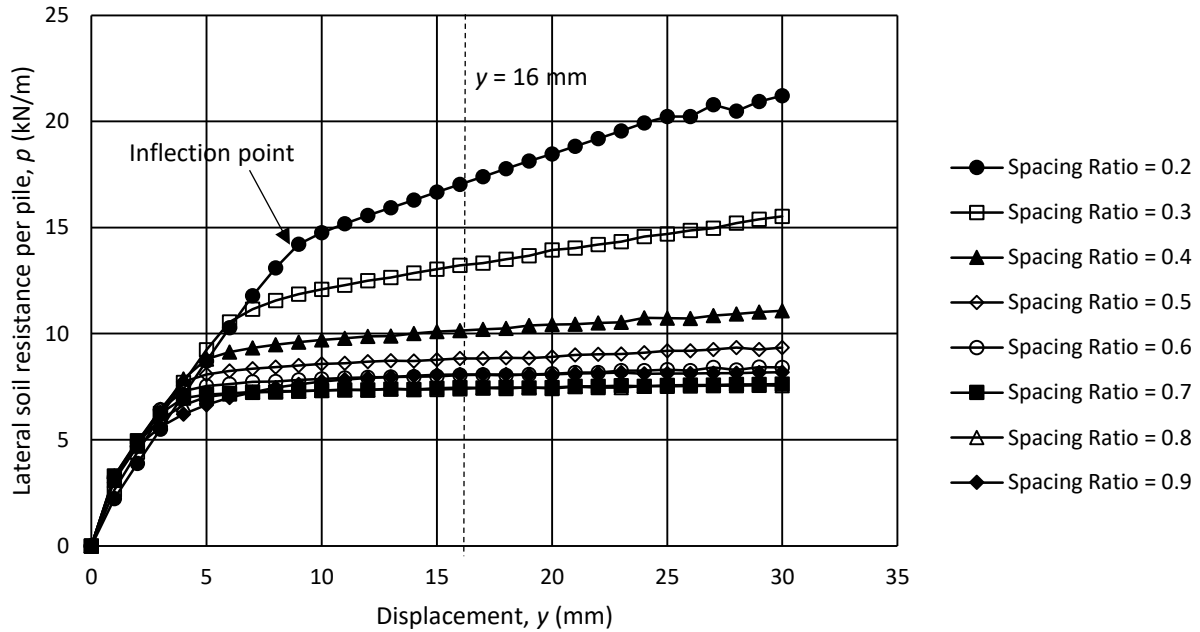
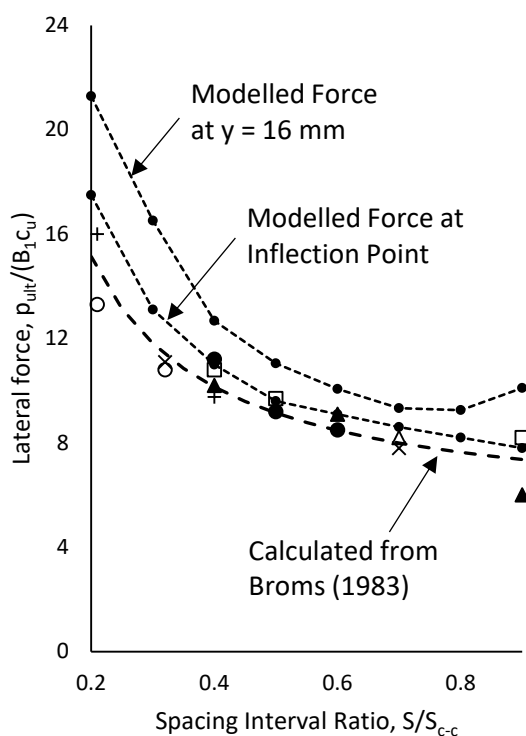


Figure 4.14: Modeled  $p$ - $y$  curve showing sensitivity to pile spacing.

Figure 4.15 shows the relationship between  $p_{ult}$  and the pile spacing interval ratio ( $S/S_{c-c}$ ) with the laboratory testing results by Broms (1983) and the 2D F.E. model results. The 2D F.E. model reasonably predicts the relationship of increasing ultimate lateral soil resistance for decreasing spacing. Selecting the magnitude of  $p_{ult}$  from Figure 4.14 requires interpretation and a range was therefore provided on Figure 4.15. The lower value for the modelled result was obtained from the inflection point illustrated on Figure 4.14. The larger value of  $p_{ult}$  was selected as the magnitude of  $p$  at a displacement of 16 mm or  $8y_{50}$  at which point  $p$  has plateaued according to the Matlock (1970)  $p$ - $y$  curve.





Lab Testing Data from Broms (1983)

$c_u$ (kPa)	b (mm)		
	20	30	40
9.8	△	●	+
16.7		□	○
22.4		▲	×

Figure 4.15: Comparison of 2D F.E. model results and laboratory testing results by Broms (1983).

#### 4.3.2.6 Sensitivity of Clay Shear Strength

A sensitivity analysis was performed on the shear strength of the clay to determine if the model accurately predicts a linearly proportional change in  $p_{ult}$  as predicted by theory. As  $c_u$  was modified, the elastic modulus, joint stiffness, and joint strength parameters were all proportionally modified according to the calibrated material properties in Table 4.1. The undrained shear strength was input as 10 kPa, 20 kPa, 50 kPa, and 100 kPa. Figure 4.16a shows the  $p$ - $y$  curves for a square pile and varying undrained shear strengths of clay and Figure 4.16b shows  $p_{ult}$  versus  $c_u$ . The value of  $p_{ult}$  was selected as the magnitude of  $p$  at  $y$  of  $8y_{50}$  or 16 mm at which point  $p$  has plateaued according to the Matlock (1970) curve. It is observed that  $p_{ult}$  and  $c_u$  have a linear relationship and therefore  $N_c$  is constant regardless of  $c_u$ , consistent with generally accepted theory.

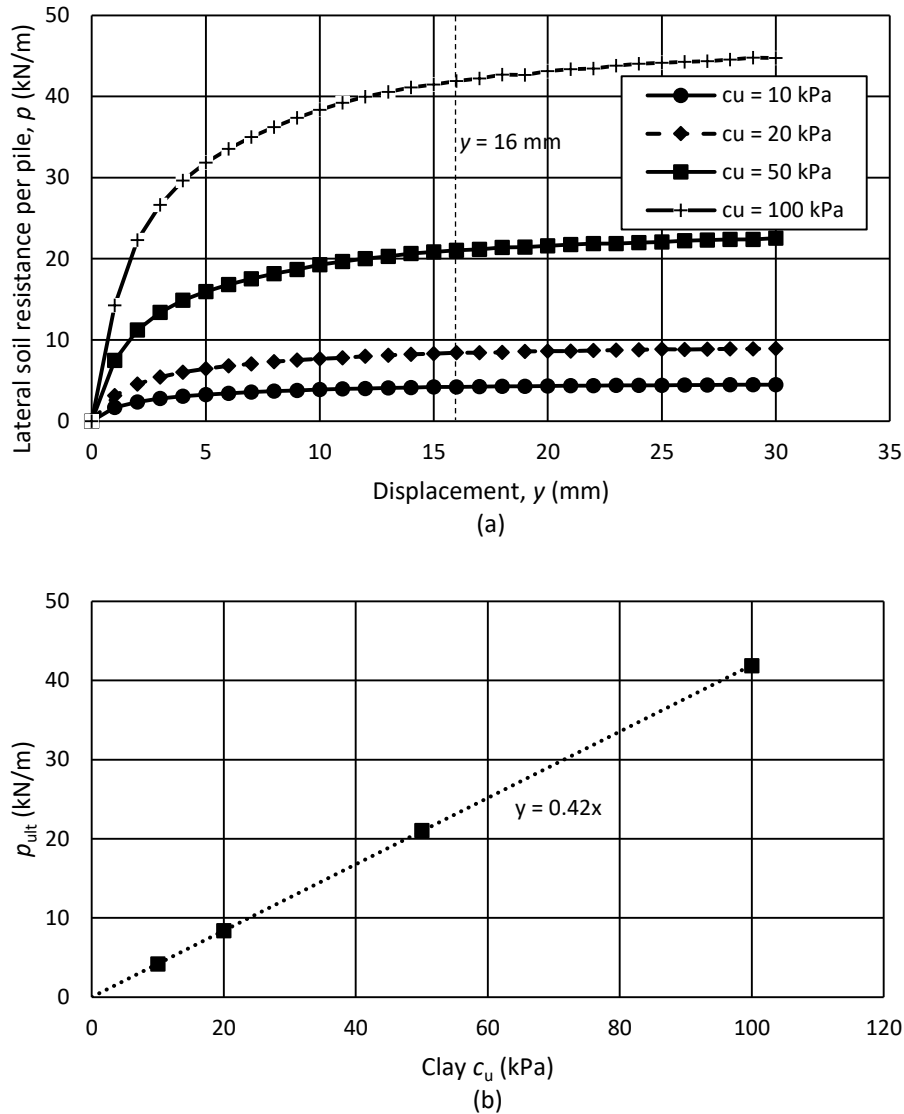


Figure 4.16: Sensitivity to clay undrained shear strength. (a)  $p$ - $y$  curves (b)  $c_u$  versus  $p_{ult}$ .

#### 4.3.2.7 Sensitivity of Pile Width

A sensitivity analysis was performed on the width ( $b$ ) of the square piles to determine if the model accurately predicts a linearly proportional change in  $p_{ult}$  as predicted by theory. The pile width was input as 40, 80, and 160 mm. Figure 4.17a shows the  $p$ - $y$  curves for varying pile widths and Figure 4.17b shows  $p_{ult}$  versus  $b$ .  $p_{ult}$  was again selected at  $y$  of  $8y_{50}$  or  $y$  equal to 16 mm, 32 mm, and 64 mm for  $b$  of 0.04 m, 0.08 m, and 0.16 m, respectively. It is observed that  $p_{ult}$  and  $b$  have a linear relationship and therefore  $N_c$  is constant regardless of  $b$ , consistent with generally accepted theory.

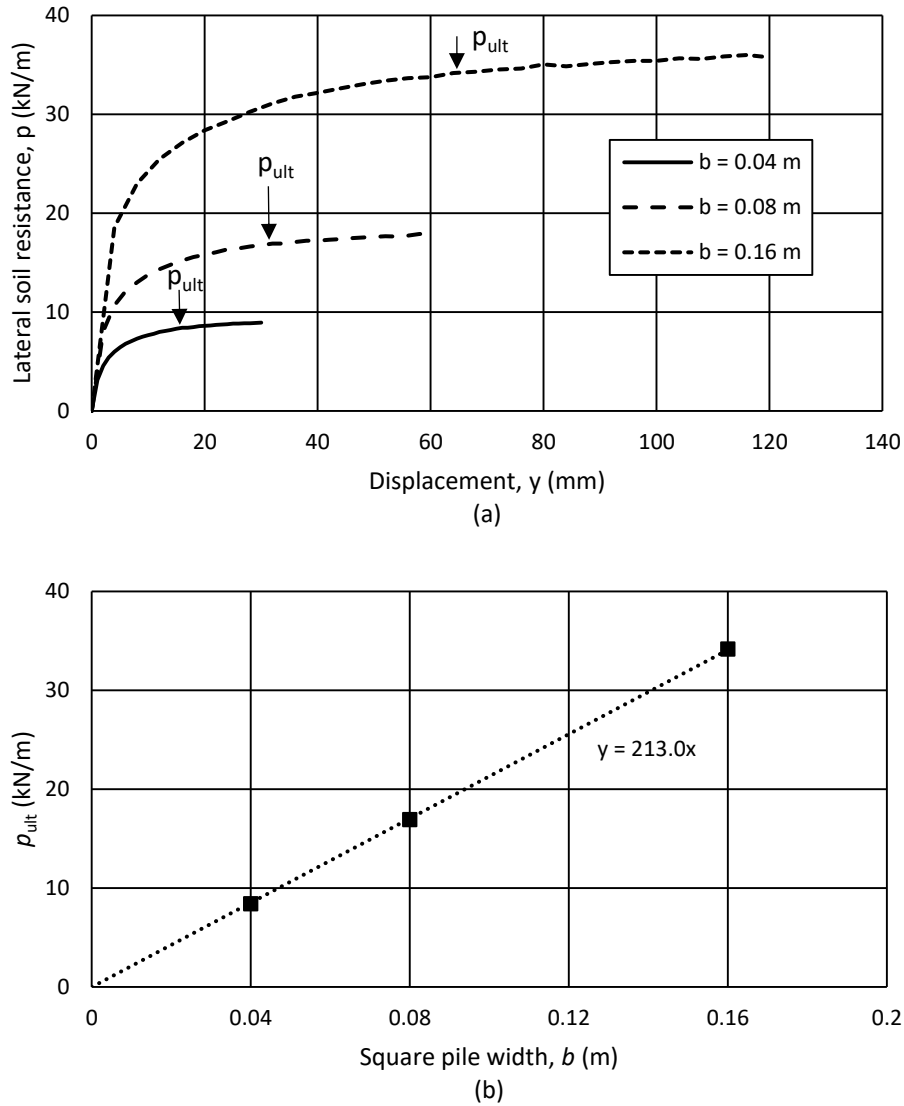


Figure 4.17: Sensitivity to square pile width. (a) Modeled  $p$ - $y$  curves (b) Pile width versus  $p_{ult}$ .

### 4.3.3 Sheet Pile Geometry Effects

After calibrating the 2D F.E. model to reasonably reflect the laboratory testing results by Broms (1983) and the field testing results by Matlock (1970), the pile geometry was then modified to represent sheet pile walls for Hardy Ribs as shown in Figure 4.18. The geometry of the sheet pile wall was simplified as a rectangle of width  $B_1$  and length  $B_2$ . The spacing between piles was large with a spacing ratio  $S/S_{c-c}$  of 0.95 to prevent interference between the adjacent piles. With a constant pile width of 40 mm, the pile length was modeled at varying ratios of  $B_2/B_1$  of 1, 2, 4, 8, and 16.

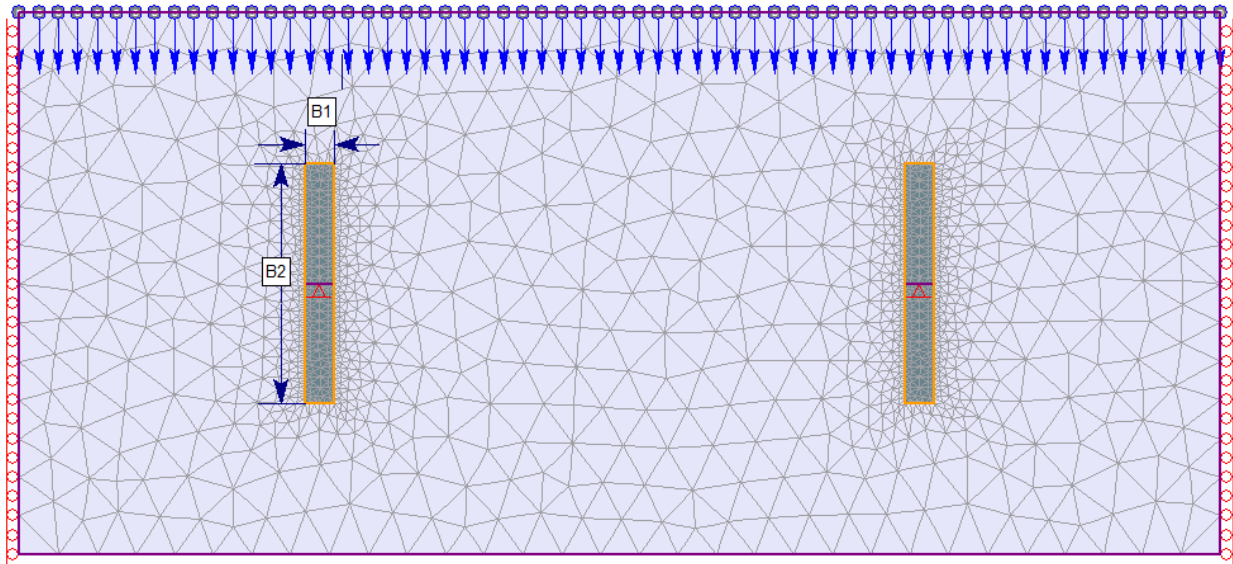
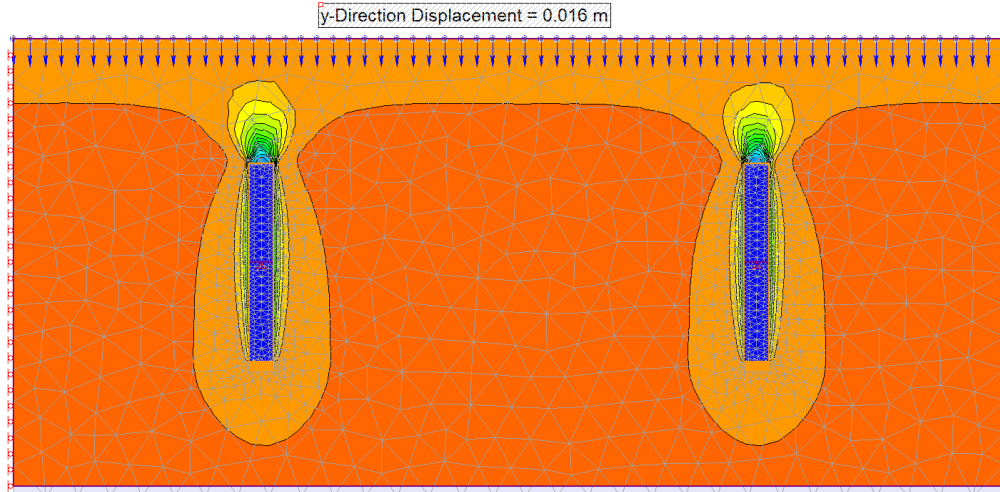
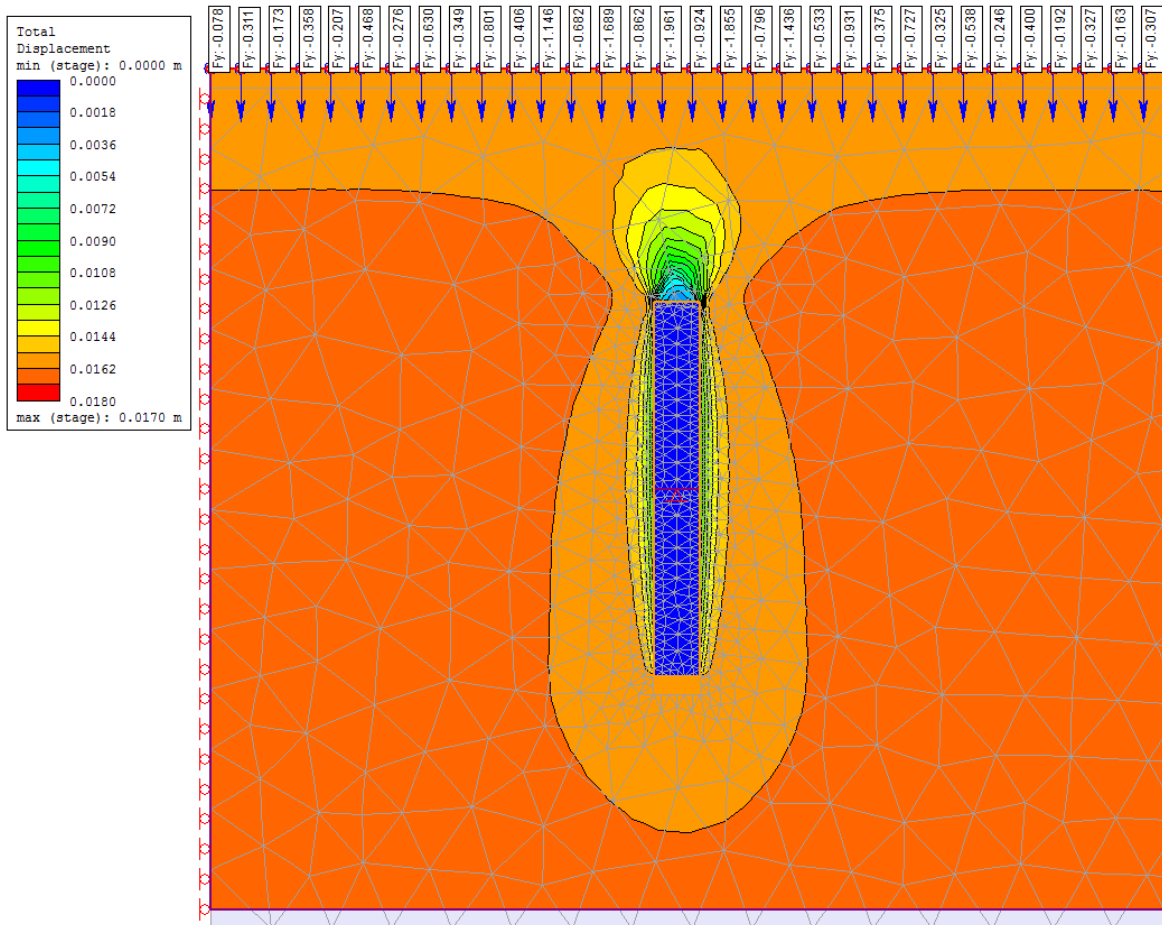


Figure 4.18: RS<sup>2</sup> model showing sheet pile geometry.

Output from RS<sup>2</sup> for a rectangular pile with  $B_2/B_1$  equal to 8 is shown below in Figure 4.19 below for a displacement of 16 mm along the top boundary. Figure 4.19a shows the entire model geometry and Figure 4.19b shows the left half of the model geometry to show a larger scale and more clearly display the results. Contours of total displacement are shown as well as the deformed mesh. The y-direction force is also shown in figure 4.19b for each node along the top boundary.



(a)



(b)

Figure 4.19: RS<sup>2</sup> output for model of rectangular piles. (a) Entire model geometry (b) Left half of model geometry.

The  $p$ - $y$  curves for each of the  $B_2/B_1$  ratios is shown in Figure 4.20a. The  $p$ - $y$  curve is observed to have greater stiffness at small displacements for increasing ratios of  $B_2/B_1$ . The magnitude of  $p_{ult}$  is also observed to increase and is plotted versus  $B_2/B_1$  in Figure 4.20b.  $p_{ult}$  is observed to increase linearly with increasing  $B_2/B_1$ . Figure 4.21 shows the model results when the joint shear strength is equal to half of the clay shear strength which is representative of an adhesion factor of 0.5 at the pile-soil interface. The value of  $p_{ult}$  was again selected as the magnitude of  $p$  at a displacement of  $8y_{50}$  or 16 mm.

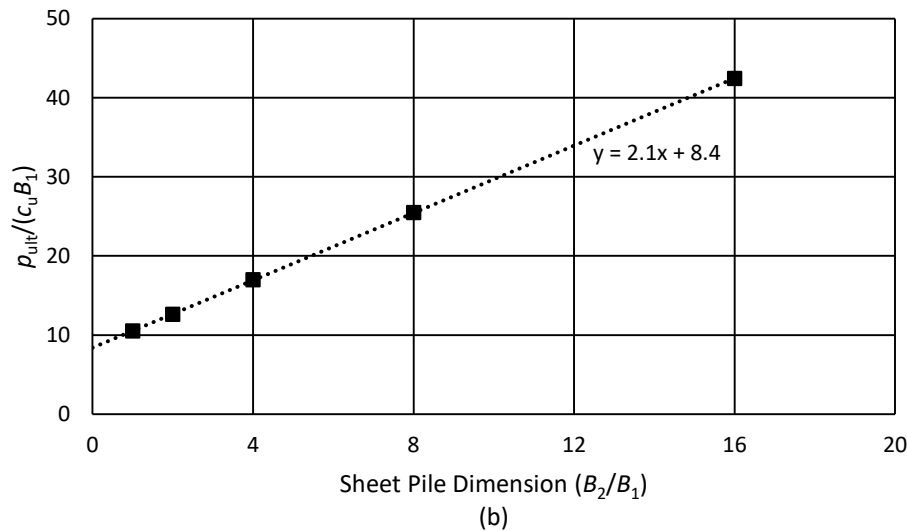
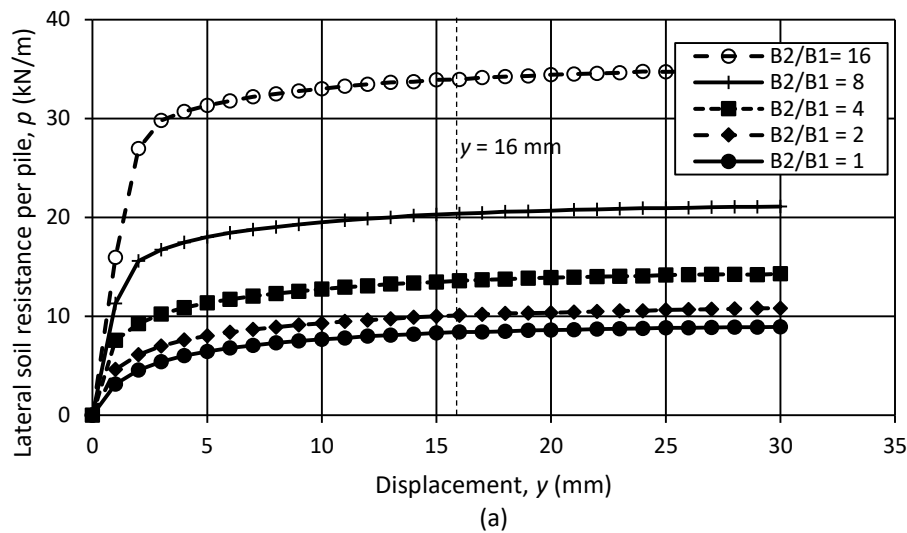


Figure 4.20: Sensitivity to sheet pile dimensions with adhesion factor of 1.0. (a) Modeled  $p$ - $y$  curves (b)  $B_2/B_1$  versus  $p_{ult}$ .

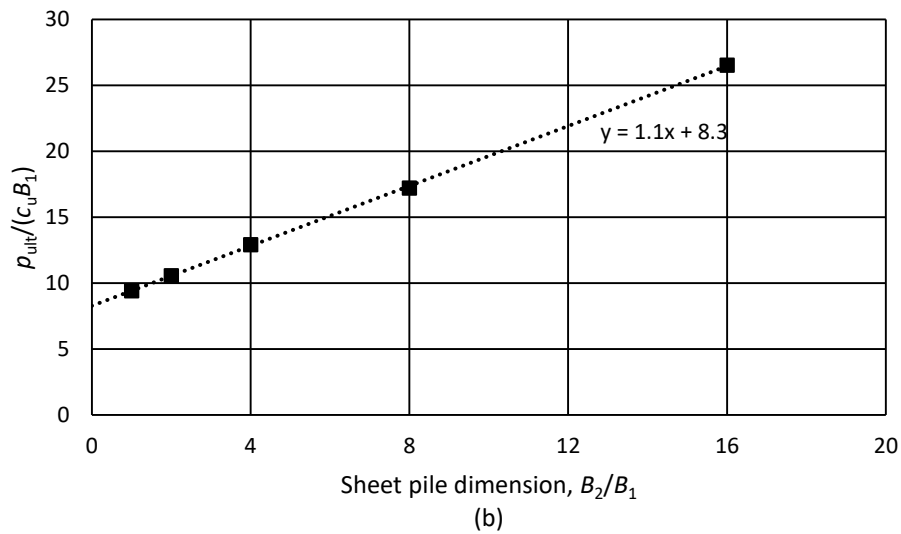
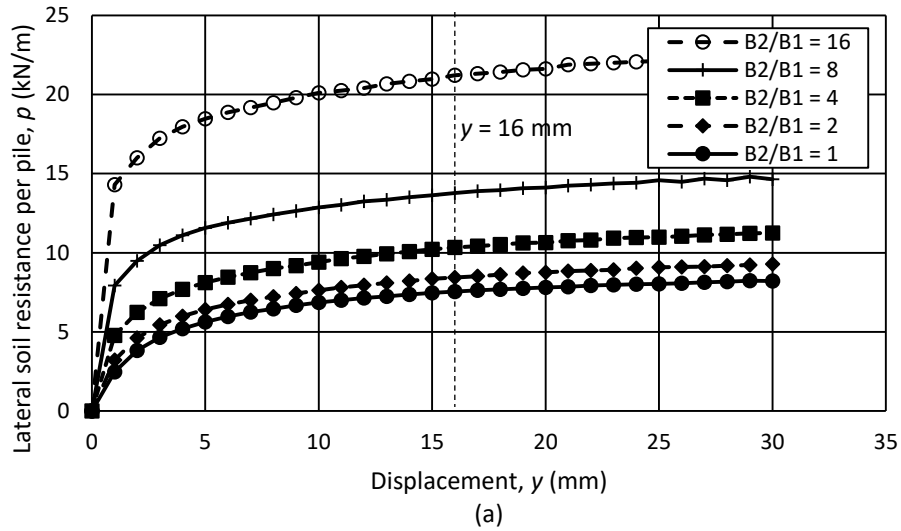


Figure 4.21: Sensitivity to sheet pile geometry with adhesion factor of 0.5. (a) Modeled  $p$ - $y$  curve (b)  $B_2/B_1$  versus  $p_{ult}$ .

Based on the linear line of best in Figure 4.20b and Figure 4.21b, there appears to be a component of the ultimate lateral resistance related to the sheet pile width and is approximately equal to  $8.4c_u B_1$ . The slope of the line indicates that  $p_{ult}$  increased with an increasing sheet pile length due to the increase in frictional resistance along the sides of the rectangular pile. The slope of the line of best fit in Figures 4.20b and 4.21b are both approximately equal to  $2a$ . This is expected considering the frictional resistance would have to be exceeded on both sides of the rectangular pile to reach the ultimate resistance.

Based on the 2D F.E. model of rectangular piles, the ultimate lateral resistance of a single sheet pile can be estimated from:

$$p_{ult} = 8.4c_u B_1 + 2ac_u B_2 \quad 4-6$$

This formula is only accurate for plane-strain conditions and for a single sheet pile wall or sheet pile walls that are spaced sufficiently far apart.

#### 4.4 Summary of Laterally Loaded Sheet Pile Walls

Three methodologies were used to estimate the ultimate lateral soil resistance for the flow-around failure mode of a single laterally loaded sheet pile wall. This included extending the block-soil model by Reese (1958) to a rectangular pile, applying Broms (1983) theoretical equation to rectangular piles, and performing 2D F.E. modeling. Each of the methodologies resulted in similar expressions for calculating  $p_{ult}$ . These included a lateral end-bearing component related to the sheet pile width and a frictional component that is proportional to two times the sheet pile length. The 2D F.E. modeling provided the most insight into the load-deformation behaviour and it appears that increasing the sheet pile length results in a greater initial stiffness in the  $p$ - $y$  curve.

The expressions developed for calculating  $p_{ult}$  for a sheet pile wall can be compared to the value calculated using an equivalent circular diameter ( $b_{eq}$ ) from Equation 2-11 by Reese & Van Impe (2011). Assuming that  $N_c$  for a circular pile is equal to 9, then  $p_{ult}$  for a rectangular pile or sheet pile wall can be calculated based on  $b_{eq}$  as:

$$p_{ult} = 9c_u b_{eq} = 9c_u \left[ B_1 \left( \frac{9c_u B_1 + 2 \left( B_2 - \frac{B_1}{2} \right) ac_u}{9c_u B_1} \right) \right] = (9 - a)c_u B_1 + 2ac_u B_2 \quad 4-7$$

Based on this expression, the lateral end bearing component ranges from 9 for when  $a = 1$  to 8 when  $a = 0$ . There is similarly a component of the lateral resistance related to the pile length. Therefore the solutions provided in Sections 4.1 through 4.3 provide relatively consistent results with the expression developed by Reese & Van Impe (2011).



The proposed distribution of ultimate lateral resistance with depth is shown below in Figure 4.22.  $p_{ult}$  for the near-surface soil where a passive wedge will develop is estimated to be equal the equation proposed by Matlock (1970) for circular piles plus an additional frictional force along the sides of the sheet pile. This distribution of  $p_{ult}$  with depth is only suitable however for a single sheet pile whereas the Hardy Ribs system consists of a series of sheet piles that are closely spaced together. The effects of spacing for a row of sheet piles is discussed in detail in Chapter 5.0.

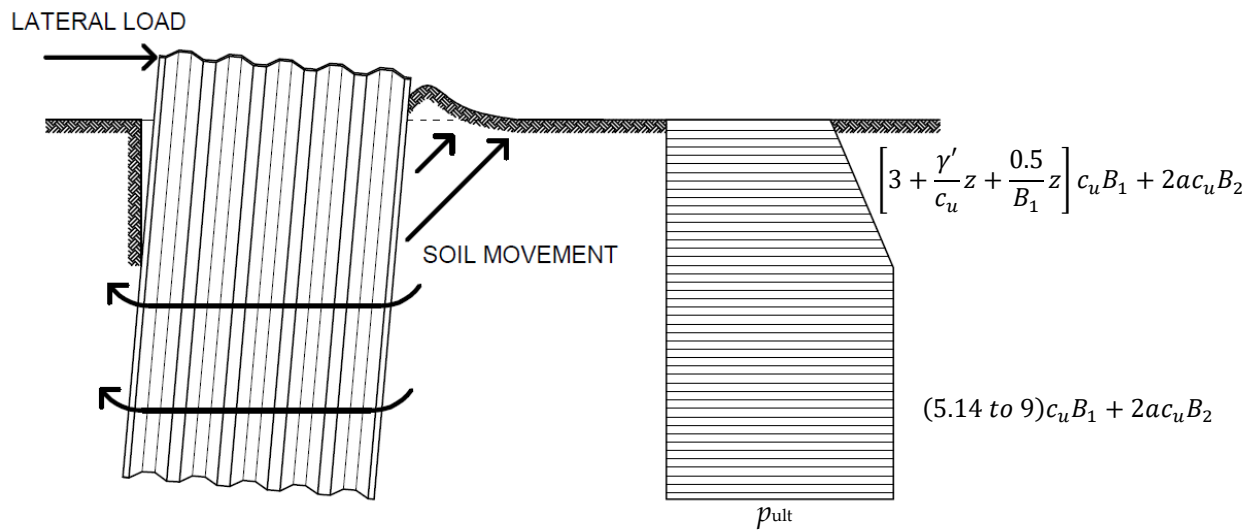


Figure 4.22: Distribution of ultimate soil resistance with depth.

## 5.0 SHEET PILE WALL SPACING EFFECTS

When adjacent sheet pile walls in a Hardy Ribs system are spaced close together, the ultimate lateral resistance for each sheet pile will be reduced due to spacing effects. This differs from the spacing effects studied in Section 4.3.2.5 where the 2D F.E. model and the lab testing data by Broms (1983) represented plane strain conditions. The resisting force per linear metre along the landslide will however increase as sheet pile wall spacing decreases until a critical spacing. For spacing less than this critical spacing, the soil between laterally loaded sheet pile walls will move with the sheet pile walls and the system acts as a continuous wall. This critical spacing between sheet pile walls is studied in Section 5.1. Three dimensional (3D) finite element modeling was performed to examine the findings and is discussed in Section 5.2.

### 5.1 Critical Sheet Pile Spacing

A limit equilibrium solution was developed to calculate this critical spacing that prevents soil from squeezing between adjacent sheet pile walls and to calculate the ultimate lateral soil resistance. The Hardy Ribs spacing findings are discussed for cohesive soil in Section 5.1.1 and for cohesionless soil in Section 5.1.2.

#### 5.1.1 Cohesive Soil

To prevent soil from squeezing between the parallel rows of sheet piles and to force the soil to move in unison with the sheet piles, a sufficiently long sheet pile length ( $B_2$ ) and a sufficiently small spacing ( $S$ ) between sheet piles is required (Figure 5.1a). If the piles are spaced closely, a continuous wall of soil will move at the leading edge of the sheet pile walls. This will cause a passive wedge to fail and an active wedge failure would occur on the opposite end of the sheet pile walls. A block of clay between two sheet piles is considered as shown in Figure 5.1b. The forces acting on the wedge include the shear force from the side of the sheet piles, the driving force from the continuous active wedge and the resisting force from the continuous passive wedge. The maximum forces acting on the clay block from the side cohesion of the sheet piles and the passive earth-pressure are illustrated in Figure 5.1c. The passive and active earth-pressure can be estimated by Rankine's theory for undrained conditions.

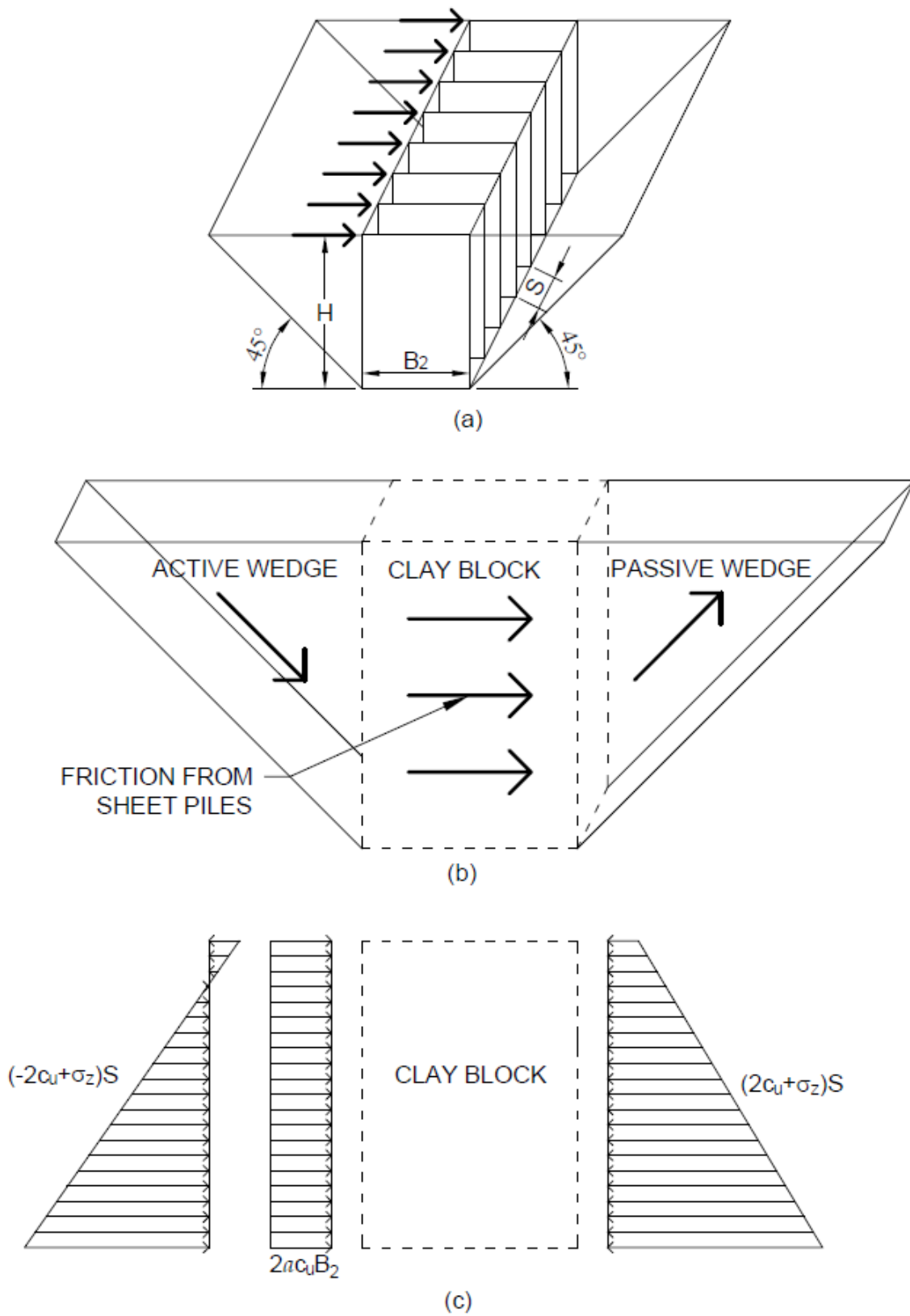


Figure 5.1: Closely spaced sheet pile walls in cohesive soil.

In order to force the Hardy Ribs system to act as a continuous wall, the critical failure mechanism must be controlled such that force resulting from the passive and active earth-pressures is less than the resulting force from the cohesion along the sheet pile walls along the entire depth of the sheet piles. This relationship is given for any depth as:

$$[(2c_u + \gamma z) - (-2c_u + \gamma z)]S < 2ac_u B_2 \quad 5-1$$

where  $c_u$  is the undrained shear strength,  $\gamma$  is the unit weight of the soil,  $z$  is the depth below ground surface,  $S$  is the spacing between sheet pile walls, and  $B_2$  is the length of the sheet pile walls. This expression can be simplified and rearranged to solve for a maximum spacing for a given sheet pile length given by:

$$S < \frac{aB_2}{2} \quad 5-2$$

Alternatively, this expression can be rearranged to solve for a minimum sheet pile length for a given spacing given by:

$$B_2 > \frac{2S}{a} \quad 5-3$$

If an appropriate combination of sheet pile length and spacing are selected based on the equation above, then any sheet pile width ( $B_1$ ) can be selected and the Hardy Ribs system will act as a continuous wall. The ultimate lateral load capacity at a given depth can then be calculated for the sheet piles of the Hardy Ribs provided that the system moves as a continuous wall. This can be calculated as the difference of passive and active earth-pressures multiplied by the centre-to-centre spacing between sheet pile walls. The ultimate lateral load capacity is given by:

$$p_{ult} = [(2c_u + \gamma z) - (-2c_u + \gamma z)](S + B_1) = 4c_u S_{c-c} \quad 5-4$$

where  $z$  is the depth below ground surface,  $B_1$  is the sheet pile wall width, and  $S_{c-c}$  is the centre-to-centre spacing between sheet pile walls. Where the active earth pressure is negative, it should be neglected and treated as equal to 0 to be conservative and not rely on the tensile strength of the cohesive soil. When neglecting tension,  $p_{ult}$  can be calculated as:

$$p_{ult} = (2c_u + \gamma z)(S + B_1) = (2c_u + \gamma z)S_{c-c} \quad 5-5$$

An appropriate magnitude of  $p_{ult}$  can be determined by calculating with depth and selecting as the lesser value from Equation 5-4 and Equation 5-5.

### 5.1.2 Cohesionless Soil

A similar expression is proposed for cohesionless soil to calculate the critical spacing between sheet piles in a Hardy Ribs system to ensure the sheet piles and soil between the sheet piles move as a continuous wall. An infinite series of sheet pile walls is considered that undergo horizontal displacement as illustrated in Figure 5.2. The forces acting on a block of soil between sheet piles is illustrated in Figure 5.2b. This includes the frictional force acting along the sides of the soil block, the resisting force from a continuous passive wedge, and a driving force from a continuous active wedge. The active and passive earth pressures are estimated by Rankine's theory. The maximum forces acting on the sand block from horizontal displacement of the sheet piles is shown in Figure 5.2c. This includes the side friction of the sheet piles and the passive and active earth-pressures.

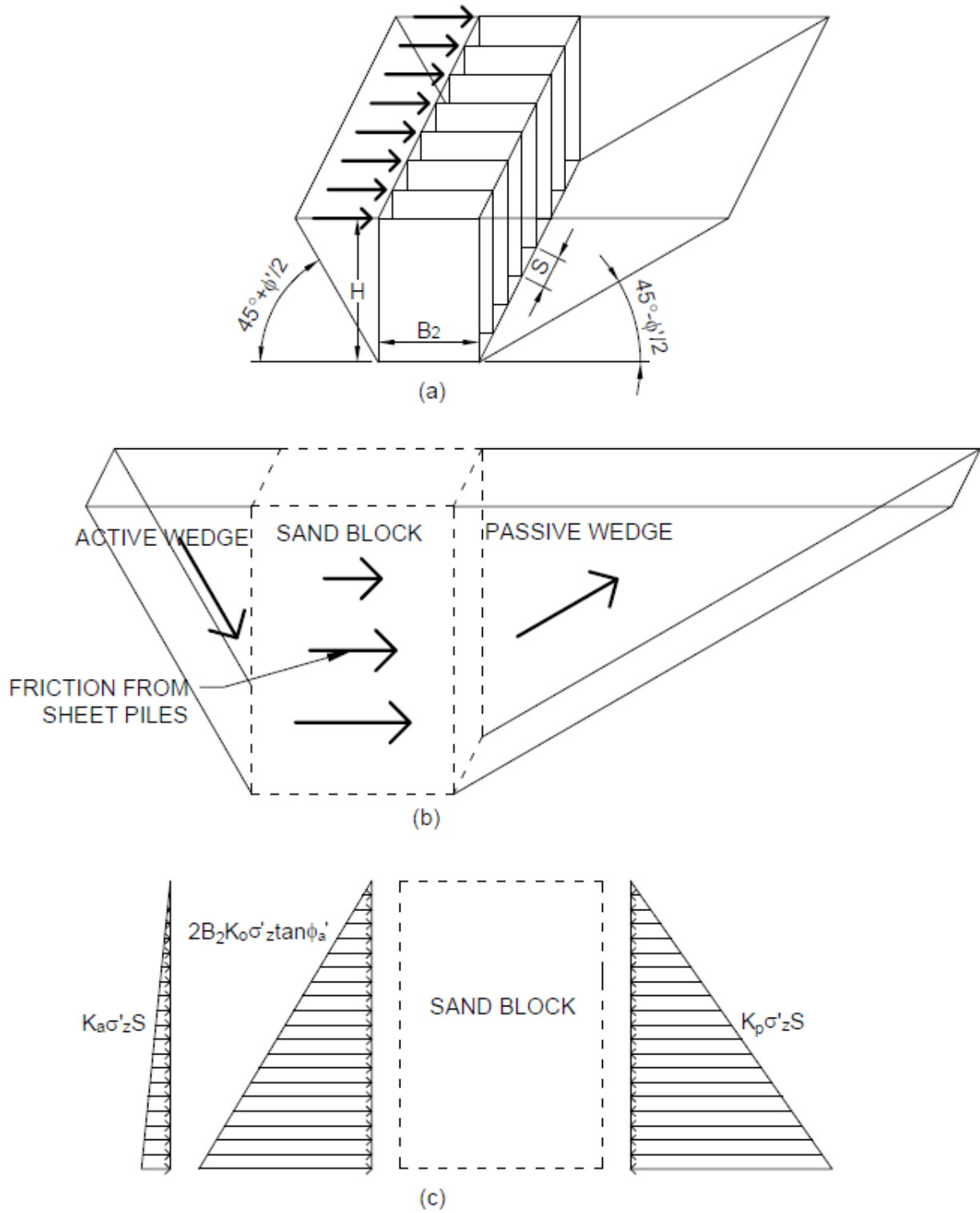


Figure 5.2: Closely spaced sheet pile walls in cohesionless soil.

To achieve the maximum lateral resistance, the performance of the Hardy Ribs system must be forced to act as a continuous wall. The critical failure mechanism must be controlled such that the force resulting from the passive and active earth-pressures is less than the force from the friction along the sheet pile walls. This relationship is given by:

$$\gamma'z(K_p - K_a)S < 2B_2K_0\gamma'z\tan\phi_a \quad 5-6$$

where  $\gamma'$  is the effective unit weight,  $z$  is the depth below ground surface,  $K_p$  is Rankine's passive earth pressure coefficient,  $K_a$  is Rankine's active earth pressure coefficient,  $K_0$  is the at-rest earth pressure coefficient,  $S$  is the spacing between sheet pile walls,  $B_2$  is the sheet pile wall length, and  $\phi_a$  is the friction angle between the sheet pile and soil interface. Equation 5-6 can be simplified and rearranged to solve for a maximum spacing for a given sheet pile length given by:

$$S < \frac{2B_2K_0\tan\phi_a}{(K_p - K_a)} \quad 5-7$$

The expression can similarly be rearranged to solve for a minimum sheet pile wall length for a given spacing given by:

$$B_2 > \frac{S(K_p - K_a)}{2K_0\tan\phi_a} \quad 5-8$$

If an appropriate combination of sheet pile length and spacing are selected based on the equation above, then any sheet pile width can be selected and the Hardy Ribs system will act as a continuous wall. The ultimate lateral load capacity at a given depth can then be calculated for the sheet piles of a Hardy Ribs provided that the system moves as a continuous wall. This can be calculated as the difference of passive and active earth-pressure multiplied by the centre-to-centre spacing between sheet pile walls expressed by:

$$p_{ult} = \gamma'z(K_p - K_a)(S + B_1) = \gamma'z(K_p - K_a)S_{c-c} \quad 5-9$$

where  $z$  is the depth below ground surface,  $B_1$  is the sheet pile wall width and  $S_{c-c}$  is the centre-to-centre sheet pile wall spacing.

## **5.2 Three-Dimensional Finite Element Modeling**

Three dimensional (3D) finite element (F.E.) modelling was performed using RS<sup>3</sup> (Rocscience, 2016) to investigate the critical spacing that prevents soil from squeezing between sheet piles in cohesive soil. This enables the Hardy Ribs to act as a continuous wall.

### **5.2.1 3D F.E. Model Geometry and Mesh**

The general geometry of the 3D F.E. model consists of a rectangular prism of clay with a row of tall and narrow rectangular prisms to represent sheet pile walls. At the base of the clay and sheet pile walls is a thin layer with low stiffness to act as a sliding plane. A schematic of the general geometry from the RS<sup>3</sup> model is shown in Figure 5.3. The clay material and sheet piles both extend from ground surface to a depth of 8.0 m. The sheet piles were modelled with a width ( $B_1$ ) of 0.1 m and a length ( $B_2$ ) of 7.0 m. The width was selected with the intention to make the sheet piles as thin as possible to minimize any lateral end bearing resistance from the soil. For practical reasons to limit the number of elements required and maintain quality dimensions of the mesh, the sheet piles were not made thinner than 0.1 m.



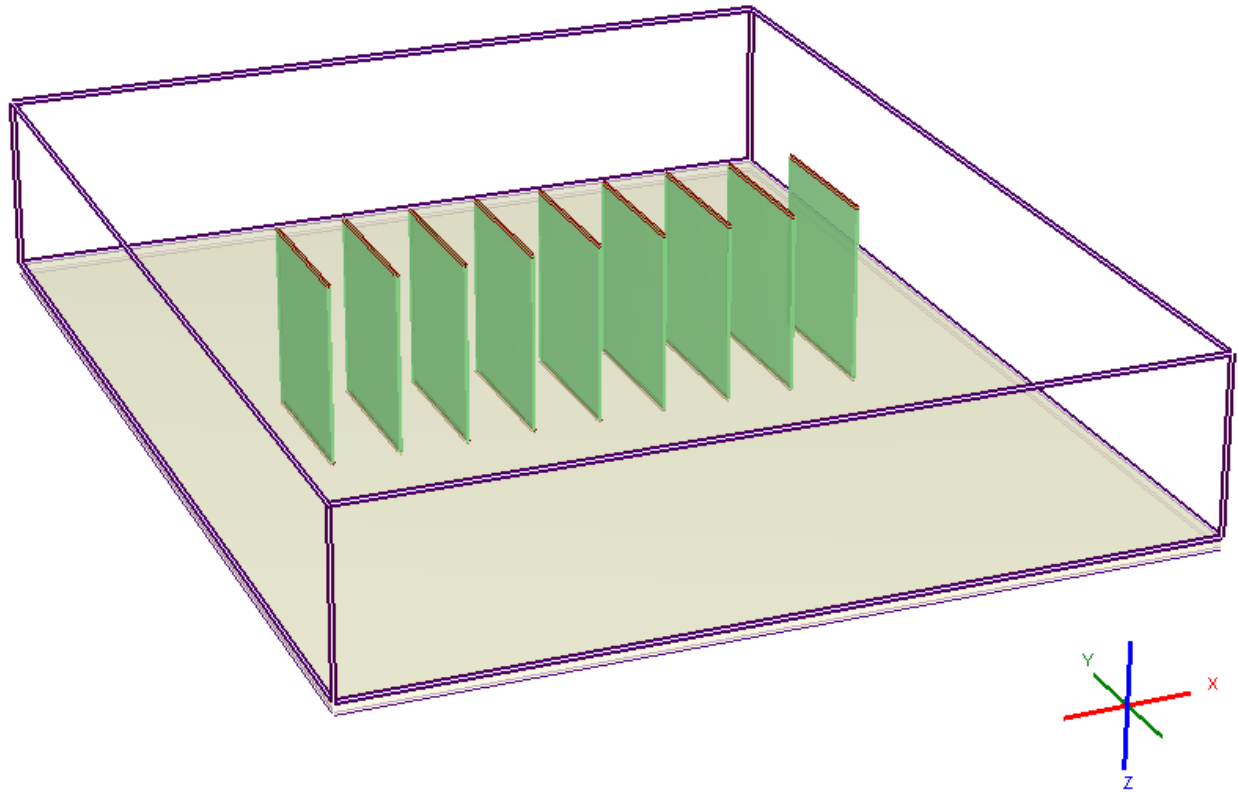


Figure 5.3:  $RS^3$  model geometry.

A graded mesh with 10 noded tetrahedron elements was used to develop the mesh shown in Figure 5.4. The quality of the mesh was checked with the  $RS^3$  to search for bad elements. The bad elements were defined as elements with an aspect ratio greater than 27, minimum dihedral angle less than  $2^\circ$ , maximum dihedral angle greater than  $168^\circ$ , or edge length ratio greater than 18. The element density was increased for the sheet pile volume to create a quality mesh with zero bad elements. The initial element loading was defined by field stress and body force where the body force represents the self-weight of the elements derived from the unit weight of the material and the field stress is derived from gravity to lock in the initial stress.

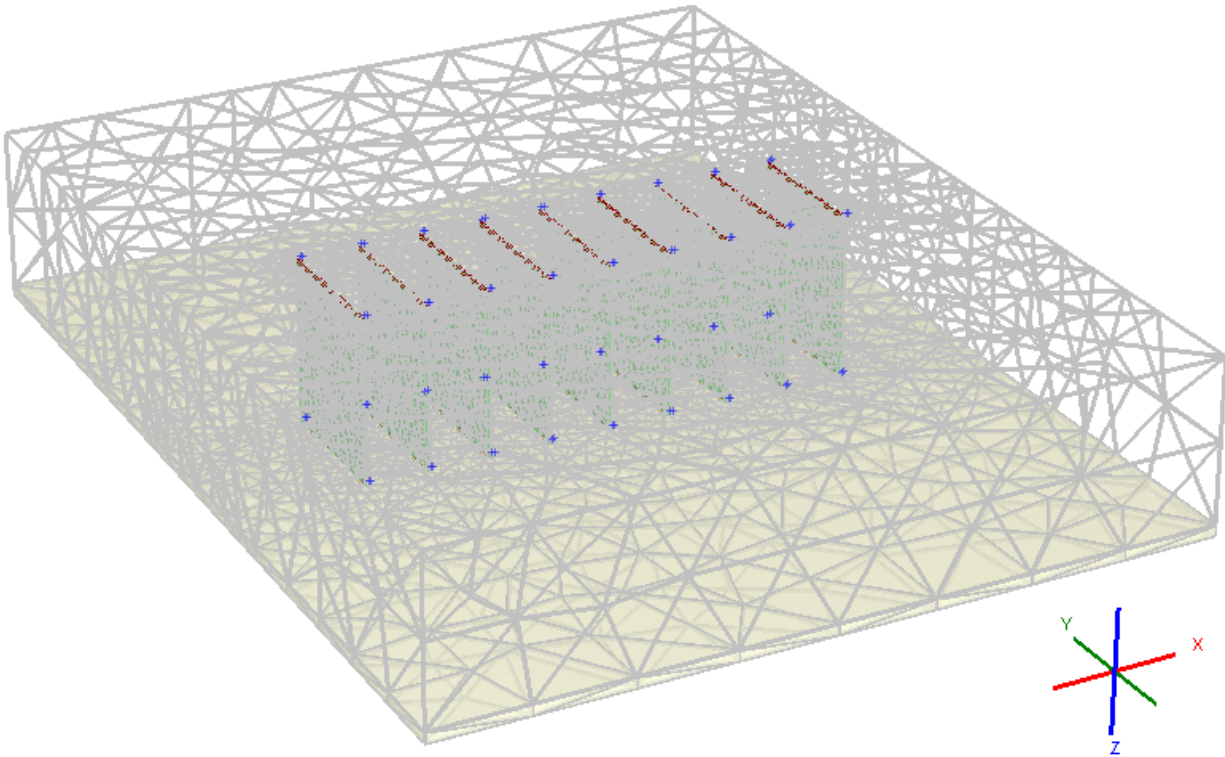


Figure 5.4: Mesh of RS<sup>3</sup> model.

#### 5.2.1.1 Boundary Conditions

The sheet piles are modelled as a rectangular prism material boundary within the boundaries of the model. The outer side boundaries and bottom boundary of the model are fixed in the x-direction, y-direction, and z-direction. Displacement of the piles is modeled by applying a displacement to the thin surface of the sheet pile in the positive y-direction which is parallel to the sheet pile length. The displacement was applied in stages of 10 mm per stage to a maximum of 160 mm. At 160 mm, a continuous passive wedge failure can be expected to develop based on the suggestion in the Canadian Foundation Engineering Manual that passive failure will occur at 0.02 times the wall height (Canadian Geotechnical Society, 2006). The boundary conditions applied to the model are shown in Figure 5.5. The modelled boundary conditions differ from those in the applications of Hardy Ribs in the field where soil moves towards the sheet pile walls which are embedded in a stronger and stiffer soil. The boundary conditions applied in the model

are intended to study the spacing effects of the ribs from the relative displacement between soil and the ribs.

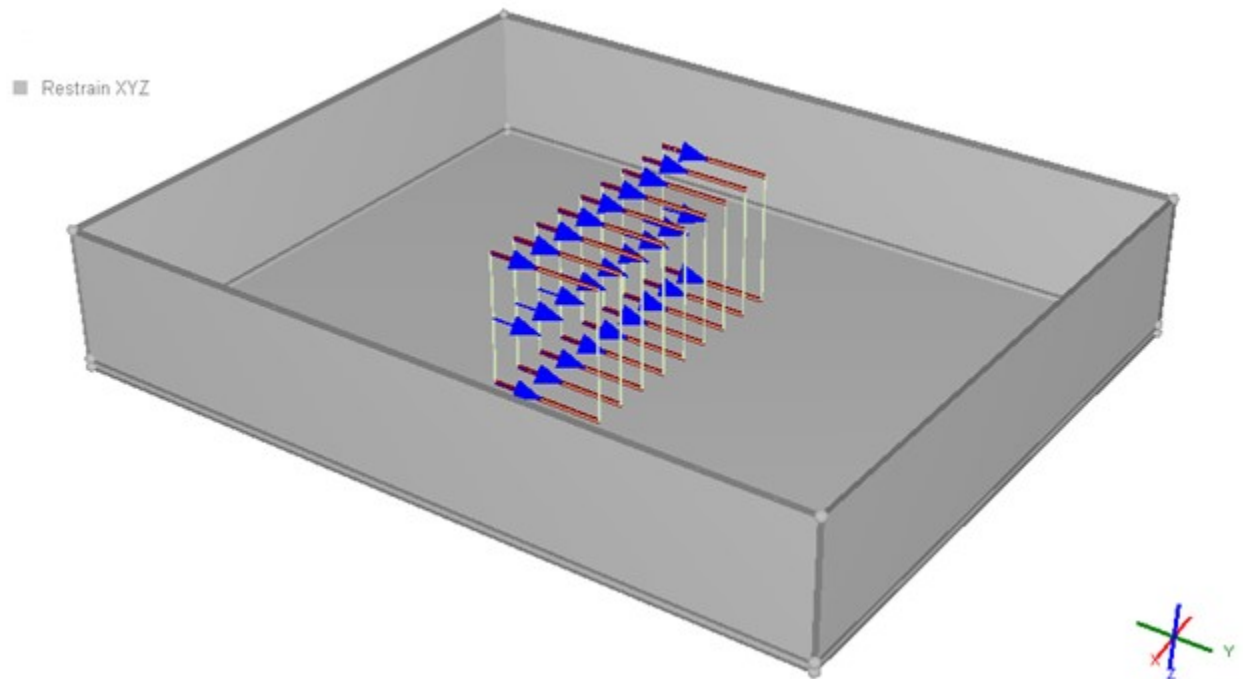


Figure 5.5: Boundary conditions of RS<sup>3</sup> model.

### 5.2.1.2 Material Properties

An elastic-plastic constitutive model was applied to the clay with the shear strength governed by purely cohesive soil. The tensile strength of the clay was input as two times the cohesion. There was no reduction of shear strength or tensile strength for the input residual strength. Consistent with the 2D F.E. modeling and the calibration of the material stiffness, the Young's modulus was input as 275 times the undrained shear strength and Poisson's ratio was input as 0.45. The clay was modelled with varying undrained shear strength of 20 kPa and 50 kPa to compare the results.

An elastic constitutive model was applied to the sheet pile material properties. An elastic modulus of 200 GPa was applied to this material type with Poisson's ratio ( $\nu$ ) of 0.3 to be representative of the elastic properties of steel. The pile material is considerably stiff compared to the clay.

The sliding material layer was modelled with an elastic constitutive model with a very low stiffness to allow the sheet piles and soil to slide on top of this material layer. An elastic modulus of 55 kPa was input which is 1% of the stiffness of the clay with an undrained shear strength of 20 kPa. The Poisson's ratio of 0.45 was input for this material. The soft material properties were applied so that the lateral resistance is predominantly developed from the clay at the ends of the sheet piles and not from sliding resistance at the base of the sheet piles. In the application of Hardy Ribs in the field, sliding resistance at the base would be developed, but the model is intended to study spacing effects based on the lateral resistance only.

### 5.2.2 Sheet Pile Spacing Results

To support the validity of Equation 5-2 for calculating the critical spacing at which the Hardy Ribs act as a continuous wall, the sheet pile walls were modelled at various spacing and the results were compared to the limit equilibrium solution. The centre-to-centre spacing was modelled at 1.0 m, 2.0 m, 3.0 m, 4.0 m, 5.0 m, and 6.0 m. Because the sheet pile walls were modelled with a width of 0.1 m, the clear spacing was 0.9 m, 1.9 m, 2.9 m, 3.9 m, 4.9 m, and 5.9 m. The sheet pile walls were modelled with a length ( $B_2$ ) of 7.0 m. The clay was modelled with an input undrained shear strength of 20 kPa, a tensile strength of 40 kPa, and Elastic modulus of 5,500 kPa. There are no joints modelled between the clay and steel interface, therefore the adhesion factor ( $a$ ) is equal to 1. Based on the limit equilibrium analysis, the critical spacing for the modelled Hardy Ribs geometry is calculated using Equation 5-2 as:

$$S < \frac{aB_2}{2} < \frac{1 \cdot 7.0 \text{ m}}{2} < 3.5 \text{ m} \quad 5-10$$

Contours of the modelled total displacement is shown in Figures 5.6 to 5.11 for clear spacing of 0.9 m, 1.9 m, 2.9 m, 3.9 m, 4.9 m, and 5.9 m, respectively. The contours are shown on a plane cut through the x-y plane through the centre of the sheet pile walls at 4.0 m depth. Also shown are contours on a plane cut through the x-z plane through the centre along the length of the sheet piles walls. The results shown in Figure 5.6 through Figure 5.11 show the displacement contours when the sheet piles undergo a displacement of 160 mm. It can be observed that the difference in displacement between the centre sheet piles and the soil is minimal when the spacing is 2.9 m or

less and becomes significant when the spacing is greater than 3.9 m. This indicates that the soil is flowing or squeezing between the sheet piles for the spacing greater than 3.9 m and the sheet pile walls act as a continuous wall when spacing is less than 2.9 m. This is consistent with the critical spacing of 3.5 m calculated in Equation 5-10.

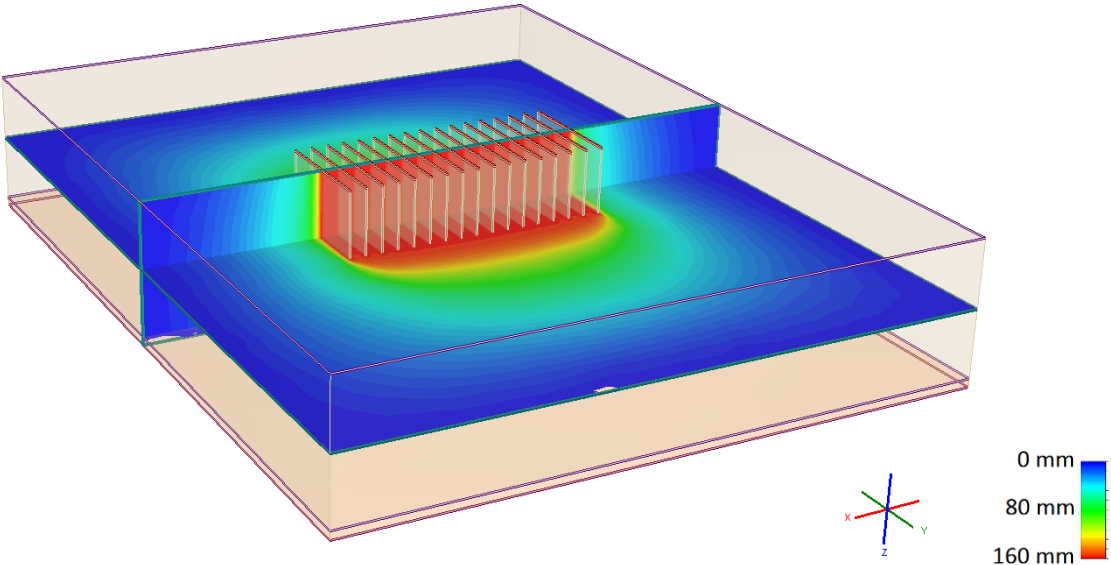


Figure 5.6: Total displacement contours for  $S=0.9$  m.

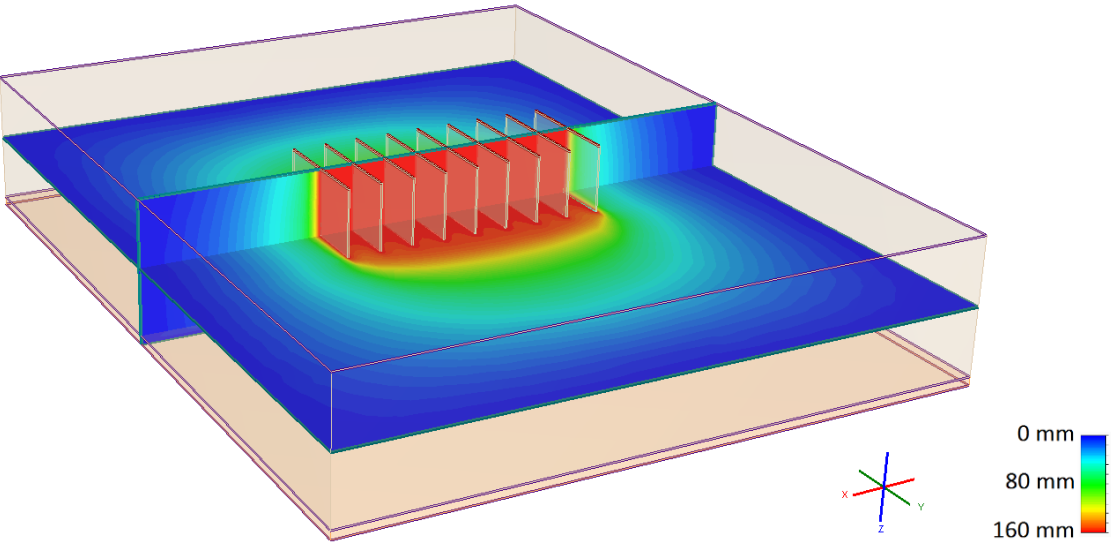


Figure 5.7: Total displacement contours for  $S=1.9$  m.

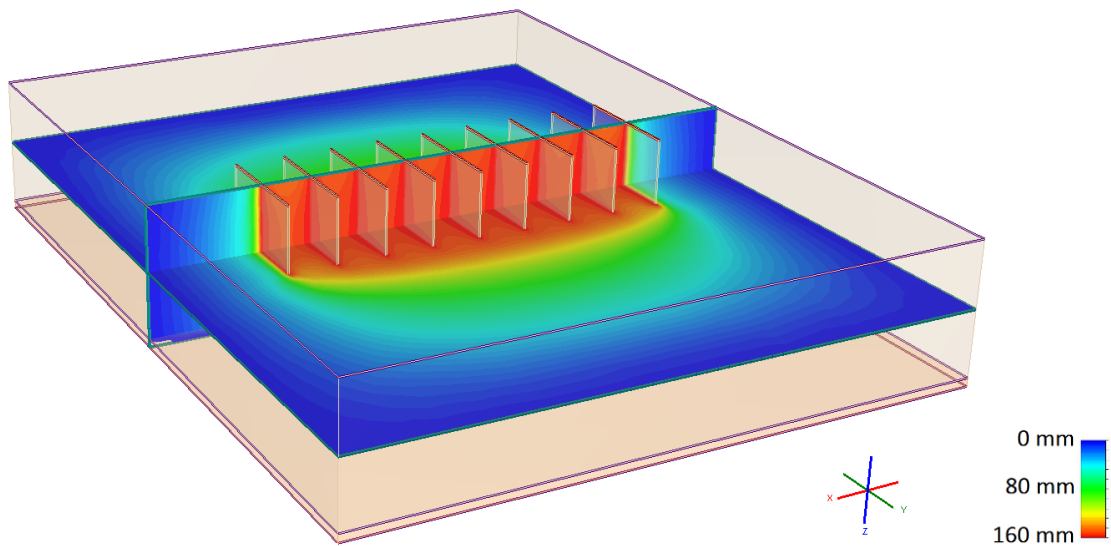


Figure 5.8: Total displacement contours for  $S=2.9$  m.

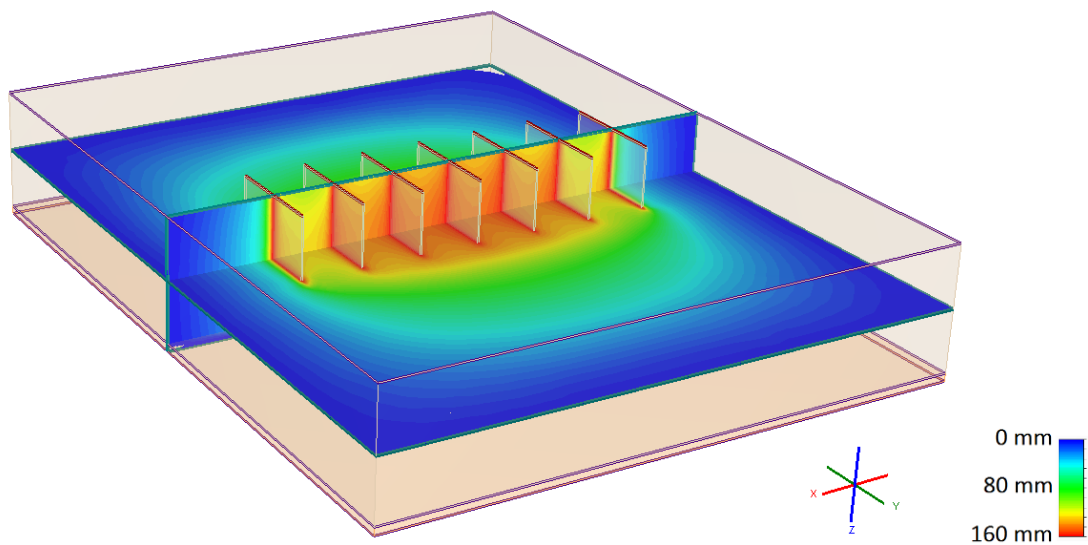


Figure 5.9: Total displacement contours for  $S=3.9$  m.

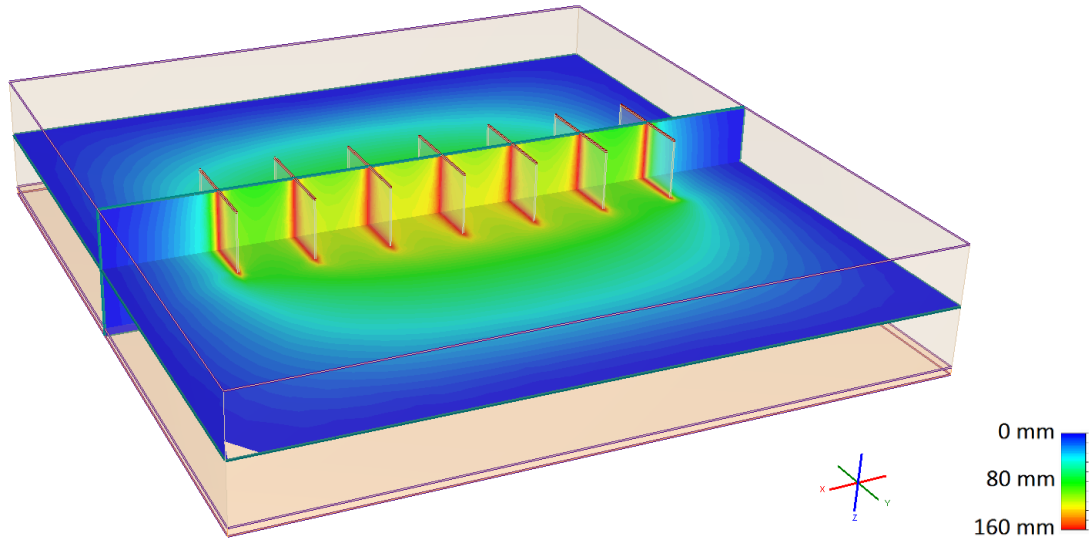


Figure 5.10: Total displacement contours for  $S=4.9$  m.

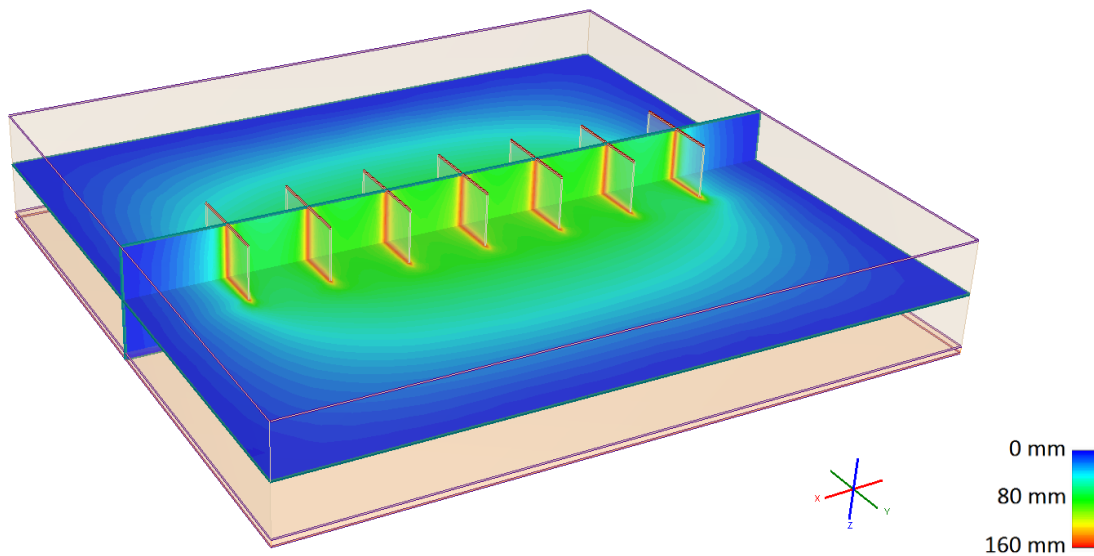


Figure 5.11: Total displacement contours for  $S=5.9$  m.

Contours of the yielded elements are shown in Figures 5.12 through 5.17 for the identical planes shown in Figures 5.6 to 5.11. The contours show the percentage of the yielded elements for the number of elements attached to a node. The yellow contours represent 100% yielded elements and the blue represents 0% yielded elements. The results shown in Figures 5.12 through 5.17 further support Equation 5-2 for calculating the critical spacing. The soil does not yield between

the sheet piles for spacing less than 2.9 m indicating that this arrangement of sheet piles acts as a continuous wall. When the spacing is greater than 3.9 m, the soil yields along the sides of the sheet piles indicating that the soil is squeezing or flowing between the sheet piles. This is consistent with the critical spacing of 3.5 m calculated in Equation 5-10.

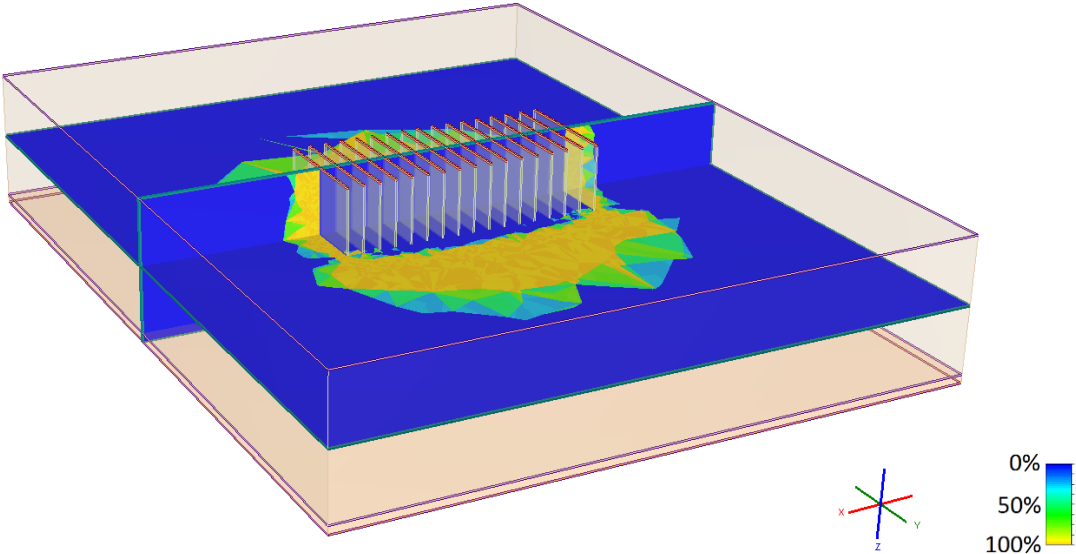


Figure 5.12: Yielded elements contours for  $S=0.9$  m.

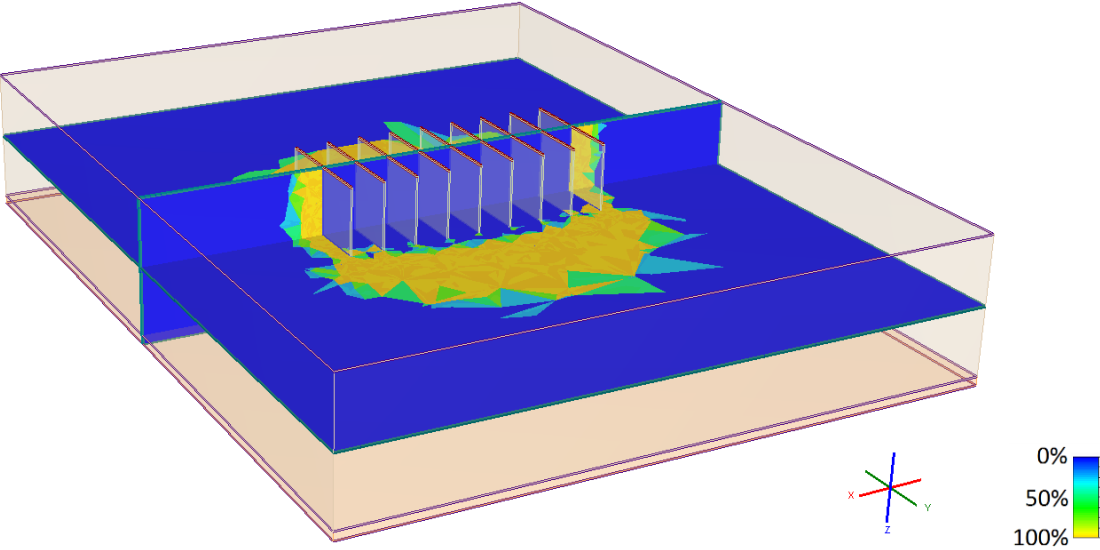


Figure 5.13: Yielded elements contours for  $S=1.9$  m.



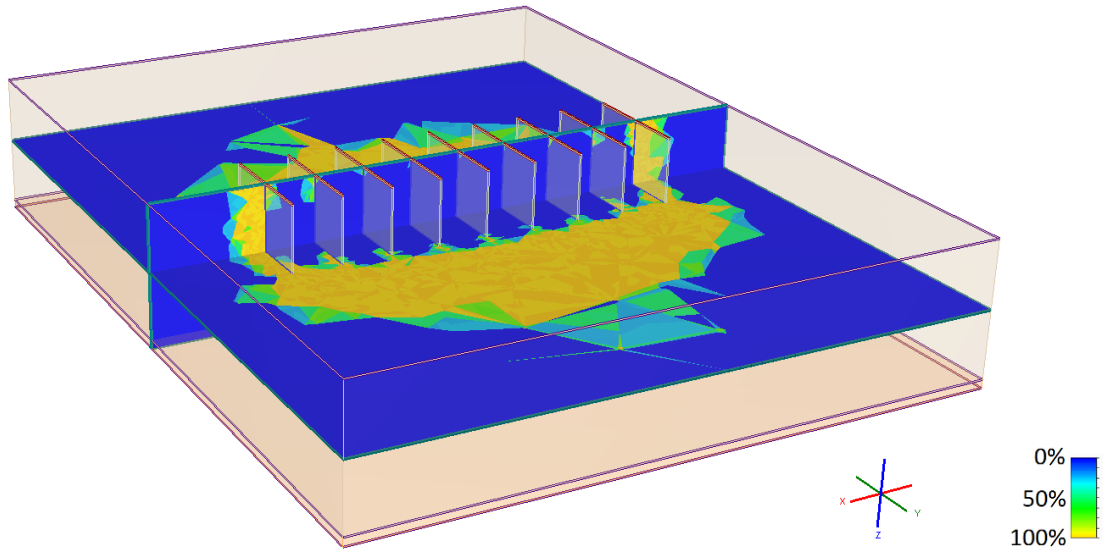


Figure 5.14: Yielded elements contours for  $S=2.9$  m.

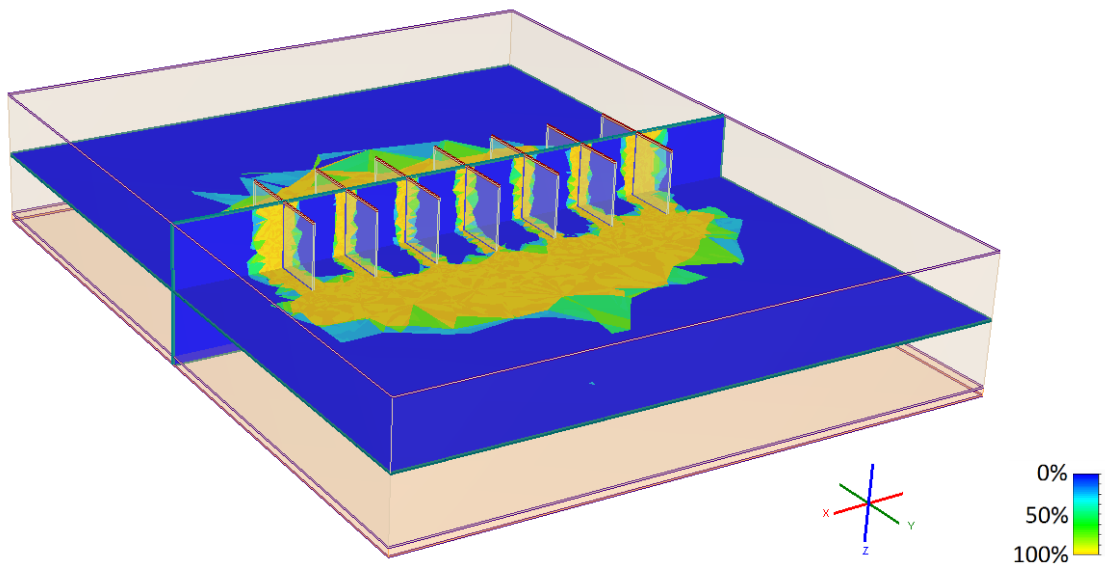


Figure 5.15: Yielded elements contours for  $S=3.9$  m.

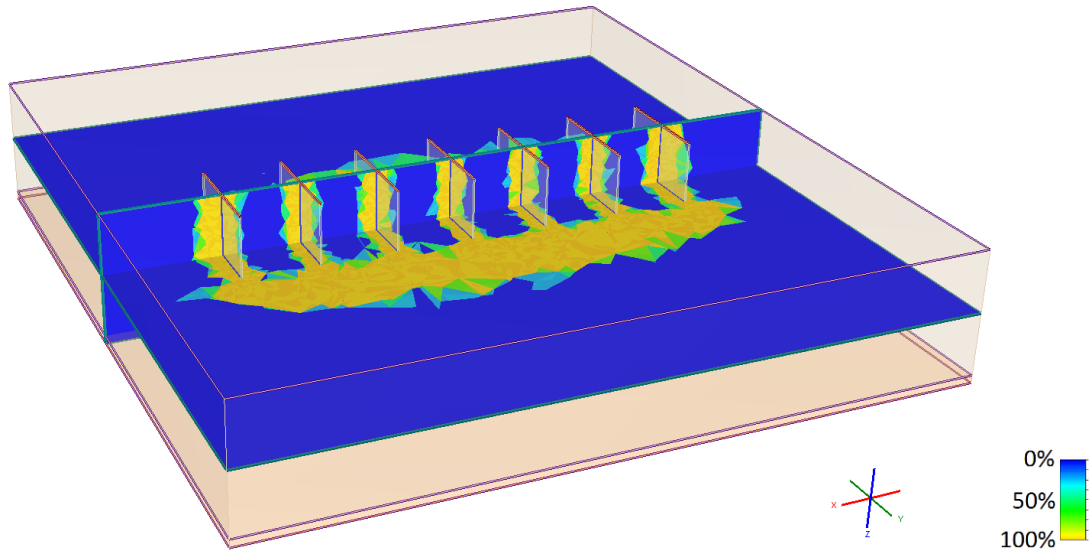


Figure 5.16: Yielded elements contours for  $S=4.9$  m.

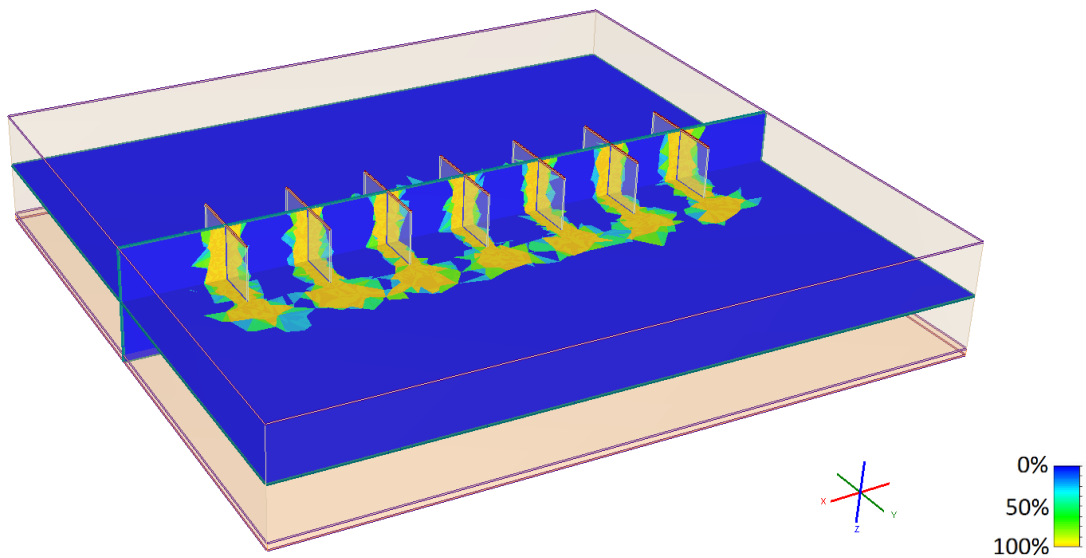


Figure 5.17: Yielded elements contours for  $S=5.9$  m.

An additional contour plot showing the total displacement along a y-z plane through the centre sheet pile is shown in Figure 5.18 along with vectors showing the displacement direction. The length of the vectors has been multiplied by a factor of 20. The clear spacing in this case is equal to 1.9 m and therefore there soil does not fail by squeezing between sheet piles. It can be observed that the soil at the leading edge of the sheet piles moves upward and away from the sheet piles consistent with the development of a passive wedge failure. The soil on the opposite side of the

sheet piles is observed to move downward and toward the sheet piles consistent with the development of an active wedge failure. This further supports the assumption that the ultimate lateral resistance for Hardy Ribs will be governed by the difference of the passive and active earth pressures. The spacing between sheet piles is required to be sufficiently small however such that the Hardy Ribs acts as a continuous wall.

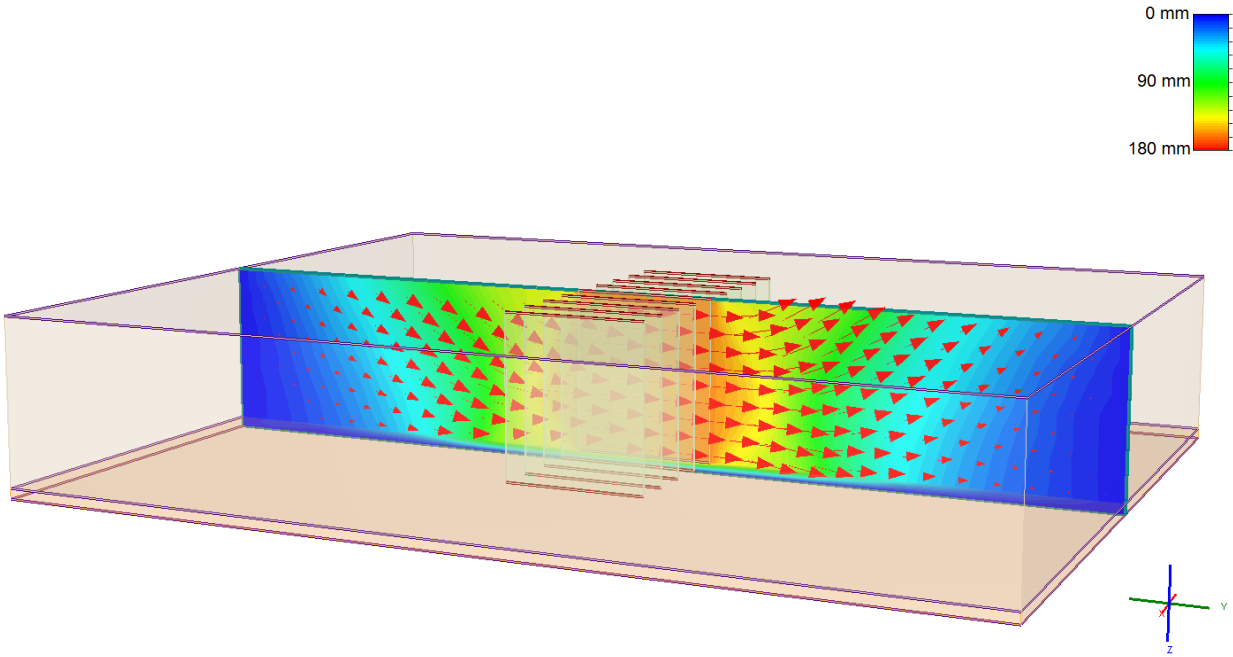
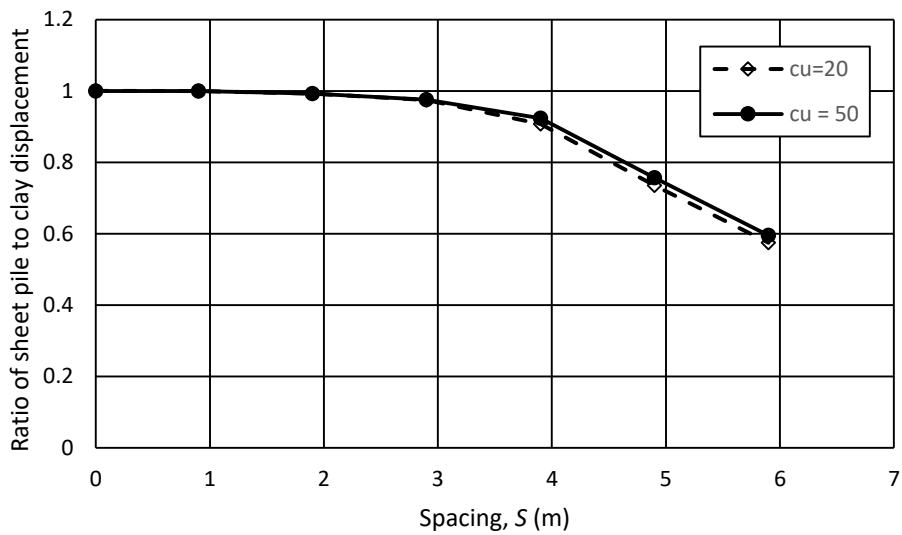


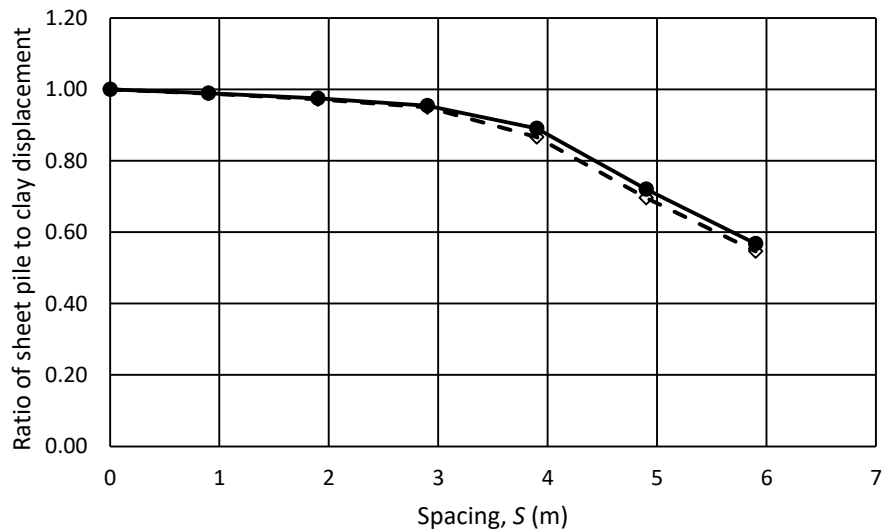
Figure 5.18: Total displacement contours and vectors for 160 mm for sheet pile displacement with spacing of 1.9 m.

Equation 5.2 predicts that the appropriate spacing for the Hardy Ribs in cohesive soil is dependant only on the sheet pile geometry and the adhesion factor. To further investigate the limits of Equation 5-2, the material properties of the clay in the 3D F.E. model were modified. The clay was modified with an undrained shear strength of 50 kPa, tensile strength of 100 kPa, elastic modulus of 13,750 kPa and Poisson's ratio of 0.45. After increasing the shear strength, tensile strength, and elastic modulus, the displacement contours and yielded elements contours similarly suggest that the sheet piles act as a continuous wall for spacing 2.9 m or less. The soil similarly fails by squeezing or shearing between sheet piles for spacing 3.9 m or greater. This suggests the critical spacing of 3.5 m calculated in Equation 5-10 is accurate for varying strengths of cohesive soil. To quantifiably compare the results when the undrained shear strength is 20 kPa

versus 50 kPa, the ratio of the total displacement at the centre sheet pile versus the soil at the midpoint between the adjacent sheet pile was calculated. The displacement at the mid-depth of the sheet piles of 4.0 m below the ground surface was compared at both the leading edge of the sheet piles and at the mid-point along the length. As observed in Figure 5.19, the results are nearly identical regardless of the soil strength and stiffness. For spacing less than 3.5 m, there is very little difference in displacement between the sheet pile and soil. This further suggests the Hardy Ribs will act as a continuous wall for spacing calculated using Equation 5-2.



(a)



(b)

Figure 5.19: RS<sup>3</sup> results of sheet pile spacing vs clay deflection. (a) Leading edge of sheet piles (b) At mid-length of sheet piles.

### 5.3 $p$ - $y$ Curves for Closely Spaced Sheet Pile Walls

The  $p$ - $y$  curves developed for laterally loaded circular piles have been successfully used for a flexible retaining walls or a row of contiguous piles which is essentially a continuous wall, where magnitude of  $p_{ult}$  is modified (Cornforth, 2005; Wang et al., 2013). Therefore, it would be reasonable to use these same  $p$ - $y$  curves for the Hardy Ribs system provided that the sheet pile walls and soil block between move in unison and act as a continuous wall. The value of  $p_{ult}$  for a contiguous row of circular piles is less than that of a single circular pile and therefore changes the shape of the  $p$ - $y$  curve. A typical reduction factor for a contiguous row of circular piles can be selected as 0.5 as recommended by Reese et al. (1992) or 0.64 as recommended by Reese and Van Impe (2011). Wang et al. (2013) suggest applying a reduction factor between 0.5 as a lower bound to 0.7 as an upper bound. Typical  $p$ - $y$  curves have been developed by Matlock (1970) for piles in soft clay, Welch & Reese (1972) for stiff clay without free water, and Reese et al. (1974) for sand, among others as reviewed in Section 2.4.

For the Hardy Ribs system, two alternatives are proposed for calculating the magnitude of  $p_{ult}$  in formation of the  $p$ - $y$  curve. The first alternative (Option 1) is to use Equations 5-4 and 5-5 for cohesive soil or Equation 5-9 for cohesionless soil. The second alternative (Option 2) for formulating  $p$ - $y$  curves is to use the magnitude of  $p_{ult}$  as calculated for a circular pile and applying a reduction factor. This option treats the Hardy Ribs system as an equivalent series of circular pile with an equivalent pile diameter. The centre to centre spacing ( $S_{c-c}$ ) between sheet piles for the Hardy Ribs can be treated to be equivalent to the circular pile diameter ( $b_{eq}$ ) and this alternative is referred to as Option 2a. Alternatively, Equation 2-11 can be used to calculate an equivalent circular pile diameter ( $b_{eq}$ ) for the sheet pile geometry. The modified magnitudes of  $p_{ult}$  calculated using Option 1 or Option 2 can then be input into the typical  $p$ - $y$  curves. The two options for calculating  $p_{ult}$  and developing  $p$ - $y$  curves for Hardy Ribs are compared in detail in Section 6.1.4.

### 5.4 Summary of Spacing Effects

Since the Hardy Ribs consist of a series of parallel sheet pile walls, it was necessary to study the effect of the spacing between sheet pile walls. The lateral resistance per sheet pile wall for a row

of sheet pile walls decreases as the regions of the passively loaded soil overlap. The overall available resistance against landslide loading does however increase with decreasing spacing. The maximum landslide resistance can be achieved when the sheet pile walls are spaced close enough together such that the Hardy Ribs act as a continuous wall.

A limit equilibrium solution was developed to calculate this critical spacing that prevents soil from squeezing between adjacent sheet pile walls. The critical spacing was further investigated using 3D F.E. modelling and the results support the use of Equation 5.2 to calculate the spacing in cohesive soil. If the spacing between sheet pile walls is sufficiently small that the Hardy Ribs act as a continuous wall, then the ultimate lateral resistance can be estimated as the difference of Rankine's passive and active lateral earth pressures. Finally,  $p$ - $y$  curves can be developed based on typical  $p$ - $y$  curves for circular piles with a modified magnitude of  $p_{ult}$ . These findings are used to develop the proposed design methodology for Hardy Ribs discussed in Chapter 6.

## 6.0 PROPOSED DESIGN METHODOLOGY FOR HARDY RIBS

A methodology or procedure has been proposed to design a Hardy Ribs system for landslide stabilization. The procedure is based on the estimated behaviour of laterally loaded sheet pile walls for Hardy Ribs discussed in Chapter 4, the estimated spacing effects discussed in Chapter 5, and a review of existing design methodologies for stabilizing landslides using circular piles. This chapter discusses the proposed design methodology in detail which is comprised of the following seven steps:

1. Determine landslide loads and required increase in resisting force to achieve target FS.
2. Develop strength parameters for laterally loaded pile analysis.
3. Determine critical spacing to prevent soil squeezing between sheet piles.
4. Develop suitable  $p$ - $y$  curves.
5. Determine soil-pile interaction using numerical models.
6. Check structural capacity of sheet pile wall.
7. Select the location on the slope to install the Hardy Ribs.

This methodology is suitable for translational landslides with a discrete shear zone. Any contribution of shear resistance along the base of the Hardy Ribs is ignored and only lateral soil resistance is considered. The procedure assumes that there is no sliding along the joints of the sheet pile sections. This results in a very large bending stiffness of the sheet pile walls and they are expected to behave as short piles. If the sheet pile sections are free to move independently, they may behave as a series of in-line long piles. In reality, there may be some displacement along the joints, however there will also be frictional forces along the joints acting to resist this movement along joints.

The seven design steps are described in detail in Section 6.1. An example of the calculations for the proposed design steps are provided for the Hardy Ribs example at CN Mile 191.4 River Subdivision in Section 6.2. The results are compared to an analysis using Viggiani's (1981) method in Section 6.3.

## 6.1 Details of Proposed Design Steps

A detailed description of each of the seven design steps is provided for the proposed design methodology for Hardy Ribs. Steps 1 through 7 are discussed in Sections 6.1.1 through 6.1.7, respectively.

### 6.1.1 Determine Landslide Loads

The proposed design methodology consists of a de-coupled approach, where a two-dimensional (2D) limit equilibrium analysis is performed to determine the landslide loads and the required increase in resisting force to achieve the target factor of safety. Step 1 includes calculating the required increase in resisting force from the Hardy Ribs to achieve the target factor of safety.

A number of 2D limit equilibrium slope stability analysis software are available that are suitable to estimate the landslide loads. Adequate site information is required including topography, stratigraphy with appropriate shear strength parameters, groundwater conditions, and identification of the slide plane of the landslide. A back analysis can be performed to calibrate the model knowing that the actual factor of safety ( $FS$ ) is approximately equal to 1.0. The sum of disturbing forces along the critical surface ( $\Sigma F_D$ ) can be determined from the back analysis results using the 2D slope stability analysis software. A target factor of safety ( $FS_T$ ) needs to be selected in consideration of the risk of ongoing landslide displacement and the impact on the infrastructure, environment, and human safety amongst other possible considerations. The expression suggested by Poulos (1995):

$$\Delta R = \Sigma F_D (FS_T - FS) \quad 6-1$$

can then be used to calculate the required increase in resisting force ( $\Delta R$ ) per m along the slope to achieve the target factor of safety.

### 6.1.2 Strength Parameters for Laterally Loaded Pile Analysis

Step 2 consists of selecting the parameters for the soil/rock above and below the slide plane to perform the laterally loaded pile analysis. Typical  $p$ - $y$  curves were discussed in Section 2.4 which require undrained shear strength parameters for laterally loaded piles in clay soils, drained shear



strength parameters for laterally loaded piles in sand, and the compressive strength for laterally loaded piles in weak rock. Suitable strength parameters and unit weight of the soil/rock above and below the slide plane must be selected. An appropriate groundwater level used in the lateral loaded pile analysis must also be selected.

### 6.1.3 Determine Critical Spacing of Sheet Pile Walls

The spacing between adjacent sheet pile walls should be designed such that the possibility of soil squeezing between sheet pile walls is prevented to maximize the resistance against landslide loading. A solution to select the appropriate spacing was derived in Section 5.1. Step 3 consists of selecting an adequate spacing between sheet pile walls. That spacing ( $S$ ) can be estimated for cohesive soils using:

$$S < \frac{aB_2}{2} \quad 6-2$$

or for cohesionless soil using:

$$S < \frac{2B_2K_0 \tan \phi_a}{(K_p - K_a)} \quad 6-3$$

Since Equations 6-2 and 6-3 were derived assuming very thin sheet pile walls, lateral end bearing was not considered. Therefore the spacing is suitable regardless of the width ( $B_1$ ) of the sheet pile walls. The centre-to-centre spacing ( $S_{c-c}$ ) is equal to the clear spacing plus the sheet pile width.

An appropriate spacing to ensure that soil does not squeeze between sheet pile walls and the Hardy Ribs acts as a continuous wall must be calculated for each stratigraphic layer. The calculation must also be performed for the soil/rock below the slide plane to achieve the maximum resistance from the underlying stable layer. Equation 6.2 should be performed for each cohesive soil layer as the adhesion ( $a$ ) may vary. Equation 6.3 should be performed for each cohesionless soil layer. The clear spacing ( $S$ ) should be selected that satisfies Equation 6.2 and Equation 6.3 for the entire depth of the sheet piles.

#### 6.1.4 Develop $p$ - $y$ Curves

Typical  $p$ - $y$  curves for a single laterally loaded circular pile were discussed in Section 2.4 and these functions are built-in to laterally loaded pile analysis software such as LPILE by Ensoft, Inc. and RSPile by Rocscience Inc. These  $p$ - $y$  curves are also suitable for flexible retaining walls such as a contiguous row of circular piles or sheet pile walls provided that a reduction in  $p_{ult}$  is considered (Cornforth, 2005; Wang et al., 2013). After selecting an appropriate spacing between sheet pile walls for the Hardy Ribs in Step 3, the Hardy Ribs will act as a continuous wall similar to a flexible wall. Therefore, the typical  $p$ - $y$  curves for circular piles would be reasonable to use for Step 4 with a modified/reduced magnitude of  $p_{ult}$ . Two options are proposed for calculating the reduced value of  $p_{ult}$  to input into the laterally loaded pile analysis. Option 1 considers the Hardy Ribs to act as a continuous wall and the magnitude of  $p_{ult}$  is estimated by Rankine's passive and active earth pressure theory. Option 2 considers each sheet pile wall of the Hardy Ribs to be equivalent to a circular pile with an equivalent diameter.

##### 6.1.4.1 Option 1: Assumed Continuous Wall

An expression to calculate  $p_{ult}$  for Hardy Ribs was derived in Section 5.1 based on Rankine's active and passive earth pressure theory. The calculation of  $p_{ult}$  for cohesive soils should be calculated with depth and taken as the lesser of Rankine's passive earth pressure:

$$p_{ult} = (2c_u + \gamma z)(S + B_1) = (2c_u + \gamma z)S_{c-c} \quad 6-4$$

or the difference between Rankine's passive and active earth pressure:

$$p_{ult} = 4c_u(S + B_1) = 4c_u S_{c-c} \quad 6-5$$

For cohesionless soils,  $p_{ult}$  can be calculated with depth as:

$$p_{ult} = \gamma' z (K_p - K_a) S_{c-c} \quad 6-6$$

A custom  $p$ - $y$  curve can be constructed by inputting  $p_{ult}$  from Equation 6-4 or 6-5 into a typical  $p$ - $y$  curve equation such as the curve developed by Matlock (1970) for a laterally loaded pile in

soft clay for example. To input a custom  $p$ - $y$  curve into LPILE or RSPile, custom  $p$ - $y$  curves must be constructed based on the normal stress at the top and bottom of the stratigraphic layer. The software can then linearly interpolate the  $p$ - $y$  curve for depths between the top and bottom. Option 1 seems suitable to develop  $p$ - $y$  curves by modifying the curve developed by Matlock (1970) for soft clays and the Welch & Reese (1972) curve for stiff clay without access to free water. For these functions, modifying  $p_{ult}$  proportionally modifies the stiffness of the curve as well as the magnitude of  $p_{ult}$ . The  $p$ - $y$  curves for sand by Reese et al. (1974) or stiff clay with access to free water by Reese et al. (1975) are more complex and require additional input parameters to define the curve. Simply modifying the magnitude of  $p_{ult}$  may not be appropriate for these functions. Therefore Option 1 is only recommended for soft clays and stiff clay without access to free water and other soil types should consider Option 2 for defining the  $p$ - $y$  curves.

#### 6.1.4.2 Option 2: Assumed Equivalent Pile Diameter

A proposed alternative to develop  $p$ - $y$  curves consists of treating each sheet pile wall of the Hardy Ribs as an equivalent circular pile and applying a reduction factor to the  $p$ - $y$  curves. Since the Hardy Ribs have been designed to act as a continuous wall, the equivalent circular pile diameter can be taken as the centre-to-centre spacing between sheet piles. This option is referred to as Option 2a and is equivalent to a contiguous row of circular piles. Another proposed alternative (Option 2b) is to use Reese & Van Impe's (2011) calculation to determine the equivalent pile diameter as:

$$b_{eq} = B_1 \left[ \frac{p_{ult,c} + 2 \left( B_2 - \frac{B_1}{2} \right) a c_u}{p_{ult,c}} \right] \quad 6-7$$

Depending on whether Option 2a or Option 2b is utilized, the ratio of  $S_{c-c}/b_{eq}$  will vary and therefore the reduction factor will vary. This is illustrated in Figure 6.1 where  $S_{c-c}$  is equal to  $b_{eq}$  in Option 2a and  $S_{c-c}$  is not necessarily equal to  $b_{eq}$  in Option 2b.

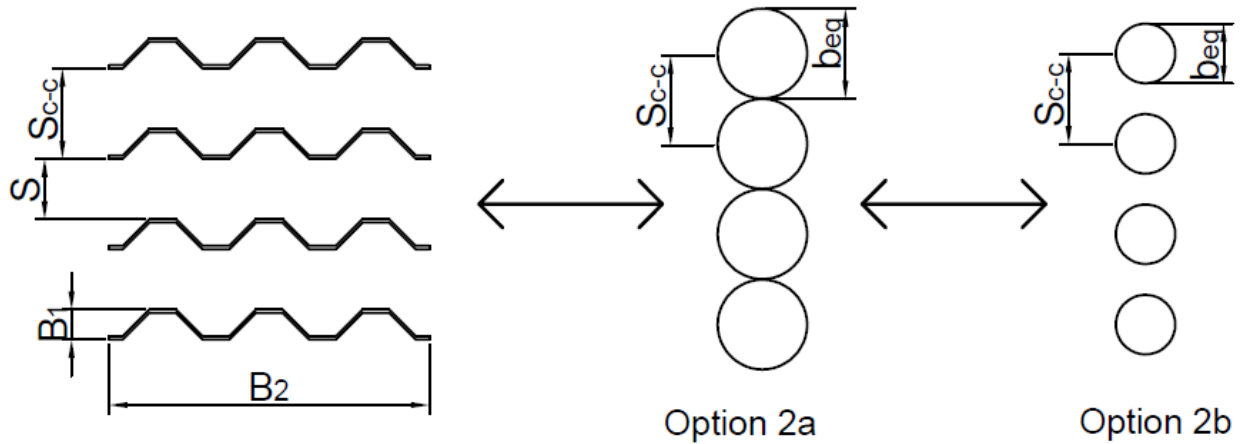


Figure 6.1: Equivalent pile diameter for Option 2a and Option 2b.

This methodology can be analyzed using LPILE or RSPILE as a customized  $p$ - $y$  curve does not have to be input and a reduction factor less than 1 can be applied to the magnitude of  $p$ . By applying a reduction factor to the  $p$ - $y$  curve, the stiffness of the curve and the magnitude of  $p_{ult}$  are both modified. Option 2 is suitable for laterally loaded piles in all soil types. The challenge with Option 2 is to select an adequate reduction factor; e.g. see Reese & Vane Impe (2011), Reese et al. (1992) and Wang et al. (2013). Selecting an appropriate reduction factor remains a challenge for the use of  $p$ - $y$  curves for all shear pile wall and flexible retaining wall designs.

### 6.1.5 Numerically Model Soil-Pile Interaction

Step 5 involves using laterally loaded pile analysis software such as LPILE or RSPILE to calculate the deflection, shear stress, and bending moment profile developed in the laterally loaded piles for a given soil displacement along the landslide plane.

The Hardy Ribs sheet piles are short piles that have the potential to fail in lateral translation or overturning. This mode of failure differs from typical shear piles for slope stabilization works which comprise of long piles. The critical failure mechanism for long piles is bending failure of the piles. If the strength of the stable soil mass below the slide plane is greater than that of the sliding soil mass, the controlling stresses and bending moments, and the soil reactions of concern, are located below the slide plane (Vessely et al., 2007). The design methods presented by Reese et al. (1992), Vessely et al. (2007), and Cornforth (2012) for circular shear piles consist of performing

the laterally loaded pile analysis only on the length of pile below the slide plane. An equivalent moment and shear force from the sliding soil is applied to the top of the pile (ie. at the slide plane). Since the sheet pile walls that comprise the Hardy Ribs have a very large moment of inertia and relatively shallow installation depth below the slide plane, these piles behave as short piles. Therefore, the maximum bending moments will develop above the slide plane and the design methods that consist of performing the laterally loaded pile analysis on the portion of soil / rock below the slide plane only is not suitable. A more suitable loading condition to represent the landslide would be to apply a lateral soil displacement above the slide plane that is constant in magnitude from the ground surface to the slide plane.

To perform the beam-column calculations, properties of the sheet pile wall are required including the moment of inertia and the elastic modulus of the steel. When using Option 1 to develop  $p$ - $y$  curves, the custom  $p$ - $y$  curve must be input for the top and bottom of each layer and the software can linearly interpolate appropriate  $p$ - $y$  curves for depths in between the top and bottom. When using Option 2 to develop  $p$ - $y$  curves, the equivalent pile diameter must be applied to the pile properties and a reduction factor to the magnitude of  $p$  that is less than 1 must be applied.

A constant soil displacement can be applied above the slide plane and the software will output the pile deflection, shear stress, and bending moment distribution with depth. RSPile can provide the profile with depth for the ultimate lateral resistance or for a maximum allowable displacement along the slide plane. To numerically model the soil-pile interaction with moving soil, RSPile calculates the soil reaction using the relative soil and pile displacement. The maximum shear stress along the profile of the pile will develop at the slide plane and this force is equal to the magnitude of the additional resisting force against landslide loading per sheet pile wall. By dividing this magnitude by  $S_{c-c}$ , the resistance to landslide loading per unit m along the landslide can be determined and compared to  $\Delta R$  calculated in Step 1. The maximum bending moment that develops in the pile should also be noted.

### 6.1.6 Check Structural Capacity of Sheet Piles

The shear stress and bending moment profile with depth will be obtained from Step 5. Step 6 includes checking the structural capacity of the sheet piles. The yield shear stress ( $V_y$ ) of the sheet pile wall can be determined using:

$$V_y = \tau_y A_p \quad 6-8$$

where  $\tau_y$  is the yield shear stress and  $A_p$  is the cross-sectional area of the sheet pile wall. The yield bending moment ( $M_y$ ) can be determined using:

$$M_y = \frac{I_p \sigma_y}{Y} \quad 6-9$$

where  $I_p$  is the moment of inertia of the sheet pile wall geometry,  $\sigma_y$  is the yield tensile stress of the steel, and  $Y$  is the distance from the outer fiber of the cross section to the neutral axis. The sheet pile walls are treated as a continuous section and the potential for sliding of connections between individual sheet pile sections has been ignored. The calculated shear stress and moment from Step 5 should then be compared to the allowable for the particular sheet piles chosen.

### 6.1.7 Select Location to Install Hardy Ribs

Step 7 consists of selecting an appropriate location on the slope to install the Hardy Ribs. The location of the proposed Hardy Ribs has not been considered through Steps 1 to 6 which consists of the de-coupled slope stability analysis and laterally loaded pile analysis. The following two recommendations by Poulos (1995) for selecting the location of circular shear piles for landslide stabilization are similarly recommended for selecting the location of Hardy Ribs:

1. The piles must extend sufficiently deep beyond the critical failure surface so that it is not shifted downward below the piles with a factor of safety less than the target value.
2. The piles should be located near the centre of the moving landslide mass in order to prevent shifting the critical failure surface behind or in front of the piles.

These potential slide planes are illustrated in Figure 6.2. Alternative slide planes can be analyzed using the 2D limit equilibrium slope stability model. The factor of safety can be calculated for potential slide planes that extend below the existing slide plane and below the depth of the sheet pile walls. Alternative slide planes that exit the slope before the sheet pile wall location or originate downslope of the sheet pile walls can also be analyzed. This additional stability modeling is required to ensure that the overall stability of the slope is greater than the target factor of safety when considering different potential landslide failure geometries.

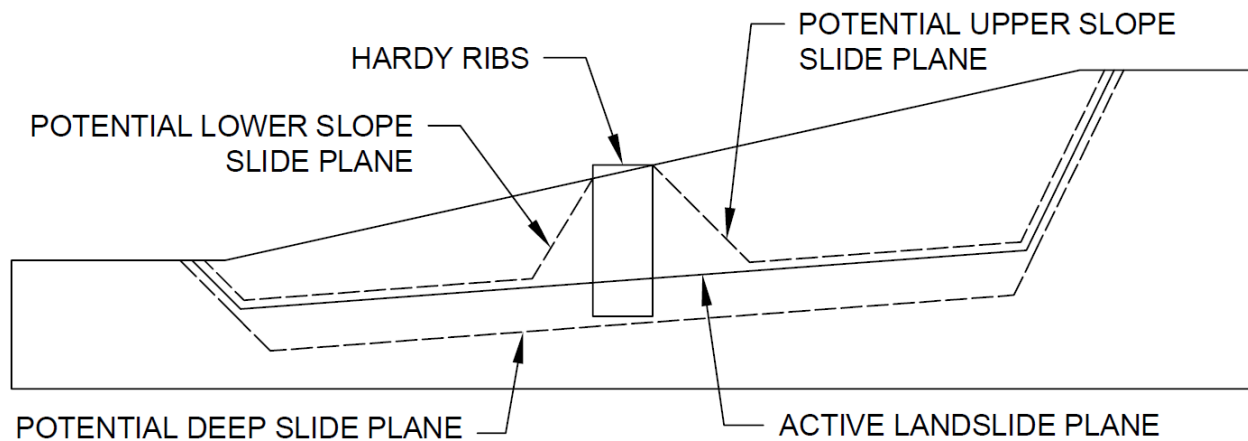


Figure 6.2: Potential slide planes.

## 6.2 Example Calculations for Hardy Ribs at CN Mile 191.4 Rivers Subdivision

An example of the calculations for the proposed seven step design methodology is applied for the Hardy Ribs that were constructed at CN Mile 191.4 Rivers Subdivision in western Manitoba. Steps 1 through 7 are performed and described in Sections 6.2.1 through 6.2.7, respectively. This study site and the design of the Hardy Ribs was described in detail in Chapter 3.

### 6.2.1 Landslide Loads at CN Study Site

A 2D limit equilibrium analysis was performed to determine the landslide loads and to determine the required increase in resisting force to achieve the target factor of safety. Slide 7.0 (Rocscience, 2016) was used to calculate the landslide loads. The existing  $FS$  was approximately equal to 1.0 prior to landslide remediation works considering the landslide was active. The method of vertical slices was used in the slope stability analysis. Both the Morgenstern-Price method with a half sine

interslice force function and the Janbu simplified method were used. The cross section modeled in Slide 7.0 is shown in Figure 6.3 which shows the material regions and the modelled material properties. In the slope stability model, there is a thin material region of residual strength shale that is between the intact shale and the disturbed shale layers. The intact shale and valley wall were modeled with infinite-strength whereas all other material types were modeled with Mohr-Coulomb strength parameters. The porewater pressure was calculated from the drawn piezometric surface and assuming static groundwater conditions. The modelled material regions and material properties are consistent with a previous slope stability back analysis performed for CN by Clifton Associates (2015).

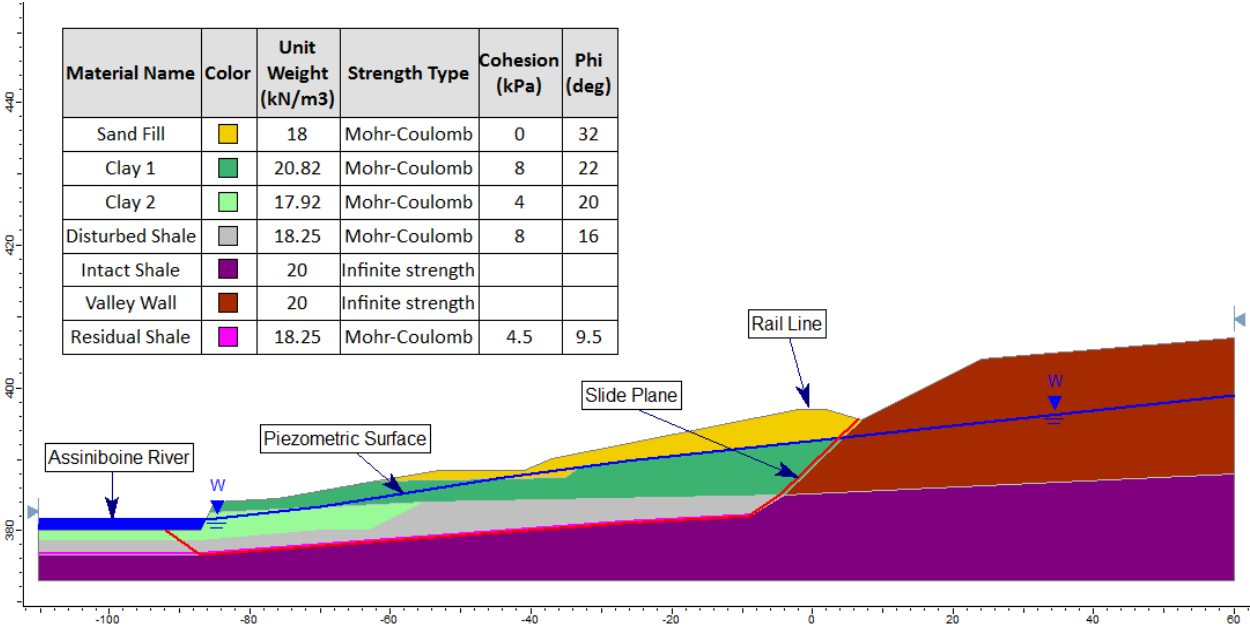


Figure 6.3: Slide 7.0 model of cross section at CN Mile 191.4 River Subdivision

Results from the slope stability model are shown in Table 6.1 including the calculated *FS*, the total driving force and resisting force along the slide plane, and the total driving and resisting moments where applicable for the Morgenstern-Price and the Janbu simplified method.



Table 6.1: Estimated FS before remediation at CN Mile 191.4 Rivers Subdivision.

Method	Estimated FS	Driving Horizontal Force (kN)	Resisting Horizontal Force (kN)	Driving Moment (kN·m)	Resisting Moment (kN·m)
Morgenstern-Price	1.03	2309.46	2379.60	271094	279327
Janbu simplified	1.01	2362.24	2384.11	-	-

The required increase in resisting force to achieve the target factor of safety ( $FS_T$ ) can then be calculated. In this case, the Hardy Ribs were intended to increase the  $FS$  to 1.3 and the existing  $FS$  prior to remediation was approximately equal to 1.0. The sum of the horizontal driving force ( $\Sigma F_D$ ) was approximately equal to 2360 kN based on the Janbu simplified method. The required increase in resisting force ( $\Delta R$ ) can be calculated as:

$$\Delta R = \Sigma F_D(FS_T - FS) = 2360(1.3 - 1.0) = 708 \text{ kN/m} \quad 6-10$$

Based on the 2D limit equilibrium analysis and the calculation shown in Equation 6-10, the Hardy Ribs are required to provide an increase of 708 kN/m along the valley to increase the  $FS$  to 1.3. A laterally loaded pile analysis is required to estimate the resistance provided from the Hardy Ribs design.

### 6.2.2 Strength Parameters at CN Study Site for Laterally Loaded Pile Analysis

Shear strength parameters of the soil are required to perform the laterally loaded pile analysis. To simplify the laterally loaded pile analysis, the stratigraphy was simplified into two layers with an unstable soil mass above the slide plane and a stable soil mass below the slide plane as shown in Figure 6.4. The soil was considered saturated with a piezometric surface at ground surface. Actual groundwater monitoring data near the alignment of the Hardy Ribs at BH14-2 in December, 2014 indicated a piezometric surface at approximately 1.3 m below ground surface and approximately 0.6 m below the thin sand and gravel fill at surface. The sand layer at surface was not encountered along the entire alignment of the Hardy Ribs during the geotechnical site investigation. The conservative assumption that the piezometric surface could be at ground surface without the added drainage benefit of the sand layer was made.

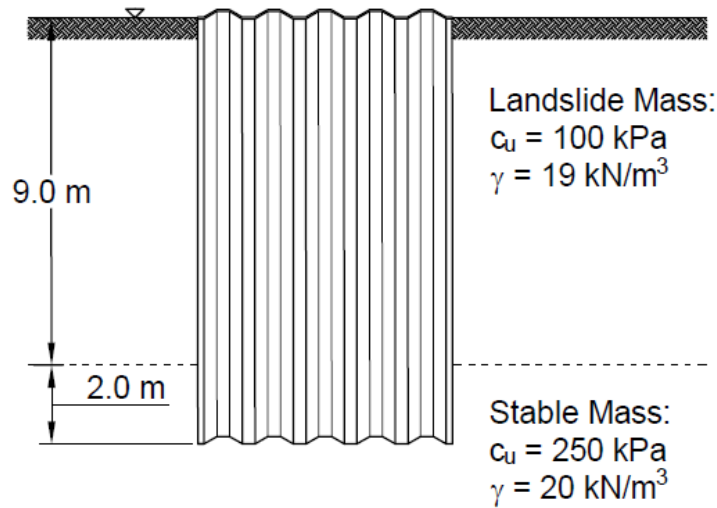


Figure 6.4: Simplified soil properties for laterally loaded pile analysis at CN Mile 191.4 Rivers Subdivision.

The unstable soil mass was simplified into one unit in consideration of the fact that the fill layer was relatively thin or not encountered along the alignment of the Hardy Ribs. The clay and disturbed shale layers had similar consistency and shear strength parameters based on the geotechnical site investigation and laboratory testing program. The clay was described as firm to very stiff whereas the disturbed shale was described as firm to very hard (Clifton Associates, 2015). The estimated undrained shear strength of the clay, as measured by lab vane and pocket penetrometer testing, ranged from approximately 35 kPa to 130 kPa. The undrained shear strength of the disturbed shale ranged from approximately 135 kPa to 170 kPa. The unstable soil above the slide plane was considered to be a homogenous layer with an undrained shear strength of 100 kPa and a unit weight of 19 kN/m<sup>3</sup> for the purpose of the laterally loaded pile analysis.

The stable layer below the slide plane consists of intact shale. The intact shale was described as hard to very hard in consistency (Clifton Associates, 2015). A fine-grained cohesive soil with a consistency that is described as hard can be expected to have undrained shear strength greater than 200 kPa based on the description of soil consistency in the Canadian Foundation Engineering Manual (Canadian Geotechnical Society, 2006). The estimated undrained shear strength of the intact shale, as measured by lab vane and pocket penetrometer testing, ranged from 250 to 285 kPa. The stable soil below the slide plane was considered as a homogeneous layer with an

undrained shear strength of 250 kPa and a unit weight of 20 kN/m<sup>3</sup> for the purpose of the laterally loaded pile analysis.

### 6.2.3 Critical Spacing of Sheet Pile Walls at CN Study Site

The spacing between sheet pile walls must be selected such that the Hardy Ribs act as a continuous wall and soil does not squeeze between the adjacent rows of sheet pile walls (See Section 5.1 for details). The critical spacing for the Hardy Ribs can be found using:

$$S < \frac{aB_2}{2} < \frac{0.75 \cdot 7.08}{2} < 2.66 \quad 6-11$$

where the adhesion factor ( $a$ ) was selected as 0.75 and the sheet pile wall length ( $B_2$ ) was 7.08 m. The shear surface along the sides of the sheet pile walls includes shearing between the clay-steel interface and shearing through clay entirely due to the corrugated geometry of the sheet piles.  $a$  of 0.5 would be expected between the steel and a stiff clay and the shear strength of the potential failure through the soil alone will be equal to  $c_u$ . Therefore, a weighted average  $a$  of 0.75 was selected. The actual clear spacing between sheet piles installed at CN Mile 191.4 was 2.55 m which is expected to be adequate to prevent soil from squeezing between sheet piles based on Equation 6-11.

### 6.2.4 $p$ - $y$ Curves for CN Study Site

$p$ - $y$  curves were developed based on Matlock (1970) and Welch & Reese (1972) which are defined by:

$$\frac{p}{p_{ult}} = 0.5 \left( \frac{y}{y_{50}} \right)^\psi \quad 6-12$$

where  $\psi = 1/3$  (Matlock, 1970) or  $\psi = 1/4$  (Welch & Reese, 1972). Matlock's (1970)  $p$ - $y$  curve for laterally loaded piles in soft clay was selected for the unstable mass or the clay and disturbed shale. The Welch & Reese (1972)  $p$ - $y$  curve for stiff clay without access to free water was selected for the stable mass or the intact shale. The deflection at one-half the ultimate resistance ( $y_{50}$ ) can be estimated as  $2.5\varepsilon_{50}B_1$  where  $\varepsilon_{50}$  is the strain corresponding to one-half the maximum principal

stress difference.  $\varepsilon_{50}$  was estimated to be equal to 0.005 for the unstable mass as suggested by Peck et al. (1974) for clay with an undrained shear strength between 96 and 192 kPa.  $\varepsilon_{50}$  was estimated as 0.005 for the stable mass as suggested by Reese & Van Impe (2011) for overconsolidated clay when laboratory testing data is not available.

The  $p$ - $y$  curves will vary with depth considering the magnitude of  $p_{ult}$  varies with depth. Assuming that the Hardy Ribs act as a continuous wall,  $p_{ult}$  can then be estimated to be controlled by Rankine's passive and active earth pressure theory. This method is referred to as Option 1 as described in Section 6.1.4. For Option 1,  $p_{ult}$  can be calculated with depth based on the lesser of Equation 5-4 and Equation 5-5. Alternatively, Option 2a considers the sheet pile walls to be equivalent to a series of contiguous circular piles as described in Section 6.1.4. With Option 2a,  $b_{eq}$  is equal to 3.0 m and a reduction factor of 0.64 was applied based on Equation 2-16 suggested by Reese & Van Impe (2011). With Option 2b, the Hardy Ribs are similarly compared to an equivalent series of circular piles where  $b_{eq}$  is calculated to be equal to 1.59 m based on Equation 2-11. The reduction factor of 0.79 was applied for Option 2b based on Equation 2-16 suggested by Reese & Vane Impe (2011). For Option 2a and Option 2b,  $p_{ult}$  was selected for the landslide mass from Matlock (1970) as the lesser of:

$$p_{ult} = 9c_u b \quad 6-13$$

$$p_{ult} = \left[ 3 + \frac{\gamma'}{c_u} z + \frac{0.5}{b} z \right] c_u b \quad 6-14$$

For the underlying stable soil,  $p_{ult}$  was selected from Welch & Reese (1972) as the lesser of:

$$p_{ult} = 9c_u b \quad 6-15$$

$$p_{ult} = \left[ 3 + \frac{\gamma'}{c_{u,a}} z + \frac{0.5}{b} z \right] c_{u,a} b \quad 6-16$$

A comparison of  $p_{ult}$  with depth as calculated using Option 1, Option 2a and Option 2b is shown in Figure 6.5. The method of Georgiadis (1983) was used to calculate  $p_{ult}$  for stable mass because

of the change in soil properties. The magnitude of  $p_{ult}$  with depth is approximately the same for Option 1 and Option 2a. The magnitude of  $p_{ult}$  is noticeably lesser when estimated using Option 2b. Option 2a and Option 2b are controlled by the potential wedge type failure which is more critical than the flow-around failure method calculation for the entire depth of the sheet pile wall.

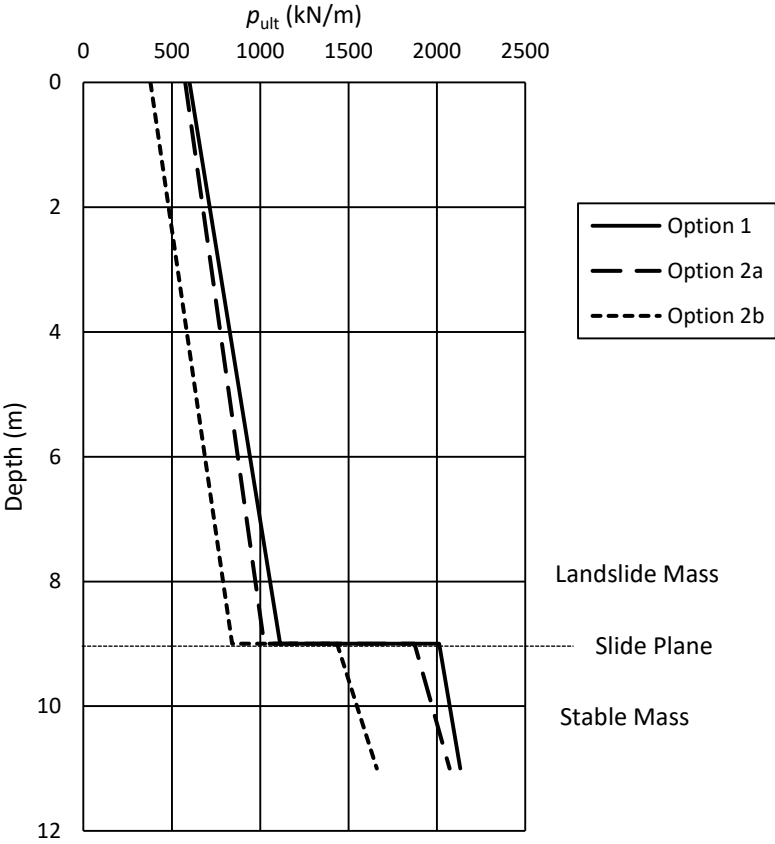


Figure 6.5:  $p_{ult}$  with depth at CN Mile 191.4 Rivers Subdivision.

The custom  $p$ - $y$  curves that were developed for Option 1 for the numerical soil model are shown in Figure 6.6. Developing a custom  $p$ - $y$  curve was not required for Option 2a or Option 2b however since the laterally loaded pile analysis software used in Step 5 has built-in functions by Matlock (1970) and Welch & Reese (1972) circular piles.

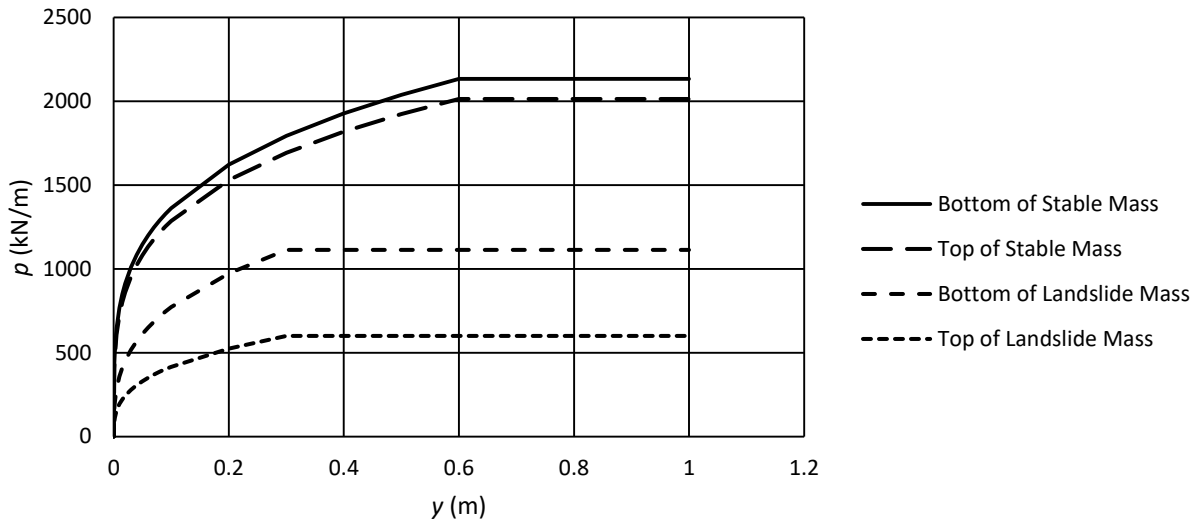


Figure 6.6: Custom  $p$ - $y$  curves for Option 1.

### 6.2.5 Soil-Pile Interaction at CN Study Site

RSPile (Rocscience, 2016) was used to numerically model the soil-pile interaction where the sheet pile walls are modelled as an elastic beam-column and the lateral soil resistance is governed by the  $p$ - $y$  curves developed in Step 4.

To solve the differential equation for a beam column shown in Equation 2-30, the flexural rigidity of the pile ( $E_p I_p$ ) is required. The series of ten PZC-26 sheet piles has a moment of inertia ( $I_p$ ) of approximately  $0.5854 \text{ m}^4$  and the steel has a Young's modulus ( $E_p$ ) of 200 GPa. The pile was modeled with a depth below ground of 11.0 m which extends 2.0 m below the slide plane depth of 9.0 m depth and into the stable layer.

The  $p$ - $y$  curves developed in Section 6.2.4 were applied to the unstable soil layer which extended to a depth of 9.0 m below ground surface and the underlying stable mass. The soil-pile interaction was numerically modeled based on the three methodologies for developing  $p$ - $y$  curves described as Option 1, Option 2a, and Option 2b. The custom  $p$ - $y$  curve for Option 1 was manually input into the model by inserting a series of  $p$ - $y$  coordinates to define the curve. For Option 2a and Option 2b, the built-in  $p$ - $y$  curves in RSPile were used. For Option 2a, the pile was idealized as a circular pile with an equivalent pile diameter of 3.0 m and a reduction factor of 0.64. For Option

2b, the pile was idealized as a circular pile with an equivalent pile diameter of 1.59 m and a reduction factor of 0.79.

The landslide loading was modelled by applying a boundary condition consisting of a uniform lateral soil displacement from the ground surface to the sliding depth. This is shown in the RSPile output in Figure 6.7. This figure shows the results from using the Option 2a  $p$ - $y$  curve and applying a landslide displacement of 25 mm. The calculated lateral displacement of the pile, the bending moment profile, and the shear force profile are given in Figure 6.7.

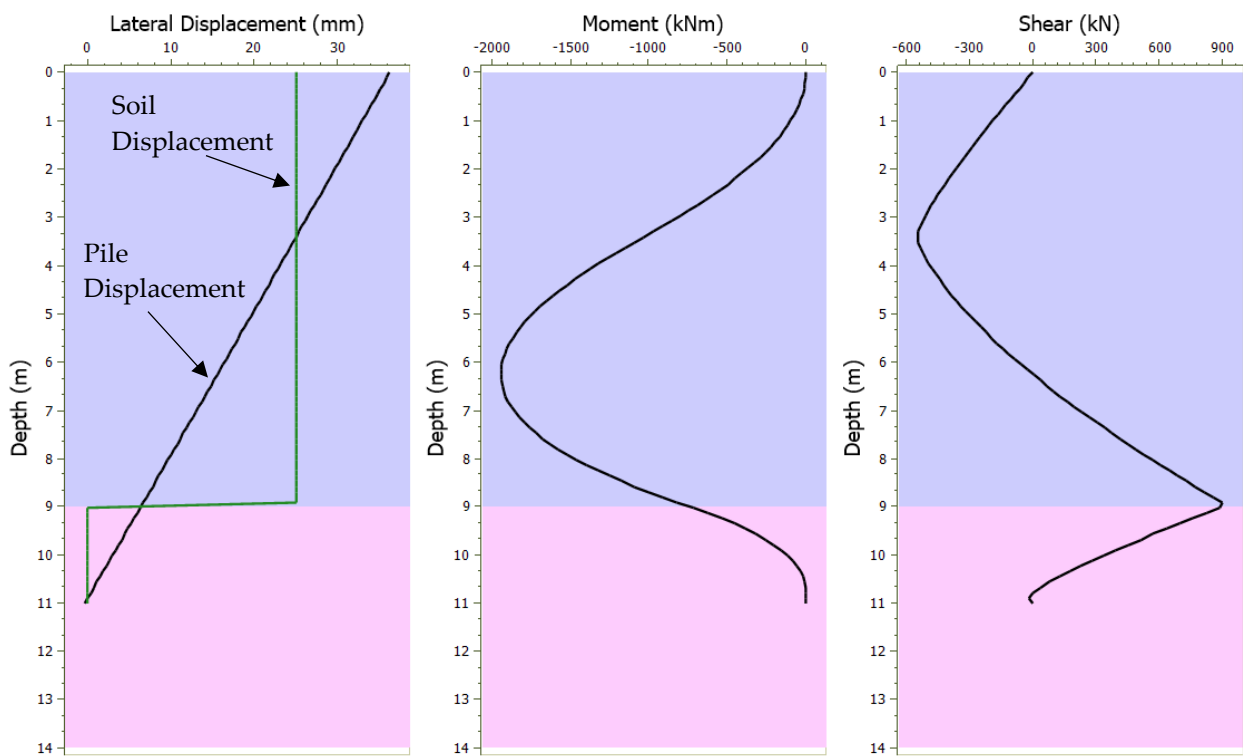


Figure 6.7: RSPile output showing pile displacement, moment, and shear force from soil displacement.

In RSPile, an ultimate lateral resistance analysis can be performed to determine the available resistance against landslide loading. Substantial soil movement is typically required to mobilize resistance along the length of the pile (Loehr and Brown, 2008). A value of 0.3 m of soil displacement has been considered failure for the ultimate lateral resistance analysis even if transverse resistance in the pile has not been fully mobilized to that point. The estimated deflection of the piles for an ultimate lateral resistance analysis with a maximum 0.3 m of lateral

soil displacement is shown in Figure 6.8. The results are shown for the three options for developing the  $p$ - $y$  curves. The corresponding bending moment and shear forces for the ultimate lateral resistance are provided in Figure 6.9 and Figure 6.10, respectively.

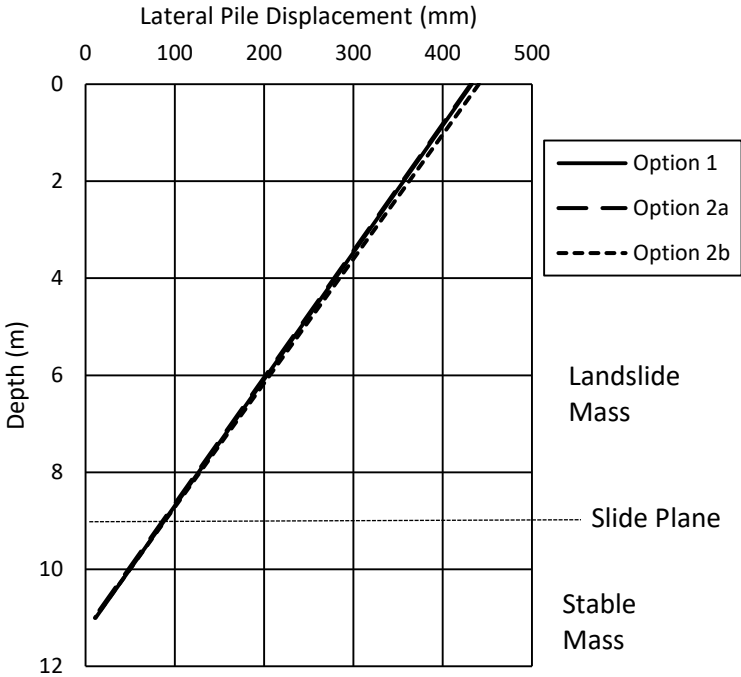


Figure 6.8: Estimated lateral displacement of sheet pile.



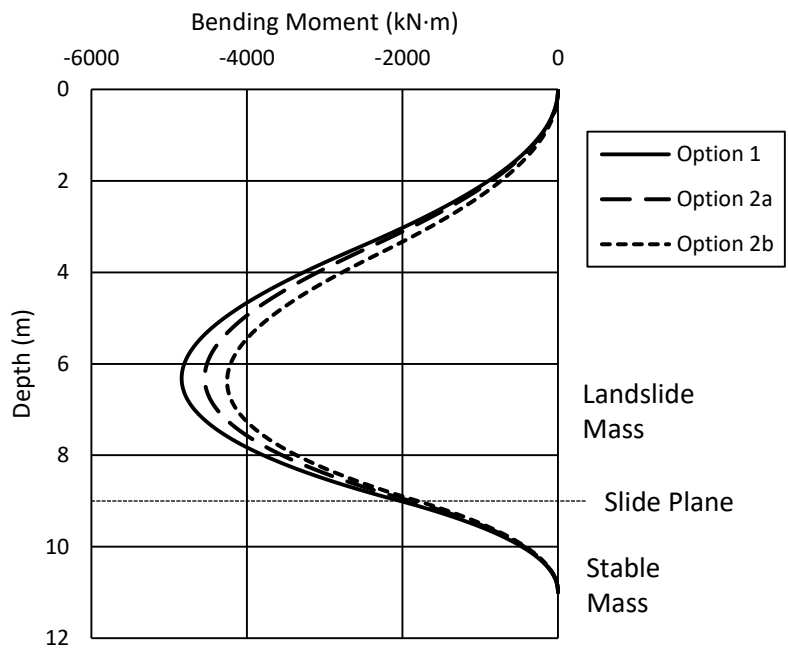


Figure 6.9: Estimated bending moment profile of sheet pile.

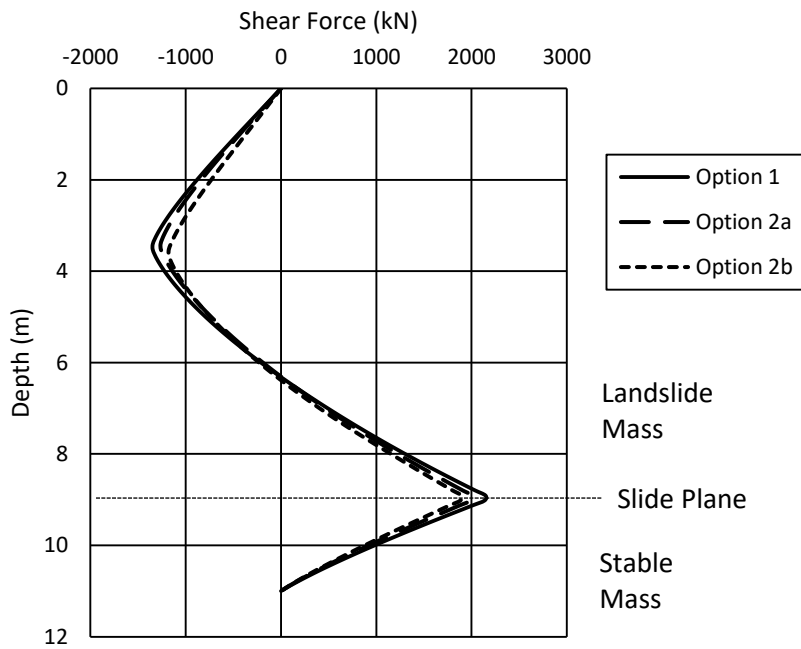


Figure 6.10: Estimated shear force profile of sheet pile.

As shown in Figures 6.8 through Figure 6.10, the estimated performance of the sheet piles that comprise the Hardy Ribs is relatively consistent regardless of which method of developing the  $p$ - $y$  curve is selected. Figure 6.8 shows that there is very little expected bending deflection of the sheet pile and that sheet piles are expected to fail in overturning by rotating about the base of the piles. This behaviour would be expected for this short pile design due to the very high flexural rigidity of the selected sheet pile wall section and the relatively small embedment depth into the intact shale. For each option, the maximum expected pile displacement is approximately 435 mm at ground surface. Figure 6.9 shows that the peak bending moment is expected to occur above the slide plane and at approximately 6.5 m depth below ground surface. Figure 6.10 shows that the maximum shear force is expected to occur at the slide plane at 9.0 m depth below ground surface. This shear force is equal to the resisting force that each sheet pile wall can contribute to resisting the landslide. By dividing the shear force at the slide plane by the 3.0 m centre-to-centre spacing between sheet pile walls, the resisting force per metre along the slope can be determined. Table 6.2 summarizes the magnitudes of the maximum bending moments, the maximum shear force, and the resisting force against landslide loading.

Table 6.2: Maximum bending moment and shear force in sheet pile walls.

<b><math>p</math>-<math>y</math> Curve</b>	<b>Maximum Bending Moment (kN·m)</b>	<b>Maximum Shear Force (kN)</b>	<b>Landslide Resistance (kN/m)</b>
Option 1	4839	2147	716
Option 2a	4543	2008	669
Option 2b	4256	1894	631

The magnitude of the maximum bending moment and shear force are greatest for Option 1 and are the smallest for Option 2b. This is expected when reviewing the magnitude of  $p_{ult}$  with depth for the various options in Figure 6.5 as  $p_{ult}$  is greatest for Option 1 and the lowest for Option 2b. The maximum bending moment and shear force for Option 2a are 6% less than Option 1 and for Option 2b are 12% less than Option 1.

It was determined in Step 1 that an increase of horizontal resting force of 708 kN/m was required to achieve the target factor of safety. Based on the numerical analysis of the pile-soil interaction, the Hardy Ribs design is expected to increase the horizontal resisting force by 716 kN/m based

on Option 1 and is therefore sufficient to achieve the target factor of safety of 1.3 based on the assumptions in the analysis. Using Option 2a or Option 2b for the  $p$ - $y$  curves provides a more conservative result for the landslide resistance force and the estimated factor of safety after remediation is slightly below 1.3.

#### 6.2.6 Structural Capacity of Sheet Pile Walls at CN Study Site

Step 6 involves checking the structural capacity of the sheet pile walls. The yield shear strength ( $V_y$ ) is calculated as:

$$V_y = \tau_y A = 0.577 \cdot \sigma_y \cdot A_p = 0.577 \cdot 250000 \text{ kPa} \cdot 0.1401 \text{ m}^2 = 20209 \text{ kN} \quad 6-17$$

where  $\tau_y$  is the yield shear stress,  $\sigma_y$  is the yield tensile strength, and  $A_p$  is the cross-sectional area of the sheet pile wall. The yield tensile strength is 250 MPa and the cross-sectional area of the sheet pile wall is 0.1401 m<sup>2</sup>. The yield bending moment ( $M_y$ ) is calculated as:

$$M_y = \frac{I_p \sigma_y}{Y} = \frac{0.5854 \text{ m}^4 \cdot 250000 \text{ kPa}}{3.54 \text{ m}} = 41342 \text{ kN} \cdot \text{m} \quad 6-18$$

Where  $I_p$  is the moment of inertia and  $Y$  is the distance from the outer fiber of the cross section to the neutral axis.  $I_p$  is approximately equal to 0.5854 m<sup>4</sup> and  $Y$  is equal to 3.54 m for the sheet pile walls.

When the maximum shear and maximum bending moment developed in the sheet pile walls in Table 6.2 are compared, the yield strength is considerably greater. Therefore, the arrangement of ten PZC-26 sheet piles is sufficient. It was assumed that there is no sliding along the connections between the individual sheet pile sections and the wall acts as a continuous section.

#### 6.2.7 Location of Sheet Pile Walls at CN Study Site

The final step consists of selecting an appropriate location for the Hardy Ribs. Poulos (1995) recommended that shear piles extend deep enough such that the landslide does not progress downward below the piles with a factor of safety less than the target value. Poulos (1995) also recommended that the piles are installed near mid-slope to prevent a landslide from occurring

upslope or downslope of the piles. Additional 2D limit equilibrium slope stability analyses were performed using Slide 7.0 with the same cross-section and material properties modeled in the back analysis described in Section 6.2.1. The Morgenstern-Price method with a half-sine interslice force function was used to calculate the factor of safety.

A 2D limit equilibrium stability analysis was performed to estimate the factor of safety of a potential landslide that could occur upslope of the Hardy Ribs and a potential landslide that could occur downslope of the Hardy Ribs. The cross sections from Slide 7.0 are shown in Figure 6.11 for the potential upper slope failure and Figure 6.12 for the potential lower slope failure surface.

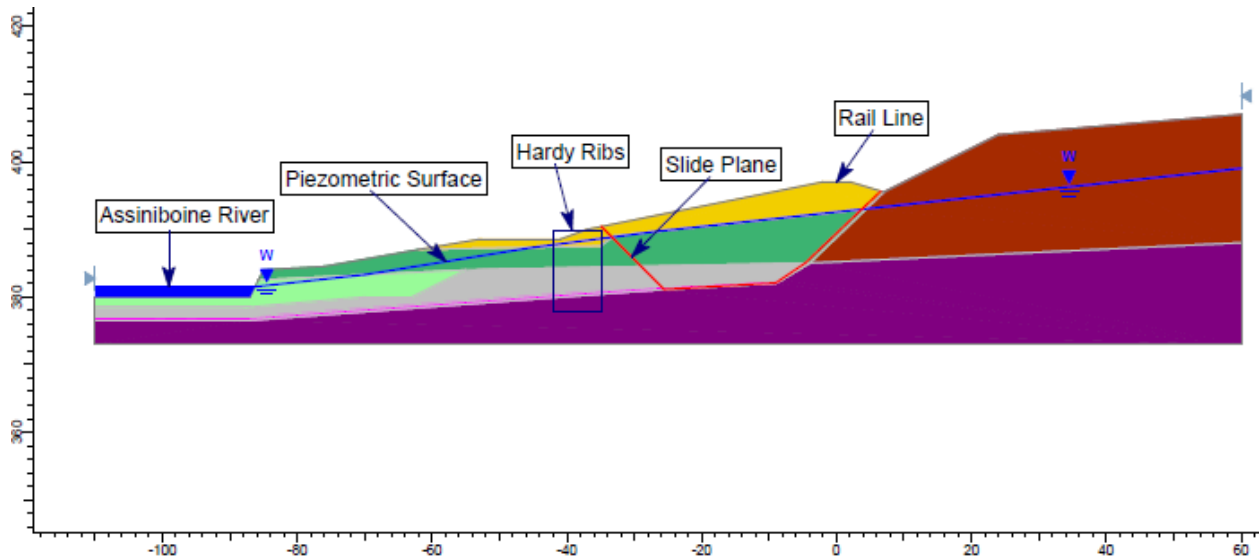


Figure 6.11: Slide 7.0 model of potential upper slope slide plane.

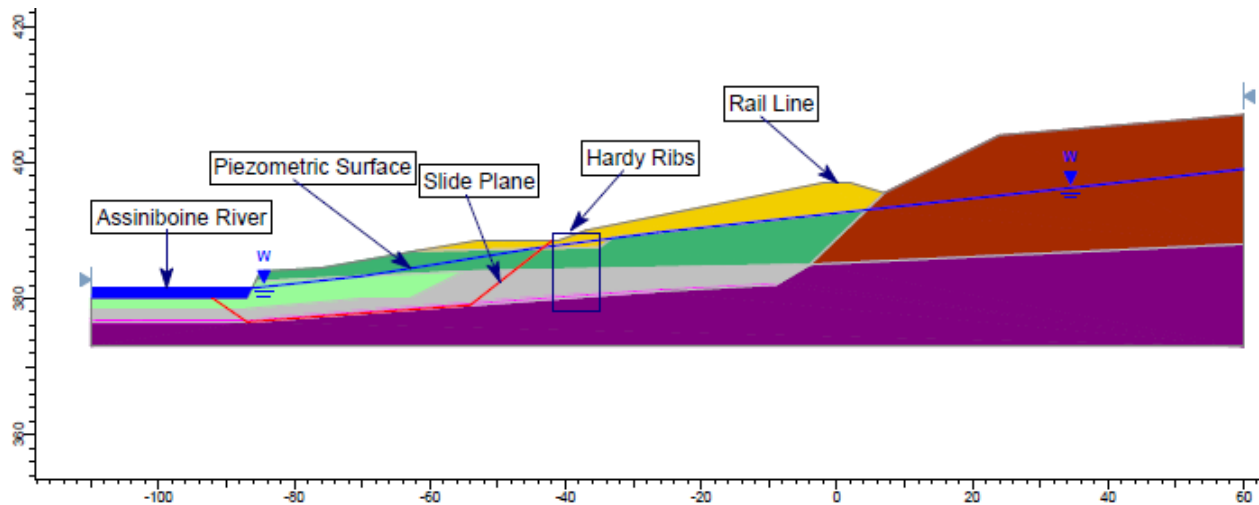


Figure 6.12: Slide 7.0 model of potential lower slope slide plane.

The estimated factor of safety of the potential upper slope slide plane was calculated to be 2.29. Therefore a potential landslide that would exit the slope upslope of the Hardy Ribs and affect the rail line is not expected to be of concern. The estimated factor of safety of the potential lower slope slide plane was calculated to be 1.12 which is less than the target factor of safety of 1.3. Although this potential landslide would not impact the rail line, the Hardy Ribs rely on the passive resistance from the downslope soil. If excessive landslide displacements occur downslope of the Hardy Ribs, the Hardy Ribs will not be able to provide the intended stabilizing force.

A 2D limit equilibrium stability analysis was also performed to estimate the *FS* of a potential slide plane that extends below the Hardy Ribs. This was executed by applying the disturbed shale material properties to the base of the Hardy Ribs. This material region of disturbed shale extends from the residual shale shear plane to the base of the Hardy Ribs at 45°. This angle is representative of the active and passive failure wedge that would develop assuming that the intact shale behaves as a purely cohesive material. The cross section from Slide 7.0 showing the analyzed slide plane and the modified material regions is shown in Figure 6.13.

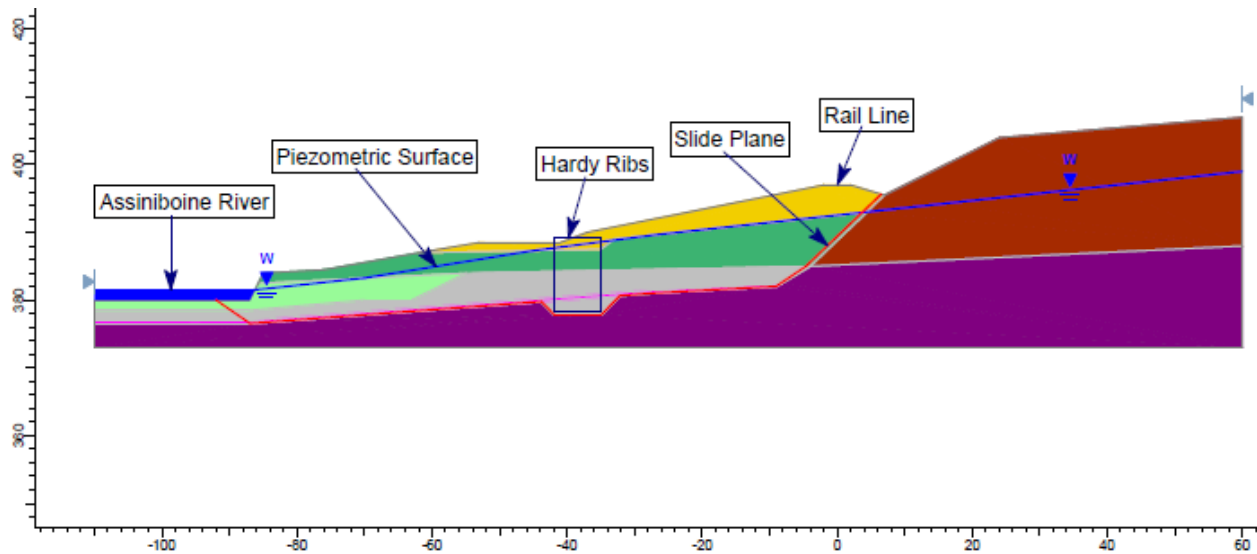


Figure 6.13: Slide 7.0 model of potential deep slide plane.

The estimated factor of safety of the potential slide plane that extends beneath the Hardy Ribs was calculated to be 1.29. This is approximately equal to the target factor of safety and approximately equal to the estimated factor of safety of the original slide plane after remediation from the Hardy Ribs. Therefore, extending the sheet piles to a depth of 2.0 m below the slide plane is sufficient.

### 6.3 Comparison to Viggiani's (1981) Method

As an alternative to Steps 4 and 5, the method suggested by Viggiani (1981) could be used to estimate the increase in resisting force against landslide loading. This method only applies to the ultimate state and does not indicate the development of pile resistance with soil displacement (Poulos, 1995). Also, this method only considers  $p_{ult}$  to be constant with depth for both the unstable soil mass and the underlying stable soil. Viggiani (1981) suggested using lateral end bearing coefficients of 4 for the unstable soil and 8 for the stable soil.

For this analysis, each sheet pile wall was treated as an equivalent circular pile, consistent with Option 2a and Option 2b in Steps 4 and 5. The ratio of the soil depth ( $\lambda$ ) is calculated as:

$$\lambda = \frac{l_2}{l_1} = \frac{2 \text{ m}}{9 \text{ m}} = 0.222 \quad 6-19$$

where the pile embedment depth below the slide plane ( $l_2$ ) is 2 m and the depth above the slide plane ( $l_1$ ) is 9 m. The ratio of lateral load capacity ( $\chi$ ) of the unstable and stable layers is calculated as:

$$\chi = \frac{N_{c1}c_{u1}}{N_{c2}c_{u2}} = \frac{4 \cdot 100 \text{ kPa}}{8 \cdot 250 \text{ kPa}} = 0.2 \quad 6-20$$

The estimated shear resistance at the slide plane can then be calculated for the various potential failure modes of a short pile which include overturning, lateral translation, or flowing soil around the piles which remain stationary. It was determined that the overturning failure mode was the most critical based on Equation 2-20, Equation 2-21, and Equation 2-24. If the sheet pile wall is analyzed as an equivalent 3.0 m diameter ( $b$ ) circular pile with reduction factor ( $P$ ) of 0.64, then the shear force for the overturning failure mode ( $T_B$ ) is calculated as:

$$\begin{aligned} T_B &= PN_{c1}c_{u1}bl_1 \left[ \sqrt{\left(\frac{1+\lambda}{1+\chi}\right)^2 + \frac{\lambda^2 + \chi}{\chi(1+\chi)}} - \frac{1+\lambda}{1+\chi} \right] \quad 6-21 \\ &= 0.64 \cdot 4 \cdot 100 \cdot 3 \cdot 9 \cdot [0.422] = 2920 \text{ kN} \end{aligned}$$

If the sheet pile wall is analyzed as an equivalent 1.59 m diameter ( $b$ ) circular pile with reduction factor ( $P$ ) of 0.79, then the shear force for the overturning failure mode ( $T_B$ ) is calculated as:

$$\begin{aligned} T_B &= PN_{c1}c_{u1}bl_1 \left[ \sqrt{\left(\frac{1+\lambda}{1+\chi}\right)^2 + \frac{\lambda^2 + \chi}{\chi(1+\chi)}} - \frac{1+\lambda}{1+\chi} \right] \quad 6-22 \\ &= 0.79 \cdot 4 \cdot 100 \cdot 1.59 \cdot 9 \cdot [0.422] = 1910 \text{ kN} \end{aligned}$$

The estimated shear force at the landslide plane is calculated to be 2920 kN for an equivalent 3.0 m diameter circular pile which is approximately 36% to 54% greater than the values provided in Table 6.2 from performing the numerical analyses utilizing  $p$ - $y$  curves. The estimated shear force at the landslide plane is calculated to be 1910 kN for an equivalent 1.59 m diameter circular pile which is within the range of values shown in Table 6.2. As shown in this example, it is possible to select parameters such that the calculated shear stress is consistent with the values calculated using a numerical analysis with  $p$ - $y$  curves. However, the analysis using  $p$ - $y$  curves in Section 6.2.5. defined failure as 0.3 m of lateral soil displacement and transverse resistance in the pile has not been fully mobilized to that point. The mobilization of resistance with soil displacement can't be estimated with Viggiani's (1981) method. Therefore, the results are not directly comparable unless substantial lateral soil displacement is applied in the analysis using  $p$ - $y$  curves.

There is considerable uncertainty in selecting an appropriate value for the equivalent circular pile diameter, the lateral end bearing coefficients above and below the slide plane as well as the reduction factor. Therefore, Viggiani's (1981) method is not recommended for estimating the available shear resistance. Since the calculations for this method are very simple to perform, it may be beneficial to provide an initial estimate of the shear resistance in the correct order of magnitude and to estimate the impact that varying the installation depth of the piles can have.

#### **6.4 Summary of Design Methodology**

A methodology was developed for the design of Hardy Ribs and consists of seven steps. This design methodology utilizes similar procedures developed for the design of a row of circular piles for slope stabilization. A de-coupled approach is used consisting of a 2D limit equilibrium slope stability analysis and a laterally loaded pile analysis to determine the additional shear resistance. This procedure is intended for translational landslides with a discrete slide plane.

The Hardy Ribs installed at CN Mile 191.4 Rivers Subdivision were analyzed based on the seven step design procedure. It was determined from the 2D limit equilibrium slope stability analysis that approximately 708 kN/m in additional shear resistance along the valley is required to increase the factor of safety to 1.3. For the laterally loaded pile analysis, the stratigraphy and shear



strength parameters were simplified into two regions, the landslide mass and the underlying stable soil mass. The  $p$ - $y$  curves were modified from existing curves for soft clay (Matlock, 1970) and stiff clay without access to free water (Welch & Reese, 1972). The estimated increase in shear resistance from the Hardy Ribs is in the range of 631 kN to 716 kN, and the estimated factor of safety after is approximately equal to 1.3.

The CN case study was also analyzed using Viggiani's (1981) method and treating the sheet pile walls as equivalent circular piles. It was determined that this method can results in a consistent estimate of the stabilizing force compared to the developed design procedure. The uncertainty in selecting a value for the equivalent circular pile diameter, the lateral end bearing coefficients above and below the slide plane, and the reduction factor can lead to considerable variation in the estimated shear resistance. Therefore, this method is only recommended for a very preliminary estimate of the shear resistance for Hardy Ribs.

## 7.0 CONCLUSIONS

This chapter provides conclusions of this thesis including key contributions on the topic of Hardy Ribs, a summary of the Hardy Ribs study site at CN Mile 191.4 Rivers Subdivision, and recommendations for future research on Hardy Ribs.

### 7.1 Key Contributions

The following key contributions related to laterally loaded sheet pile walls and Hardy Ribs were made from this research.

- An expression was developed for calculating the magnitude of  $p_{ult}$  for a sheet pile wall or rectangular pile that is loaded laterally parallel to the length of the pile as described in Chapter 4. Both the possibility of a wedge-type failure near ground surface and a flow-around failure mechanism at depth were considered. The expression for the flow-around failure mechanism was derived from a calibrated 2D finite element model.
- An expression was proposed for calculating an appropriate spacing between adjacent sheet pile walls in cohesive and cohesionless soils such that the Hardy Ribs act as a continuous wall as described in Chapter 5. This will result in the maximum resistance to landslide loading. This expression was derived from limit equilibrium analyses and was supported by 3D finite element modelling.
- Where the Hardy Ribs act as a continuous wall, an expression was proposed to calculate  $p_{ult}$  that is equal to the difference of the passive and active earth pressures acting on the Hardy Ribs as described in Chapter 5. The tensile strength near ground surface for cohesive soils should be ignored and not relied upon in design of Hardy Ribs.
- A methodology was proposed for using existing  $p$ - $y$  curves developed for circular piles for Hardy Ribs where the magnitude of  $p_{ult}$  is modified as described in Chapter 5. Two general options were proposed consisting of calculating  $p_{ult}$  from the difference of passive and active earth pressures or treating the Hardy Ribs as an equivalent series of circular piles.

- A methodology was proposed for the analysis and design of Hardy Ribs which includes seven steps as described in Chapter 6. The steps include: 1) determine the landslide loads, 2) select material properties for a laterally loaded pile analysis, 3) calculate the minimum spacing to prevent soil from squeezing between sheet pile walls, 4) develop  $p$ - $y$  curves, 5) numerically model the soil-pile interaction to determine the resisting force against landslide loading, 6) check the structural capacity of sheet pile walls, and 7) select the location on the slope to install the Hardy Ribs. This methodology ignores any contribution to resistance from shearing along the base of the Hardy Ribs and the estimated resistance is entirely developed from the lateral soil resistance.

## 7.2 Summary of CN Mile 191.4 Rivers Subdivision

The performance of the landslide at CN Mile 191.4 of the Rivers Subdivision was studied where landslide remediation works consisting of Hardy Ribs were constructed in the summer of 2015. Summarizing points related to the performance and analysis of the site are provided below:

- The stratigraphy at the site consisted of a thin layer of fill comprising the rail embankment, underlain by clay and clay shale bedrock. A slide plane was identified within the shale bedrock based on slope inclinometer monitoring data. The landslide was observed to be moving at approximately 1 mm per day in November and December of 2014 prior to the construction of remediation works.
- The Hardy Ribs design at CN Mile 191.4 Rivers Subdivision consisted of 37 rows of sheet pile walls spaced 3.0 m apart centre-to-centre to span approximately 108 m along the valley. Each wall consisted of ten PZC-26 pile which had a length of approximately 7.08 m and were installed to approximately 2.0 m below the slide plane.
- Monitoring data from a slope inclinometer installed upslope of the Hardy Ribs has indicated that landslide displacement has significantly decreased since completion of the remediation works. The monitoring data from December, 2015 to December, 2016 indicates downslope displacement along the entire depth of the sheet pile walls. The maximum displacement has occurred in the disturbed shale, however the rate of displacement has decreased to less than 1 mm per month over this time period. Some

displacement is expected as the Hardy Ribs are a passive system and require to undergo lateral displacement to develop resistance and provide a stabilizing force. Continued long term displacement may occur due to creep behaviour of the clay and shale bedrock.

- Based on the proposed theoretical limit equilibrium solution for calculating and selecting an appropriate sheet pile wall spacing, the spacing at CN Mile 191.4 Rivers Subdivision is expected to be sufficiently small such that the Hardy Ribs act as a continuous wall. The slope inclinometer data does however indicate that there is greater displacement in the shale bedrock than the clay above which suggests that there could be shearing between the side of the sheet pile walls and the shale bedrock. This could be from the highly disturbed nature of the clay shale above the slide plane. The adhesion value ( $a$ ) was selected as 0.75 in the analysis, however a lower value may have been more appropriate which would require a smaller spacing between sheet piles to prevent the shale from squeezing between sheet piles.
- Based on a 2D limit equilibrium slope stability analysis, approximately 708 kN/m of landslide stabilization force along the valley is required to increase the estimated factor safety to the target value of 1.3.
- Based on a laterally loaded pile analysis utilizing  $p$ - $y$  curves, the Hardy Ribs are expected to increase to provide a resisting force of 716 kN/m which is sufficient to achieve the target FS. This is based on the simplified soil stratigraphy and shear strength parameters described in Section 6.2 and neglects shear resistance along the base of the Hardy Ribs.
- The shear strength and bending strength of sheet pile walls are expected to be adequate to prevent yielding. The sheet pile walls were considered to behave as a continuous section.
- A potential landslide plane originating downslope of the Hardy Ribs was analyzed and the estimated factor of safety was calculated to be approximately 1.12. This site is located along the outside bend of the Assiniboine River and signs of ongoing erosion at the toe of the slope have been observed. This toe erosion can further reduce the factor of safety for this potential slide plane. If considerable landslide displacement were to occur downslope

of the Hardy Ribs, the passive resistance would be lost and the Hardy Ribs would no longer function as intended.

### **7.3 Recommendations for Future Research**

The key findings from this research on Hardy Ribs were largely derived from limit equilibrium analyses and supporting numerical models. There is still a significant lack of empirical field data and no lab scale data on the performance of laterally loaded sheet pile walls that comprise Hardy Ribs. The following research topics and tasks are recommended.

- Laboratory scale testing of laterally loaded rectangular piles or sheet pile walls is recommended to verify the calculation of the critical spacing where the Hardy Ribs act as a continuous wall. It may be difficult to replicate the displacement of soil towards the piles, however displacement could be applied to piles in a fixed container of soil to measure the resistance due to the relative displacement between pile and soil. Visual observations can be made to describe whether squeezing between piles occurs and the force applied to the piles can be measured to quantify the resistance for varying pile spacing. Reduction factors can also be developed for the lateral load capacity of the piles where they are spaced further apart such that shearing along the sides of the piles occurs.
- Monitoring of additional Hardy Ribs study sites is recommended with the installation of more instrumentation to gather more empirical performance data. The geotechnical investigation should include more insitu and laboratory testing of the soil and bedrock for a more accurate estimation of the material properties. As part of the instrumentation program, the following instruments and locations should be considered.
  - Slope inclinometers or ShapeAccelArrays installed upslope and downslope of the Hardy Ribs and between sheet pile walls to compare horizontal displacements upslope, downslope, and within the Hardy Ribs. The slope inclinometers should be monitored before, during, and after construction of the Hardy Ribs. Additionally, a slope inclinometers installed in the corrugations of connected sheet piles would provide an accurate measurement of whether the sheet piles undergo lateral translation or rotation.

- Monitoring pins on the sheet pile walls and on the ground surface between sheet pile walls for survey monitoring to compare the displacement and determine if the soil is squeezing between the sheet pile walls. If the sheet pile walls are to be buried following installation, rebar can be welded to the sheet pile walls to allow for survey monitoring at ground surface.
- Horizontally installed slope inclinometers perpendicular to the sheet pile walls and immediately upslope or downslope of the sheet piles. This displacement profile measured would indicate whether soil is squeezing between the sheet pile walls at that particular depth. The installation could practically only occur near the ground surface and trenches would be required at both ends of the slope inclinometer casing to pull the probe through.
- Strain gauges on the sheet pile walls to measure strain and determine if the bending stresses are distributed through the entire arrangement of sheet piles. Careful consideration would be required to install the strain gauges and ensure that they are not damaged from the pile driving process.
- Studying the orientation of the sheet piles that comprise the Hardy Ribs is recommended. Instead of being installed perfectly parallel to each other, the sheet pile walls could be installed in an alternating skewed fashion such that the ends of adjacent sheet pile walls touch. This would essentially create a continuous wall in a zig-zag formation, eliminating the possibility of soil squeezing between the walls. The structural capacity of the sheet piles would decrease however as the bending moment would no longer be applied in the orientation of the maximum moment of inertia.

## REFERENCES

- Abdelaziz, T.S., Proudfoot, D.W., & Skirrow, R. (2011). Stabilization of Alberta highway landslides using pile walls. *Proceeding of the 2011 Pan-am CGS Geotechnical Conference, Toronto, Ontario*. Richmond: Canadian Geotechnical Society.
- Bowles, J.E. (1996). *Foundation Analysis and Design*. Peoria, Illinois: McGraw-Hill.
- Broms, B.B. (1964). Lateral resistance of piles in cohesive soils. *J. Soil Mech. and Found. Div., ASCE* 90 (SM2): 27-63.
- Broms, B.B. (1964). Lateral resistance of piles in cohesionless soils. *J. Soil Mech. and Found. Div., ASCE* 90 (SM3): 123-156.
- Broms, B.B. (1983). Earth pressures on piles in a row due to lateral soil movements. *Discussion, Soils and Foundations*, 23(3): 127-129.
- Bunce, C. & Chadwick, I. (2012). GPS monitoring of a landslide for railways. *Proceedings of the 11<sup>th</sup> International and 2<sup>nd</sup> North American Symposium on Landslides and Engineered Slopes, Banff, Alberta, Vol. 2: 1373-1379*. Leiden: CRC Press.
- Canadian Geotechnical Society (2006). *Canadian foundation engineering manual 4<sup>th</sup> edition*. Richmond B.C.: Canadian Geotechnical Society.
- Clifton Associates (2015). *Canadian National Railway Company Slope Stability Analysis and Remedial Design* (Unpublished Report). Regina, Saskatchewan.
- CloudCompare (2017). [GPL Software]. v2.8. Retrieved from <http://www.cloudcompare.org/>
- Conte, E. & Troncone, A. (2004). An analysis of piles used to stabilize slopes. *Proceedings of the Ninth International Symposium on Landslides, Rio de Janeiro, Brazil: 1599-1605*. New York: A.A. Balkema.

- Cornforth, D.H. (2005). *Landslides in Practice*. Hoboken, NJ: John Wiley & Sons.
- Cornforth, D.H. (2012). Advances in investigation and analysis for landslides: Three selected topics. *Proc. 11<sup>th</sup> Int. Symposium on Landslides and Eng. Slopes, Banff 2012*: 59-71. Leiden: CRC Press.
- Cox, W.R., Dixon, D.A., & Murphy, B.S. (1984). Lateral load tests of 25.4 mm diameter piles in very soft clay in side-by-side and in-line groups. *Laterally Loaded Deep Foundations: Analysis and Performance, ASTM, SPT835*: 122-1390. Philadelphia, Pa.: ASTM.
- Cruden, D.M. & Varnes, D.J. (1996). Landslide types and processes, In; Turner, A.K. & Schuster, R.L. (editors), *Landslides: Investigation and Mitigation*. (Special Report 247, Transportation Research Board, National Research Council, 36-75). Washington, DC.
- Georgiadis, M. (1983). Development of p-y curves for layered soils. *Proceedings of the Geotechnical Practice in Offshore Engineering, ASCE*: 536-545. New York, ASCE.
- Hetenyi, M. (1946). *Beams on elastic foundation*. Ann Arbor, Michigan: University of Michigan Press.
- Klassen, R.W. (1975). *Quaternary geology and geomorphology of Assiniboine and Qu'Appelle valley of Manitoba and Saskatchewan* (Geological Survey of Canada, Department of Energy, Mines and Resources). Ottawa: Geological Survey of Canada.
- Lieng, J.T. (1988). *Behaviour of laterally loaded piles in sand – large scale model tests* (Ph.D. Thesis). Department of Civil Engineering, Norwegian Institute of Technology, Trondheim, Norway.



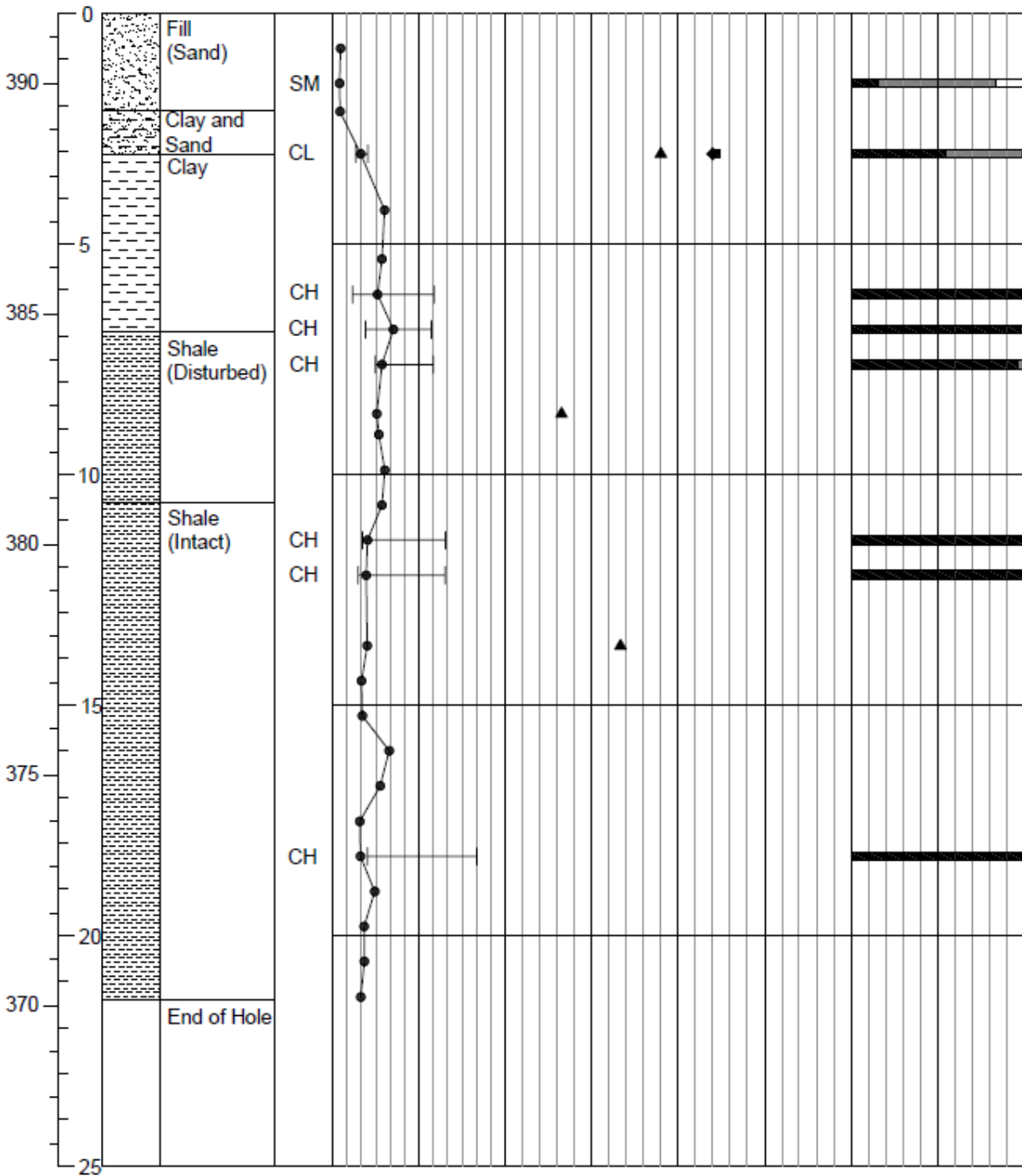
- Loehr, E.J. & Brown, D.A. (2008). *A method for predicting mobilization of resistance for micropiles used in slope stabilization applications*. A report prepared for the joint ADSC/DFI micropile committee.
- Matlock, H. (1970). Correlations for design of laterally loaded piles in soft clay. *Proceedings, Second Annual Offshore Technology Conference, Houston, Texas, Vol. 1: 577-594*. New York: IEEE.
- Pariseau, W.G. (2007). *Design Analysis in Rock Mechanics*. Leiden, The Netherlands: Taylor and Francis.
- Peck, R.B., Hanson W.E., & Thorburn, T.H. (1974). *Foundation Engineering, 2<sup>nd</sup> edition*. New York: Wiley.
- Poulos, H.G. (1995). Design of reinforcing piles to increase slope stability. *Canadian Geotechnical Journal* 32: 808-818.
- Poulos, H.G. & Davis, E.H. (1980). *Foundation analysis and design*. New York: John Wiley and Sons.
- Prakash, S. (1962). *Behaviour of pile groups subjected to lateral loads*. Unpublished dissertation, University of Illinois.
- Randolph, M.F. & Houlsby, G.T. (1984). The limiting pressure on a circular pile loaded laterally in cohesive soil. *Geotechnique*, 34(4): 613-623.
- Reese, L.C. (1958). Discussion of soil modulus for laterally loaded piles, by McClelland, B. and Focht, J.A., Jr. *Transactions ASCE Vol. 123: 1071-1074*.
- Reese, L.C. (1984). *Handbook on design of piles and drilled shafts under lateral load*. (Report No. FHWA-IP-84-11, U.S. Department of Transportation Federal Highway Administration). McLean, Va: U.S. Department of Transportation.

- Reese, L.C. (1997). Analysis of laterally loaded piles in weak rock. *Journal of Geotechnical and Geoenvironmental Engineering, ASCE, vol 123 (11) Nov: 1010-1017.*
- Reese, L.C., Cox, W.R., & Koop, F.D. (1974). Analysis of laterally loaded piles in sand. *Proceeding of the VI Annual Offshore Technology Conference, Houston, Texas, 2(OTC 2080): 473-485.*
- Reese, L.C., Cox, W.R., & Koop, F.D. (1975). Field testing and analysis of laterally loaded piles in stiff clay. *Proceeding of the VII Annual Offshore Technology Conference, Houston, Texas, 2(OTC 2312): 671-690.*
- Reese, L.C. & Van Impe, W.F. (2011). *Single piles and pile groups under lateral loading, 2<sup>nd</sup> edition.* Boca Raton, Florida: Taylor and Francis Group.
- Reese, L.C., Wang, S.T., & Fouse, J.L. (1992). Use of drilled shafts in stabilizing a slope. *Stability and Performance of Slopes and Embankments – II, Geotechnical Special Publication No. 31, ASCE, Vol. 2: 1318-1332.* New York, N.Y.: ASCE.
- Rocscience Inc. (2016). RSPile 1.0 [Computer Software], v1.004.
- Rocscience Inc. (2016). RS2 9 [Computer Software], v9.016.
- Rocscience Inc. (2016). RS3 1.0 [Computer Software], v1.020.
- Rocscience Inc. (2016). Slide 7.0 [Computer Software], v7.017.
- Vessely, D.A., Yamasaki, K. & Strom, R. (2007). Landslide stabilization using piles. *Proceedings, First North American Conference on Landslides. Vail Colorado: 1173-1183.* Madison, Wisconsin: Omnipress.
- Viggiani, C. (1981). Ultimate lateral load on piles used to stabilize landslides. *Proceedings of the 10<sup>th</sup> International Conference on Soil Mechanics and Foundation Engineering, Stockholm, Vol. 3: 555-560.* Rotterdam: Balkema.

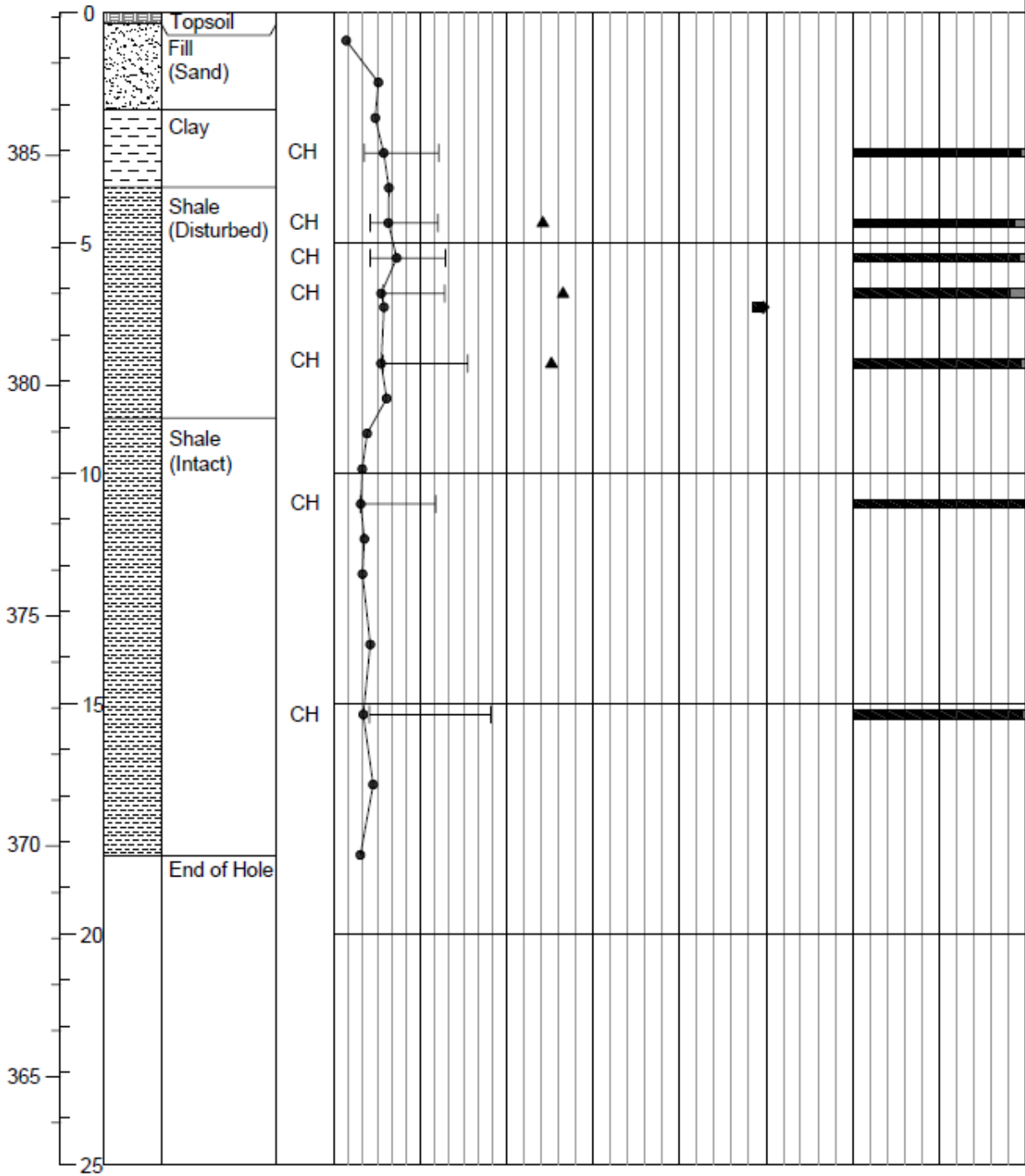
- Wang, S.T. & Reese L.C. (1986). *Study of design method for vertical drilled shaft retaining walls* (Research Report 415-2F, Texas State Department of Highway and Public Transportation, U.S. Department of Transportation Federal Highway Administration). Austin Texas, Center for Transportation Research, The University of Texas at Austin.
- Wang, S.T., Vasquez, L. & Xu, D. (2013). Application of soil-structure interaction (SSI) in the analysis of flexible retaining walls. *Proceedings of the IACGE International Conference on Geotechnical and Earthquake Engineering, Chengdu, China: 567-577.*
- Welch, R.C. & Reese L.C. (1972). *Laterally loaded behaviour of drilled shafts* (Research Report No. 3-5-65-89, Texas State Department of Highway and Public Transportation, U.S. Department of Transportation Federal Highway Administration). Austin, Texas, Center for Transportation Research, The University of Texas at Austin.

## **APPENDIX A: BOREHOLE LOGS**

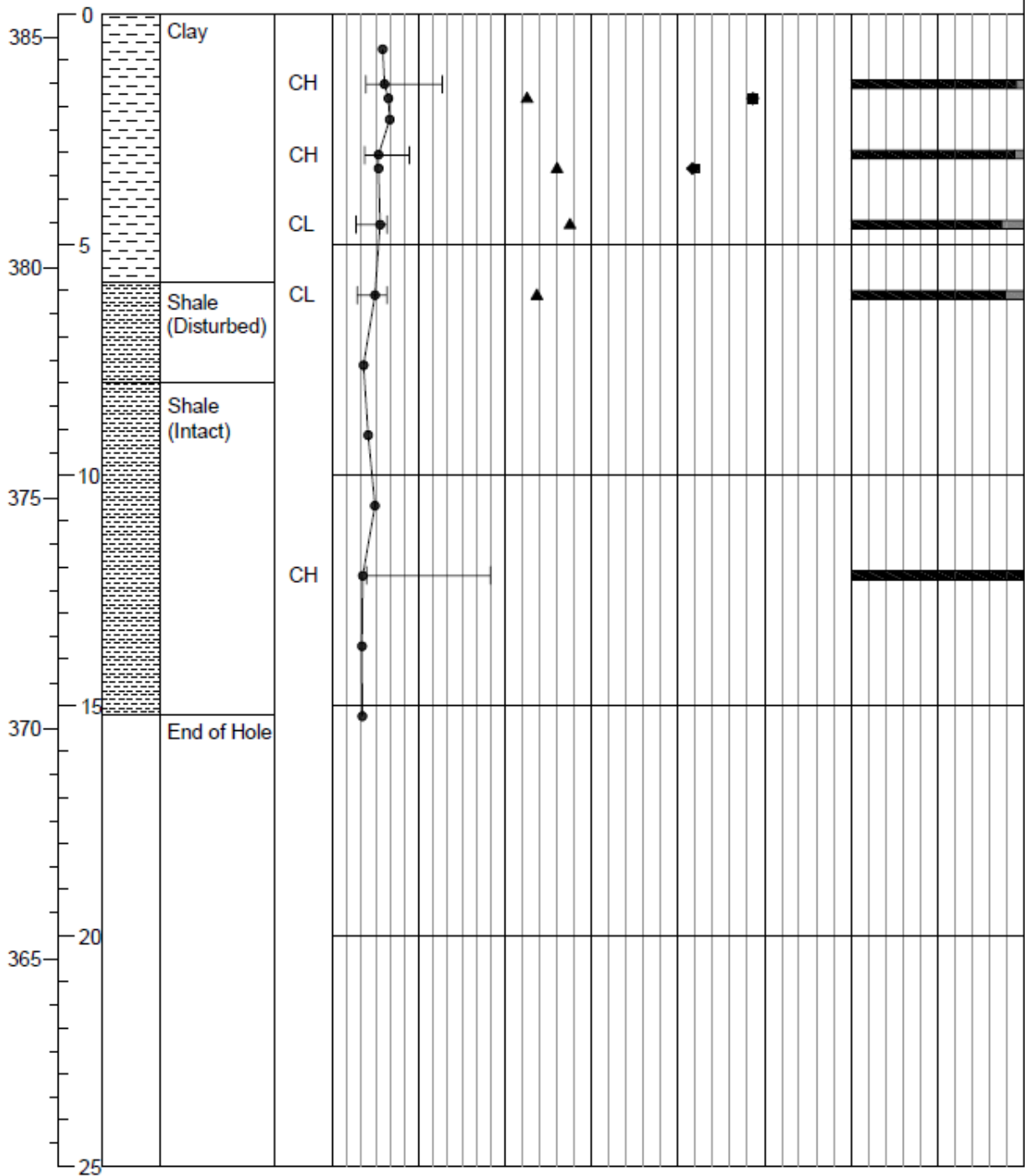
<b>Borehole: BH14-1</b>				Northing: 5572125.201 m		Easting: 343920.159 m		Ground Elevation: 391.521 m								
Elev (m)	Depth (m)	Symbol	Soil Description	USCS	Water Content (%)			Dry Density (kg/m <sup>3</sup> )	Undrained Shear Strength (kPa)		Particle Size Distribution (%)					
					PL	w	LL		-LAB VANE	-POCKET PEN	Clay & Silt	Sand	Gravel			
					0	60	120	1200	1500	1800	0	150	300	0	50	100



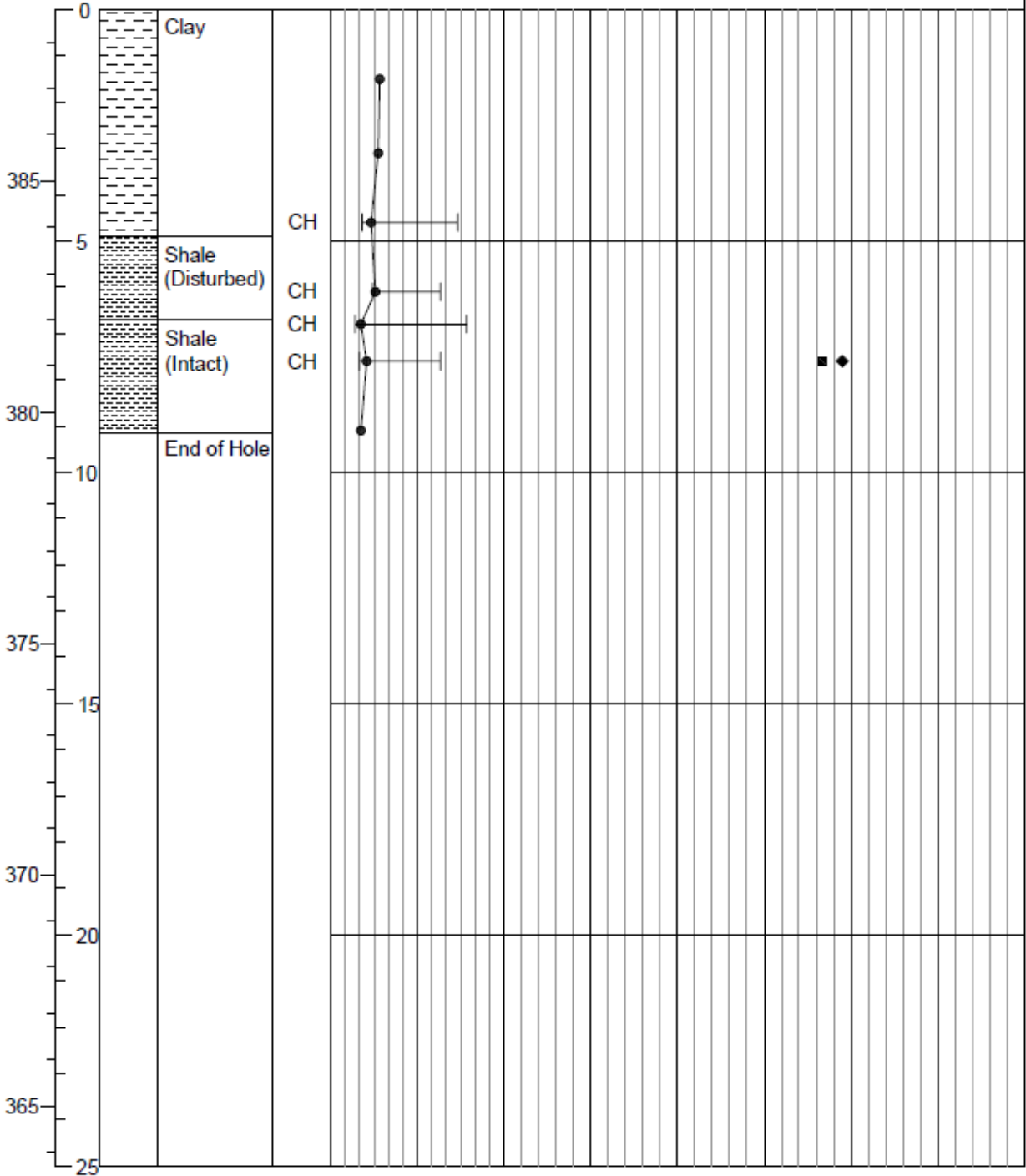
<b>Borehole: BH14-2</b>				Northing: 5572126.245 m												
				Easting: 343900.160 m												
				Ground Elevation: 388.099 m												
Elev (m)	Depth (m)	Symbol	Soil Description	USCS	Water Content (%)			Dry Density (kg/m <sup>3</sup> )	Undrained Shear Strength (kPa)		Particle Size Distribution (%)					
					PL	w	LL		-LAB VANE	-POCKET PEN	Clay & Silt	Sand	Gravel			
					0	60	120	1200	1500	1800	0	150	300	0	50	100



<b>Borehole: BH14-3</b>					Northing: 5572125.338 m Easting: 343877.197 m Ground Elevation: 385.513 m			
Elev (m)	Depth (m)	Symbol	Soil Description	USCS	Water Content (%)	Dry Density (kg/m <sup>3</sup> )	Undrained Shear Strength (kPa)	Particle Size Distribution (%)
					PL    w    LL 			

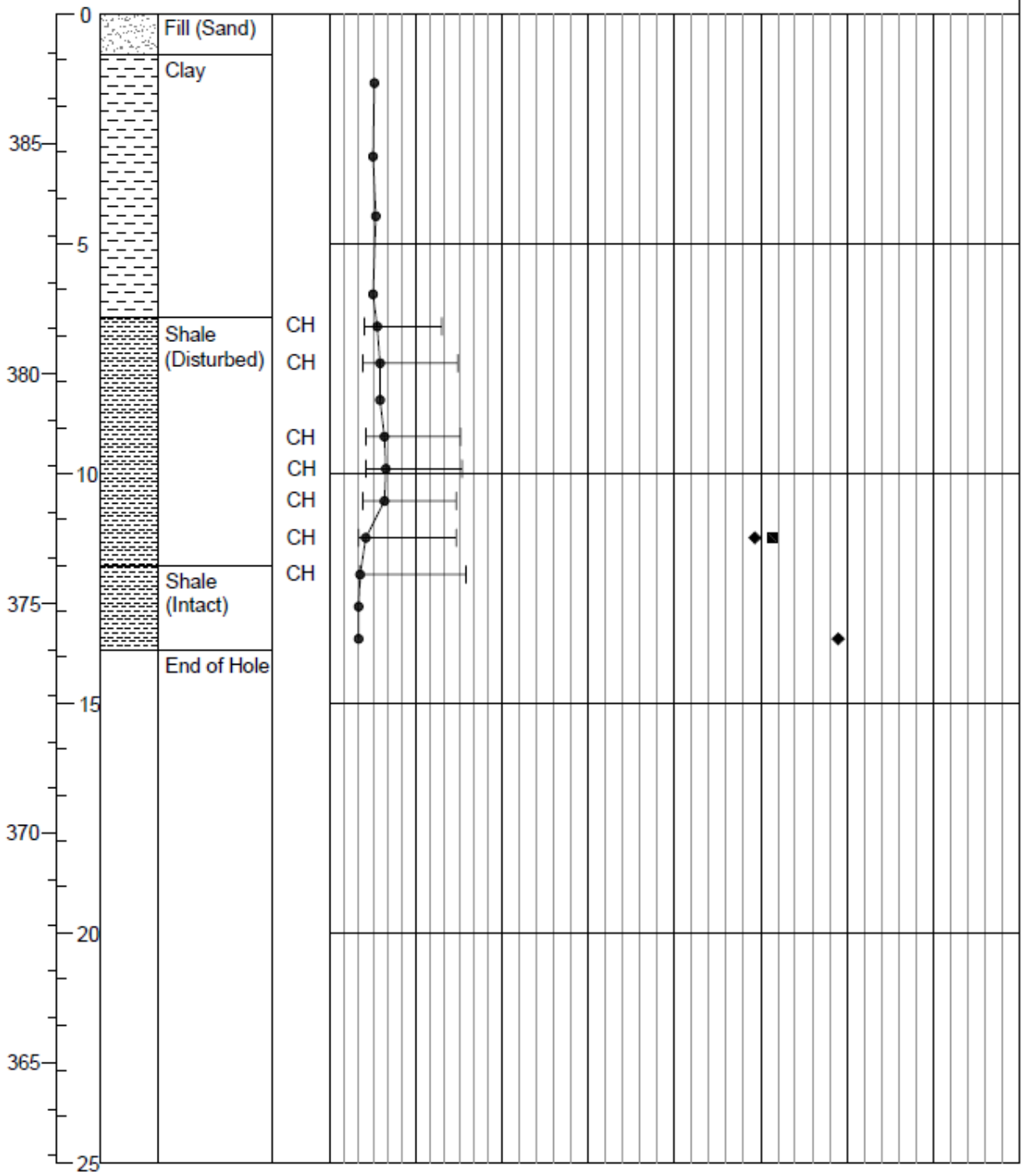


<b>Borehole: BH15-1</b>					Northing: 5572067.44 m Easting: 343907.95 m Ground Elevation: 388.7 m			
Elev (m)	Depth (m)	Symbol	Soil Description	USCS	Water Content (%) PL    w    LL	Dry Density (kg/m <sup>3</sup> ) ▲	Undrained Shear Strength (kPa) ■ -LAB VANE ◆ -POCKET PEN	Particle Size Distribution (%) Clay & Silt    Sand    Gravel
					0    60    120	1200    1500    1800	150    300	0    50    100





<b>Borehole: BH15-2</b>					Northing: 5572166.82 m Easting: 343905.91 m Ground Elevation: 387.84 m			
Elev (m)	Depth (m)	Symbol	Soil Description	USCS	Water Content (%)	Dry Density (kg/m <sup>3</sup> )	Undrained Shear Strength (kPa)	Particle Size Distribution (%)
					PL    w    LL 			



<b>Borehole: BH15-3</b>					Northing: 5572123.978 m Easting: 343913.052 m Ground Elevation: 390.559 m			
Elev (m)	Depth (m)	Symbol	Soil Description	USCS	Water Content (%)	Dry Density (kg/m <sup>3</sup> )	Undrained Shear Strength (kPa)	Particle Size Distribution (%)
					PL    w    LL 			

